7-22-2012

International Conference on Mechanical & Industrial Engineering

Prof.Srikanta Patnaik Mentor
IRNet India, patnaik_srikanta@yahoo.co.in

Proceedings of International Conference on

MECHANICAL & INDUSTRIAL ENGINEERING

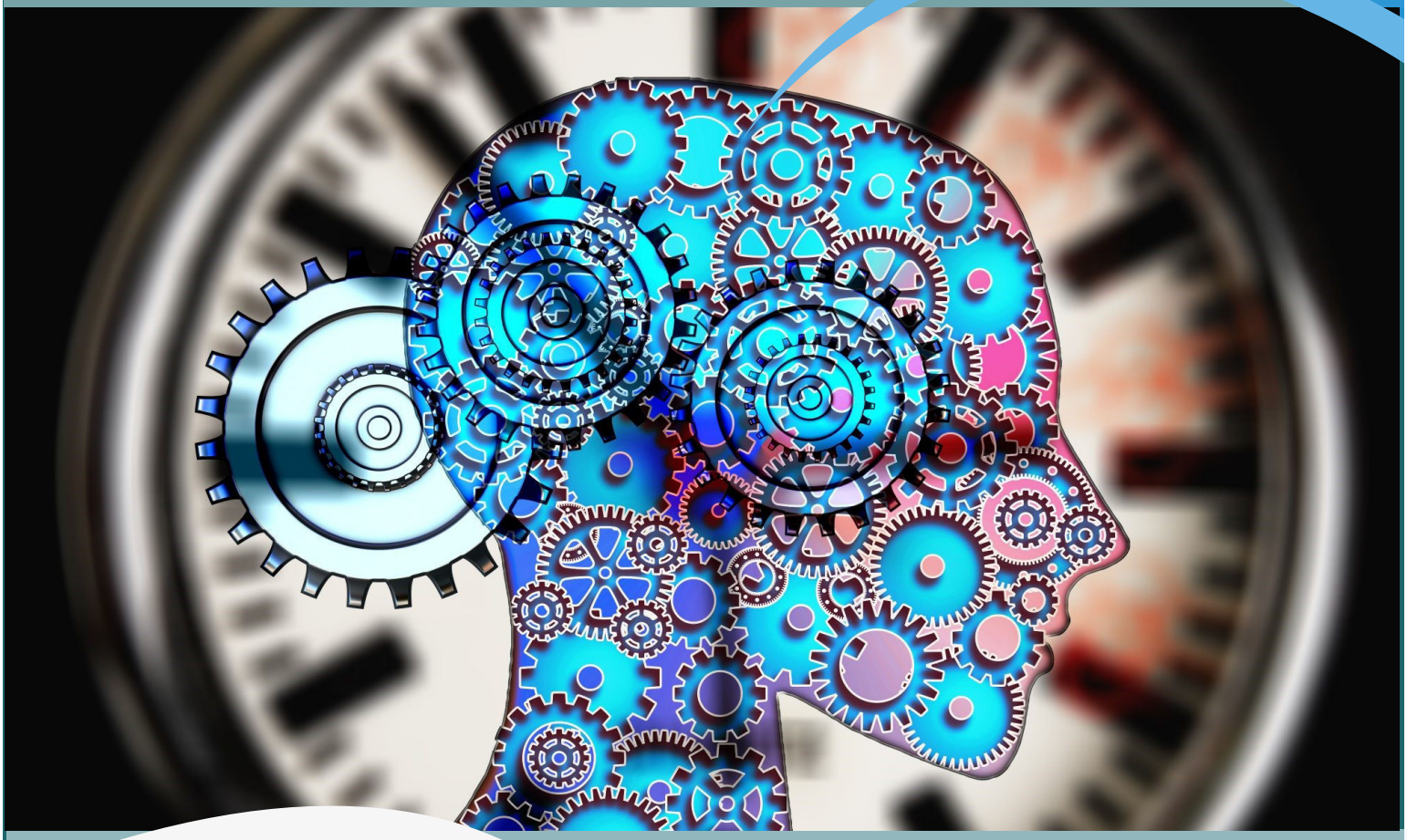

(ICMIE-2012)
22nd July, 2012
BANGALORE, India

Interscience Research Network (IRNet)
Bhubaneswar, India

Editorial

India is quickly overpopulating with growth outstripping China's . The big question is whether the land can sustain such huge pressure. For example in spite of being gifted with abundant water, huge population is making per-capita clean water scarcer. No one knows if India's economy will be strong enough to rescue such a huge mass of poor people. Recently, to tackle this problem, the Indian Government has started a mass employment program to help employ civilians living in rural areas. However, some note that this will be a "spoonful of reform for a sea of misery. India desperately needs to improve its social infrastructure such as roads, rail, power grid, water, communications infrastructure, housing. Since the turn of the century, the global recession has affected most businesses, including Mechanical Engineering. As a result of globalization there is tremendous pressure to perform or deliver. Hence the technologies to be adopted by the industries are to be latest and most efficient to facilitate growth. Significant achievements have been made worldwide in the area of mechanical engineering like Diesel Engines, Pumps, Hydraulic and Pneumatic, Compressors, Gears, Bearing, Drilling , thermal systems etc and still considerable innovative research is being continued to address the technical and economical challenges.

In such a scenario it is necessary to discuss the recent developments in the field of mechanical engineering and its allied areas. Computational Fluid Dynamics (CFD) is one more advancement which also has a bright Computational fluid dynamics (CFD) is one of the branches of fluid mechanics that uses numerical methods and algorithms to solve and analyze problems that involve fluid flows. Computers are used to perform the millions of calculations required to simulate the interaction of fluids and gases with the complex surfaces used in engineering. Even with simplified equations and high-speed supercomputers, only approximate solutions can be achieved in many cases. Ongoing research, however, may yield software that improves the accuracy and speed of complex simulation scenarios such as transonic orturbulent flows. Initial validation of such software is often performed using a wind tunnel with the final validation coming in flight test.Electro chromatic mirrors / Auto dimming mirrors use a combination of opto electronic sensors and complex electronics (sensors, circuit boards, micro-controllers, etc.) that constantly monitor ambient light and the intensity of light shining directly on the mirror. As soon as sensors detect glare, the electro chromatic surface of the mirror becomes darker to protect driver’s eyes and their concentration.

The conference designed to stimulate the young minds including Research Scholars, Academicians, and Practitioners to contribute their ideas, thoughts and nobility in these disciplines of engineering. It’s my pleasure to welcome all the participants, delegates and organizer to this international conference on behalf of IOAJ family members. We received a great response from all parts of country and abroad for the presentation and publication in the proceeding of the conference. I sincerely thank all the authors for their invaluable contribution to this conference. I am indebted towards the reviewers and Board of Editors for their generous gifts of time, energy and effort.

Editor-in-Chief
Dr. SrikantaPatnaik
Chairman, I.I.M.T., Bhubaneswar
Intersceince Campus,
At/Po.: Kantabada, Via-Janla, Dist-Khurda
Bhubaneswar, Pin:752054. Orissa, INDIA.

Vibration Suppression Using Mechatronic Systems

[1]PRATHAP NARAYANAPPA & [2]Y.V. DASESWARARAO

[1,2]Department of Mechanical Engineering
Birla Institute of Technology & Science (BITS)-Pilani, Hyderabad Campus
Hyderabad - 500078, Ranga Reddy (Dist) (AP), INDIA

***Abstract*—** Vibration suppression has always been an important issue in developing efficient motion control systems. Traditionally, in a mechanical system, the vibrations are suppressed by adding more material to the system in order to increase the rigidity. However, recent advancements in mechatronics, has provided with many alternative solution that avoids excess material addition and increased performance. This paper attempts to summarize various methods that are being developed for vibration detection and suppression. The techniques included in this paper are motion control strategies based on sensors, sensor-actuator and sensorless controllers.

Keywords-*Vibration suppression; Sensorless control technique; piezoelectric; shape memory alloy;PID; Input shaping*

I. INTRODUCTION

The vibration in machine structure has a significant effect on machine's performance. There is a need to develop systems for damping and control of vibrations in order to have high precision and speed. Due to the global demand for mass production, automation systems have to be consistently efficient to meet the requirements. An important issue for such systems is the jerk and vibration caused by the inappropriate acceleration or deceleration motion, which results in decreased accuracy and increased settling time to the motion control systems in the equipment. Moreover, motion induced vibration also occurs in such systems. The occurrence of vibration leads to an additional settling time before the new maneuver can be initiated. Therefore, in order to achieve a fast system response, it is imperative that this vibration is reduced.

Traditional method to suppress vibrations was to increase the rigidity of the system in order to resist the vibrations. Recent advancements in mechatronics have given rise to alternate solution in the form of a smart structure which would suppress the vibrations without significant increase the overall weight of the equipment. A smart structure used in vibration control can be defined as a structure of structure's component with bonded of embedded sensors and actuators as well as an associated control system, which enable the structure to respond simultaneously to external stimulus exerted on it and then suppress undesired effects of enhance desired effects. Various approaches have been proposed to reduce vibration in flexible systems. They can be broadly categorized based on control system used as feed-forward, feedback or a combination of both methods.

This paper talks about various smart materials and control strategies, used in passive and active vibration control. Smart materials like piezo-ceramics and shape memory alloys are extensively being studied for vibration suppression. However, there are other methods where the various control strategies are used in order to achieve the optimum damping characteristics with and without these smart materials. Few such methods are discussed in this paper.

II. PIEZOELECTRIC VIBRATION SUPPRESSION SYSTEMS

A. Bonded Piezoelectric Sensors and Actuators

Piezoceramics are well known smart materials for being lightweight, low-cost. They offer sensing and actuation capabilities that can be utilized for passive and active vibration control. Active vibration control (AVC) is well known nowadays as an optimum technique in vibration suppression of flexible structures. In AVC, constrained viscoelastic damping layers are usually used to attenuate the vibration of vibrating bodies. Gou Xinke Tian Haimin [1] presented a numerical study on the active vibration control of piezoelectric cantilever beam. In his study, he analyzed optimum position for placement of piezoelectric actuators on a cantilever beam.

In AVC, a controller receives the information about the induced vibration and supplies suitable control signals to actuators in order to suppress the vibration. From the results of Gou Xinke Tian Haimin's work it was evident that controlled dynamic response of displacement at the free end of the piezoelectric cantilever beam had significant less compared to uncontrolled dynamic response. It was further observed that application of LQR optimal control algorithm suppresses excessive vibration when sensors and actuators are placed at fixed end of the cantilever beam as shown in figure 1.

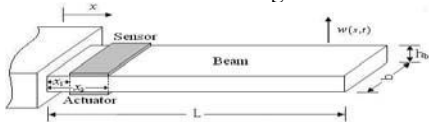

Figure 1 Cantilever Smart Sensor [1]

B. Active Force Control Strategy

In Active Force Control (AFC), a controlled varying force is applied by the actuators in order to suppress the vibrations. In AFC, it has been shown that the system subjecting to a number of disturbances remains stable and robust via the compensating action of the AFC control strategy [2]. The main concern in the AFC scheme is regarding the estimation of mass of the dynamic system to ensure correct estimation of total force to be applied by the actuator. This mass being estimated is virtual mass that represents mass of dynamic system. There are several methods to find correct value of mass matrix such as genetic algorithm, iterative learning algorithm, fuzzy logic and etc.

Zahidi Rahman's [3] experimental study of the vibration control of flexible structure using AFC method is chosen for discussion. He used heuristic method to estimate the mass matrix of flexible system along with an assumption that transfer function of actuator is unity. In this study, collocation of sensor and actuator was implemented. Thus an accelerometer was placed at the opposite side of piezoelectric patch actuator at the same flexible plate.

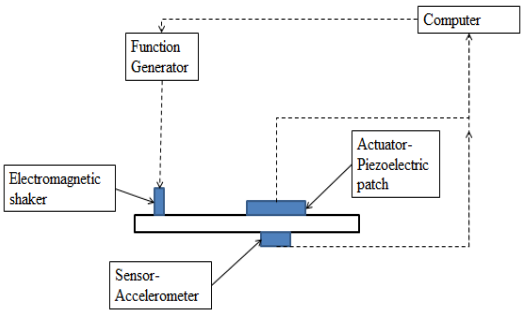

Figure 2 Schematic diagram of Active Force Control System [3]

Piezoelectric patch transducer was chosen to attenuate the disturbance vibration force from the plate. The transducer contracted when voltage is applied to create counter force.

The results of above mentioned study clearly indicates that AFC possessed the ability to attenuate the unwanted vibration of flexible system as long as a proper method is chosen to estimate the mass matrix of the system to ensure correct estimation of counter force subjected to the system.

III. CONTROL STRATEGIES FOR VIBRATION SUPPRESSION

C. Input-Shaping with PID

The command shaping technique is widely employed in control of flexible manipulators and aircraft [4, 5]. The design method involves convolving a desired command with a sequence of impulses known as an input shaper. The shaped command that results from the convolution is then used to drive the system. The method has been effective in reducing motion-induced vibration [6, 7].The performance of the feedback control can be improved by adding the feed forward control component, by achieving reduction in the system vibration. This is important for the fast maneuvering platforms, where the command signals change rapidly.

However, when the feed-forward control component is augmented with feedback component it causes additional delay in the system response. To resolve this issue, an objective function is created to tune the PID controller within the augmented strategy that gives the smallest overshoot, fastest rise time, quickest settling time and very small steady state error. In order to combine all these objectives, multiple objective functions are used to minimize the output error of the controlled system. To get optimum performance of a PID controller its parameters were tuned using GA optimization process by Fareg Aldebrez [8]. The population is represented by real valued numbers or binary strings each of 16 bits called a chromosome. Each chromosome consists of three separate strings constituting a Kp, Ki and Kd terms, as defined with in specific range, which can ensure stability. The response due to shaped step input is stored and error is assessed taking the difference between the desired and actual response. This error signal is processed based on different criteria to evaluate the performance and assign a fitness value to that individual. Using the fittest individuals, the next population is generated through a process of shuffle crossover with reduced surrogate and mutation operation [9].

This method was experimentally implemented on a 4-impulse input shaper, designed on the basis of vibration frequency and damping ratio of the main rotor system. The designed input shaper was used for pre-processing the reference signal. It was observed that oscillation in the system response has been significantly reduced due to the shaped reference signal. The system performance after GA tuning process recorded further reduction in settling time. This study has proven that with proper tuning, a PID controller can be used to controls an augmented feed-forward control component combined with feedback control component to achieve significant improvement in the dynamic system response with satisfactory level of vibration reduction.

D. Acceleration Profile Control

An important issue in high precision and high speed automatic equipment is the jerk and vibration caused by inappropriate acceleration or deceleration motion, which results in decreased accuracy and increased settling time to the positioning table. To solve such problems and reach a high production efficiency level, the motion control must have the capability to plan trajectory and generate motion profile in such a way that the accelerating and decelerating phases become much smoother to reduce inertia force and decrease residual vibration of point-to-point motion. A typical point-to-point motion profile can be divided into three phases: accelerating, constant speed and decelerating.

To improve the performance, the velocity profile is modified to have an s-shape during the acceleration and deceleration periods to reduce the residual vibrations caused in a mechanical system by a moving mass. In such s-curve velocity profile, the trajectory ramps up to peak acceleration and ramps down to constant speed. Though s-curve motion profile gives faster and more precise motion compared to trapezoidal velocity profile, it is noted that s-curve profile still exhibits a sudden jerk profile, and the finite jerk spreads out over a period of time [10].

A method proposed by H.Z.Li [11] smoothens the acceleration profile using sine wave function to achieve smoother jerk profile. The main objective of this method was to minimize the high acceleration induced jerk in high-speed and high-precision motion control. The DSP controller performs the servo motion control by providing motion profile generation, position determination, position error calculation, and motion commands creation in real time. In this method, the profile data was calculated using Matlab script and the values for the constant velocity and deceleration parts are calculated by the DSP. The results showed that it is possible to reduce the motion-induced transient vibration of a structure by using a sine wave profile.

E. Sensorless Control Technique

When vibration in a flexible system has to be suppressed, using motion control system with sensors, multiple sensors will be required. Multiple sensors require multiple wiring along with their associated electronic setups. Moreover, using certain sensors increases the mechatronic products' cost tremendously, especially if force/torque feedback is required. In addition, control of flexible systems requires using sensors with certain specifications such as fatigue resistance to withstand the everlasting fluctuations due to simplest maneuvers. To overcome most of such issues sensorless control techniques are being developed. Sensorless techniques reduce the hardware sophistication that is added when sensors are utilized.

Action-reaction event normally occurs at the actuator-plant's point of interface. Actuator's action on any given dynamical system is naturally followed by an instantaneous dynamical system reaction. The actuator's action and dynamical system's reaction are related. Therefore, one can get the information about the plant's dynamics and parameters through measurement taken from the other system that imposes the action. Gulnihal Cevik [12] discusses about one such sensorless technique where based on the measurements from system imposing action, an estimation algorithm combined with regular LQR is capable of achieving motion control and vibration suppression without taking any measurement from the flexible plant. The correctness of the whole analysis discussed in [12] shows that almost zero variation of the estimated displacement and real ones and the vibration is significantly decreased in comparison to a PID control. However the estimation algorithm will not compensate for unknown or sudden effects on the system. The unknown parameters can be the masses of peripherals, springs, parts of the setup etc. These external effects can be minimized be more experience and thus finding equivalent gains for these unknowns.

IV. VIBRATION CONTROL USING SHAPE MEMORY ALLOYS

Shape memory alloys (SMAs) have been widely employed as actuators and sensors in applications including smart structures, biomedical devices, and robotics. When heated above the transformation temperature, the SMAs undergo a change in the crystal structure, thereby generating large forces that can be used to actuate the control systems. However, due to the inherent nonlinear and complex dynamic behavior of the SMA actuators, it is generally difficult to design a controller that guarantees closed loop stability within the performance bounds [13, 14].

There are comparative merits and demerits of the SMA actuators with respect to the piezoelectric actuators. The SMA actuators are capable of producing large forces, withstanding large stresses and recovering large strains, unlike piezoelectric actuators, which are brittle, and when subjected to large stresses, can become depolarized and ineffective. The SMA actuators are attached to each flexible link for the vibration suppression. The SMA actuators are wires that act in pairs to provide a bidirectional control i.e., the actuators tend to counteract. The slow response of the SMAs is a major limitation in practice, and thus, loses effectiveness at high frequencies of vibration, whereas the piezoelectric actuators can operate at frequencies, of the order of 10 kHz [15]. The slow response of SMA can be partially circumvented by reducing the size of the actuators to increase the rate of heat transfer. However, the force production decreases with size, thus diminishing the advantage of the SMAs in delivering large forces. For successful implementation of the SMAs, engineers need to balance the force requirements of the application in concern with the rate of cooling that can be achieved in the operating environment.

V. CONCLUSION

This paper discusses various options available to suppress the vibrations using mechatronics system. The methods discussed serve as an alternate option to material addition which has been traditional practice to increase rigidity. It is clear from our discussion that SMAs are only limited to low frequency vibrations and is a long way from being effective in active vibration control. Though control techniques discussed were very effective in certain applications, they're limited to those applications. However, their applications can be extended by combing with an actuator and sensor. Hence it can be said that actuator-sensor based control strategies can achieve optimum vibration suppression. And as discussed, piezoelectric actuators, because of their high frequency response, can be the best option for such control strategies, as it

can be easily augmented with variety of control strategies.

◈◈◈

REFERENCES

[1] Gou Xinke Tian Haimin, "Active Vibration Control of a Cantilever Beam using Bonded Piezoelectric Sensors and actuators" The Eighth International Conference on Electronic Measurement and Instruments, IEEE, 2007,Vol-4, Page 85-88.

[2] M. Mailah, E. Pitowarno and H. Jamaluddin, "Robust Motion Control for Mobile Manipulator Using Resolved Acceleration and Proportional- Integral Active Force Control", International Journal of Advanced Robotic Systems, 2005, Vol-2, Page 125-134.

[3] T.A.Zahidi Rahman, I.Z.Mat Darus, "Active Vibration Control of a flexible plate via Active Force Control strategy", 4th International Conference of Mechatronics, 2011, Page 1-6.

[4] T. Livet, D. Fath and F. Kubica, "Robust autopilot design for a highly flexible aircraft" Proceedings of IFAC World Congress, San Francisco, California, 1996, Page 279-284.

[5] Z. M. Mohamed and M. O. Tokhi, "Vibration control of a single-link flexible manipulator using command shaping techniques," Proc. Inst. Mech. Eng., Part I, J Systems and Control Engineering, 2002, vol. 216, Page 191- 210.

[6] L. Y. Pao, "Strategies for shaping commands in the control state of flexible structures," Proceedings of Japan–USA–Vietnam Workshop on Research and Education in Systems, Computation and Control Engineering, Vietnam, 2000, Page 309-318.

[7] W. E. Singhose, N. C. Singer and W. P. Seering, "Comparison of command shaping methods for reducing residual vibration", Proceedings of European Control Conference, 1995, Page 1126-1131.

[8] Fareg M. Aldebrez, Mohammad S.Alam and M.Osman Tokhi, "Input-shaping with GA-tuned PID for target tracking and vibration reduction", Proceedings of 13th Mediterranean Conference on Control and Automation, 2005, Page 485-490.

[9] D. E. Goldberg, "Genetic algorithms in search, optimisation and machine learning," Addison Wesley Longman, Publishing Co. Inc., NY, 1989.

[10] S. Macfarlane and E. A. Croft, "Jerk-Bounded Manipulator Trajectory Planning: Design for Real-Time Applications," EE Transactions on Robotics and Automation, 2003, Vol. 19, No. 1, Page 42-52.

[11] H.Z.Li, Z.Gong, W.Lin and T.Lippa, "A new motion control approach for jerk and transient vibration suppression", IEEE International Conference on Industrial Informatics, 2006, Page 676-681.

[12] Gulnihal Cevik, Besir Celebi, Berkem Mehmet, Islam S.M. Khalis and Asif Sabanovic, "Motion Control and Vibration Suppression of Flexible Lumped Systems via Sensorless LQR", IEEE 15th Conference on Emerging Technologies & Factory Automation, 2010, Page 1-7.

[13] S.W. Rhee and L. R. Koval, "Comparison of classical with robust control for SMA smart structures," Smart Material and Structures, 1993, vol. 2, Page 162–171.

[14] S. Choi and C.C.Cheong, "Vibration control of flexible beams using smart memory alloy actuators," Journal of Guidance, Control and Dynamics, 1996, vol. 19, Page 1178–1180.

[15] S. Choi and C.C.Cheong, "Vibration control of flexible beams using smart memory alloy actuators," Journal of Guidance, Control and Dynamics, 1996, vol. 19, Page 1178–1180.

Delamination Analysis of Drilled Natural Fiber Reinforced Composite Materials

B.V.BHARGAVI[1*], IFTEKHAR HUSSAIN[2],G.DILLI BABU[3] , MIR SAFIULLA[4], M.VENKATESWARA RAO[5]

[1*] Department of Mechanical Engineering, Bapatla Engg. College, Bapatla, Guntur, India.
[2] *Department of Mechanical Engineering,* Bapatla Engg. College, Bapatla, Guntur, India.
[3] *Department of Mechanical Engineering,*V.R.Siddhartha Engineering college,Vijayawada,India.
[4] Ghousia College of Engineering, Ramanagaram, India.
[5]Bapatla Engg. College, Bapatla, Guntur, India.

Abstract-The present work deals with the machining of natural fiber composite to study the delamination effect. The natural fiber composite consists of royal palm fiber and material has matrix. And these composites have been fabricated by using hand layup method after extracting the fiber by retting method. Drilling operations has been carried out on the fabricated composite by using CNC drilling machine to study the effect of delamination.
In the first phase of the work, design of experiments software has been used for finding out the optimum number of samples for carrying out the experiment. In addition, in the second phase of the experiment the composites have been fabricated according to the norms of design of experiments. In the third phase of the work
AUTO-CAD software has been used for dimensioning the holes drilled on the fabricated composites, once again design of experiments software is used for computing the delamination effect on fabricated component by varying speed, feed and volume fraction.
This overall work emphasizes that the feed is the main parameter and the speed is almost negotiable parameter in drilling process on rice straw and royal form fiber composites for delamination. In addition, this project work lays a platform for further machining process on fiber composites.
Keywords: *Royal palm fiber, Natural fiber reinforced composites, Delamination.*

Introduction:

The word "composite" means two or more distinct parts physically bounded together. Thus a material

having two more distinct constituent material or phases may be considered as a composite material.

Fiber – reinforced composite materials consists of fiber of high strength and modulus embedded in or bonded to a matrix with distinct interfaces (boundary) between them. In this form, both fiber and matrix with retain their physical and chemical identities, yet they produce a combination of properties that cannot be achieved with either of constituent acting alone. in general, fiber are the principal load-carrying members, while the surroundings matrix keeps them in the desired location and orientation, acts as a load transfer medium between them ,and protects them from environmental damages due to elevated temperatures and humidity etc.

The properties that can be improved by forming a composite material include strength, stiffness, corrosion résistance, attractiveness, weight, fatigue life, temperature-dependent behavior, and thermal insulation, thermal conductivity, acoustical insulation and electrical insulation. Naturally, neither all of the properties are improved at the same time nor is there usually any requirement to do so.

Composite materials have a long history of usage. Their beginnings are unknown, but all recorded history contains references to some form of composite material. For example, straw was used by the Israelites to strengthen mud bricks. More recently, fiber reinforced resign composites that have high strength-to-weight and stiffness-to-weight ratios have become important in weight –sensitive applications such as aircraft and space vehicles.

Royal Palm*:* **Palm trees** are a family of plants. This family is called **Arecaceae**. Most of them are trees but some are shrubs. They grow in hot climates, but some have been planted as far north as Britain. Palms are one of the most well-known and widely planted tree families. They have had an important role to humans throughout much of history. Many common products and foods come from palms, and they are also used a lot in parks and gardens in areas that do not have heavy frosts. This Royal palm fiber is extracted from Royal palm tree which is mostly seen in gardens.

2. Experimental

2.1. Extraction of Fibers

ROYAL PALM: The outside portion of the royal palm tree is collected .it is dried in the sunlight for 4-5 days .Later the force is applied on outside portion by a hammer .Then the fiber is extracted .Later it is cut for required length.

2.2PROCEDURE OF EXPERIMENT:

2.2.1 Preparation of samples:

In the preparation of the samples, the mould is used which is prepared with the rubber shoe sole. The mould i.e., the rubber soul is attached to a flat surface with an adhesive material, and then supported with heavy loads. After one day the mould is ready to use. The fibers are cut in required length i.e. equal to the length of mould. In the laboratory the resin solution is prepared with the help of flask, accelerator, and catalyst. Resin of 100ml is taken into a flask, and 1.5ml catalyst and accelerator are added to it, then mixed thoroughly in the flask with the help of a stirrer and then poured into the mould in which the fibers are already placed. Heavy loads are placed upon the mould for proper molding. After a minimum period of 24 hours the samples are removed from the mould carefully.

2.2.2 Machining Process:

The samples are placed on a CNC machine for the machining (drilling) process. Here the varying parameters are speed and feed. The minimum and maximum value of speed and feed is taken from the available literature.

The specifications of the CNC machine are:

Length = 550mm.
Width = 540mm.
Overall height = 880mm.

Maximum Capacity:
Maximum cross travel =90mm.
Maximum longitudinal travel =170mm.
Maximum head travel=190mm.
Spindle tapes =R8
Z axis ball screw =16mmdia*5mmpitch
Y axis ball screw =16mmdia *5mm pitch
Machine resolution =0.01mm
Drill bit diameter =5mm.

The drilling operation is done on the sixteen samples with varying speed and feeds.

2.2.3 Calculations:

In the drilling process, the laminated fibers are delaminated up to a certain extent around the drilled holes. Before the drilling process the laminates are darkened with color. The drilled samples are snapped at the spindle entrance and the exit point for the identification of delaminated area, which are used for the further calculations. With the help of the AUTO CAD, the dimension of the delaminated area is calculated as per the definition (D_{MAX}/D_{MIN}).

After obtaining the values, the delamination factor is calculated. Then the volume fractions of the fibers are calculated:

The sum of volume fraction of fiber and resin is equal to one.

i. e. $V_f+Vr=1$

For weight fraction (0.5g):

Total weight of the composit =10.26g
Mass of fiber =0.5g
Mass of resin =9.76(10.26-0.5)
Volume fraction of resin= $(M_r / M_c) * (P_c / P_r)$

= (9.76/10.26)*(0.0012624/0.00134393)

= 0.8901(89.01%)

Where, M_r = Mass of Resin & M_c = Mass of Composite

Volume fraction of the fibers
=1-volume fraction of resin
= 1-0.8901
=0.1099(10.99%)

For weight fraction (0.7g):

Total weight of the composite =10.62g
Mass of the fiber =0.7g
Mass of the resin =9.96g (10.26g-0.7g)
Volume fraction of the resin = (Mr/Mc)*(Pc/Pr)

= (9.96/10.62)*(0.0012624/0.001393)
= 0.8774(87.74%)
Volume fraction of the fiber
=1-volume fraction of the resign
= 1-0.8774
= 0.1283(12.83%)

3. Results and Discussion

Delamination analysis :(Design of experiments software)

The values obtained from the above steps like delaminated values, volume fraction are given as inputs to the Design of Experiments software. In this, maximum and minimum values are given and the software calculates the model equation and determines the values at different points. The Delamination of the two reinforced composites are given to the Design of Experiment software with various parameters like speed, feed. And the graphs are obtained which are shown below. Delamination values at various parameters are shown in the table 1.

4. Conclusions

From the graph half normal plot Vs effect it is observed that the feed is more influenced than the other parameters. In the combined form of parameters the speed and feed combination is comparatively more influenced. The delamination values are ranging from 1.23457 to 2.54671 for maximum and minimum values of speed, feed and volume fraction. The residual Vs different parameters graphs indicate the limits of the experiments.

5. References

[1] S.C. Lin, I.K. Chen, Drilling of carbon fiber-reinforced composite material at high speed, Wear 194 (1/2) (1996) 156–162.

[2] W. Chen, Some experimental investigations in the drilling of carbon fibre-reinforced plastic (CFRP) composite laminates, Int. J. Mach. Tools Manuf. 37 (8) (1997) 1097–1108.

[3] R. Piquet, B. Ferret, F. Lachaud, P. Swider, Experimental analysis of drilling damage in thin carbon/epoxy laminate using special drills, Comp. Part A: Appl. Sci. Manuf. 31 (10) (2000) 1107–1115.

[4] E.U. Enemuoh, A. Sherif El-Gizawy, A. Chukwujekwu Okafor, An approach for development of damage-free drilling of carbon fiber reinforced thermosets, Int. J. Mach. Tools Manuf. 41 (12) (2001) 1795–1814.

[5] H. Zhang, W. Chen, D. Chen, L. Zhang, Assessment of the exit defects in carbon fibre-reinforced plastic plates caused by drilling, Prec. Mach. Adv. Mater. 196 (2001) 43–52.

			FACTOR 1	FACTOR 2	FACTOR 3	RESPONSE 1
STD	RUN	BLOCK	A:SPEED	B:FEED	C: VOL FRAC.	DELAMINATION
			RPM	MM/REV	PERCENTAGE	
10	1	BLOCK 1	600	0.05	12.83	1.515152
11	2	BLOCK 1	1800	0.05	12.83	2.5
8	3	BLOCK 1	1800	0.35	10.99	1.351351
9	4	BLOCK 1	600	0.05	12.83	1.587302
4	5	BLOCK 1	1800	0.05	10.99	2.272727
13	6	BLOCK 1	600	0.35	12.83	2.564103
1	7	BLOCK 1	600	0.05	10.99	1.724138
5	8	BLOCK 1	600	0.35	10.99	1.492537
12	9	BLOCK 1	1800	0.05	12.83	2.222222
7	10	BLOCK 1	1800	0.35	10.99	1.492537
16	11	BLOCK 1	1800	0.35	12.83	1.333333
3	12	BLOCK 1	1800	0.05	10.99	2.083333
2	13	BLOCK 1	600	0.05	10.99	1.960784

TABLE NO.1

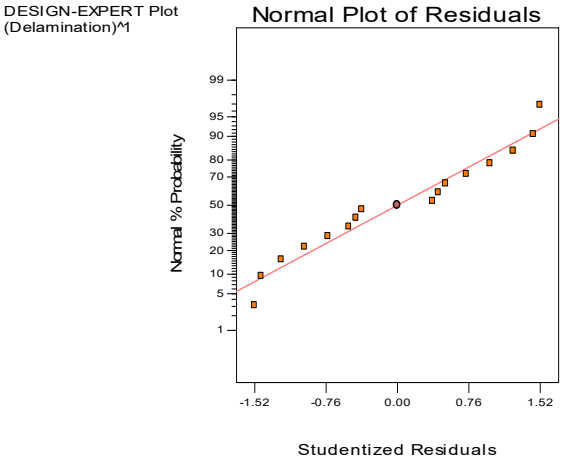
DESIGN-EXPERT Plot
(Delamination)^1
Normal Plot of Residuals
Normal % Probability
99
95
90
80
70
50
30
20
10
5
1
-1.52
-0.76
0.00
0.76
1.52
Studentized Residuals

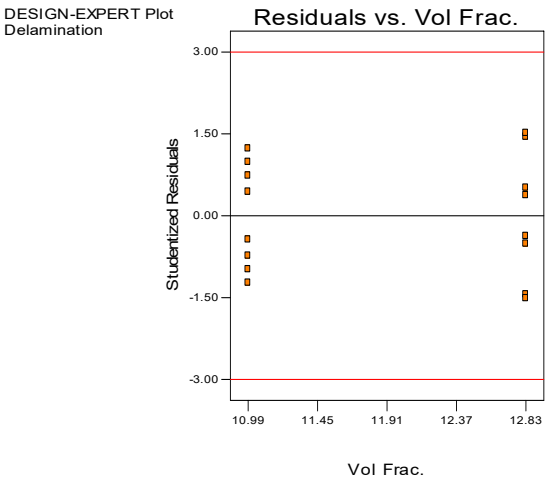
DESIGN-EXPERT Plot
Delamination
Residuals vs. Vol Frac.
Studentized Residuals
3.00
1.50
0.00
-1.50
-3.00
10.99
11.45
11.91
12.37
12.83
Vol Frac.

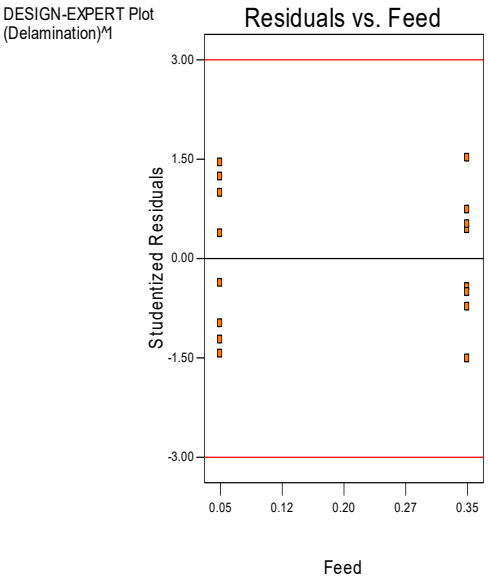
DESIGN-EXPERT Plot
(Delamination)^1
Residuals vs. Feed
Studentized Residuals
3.00
1.50
0.00
-1.50
-3.00
0.05
0.12
0.20
0.27
0.35
Feed

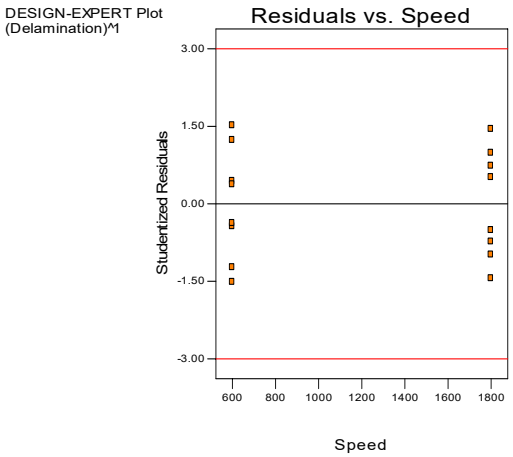
DESIGN-EXPERT Plot
(Delamination)^1
Residuals vs. Speed
Studentized Residuals
3.00
1.50
0.00
-1.50
-3.00
600
800
1000
1200
1400
1600
1800
Speed

◈◈◈

Evaluation of Mechanical properties of coir fiber reinforced polyester matrix composites

[1]P.N.E.NAVEEN & [2]T.DHARMA RAJU

[1, 2]Dept. Mechanical engineering
Godavari institute of engg. & tech.
Rajahmundry, india

Abstract— this paper "Evaluation Of Mechanical properties of coir fiber reinforced polymer matrix Composites" Natural fibres can be easily obtained in many tropical and available throughout the world. Today these fibres are considered as environment friendly materials owing to their biodegradability and renewable characteristics. The goal of this paper is to determine the mechanical (Static & Dynamic) properties of a proposed combined polymer composite which consist of a polyester matrix and coconut fibres (also known as coir fibres). The influence of fibres volume on the mechanical properties was also evaluated. Composites with volumetric amounts of coconut fibre up to 10% were fabricated and they were arranged in randomly oriented discontinues form. Tensile test was carried out to determine the strength of material by using Universal Testing Machine. The acquired results show that the tensile modulus changes with the fibre content. The strength of coconut fibre reinforced composites tends to decrease with the amount of fibre which indicates ineffective stress- transfer between the fibre and matrix.

It was observed that the effects of reinforcing polyester matrix with the coconut fibres causes the composites to be more flexible and easily deform due to high strain values. In fact, it may also be used to reduce high resonant effect.

Keywords- *Coconut Fiber, Polyester resign,Tensile test, Modal testing, Damping Ratio, Resonant.*

I. INTRODUCTION

Natural fibres can be easily obtained in many tropical and available throughout the world. Today these fibres are considered as environment friendly materials owing to their biodegradability and renewable characteristics. Natural fibres such as sisal, jute, coir, oil palm fibre have all been proved to be good reinforcement in thermoset and thermoplastic matrices (Varma *et al.* 1989; Joseph *et al.* 1996; Sreekala *et al.* 1997; Geethamma *et al.* 1998). Nowadays, the use of natural fibres reinforced composites is gaining popularity in automotive, cosmetic, and plastic lumber applications because it offers an economical and environmental advantage over traditional inorganic reinforcements and fillers (Murali & Mohana 2007).

In searching for such new material, a study has been made where coconut fibre (also known as coir fibre) is compounded with composite material. Coir is the natural fibre of the coconut husk where it is a thick and coarse but durable fibre. It is relatively water-proof and has resistant to damage by salt water and microbial degradation (Ray 2005).

COMPOSITE MATERIALS

Fiberglass, developed in the late 1940s, was the first modern composite and is still the most common. It makes up about 65 per cent of all the composites produced today and is used for boat hulls, surfboards, sporting goods, swimming pool linings, building panels and car bodies. We also may be using something made of fiberglass without knowing it.

Composite material is a material composed of two or more distinct phases (matrix phase and dispersed phase) and having bulk properties significantly different from those of any of the constituents.

- **Matrix phase**
- **Dispersed (reinforcing) phase**

TESTING METHODS

All the mechanical testing methods that were carried out were base on American Standard Testing Methods (ASTM). There were three test performed, namely Tensile Test (ASTM D638), Flexural Test (ASTM D256) and Impact Test (ASTM D790). For morphology studies, Scanning Electron Microscope (SEM) was used.

Tensile Testing: In a broad sense, tensile test is a measurement of the ability of a material to withstand forces that tend to pull it apart and to what extent the material stretches before breaking. The stiffness of a material which represented by tensile modulus can be determined from stress-strain diagram.

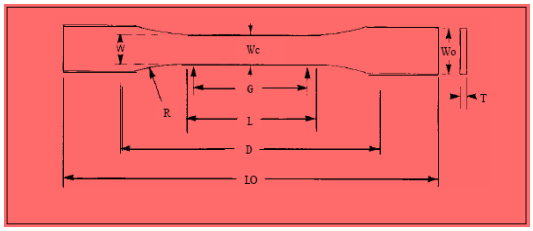

Dumbell Shaped Specimen Dimension in ASTM D638

Dimensions	Value, mm(in)
Thickness <7mm (0.28in), T	1.00 ± 0.4 (0.13 ± 0.02)
Width of narrow selection, W	13 (0.5)
Length of narrow selection, L	57 (2.25)
Width overall, WO	19 (0.75)
Length overall, LO	165 (6.5)
Gauge length, G	50 (2.00)
Distance between grips, D	115 (4.5)
Radius of fillet, R	76 (3.00)

II. LITERATURE SURVEY

Natural fibres are environment friendly materials and have proved to be a competitor for glass fibre/polyester in terms of strength performance and cost (Baiardo *et al.* 2004; Brahim & Cheikh 2006; Idicula *et al.* 2006).

Earlier studies by Brahmakumar *et al.* (2005) proved that the coir fibres can be used as effective reinforcement and bonded in polyester matrix. These fibres were hybridized with the matrix to get a better mechanical performance.

In the studies on mechanical performance and properties of short fibre reinforced polymer composites, Maries Idicula *et al.* (2006) have shown that both fibre length distribution and fibre orientation distribution play very important role in determining the mechanical properties. Sapuan *et al.* (2003) believed that mechanical properties of the natural fibre composites depend on several factors such as the stress-strain behaviours of fibre and matrix phases, the phase volume fractions and the distribution and orientation of the fibre or fillers relative to one another.

Shaikh *et al.* (2003) indicated that the volume fraction of the natural fibre has a crucial effect on the composite strength where the strength of the composite raises linearly with the increase of volume fraction.. Brahim (2006) had pointed out that the longitudinal modulus and the longitudinal stress increase with the rise of the volume fraction in fibres. This is obvious since the mechanical properties of the fibres are bigger than those of the polyester matrix. In the other hand, the strain decreases slightly from 2.7

to 2.3 when the fraction volume in fibres increases from 0% to 21% and then rises again to reach 3.1 for Vf = 44%. However, the effect on dynamic characteristics of the composite was still not known. Therefore this problem has been considered in the study since the dynamic behaviour of composite structures is very important.

In the first part of this work, the physical and mechanical properties of coconut fibres used to reinforce the studied composite material were present. An experimental investigation was carried out to study the effect of coir fibres volume (%) on the strength of composite and the results were discussed in this paper. In the second part, the dynamic test was then performed to describe the effect of fibres content and the relationship of mechanical properties on the dynamic characteristics of the developed material.

III. CLASSIFICATION OF COMPOSITES

Composite materials can be classified on the basis of the matrix material used for their fabrication:

1. Polymer matrix composites (PMC)
2. Metal matrix composites (MMC)
3. Ceramic matrix composites (CMC)

Composite Materials for Engineered Products

The reinforcing fiber provides strength and stiffness to the composite. The matrix material binds the fibers together, provides form and rigidity, transfers the load to the fibers, and protects the load-bearing fiber from corrosion and wear. For composites in structural applications, continuous or long-fiber configurations are typical, whereas for nonstructural applications, short fibers can be used.

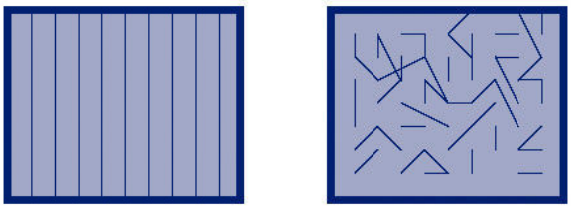

Continuous-Fiber versus Short-Fiber Composites

Reinforced polymers with continuous fiber (% by weight)						
	Density g/cc(ρ)	Tensile strength MPa (σ)	Tensile modulus GPa (E)	Specific strength (σ/ρ)	Specific modulus (E/ρ)	Max. service temp (°C)
Glass/epoxy (35%)	1.81	0.87	39.5	0.48	21.8	80-215
Reinforced polymer with short fiber (% by weight)						
Glass/epoxy (35%)	1.90	0.30	25	0.16	8.26	80-200

IV. FIBER REINFORCED COMPOSITES

Examples of natural fibers are jute, flax, hemp, remi, sisal, coconut fiber (coir), and banana fiber (abaca). All these fibers are grown as agricultural plants in various parts of the world and are commonly used for making ropes, carpet backing, bags, and so on. The components of natural fibers are cellulose micro fibrils dispersed in an amorphous matrix of lignin and hemicelluloses. Depending on the type of the natural fiber, the cellulose content is in the range of 60–80 wt% and the lignin content is in the range of 5–20 wt%. In addition, the moisture content in natural fibers can be up to 20 wt%. The properties of coir fibers in use are given below.

Property	Coir
Density (g=cm3)	1.2
Modulus (GPa)	4-6
Tensile strength (MPa)	175
Elongation to failure (%)	30
Water absorption (%)	130-180

Properties of Coir Fibers

Natural Fibers in the Automotive Industries:

Ironically, early automobile-makers employed significant quantities of wood and natural materials in the manufacturing process. Wood, horsehair, animal glues, natural adhesives are but a few examples. It is interesting, nearly a century later, than the automobile industry is integrating natural materials into design and production.

Natural fibers (hemp, flax, jute, etc.) are lightweight, remarkably strong and relatively inexpensive. Now these materials (particularly in Europe) are being used for many automotive applications:

- Doorpanels
- Dashboards
- Seat backs
- Trunk liners
- Head liners
- Package trays

Composite materials may be either **isotropic** or **anisotropic**, which is determined by the Structure of composites.

Isotropic material is a material, properties of which do not depend on a direction of measuring.

Anisotropic material is a material, properties of which along a particular axis or parallel to a particular plane are different from the properties measured along other directions.

Density

$$d_c = d_m * V_m + d_f * V_f$$

Coefficient of Thermal Expansion

$$\alpha_{cl} = (\alpha_m * E_m * V_m + \alpha_f * E_f * V_f) / (_m * V_m + E_f * V_f)$$

Modulas of elasticity

$$Ecl = \eta 0 \eta LVf\, Ef + VmEm$$

Shear modulus

$$G_{ct} = G_f G_m / (V_f G_m + V_m G_f)$$

Poisson's ratio

$$\mu_{12} = v_f \mu_f + V_m \mu_m$$

Tensile strength

$$\sigma_c = \sigma_m * V_m + \sigma_f * V_f * (1 - L_c/2L)$$

V. MANUFACTURING PROCESS

Open Molding: Hand Lay-Up Technique

Open Molding, also known as contact molding, open laminating, and wet lay-up, is the method used longest in the polymer-matrix composites industry to make thermo set composite products, and it is still the selected production process for a wide range of composite products. It is a basic process that provides many of the advantages of composites processing, using relatively basic materials technology and processing methods. The molding method involves placing reinforcements and liquid resin onto the surface of an open mold (which may or may not be pre-coated with gel coat), or onto other substrates, as, for example, when making a one-off sandwich construction, when making on-site repairs by applying a reinforcing vacuum-formed acrylic, corrosion-resistant lining on steel, or when making on-site repairs of tanks and pipes. The hand lay-up version involves applying the reinforcements and the resin by hand, while the spray-up version uses tailored spray equipment to deposit both reinforcements and resin on the mold or an alternative substrate.

MODELLING AND MANUFACTURING OF DIE

The composite die is modeled by using Catia-V5 software according to the drawing requirements as shown in fig

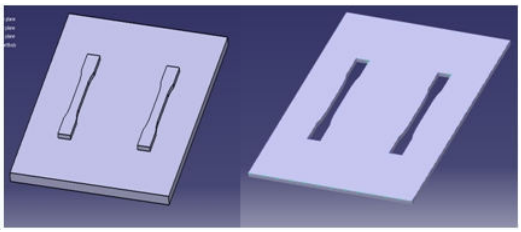

Fig: ASTM D638 Type 1 mould.

VI. EXPERIMENTAL PROCEDURE

Basically two main tasks were carried out to achieve the objectives of study. The first task was the preparation of composite material by combining the polyester and coconut coir. Then it was continued by performing the tensile test to determine the mechanical characteristics of the studied composite. Figure shows the whole processes of the study.

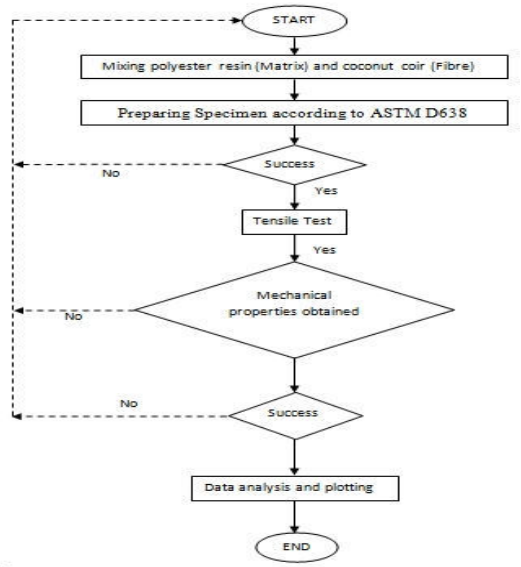

material the studied composite material is made of polyester matrix reinforced with coconut fibres which were arranged in discontinuous randomly oriented configuration.After they had been abstracted, the coir fibres will be dried at 70°C to 80°C using drying oven. In order to avoid degradation factor, the coir fibres need to go through the treatment process. This process solution for 24 hours to remove the first layer of coconut coir fibres. After that, the obtained fibres were washed abundantly with water to remove the NaOH before they dried again in furnace at 70°C to 80°C for next 24 hours. The coir fibres were then soaked into 5% of silane and 95% of methanol solution for 4 hour and dried at 70°C for next 24 hours curing time. After the drying process finished, the coconut fibres was inserted into the cutting machine to cut into smaller pieces. This form is called whiskers which its length is less than about 10 mm. The advantage of whiskers is that they can easily pour into the mixture of coconut fibres and polyester in ASTM D638 Type 1 mould (Turtle 2004). The physical properties of polyester resin are shown in Table

Mechanical properties	Polyester Resin
Density (g/cm3)	1.2-1.5
Tensile Elongation at break (%)	2
Tensile strength (MPa)	40-90
Compressive Strength (MPa)	90-250
Young's modulus (GPa)	2-4.5
Water absorption (%) 24h at 20^0C	130-180

Mechanical properties of polyester resin

Preparation of Composites

Composites having different fibres content were prepared by varying the fibres volume from 5% to 10%. In the first process of preparing the composite, a release agent was used to clean and dry the mould before the polyester can be laid up on the mould. The polyester was then mixed uniformly with the coconut fibres by using a special brush in the mixed container. The mixture was poured carefully into the moulds and flattened appropriately by using the roller before being dried for 24 hours. After the composites were fully dried, they were separated off from the moulds

VII. DYNAMIC TESTING.

Dynamic test, sometimes called modal testing is a method used to extract modal parameters such as natural frequency, damping value and mode shape from the structure experimentally. The Frequency Response Function (FRF) is a fundamental measurement produced by the testing where the displacement, velocity, or acceleration response of a structure can be measured. In the preparation of sample, the composite plate which having dimension of 210 x 210 x 5 mm was prepared. The plate was divided into 25 grid points as shown as in Figure where at these points; FRFs were measured in the range of 0-2000 Hz to identify the modal characteristics. This 25 grid points were chosen to give adequate spatial resolution to describe the global structural mode shapes.

In this case, impact hammer excitation method was chosen to determine the modal parameter of composite structure.

The sample was placed on the very soft sponge or polymeric foam to represent the free vibration test. In this type of testing, it is assumed that the sample can freely vibrate or rotate in all degree of freedom.A voltage type accelerometer was fixed at point number 1 using some bees wax in order to measure the response at single fixed point. A charge type force transducer was then mounted close to the tip of impact hammer and connected to the channel 1 of Data analyzer using cable. The hammer excitation will be roving from one point to another point to compute the FRFs. For the calculation of modal parameters, Multi-Degree of Freedom (MDOF) method was used. Some manipulation was done to obtain the resonance peaks in the plot.

VIII. RESULT AND DISCUSSION

STATIC PROPERTIES

The static properties of coir fibres reinforced composites are expected to depend on the content or volume fraction of the fibres in the composite (Murali & Mohana 2007). Even a small change in the physical nature of fibres for a given volume content of fibres may result in distinguished changes in the overall mechanical properties of composites. Therefore the influence of fibres content on mechanical properties of coir fibres reinforced composites was investigated. Table shows the static properties of coir fibres reinforced composites with fibres volume changing from 5 to 10%.

Fiber content (% vol)	Tensile Strength (MPa)	Failure Strain (%)	Young's modulus (GPa)
5	25.2	3.4	630
7.5	23.1	3.8	544.2
10	21.4	4.6	460.6

Obviously, there is a good wetting between the fibre and matrix and a strong interface is created which is lead to a strong bonding. However, high percentage of coir fibre will result in poor wetting between the coir fibre and polyester matrix. It was found lead to the less area of fibre being bonded by the matrix which can cause weak interface and thus lead to weak bonding. The composite will become more easy to deform and flexible towards the increase of fibres content. Figure shows the effect of fibres volume on the tensile strength of the composite. It indicates that the tensile strength of composites decrease with increasing fibres volume. This agrees with the conclusion of earlier work by Murali and Mohana 2007 that coir fibres do not enhance the tensile strength of composite. This result reflects the lack of interfacial adhesion between matrix and fibres which behave like voids in the continuous phase. However this behaviour make the structure become more flexible. Figure indicates that the coir fibre reinforced composites experience ductile fractures which increase with the increment of the fibres volume. The failure strain increases slightly from 3.4% to 4.6% when the volume percentage in fibres increases from 5% to 10%. It can be notified that the evolution of the composite failure strain with increasing of fibres volume is very significant since the strain at break of the coir fibres and the polyester resin are too distant.

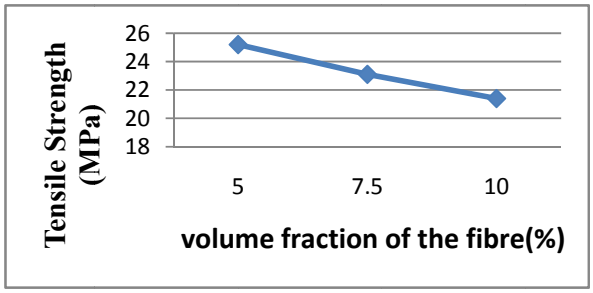

Tensile strength of composite

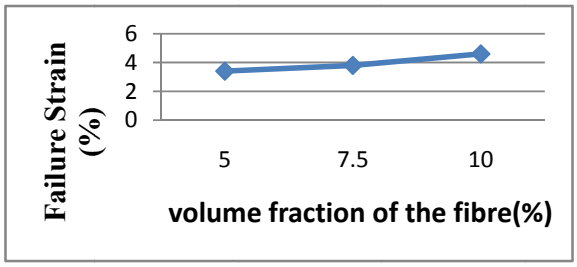

Failure strain of composite

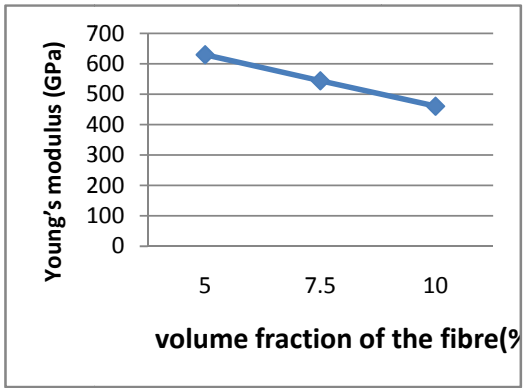

Young modulus of each percentage of coir fibre

DYNAMIC CHARACTERISTICS

The natural frequency of the each percentage of coir fibers can be determined from the plot of superimposed FRFs as shown in Figure which was obtained from point 1 until 25 during the impact hammer test. Obviously it can be easily identified by taking the frequencies corresponding to the resonance peaks (Ewins 1984). The frequency range was setting up to 2000 Hz.

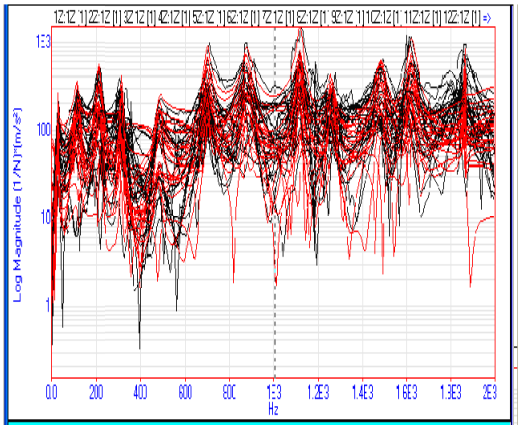

Based on the data, there are inconsistent natural frequencies for each percentage of coir fiber. This is true since the modes or resonances are inherent properties of the structure.

Resonances are determined by the material properties and the boundary conditions of the structure (Bishop 1979). Therefore if the material properties of the structure change, its modes will change.

Fiber content (vol %)	Natural frequency (HZ)									
	1	2	3	4	5	6	7	8	9	10
5 %	26.8	130	245	341	529	771	960	1170	1550	1690
7.5 %	26.1	123.5	231.5	333	510	732.5	915	1129	1415	1551
10 %	25.5	117	218	326	492	694	868	1090	1280	1420

Generally it indicates that the composite with 5% volume of coir fibers shows the maximum value of natural frequencies for the whole mode followed by 7.5% and 10% volume of coir fibers. The composite with the 7.5% volume of coir fibers shows a slightly higher frequency compared to 10% volume of coir fibers only for the first five mode frequency. Somehow for higher mode, it found that the composite with 10% coir fibers volume prove to have a higher value.

DAMPING RATIO

Based on the theoretical formulation for the damping ratio, the stiffness, mass and damping peaks can give an effect to the damping ratio value. By the incorporation of coir fibers, it appears that the damping ratio of composite is increasing only for the first five modes. However for next higher modes, the results of damping ratio are found inconsistent. In all cases, the peaks of damping ratio for each percentage of coir fibers composite was found to decrease when the modes increase. The composite with the volume of 10% of coir fiber shows the high damping ratios. These values are agreed with the theoretical formulation since any decrement of the stiffness and the mass will give an increment value of damping ratio (Avitabile 2005). By adding the coir fiber obviously gives the structure vibrating in less oscillatory motion. Therefore, it gives advantage to the structure in reducing the high resonant.

IX. CONCLUSIONS

The research was carried out to investigate the static and dynamic mechanical behavior of randomly oriented mixed coir fibers reinforced polyester composite. The effect of coir fibers volume fraction on mechanical properties and dynamic characteristic of composite were studied. The results found that the mechanical properties have a strong association with the dynamic characteristic. Both of the properties are greatly dependent on the volume percentage of fibers. In general, the composite having a coir fibers volume of 5% showed a significant result compared to high fiber loading composites due to the effect of material stiffness. Dynamic characteristics such as natural frequency of the composite can be predicted by analyzing the mechanical properties. The tensile strength of composite was found to be a linear proportional to natural frequency.

Moreover, the damping ratio was found to be increased by incorporation of coir fibers which giving an advantage to the structure in reducing the high resonant.

X. REFERENCES

1. Avitabile, P. 2005. *Modal Space in Our Own Little World.* University of Massachusetts Lowel.
2. Baiardo, M., Zini, E. & Scandola, M. 2004. Flax fibre-Polyester Composites. *Composites: Part A,* 35. 703-710.
3. Bishop, R.E.D. 1979. *Vibration: Second Edition.* Cambridge University Press,London.
4. Bledzki, A.K. & Zhang, W.Y. 2001. *Journal Reinforced Plastic Composite;* 20(14): 1263.
5. Brahim, S.B. & Cheikh, R.B. 2006. Influence of Fibre Orientation and Volume Fraction on the Tensile Properties of Unidirectional Alfa-Polyester Composite. *Composites Science and Technology,* xxx. xxx-xxx.
6. Brahmakumar, M., Pavithran, C. & Pillai, R.M. 2005. Coconut fibre reinforced polyethylene composites: effect of natural waxy surface layer of the fibre on fibre/matrix interfacial bonding and strength of composites. *Composites Science and Technology* 65: 563-569.
7. Geethamma, V.G., Mathew, K.T., Lakshmnarayanan, R. & Thomas, S. 1998. Composite of short coir fibers and natural rubber: effect of chemical modification, loading and orientation of fiber. *Polymer,* 39:1483.
8. Huang, J.H. 2001. *Composites PartA* 32:573.
9. Joseph, K., Thomas, S. & Pavithran, C. 1996. Effect of chemical treatment on the tensile properties of short sisal fiber-reinforced polyethylene composites. *Polymer,* 37:5139^15.
10. Idicula, M., Boudenne, A., Umadevi, L., Ibos, L., Candau, Y., & Thomas, S. 2006. Thermophysical Properties of Natural Fibre Reinforced Polyester Composite. *Composites Science and Technology,* 66. 2719-2725.
11. Murali, K. & Mohana, K. 2007. Extraction and tensile properties of naturalfibers: Vakka, date and bamboo. *Composite Structures* 77; 288-295.
12. Ray, D. 2005. Natural Fibres, Biopolymers and Biocomposites. *Thermoset Biocomposite in Mohanty.* Boca Ranton, Flourida: Taylor & Francis.
13. Sapuan, S.M., Harimi, M. & Maleque, M.A. 2003. Mechanical Properties of Epoxy/Coconut Shell Filler Particle Composites. *The Arabian Journal for Science and Engineering-,* 28. 1 7 1 - 1 8 1 .
14. Sreekala, M.S., Kumaran, M.G. & Thomas, S. 1997. Oil palm fibers: morphology, chemical composition, surface modification and mechanical properties. *Journal Applied Polymer Sci;* 66:8-821.

◈◈◈

AL_2O_3 Nanofluids as Heat Transfer Liquids in Automotives.

[1]M.YASASWI, [2]R.V.PRASAD & [3]T.JAYANDA KUMAR

[1,2](CAD-CAM) ,Dept. Mechanical Engineering
Godavari Institute of Engg. & Tech.
Rajahmundry, India

Abstract— the thermal conductivity of heating or cooling fluids is a very important property in the development of energy efficient heat transfer systems, which is one of the important needs of many industries. However, low thermal conductivity is a primary limitation in developing energy-efficient heat transfer fluids that are required for cooling purposes. Nanofluids are nanotechnology-based heat transfer fluids that are engineered by stably dispersing nanometer-sized (below 100nm) solid particles (such as ceramics, metals, alloys, semiconductors, nanotubes, and composite particles) in conventional heat transfer fluids (such as water, oil, diesel, ethylene glycol and mixtures) at relatively low particle volume concentrations. These suspended nanoparticles can change the transport and thermal properties of the base fluid. Adding to ethylene glycol, it has been observed that an enhancement of nearly 36 % with al2o3 nanoparticles and 40% enhancement with copper nanoparticles in the thermal conductivity. This paper focuses on some of the automotive applications such as coolant for automobiles, showcases a few of them that are believed to have the highest probability of success in this highly competitive industry and to raise the awareness on the promise of nanotechnology, its potential impact on the future of the automotive industry.

Keywords- *Nanofluids, Nanoparticles, Heat transfer, Thermal conductivity.*

I. INTRODUCTION

In the dimensional scale a nanometer is a billionth of a meter. Nanoscale science and engineering has revolutionized the scientific and technological developments in nanoparticles, nonstructured materials, nanodevices and systems. National Science Foundation defines nanotechnology as the creation and utilization of functional materials, devices, and systems with novel properties and functions that are achieved through the control of matter, atom-by-atom, and molecule by molecule or at the macro molecular level. A unique challenge exists in restructuring teaching at all levels to include nanoscale science and engineering concepts and nurturing the scientific and technical workforce of the future.

There is a great need for more efficient heat transfer fluids in many industries, from transportation to energy supply to electronics and photonics. The coolants, lubricants, oils, and other heat transfer fluids used in today's thermal management systems have inherently poor heat transfer properties. And conventional working fluids that contain millimeter- or micrometer-sized particles are not applicable to the newly emerging "miniaturized" technologies because they can clog micro channels.

Nanofluids are a new, innovative class of heat transfer fluids created by dispersing solid particles smaller than 40 nm in diameter (less than one-thousandth the diameter of a human hair) in traditional heat transfer fluids such as water, engine oil, and ethylene glycol. Solid particles are added because they conduct heat much better than liquid.

Nanofluids are nanotechnology-based heat transfer fluids that are engineered by stably dispersing nanometer-sized solid particles (such as ceramics, metals, alloys, semiconductors, nanotubes, and composite particles) in conventional heat transfer fluids (such as water, ethylene glycol, oil, and mixtures) at relatively low particle volume concentrations. Nanofluids have been considered for applications as advanced heat transfer fluids for almost two decades, since they have better suspension stability compared to micron-sized solid particles, can flow smoothly without clogging the system, and provide enhanced thermal and physical properties.

Conventional fluids, such as water, engine oil, and ethylene glycol are normally used as heat transfer fluids. Although various techniques are applied to enhance the heat transfer, the low heat transfer performance of these conventional fluids obstructs the performance enhancement and the compactness of heat exchangers. The use of solid particles as an additive suspended into the base fluid is technique for the heat transfer enhancement. Improving the thermal conductivity is the key idea to improve the heat transfer characteristics of conventional fluids. Since a solid metal has a larger thermal conductivity than a base fluid, suspending metallic solid fine particles into the base fluid is expected to improve the thermal

conductivity of that fluid. The enhancement of thermal conductivity of conventional fluids by the suspension of solid particles, such as millimeter- or micrometer- sized particles has been well-known for many years. However, they have not been of interest for practical applications due to problems such as sedimentation leading to increased pressure drop in the flow channel. The recent advance in material technology has made it possible to produce innovative heat transfer fluids by suspending nanometer-sized particles in base fluids which can change the transport and thermal properties of the base fluid. Nanofluids are solid-liquid composite materials consisting of solid nanoparticles or nanofibers with sizes typically of 1 to 100 nm suspended in liquid. The nanofluid is not a simple liquid-solid mixture the most important criterion of nanofluid is agglomerate-free stable suspension for long durations without causing any chemical changes in the base fluid. This can be achieved by minimizing the density between solids and liquids or by increasing the viscosity of the liquid by using nanometer- sized particles and by preventing particles from agglomeration, the settling of particles can be avoided. Nanofluids have attracted great interest recently because of reports of enhanced thermal properties. Extensive research has been carried out on alumina-water- and CuO-water-based systems besides few reports in Cu-water, carbon nanotubes water systems.

THE GOAL AND APPLICATIONS OF NANO FLUIDS

The most important goal in nanofluid research is to create and develop a nanofluid with stability and ultra-high thermal conductivity for industrial applications. The use of these nanofluids can have a lot of benefits which are: the improvement of heat transfer, reduction in pumping power and lower operating costs, miniaturizing of smaller and lighter heat exchangers, reduction of emissions, suitable for small flow passages like microchannels and reduction in heat transfer fluid inventory.

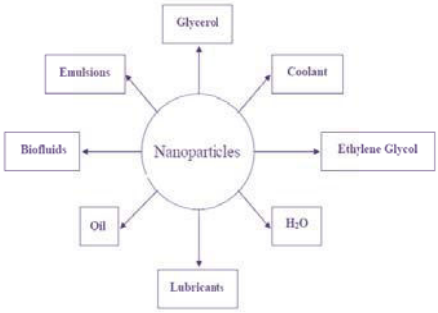

Fig: 1 A number of liquids (heat transfer fluids) that can host nanoparticles for the production of nanofluids.

The size of nanoparticles defines the surface-to-volume ratio and for the same volume concentrations suspensions of smaller particles have a higher area of the solid/liquid interface.Therefore the contribution of interfacial effects is stronger in such a suspension. Interactions between the nanoparticles and the fluid are manifested through the interfacial thermal resistance.

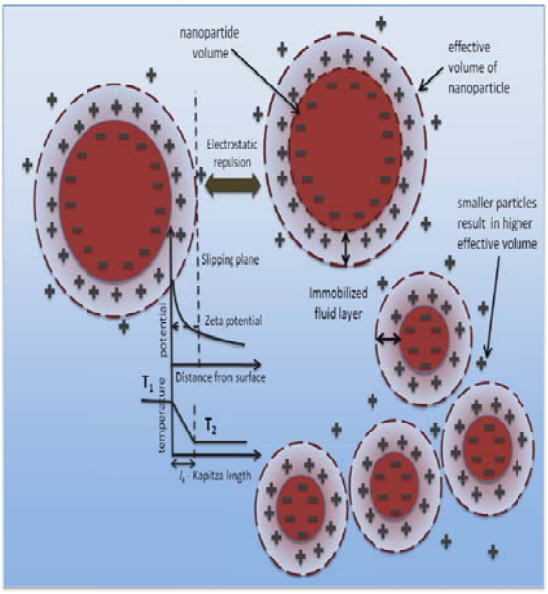

Fig: 2 Interfacial effects in nanoparticle suspensions

THE MOST PROMISING AUTOMOTIVE APPLICATIONS OF NANOTECHNOLOGY

- Improved materials with CNTs, graphene and other nanoparticles/structures
- Improved mechanical, thermal, and appearance properties for plastics
- Coatings & encapsulants for wear and corrosion resistance, permeation barriers, and appearance
- Cooling fluids with improved thermal performance
- Displays with lower cost and higher performance
- Automotive sensors with nano-sensing elements, nanostructures and nano-machines
- Self-assembly using fluid carriers
- Electrical switching including CNT transistors, quantum transistors, electronemission amplification, and more efficient solar cells

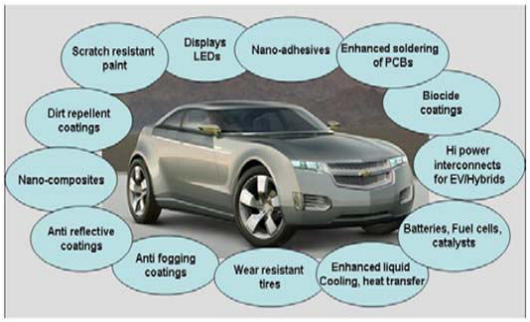

Fig: 3 automotive applications

EFFICIENT NANO FLUID BY DESIGN

In light of all the mentioned nanofluid property trends, development of a heat transfer nanofluid requires a complex approach that accounts for changes in all important thermophysical properties caused by introduction of nanomaterials to the fluid. Understanding the correlations between nanofluid composition and thermo-physical properties is the key for engineering nanofluids with desired properties.

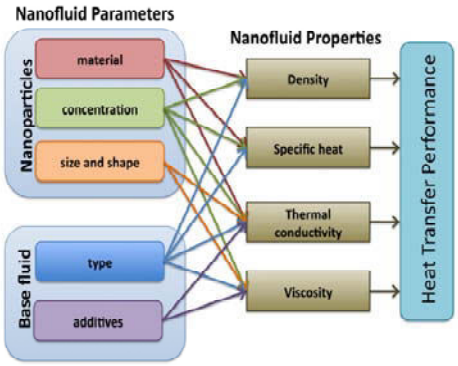

Fig: 4 Complexity and multi-variability of nanoparticle suspensions

PREPARATION OF NANO FLUIDS

Synthesis and Preparation of Nanofluids:

Preparation of nanofluids is the first key step in experimental studies with nanofluids. Nanofluids are not just dispersion of solid particles in a fluid. The essential requirements that a nanofluid must fulfill are even and stable suspension, adequate durability, negligible agglomeration of particles, no chemical change of the particles or fluid, etc. Nanofluids are produced by dispersing nanometerscale solid particles into base liquids such as water, ethylene glycol, oil, etc. In the synthesis of nanofluids, agglomeration is a major problem. There are mainly two techniques used to produce nanofluids the single-step and the two-step method.

THE SINGLE-STEP PROCESS

Various investigators have produced Al2O3 and CuO nanopowder by direct evaporation condensation method that produced 2–200 nm-sized particles.Even though this method has limitations of low vapor-pressure fluids and oxidation of pure metals; it provides excellent control over particle size and produces particles for stable nanofluids without surfactant or electrostatic stabilizers. The single-step direct evaporation approach was developed by Akoh et al.and is called the Vacuum Evaporation onto a Running Oil Substrate technique. The original idea of this method was to produce nanoparticles, but it was difficult to subsequently separate the particles from the fluids to produce dry nanoparticles. Eastman et al. developed amodified vacuum evaporation onto oil technique, in which Cu vapor is directly condensed into nanoparticles by contact with a flowing low-vapor-pressure liquid ethylene glycol. Zhu et al. presented a novel one-step chemical method for preparing copper nanofluids by reducing CuSO4・5H2O with NaH2PO2・H2O in ethylene glycol under microwave irradiation. Results showed that addition of NaH2PO2・H2O and the adoption of microwave irradiation are two significant factors which affect the reaction rate and properties of Cu nanofluids. Lo et al. developed a vacuum-based submerged arc nanoparticle synthesis system to prepare CuO, Cu2O, and Cu based nanofluids with different dielectric liquids. The morphologies of nanoparticles depended on the thermal conductivity of the dielectric liquids. An advantage of the onestep technique is that nanoparticle agglomeration is minimized, while the disadvantage is that only low vapor pressure fluids are compatible with such a process.

THE TWO STEP PROCESS

The two-step method is extensively used in the synthesis of nanofluids considering the available commercial nano-powders supplied by several companies. In this method, nanoparticles were first produced and then dispersed in the base fluids. Generally, ultrasonic equipment is used to intensively disperse the particles and reduce the agglomeration of particles. For example, Eastman et al.Lee et al, and Wang et al. used this method to produce Al2O3 nanofluids. Also, Murshed et al. prepared TiO2 suspension in water using the two-step method. Other nanoparticles reported in the literature are gold (Au), silver (Ag), silica and carbon nanotubes. As compared to the single-step method, the two-step technique works well for oxide nanoparticles, while it is less successful with metallic particles. Except for the use of ultrasonic equipment, some other techniques such as control of pH or addition of surface active agents are also used to attain stability of the suspension of the nanofluids against sedimentation. These methods change the surface

properties of the suspended particles and thus suppress the tendency to form particle clusters. It should be noted that the selection of surfactants should depend mainly on the properties of the solutions and particles. For instance, salt and oleic acid as dispersant are known to enhance the stability of transformer oil– Cu and water–Cu nanofluids, respectively. Oleic acid and cetyltrimethylammoniumbromide (CTAB) surfactants were used by Murshed et al.to ensure better stability and proper dispersion of TiO2–water nanofluids. Sodium dodecyl sulfate (SDS) was used by Hwang et al.during the preparation of water-based multi wall carbon nanotube dispersed nanofluids since the fibers are entangled in the aqueous suspension. In general, methods such as change of pH value, addition of dispersant and ultrasonic vibration aim at changing the surface properties of suspended particles and suppressing formation of particlescluster to obtain stable suspensions

.

EXPERIMENTAL INVESTIGATIONS

Measurement of Thermal Conductivity

Since thermal conductivity is the most important parameter responsible for enhanced heat transfer, many experimental works have been reported on this aspect.Alumina (Al2O3) and copper oxide are the most common and inexpensive nanoparticles used by many researchers in their experimental investigations. All the experimental results have demonstrated the enhancement of the thermal conductivity by addition of nanoparticles. Eastman et al.measured the thermal conductivity of nanofluids containing Al2O3, CuO, and Cu nanoparticles with two different base fluids: water and HE-200 oil. A 60% improvement of the thermal conductivity was achieved as compared to the corresponding base fluids for only 5 vol% of nanoparticles. They also showed that the use of Cu nanoparticles (using the one-step method) results in greater improvements than that of CuO (using the two-step method). Lee et al. suspended CuO and Al2O3 (18.6 and 23.6 nm, 24.4 and 38.4 nm, respectively) in two different base fluids: water and ethylene glycol (EG) and obtained four combinations of nanofluids: CuO in water, CuO in EG, Al2O3 in water and Al2O3 in EG. Their experimental results showed that nanofluids have substantially higher thermal conductivities than the same liquids without nanoparticles. The CuO/EG mixture showed enhancement of more than 20% at 4 vol% of nanoparticles. In the low volume fraction range (<0.05% in test), the thermal conductivity ratios increase almost linearly with volume fraction. Results suggest that not only particle shape but size is considered to be dominant in enhancing the thermal conductivity of nanofluids. The base fluids (water, ethylene glycol (EG), vacuum pump oil and engine oil) contained suspended Al2O3 and CuO nanoparticles of 28 and 23 nm average diameters, respectively. Experimental results demonstrated that the thermal conductivities of all nanofluids were higher than those of their base fluids. Also, comparison with various data indicated that the thermal conductivity of nanofluids increases with decreasing particles size. Results demonstrated 12% improvement of the effective thermal conductivity at 3 vol% of nanoparticles as compared to 20% improvement reported by Masuda et al. and 8% reported by Lee et al. at the same volume fraction of particles. Xuan and Li enhanced the thermal conductivity of water using Cu particles of comparatively large size (100 nm) to the same extent as has been found using CuO particles of much smaller dimension (36 nm). An appropriate selection of dispersants may improve the stability of the suspension. They used oleic acid for transformer oil-Cu nanofluids and laurate salt for water-Cu suspension in their study and found that Cu particles in transformer oil had superior characteristics to the suspension of Cu particles in water. Xie et al. investigated the effects of the pH value of the suspension, the specific surface area (SSA) of the dispersed Al2O3 particles, the crystalline phase of the solid phase, and the thermal conductivity of the base fluid on the thermal conductivity of nanofluids. They found that the increase in the difference between the pH value and isoelectric point (the pH at which a molecule carries no net electrical charge) of Al2O3 resulted in enhancement of the effective thermal conductivity.Also, the thermal conductivity enhancements were highly dependent on the specific surface area (SSA) of the nanoparticles. The crystalline phase of the nanoparticles did not appear to have any obvious effect on the thermal conductivity of the suspensions. Eastman et al. used pure Cu nanoparticles of less than 10 nm size and achieved a 40% increase in thermal conductivity for only 0.3% volume fraction of the solid dispersed in ethylene glycol.

Das et al. (2003c) examined the effect of temperature on thermal conductivity enhancement for nanofluids containing Al2O3 (38.4 nm) or CuO (28.6 nm) through an experimental investigation using the temperature oscillation method. They observed that a 2 to 4-fold increase in thermal conductivity can take place over the temperature range of 21oC to 52oC. The results suggest the application of nanofluids as cooling fluids for devices with high energy density where the cooling fluid is likely to work at a temperature higher than room temperature. They also mention that the inherently stochastic motion of nanoparticles could be a probable explanation for the thermal conductivity enhancement since smaller particles show greater enhancements of thermal conductivity with temperature than do larger particles. Li and Peterson conducted an experimental investigation to examine the effects of variations in the temperature and volume fraction on the effective thermal conductivity of CuO (29 nm) and Al2O3 (36

nm) water suspensions. Results demonstrated that nanoparticle material, diameter, volume fraction and bulk temperature have significant effects on the thermal conductivity of the nanofluids. For example, for Al2O3/water suspensions, increase in the mean temperature from 27 to 34.7oC results in an enhancement of nearly three times. They also derived two simple two-factor linear regressions for the discussed nanofluids (Al2O3/water)

$$(keff - kb)/kb = 0.764\varphi + 0.0187(T - 273.15) - 0.462,$$

CuO/water

$$(keff - kb)/kb = 3.761\varphi + 0.0179(T - 273.15) - 0.307 .$$

EXPERIMENTAL RESULTS ON THERMAL CONDUCTIVITY OF AL2O3 BASED NANOFLUIDS

1. Effect of temperature on thermal conductivity of Al2O3- based nanofluids

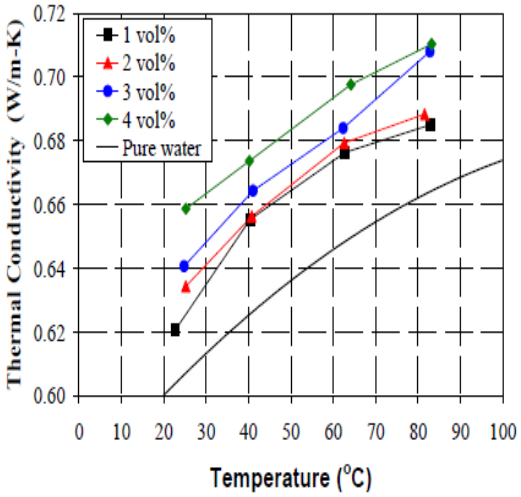

2. Thermal conductivity of Al2O3 nanofluids measured by different techniques

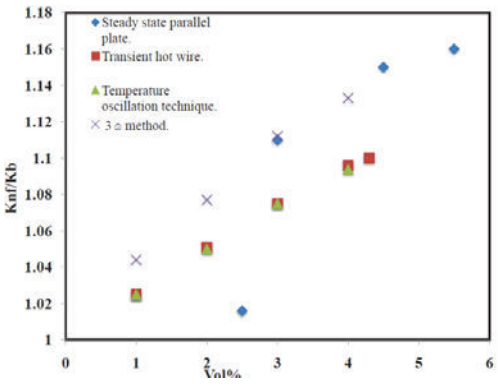

3. Effect of volume fraction of nanoparticles on thermal conductivity of Al2O3-based nanofluids

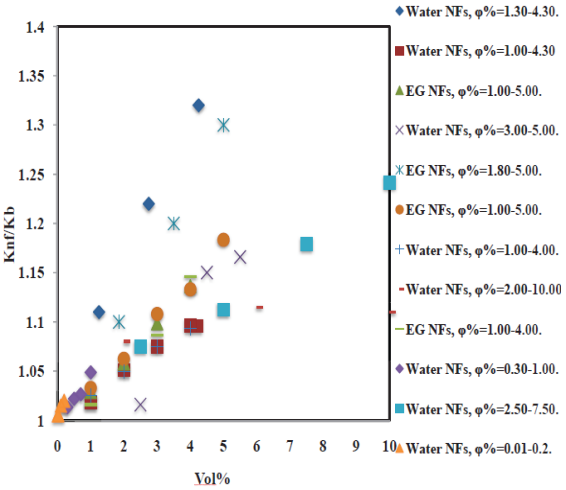

4. Effect of particle size on thermal conductivity of Al2O3 based nanofluids

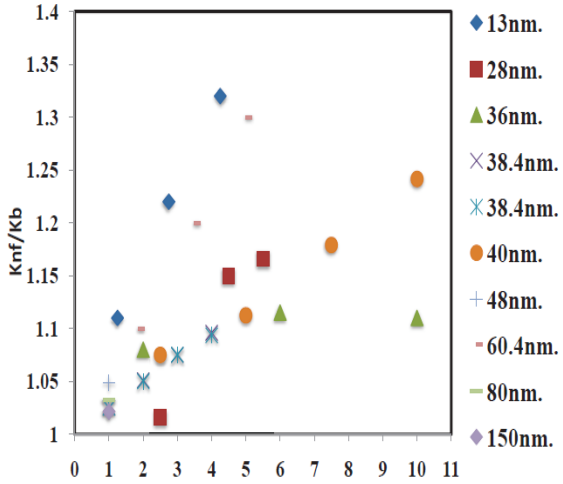

Water-based Al2O3 nanofluids

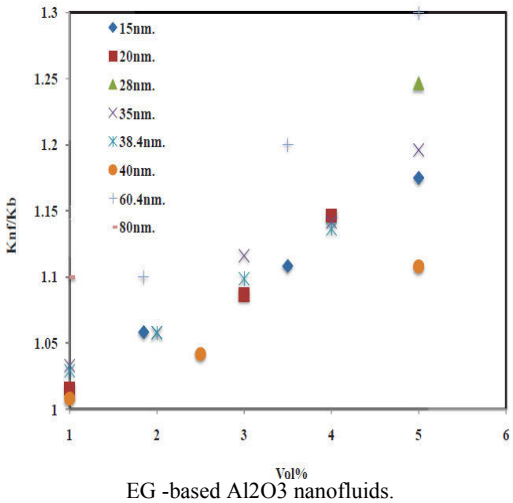

EG -based Al2O3 nanofluids.

5. Effect of base fluids on thermal conductivity of Al2O3- based nanofluids

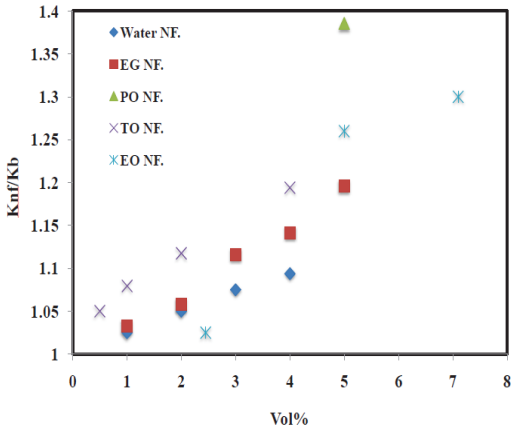

6. Effect of preparation method on thermal conductivity of Al2O3-based nanofluids

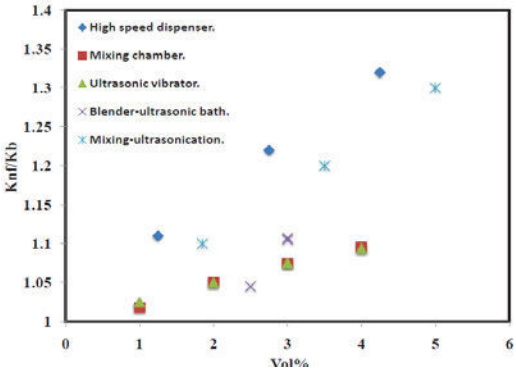

7. Effect pH on thermal conductivity of Al2O3 water-based nanofluids.

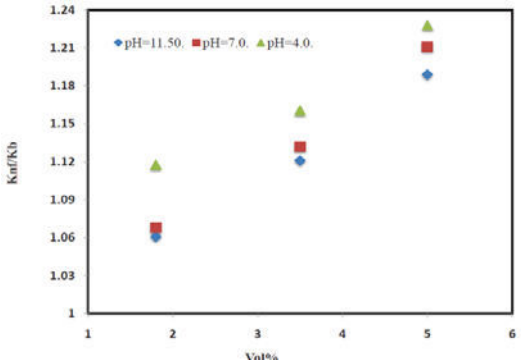

8. Effect of surface active agents on thermal conductivity of water-based Al2O3 nanofluids

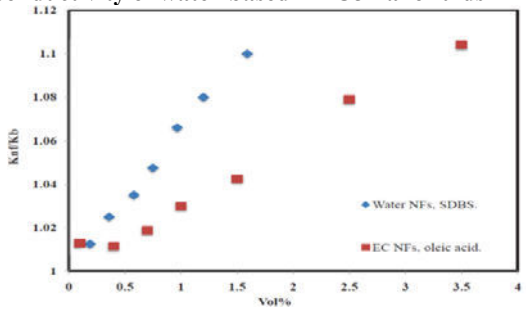

EXPERIMENTAL RESULTS ON THERMAL CONDUCTIVITY OF CU-CONTAINING -EG

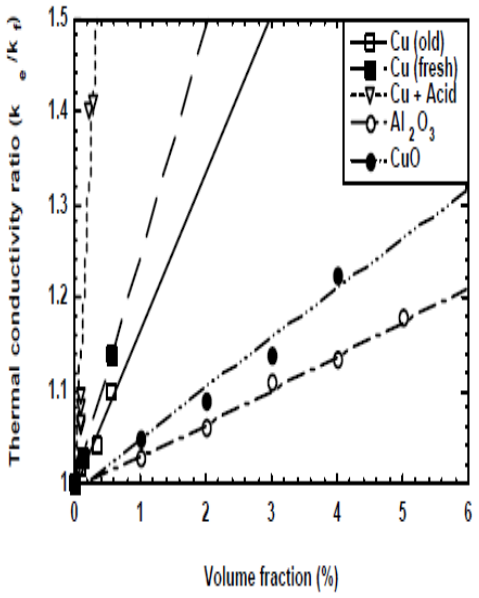

Fig 5: Thermal conductivity enhancement of copper, copper oxide, and alumina particles in ethylene glycol.

CONCLUSIONS

- Nano fluids containing copper nano particles enhance the thermal conductivity of base fluids dramatically For example; adding only 0.3 vol. % of 10-nm copper nanoparticles to ethylene glycol increased its thermal conductivity up to 40%. Further, nanotubes have yielded by far the highest thermal conductivity enhancement ever achieved in a liquid: a 150% increase in conductivity of oil at ~1 vol. % of 25-nm nanotubes.
- From the observed results, it is clearly seen that nanofluids have a greater potential for heat transfer enhancement and are suitable for application in practical heat transfer processes. The enhancement of thermal conductivity of base fluid will be a definite requirement in the future to improve the thermal efficiency of different systems.
- Researchers can concentrate on the effect of temperature and the hysteresis behavior for AL_2O_3 nanofluids and can try to increase the temperature withstanding capacity of the Al2O3 nanofluids.
- On the basis of the promising results to date, nanofluid research could lead to a major breakthrough in solid/liquid composites for numerous engineering applications, such as coolant for automobiles, air conditioning, and supercomputers.

REFERENCES

1. Lee S, Choi SUS, Li S, Eastman JA: Measuring thermal conductivity of fluids containing oxide nanoparticles. ASME J Heat Transfer 1999,121:280-89.
2. Singh AK: Thermal conductivity of nanofluids. Defence Sci J 2008,58:600-607.
3. Das SK, Putra N, Roetzel W: Pool boiling of nano-fluids on horizontal narrow tubes. Int J Multiphase Fl 2003, 29:1237-1247.
4. Paul G, Chopkar M, Manna IA, Das PK: Techniques for measuring the thermal conductivity of nanofluids: a review. Renew Sust Energ Rev 2010,14:1913-1924.
5. Wang X, Xu X, Choi SUS: Thermal conductivity of nanoparticle-fluid mixture. J Thermophys Heat Trans 1999, 13:474-480.
6. Beck MP, Sun T, Teja AS: The thermal conductivity of alumina nanoparticles dispersed in ethylene glycol. Fluid Phase Equilib 2007, 260:275-278.
7. Beck MP, Yuan Y, Warrier P, Teja AS: The thermal conductivity of alumina nanofluids in water, ethylene glycol, and ethylene glycol + water mixtures. J Nanopart Res 2010, 12:1469-1477.
8. j. a. eastman, s. u. s choi, s. li, w. yu, and l. j. thompson, "anomalously increased effective thermal conductivities of ethylene glycol-based nanofluids containing copper nanoparticles," appl. phys. lett. 78, 718 (2001).

◈◈◈

Phase Change Materials (PCM) for Thermal Control during Spacecraft Transportation

[1]ARUN KUMAR.S, [2]A.SEKAR, [3]D.N.SIDDHARTHA JAIN & [4]K.V.GOVINDA

Systems Integration Group, ISRO Satellite Centre
Old Airport Road, Vimanapura, Bangalore-17

Abstract: Phase Change materials (PCMs) absorb and release latent heat during their phase transition nearly at constant temperature. The latent heat storage phenomena using PCMs provides much higher storage density, with a smaller or zero temperature difference while storing and releasing of heat. PCMs have 5-14 times more heat capacity per unit volume than sensible storage materials that merits their usage as passive thermal control systems. They are effectively complemented with active thermal control systems in order to minimize their duty cycles and optimize the capacity. This paper discusses a passive thermal control system using PCMs to maintain the temperature within the limits inside the enclosures used for transportation of spacecrafts. Further, various applications of PCMs in the thermal control architecture as applied to spacecrafts are also discussed. The paper also discusses about the technologies such as Onboard power generation, Universal Spacecraft thermal control architecture and other significant spacecraft applications.

Key Words – *Phase Change Materials (PCM), Transportation, Thermal control system, Onboard Power Generation, Spacecraft applications.*

INTRODUCTION

Most pure substances change phase between liquid, solid or gas at some temperature and pressure. A PCM is a non- scientific expression which refers to any substance which has a single 'sharp' melting point and a sufficiently large heat of fusion that makes it of interest as a potential heat energy storage material. The latent heat per unit mass of the substance varies from substance to substance and reflects in large part, the variation in strength of the molecular bonding within the given substance at the phase change temperature. They use chemical bonds to store and release heat. The
thermal energy transfer occurs when a material changes undergoes the phase transition from a solid to a liquid or from a liquid to a solid. Initially, these solid-liquid thermal salts perform like conventional heat storage materials. When PCMs reach the temperature at which they change the phase (their melting point), they absorb large amounts of heat without getting hotter. When the ambient temperature in the space around the PCM material drops, it solidifies, releasing its stored latent heat. PCMs absorb and emit heat while maintaining a nearly constant temperature. Latent heat storage is one of the most efficient ways of storing thermal energy. Large numbers of PCMs are available that melt and solidify at a wide range of temperatures. In general, in most of the applications, PCMs are encapsulated properly for providing large heat transfer area, reduction of its reactivity with the outside environment and controlling the differences in volume of the storage materials as phase change occurs. Application of PCMs in spacecraft transportation involves calculation of heat loads such as radiative, convective and conductive heat transfer during travel, through appropriate modeling of the enclosures.

II. CLASSIFICATION & PROPERTIES OF PCM

Classification [1]:

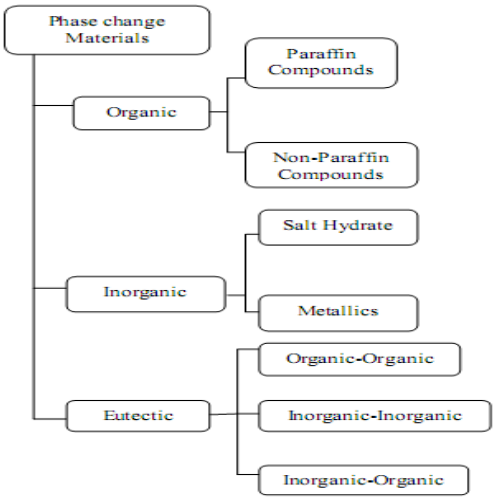

Some of the important properties required for PCM [4] are

- High latent heat of fusion per unit mass, so that a lesser amount of materials stores a given amount of energy.
- High thermal conductivity so that the temperature gradient required for charging the storage material is small.
- High density, so that a smaller container volume holds the material to obtain compact encapsulation.
- A melting point in the desired operating range of temperature as per the application.
- The phase change material should be non-poisonous, non-flammable, and non-explosive.
- No chemical decomposition, so that the system life is assured.
- No corrosiveness to the encapsulation material.

Salt hydrate PCMs are more suited for the spacecraft transportation application discussed here as against Organic and Eutectic PCMs. Organic PCMs have low thermal conductivity and are flammable and hence not a candidate for the said application. Eutectic type PCMs exhibit low phase
change temperatures generally in the sub zero range and further the metallic type PCMs have weight penalties. In addition, the technical grade Salt Hydrates are inorganic type, safe, reliable, predictable, less expensive as compared to the other types of PCMs. It provides several advantages such as high thermal conductivity, high latent heat of fusion and small volume changes on melting. Based on the above, Salt Hydrates PCMs having melting point around 17°C are selected for the application.

The table below gives the properties of commercially available salt hydrates PCMs suitable for the application.

TABLE 1:

Sl no	Phase Change Temperature (°C)	Density (kg/m^3)	Latent Heat Capacity (KJ/kg)
1	27	1530	183
2	23	1530	175
3	19	1520	160
4	17	1525	160
5	15	1510	160
6	13	1515	160
7	10	1470	155

III. HEAT LOAD ESTIMATION

There is sensible heat transfer across the container wall due to the temperature difference between the inside of the container and outside ambient. This is known as fabric heat gain or loss and the heat transfer through the container wall is analyzed taking the following considerations:

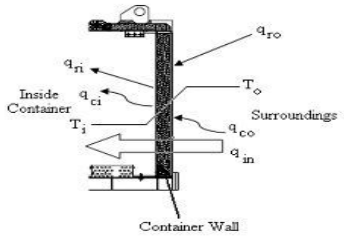

Fig 1

- Non-Homogeneous construction of container wall which includes an arrangement of Corrugation metallic sheets, Polyurethane Foam, Stainless Steel Cladding, Structural Members etc.
- Transient atmospheric conditions due to variation in solar radiation, outside temperature, wind and travel velocity, change in container orientation during shipment with respect to sun etc.
- Thermal Capacity of a container wall which introduces time lag and reduce heat transfer from ambient to inside of container.

For cooling load calculation, the conditions inside the container are assumed to be constant. However, for accurate simulation of varying outside ambient conditions, unsteady transient heat transfer analysis needs to be done. Due to the complexities involved, simplified one dimensional steady state heat transfer analysis is done for one of the Satellite

Transportation Containers (STC) to obtain an initial estimate of Phase Change Material (PCM) required. For steady heat transfer across the container wall, heat transfer network considering various heat transfer resistances is shown in Fig 2.

The variables are denoted by abbreviations as per Table 2 given in the end of the paper.

The heat transfer rate per unit area of the wall qin under steady

Writing the radiative heat transfer in terms of a linearized heat transfer coefficient and combining the convective heat transfer coefficient, we can write the heat transfer rate per unit area as:

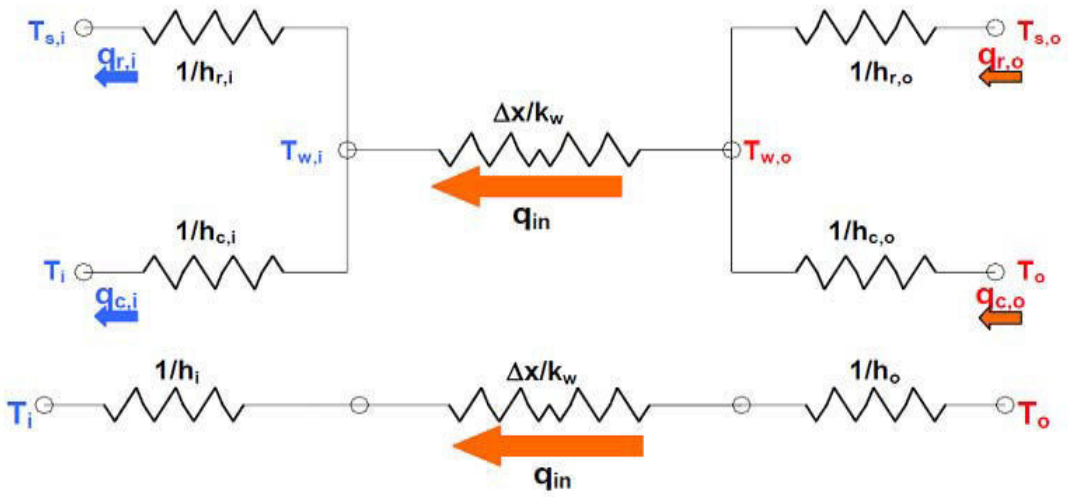

Fig 2

state is given by:

$$q_{in} = (q_{co} + q_{ro}) = (q_{ci} + q_{ri}) \quad W/m^2$$

$$q_{in} = h_o(T_o - T_{wo}) = h_i(T_{wi} - T_i) \; W/m^2$$

Eliminating the surface temperatures of the wall (Twi and Two),

the steady state heat transfer rate per unit area of the wall can

be written in terms of the indoor and outside air temperature

and the overall heat transfer coefficient:

$$q_{in} = U(T_o - T_i) \; W/m^2$$

From heat transfer network (fig 2), the expression for overall

heat transfer coefficient is given by:

$$1/U = (1/h_i + \Delta x/K_w + 1/h_o)$$

IV. CASE STUDY

Heat load was calculated for one of the existing Spacecraft Transportation Container (STC) considering the following data:

- Transportation Container Dimension: 7800 x 3000 x 3800 mm
- Container wall Insulation Thickness: 100 mm
- Thermal Conductivity of Container wall: 0.023 W/mK
- Inside Container Temperature to be maintained:
- 22±1°C
- Mean Ambient Temperature: 35 °C
- Emissivity of paint used on container: 0.8

Five walls of container were considered for heat transfer and total steady heat transfer was calculated as:

Qt = 220 Watt

Assuming steady heat transfer for continuous operation, the amount of PCM required for maintaining the temperature at 22 °C inside container can be calculated. Standard PCM with phase change temperature of 17 °C and having a Latent Heat Capacity of 160 KJ/kg is selected.

Mpcm = Heat Entering Container/Latent Heat Capacity Heat Entering Container = Qt x Cycle Time For the above case, the mass of PCM required (Mpcm) is estimated to be around 100 kg for 24 hrs duty cycle. This is an initial estimation for PCM and a more comprehensive transient heat transfer model analysis need to be done to characterize the system

for the various boundary conditions and to get more accurate results. To express the temperature gradients under various conditions, a field test to simulate the actual systems and boundaries is also planned to validate the analysis for necessary corrections and improvements on accuracies of theoretical estimation.

V. PCM IN SPACECRAFT APPLICATIONS

The application of PCM is not limited to passive thermal control for ground equipment alone. The recent research and development in PCM can be extended in novel application for spacecraft systems. In the area of heat removal and rejection, the applicable technologies for spacecraft are high thermal conductivity materials, high heat transport devices such as fixed conductance heat pipes, loop heat pipes, capillary heat pipes and low absorptivity to emissivity passive coatings [2].

The PCM is used for conserving the heat that act as a heat sink which is similar to high performance lightweight insulation, heat switches, variable emissivity coatings etc.

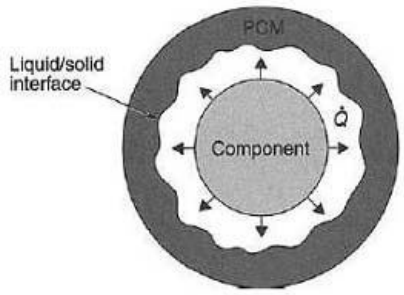

Fig 3

PCM to store energy at melt temperature. This

stored energy can then be converted into electrical power by using the large temperature difference between radiator and deep space to drive either thermionic or thermoelectric devices. Preliminary analytical and experimental studies reported by

Humphries and Griggs indicate the feasibility of this application. Electronic components having cyclic operating conditions are the ones that operate in ON or OFF cycles. The heat generated during the ON cycle, is stored in the phase change material via phase change and during the OFF cycle, the heat of fusion energy is removed via radiator, heat pipe, thermal strap or other means.

The simplest form of PCM thermal control for electronic components is the one that is used for short-duty cycle components in launch or reentry vehicles. Although such components are used only once, they generate large quantities of heat that must be removed, so that they will not overheat and subsequently fail. PCM laid at the vicinity to component can thermally protect such components, as seen in Fig.3. The generated heat is absorbed via latent heat of fusion by the PCM without an appreciable temperature rise of the component. This kind of system is totally passive and can be designed for high reliability.

Some of the applications of PCM in spacecraft technologies include:

- Onboard power generation using the thermal energy.
- Electronic components having cyclic operating conditions.
- Enhance efficiency of fluid-loop/radiator systems.
- Universal Spacecraft Thermal Control Architecture.
- Precise dimensional stability.
- Micro/nano satellites.

Onboard Power Generation [3]: With conventional photoelectric radiators, the power production ceases during the shadow portion of the orbit and energy is stored in cells or batteries for use during the OFF portion of the cycle. PCM with high melting-point can be used in conjunction With electronic power-producing systems. Radiators for collecting solar energy can be packed with

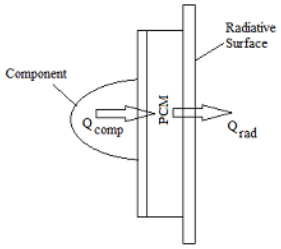

Fig 4

The alternate melting and freezing of the PCM enables the component to operate very nearly at isothermal condition at all the times minimize the gradients. The system is shown in Fig 4. Enhance efficiency of fluid-loop/radiator systems: The coolant fluid returning from the external radiators experienced sizable temperature variations during the course of an orbit cycle. PCMs works as a thermal capacitor for efficient operation of heat exchangers when applied to such heat exchange devices, where large temperature variations exists. PCMs are used as a passive system to mitigate these temperature variations by alternate melting and freezing, thus

maintaining the fluid within allowable temperature range.

Universal Spacecraft Thermal Control Architecture [2]: Thermal control design configurations vary significantly for each mission. A variety of spacecraft configurations are used in order to meet the needs of the individual missions. A universal flexible thermal design concept will be advantageous in terms of faster and less expensive design cycles. Cooling loop thermally integrates all the spacecraft subsystem using thermal switches and valves. The heat rejected from one subsystem is transferred to another subsystem where the heat is needed, to maintain its minimum temperature. Any excess heat generated in the spacecraft is contained in microencapsulated PCM for use in subsequent cycle within the loop. Precise dimensional stability: Missions requiring precise dimensional stability of the mechanical hardware are required to be designed with low thermal distortions. One way to maintain low thermal distortion and obtain high dimensional stability is to control the temperature precisely. PCMs can be used for maintaining the temperature apart from other methods of controlling. This approach is useful where there are difficulties for using materials with low thermal co-efficient of expansion. Micro/ nano satellites: Thermal control applications for micro/nano satellites where power levels are expected very low, can be well controlled by PCM.

VI. CONCLUSION

The basis for phase change material is the fact that these materials can absorb large amount of heat energy at constant temperature. This unique property as discussed in this paper finds multiple applications in the ground systems and spacecraft systems. The use of PCM for the passive thermal Control during spacecraft transportation provides more reliable and cost effective method of temperature control. The low temperature variations within the sealed containers result in precise humidity control too. The foregoing technique eliminates the need of complex active temperature control systems for the transportation of spacecrafts and allied hardware. Further, PCM finds its use for applications in onboard spacecraft systems. PCM material heat sinks have been recognized as an important tool in optimizing thermal control systems for space exploration vehicles and habitats with widely varying thermal loads and environment. Using appropriate PCMs in conjunction with the conventional thermal control systems, considerable optimization and improvement can be imparted to spacecraft systems design to minimize the mass of spacecraft and achieve considerable cost saving.

VII. REFERENCES

[1] Atul sharma, V.V. Tyagi, C.R.Chen, D.Budhi, Review on thermal energy storage with phase change change materials and applications, Science Direct, Renewable and Sustainable Energy Reviews 13 (2009) .

[2] Gajanana C.Birur, Timothy O'Donnell, Advanced Thermal Control Technologies for Space Science Missions at JPL, Jet Propulsion Laboratory, California Institute of Technology, Pasadena, California.

[3] Mohammed M.Farid etal, A review on Phase change storage: materials and applications, Elsevier, Energy Conversion and Management 415 (2004).

[4] M. Ravikumar, Dr. PSS.Srinivasan, Phase change Materials as a thermal energy storage material for cooling of a building, Journal of Theoretical and
Applied Information Technology.

VIII. ABBREIVIATIONS, NOTATIONS AND UNITS

TABLE 2 :

ABBREIVATIONS AND NOTATIONS	UNIT
q_{in} = Heat Transfer rate per unit area	W/m^2
T= Temperature	°K
h= Heat transfer coefficient	W/m^2
Δx= Container wall thickness	m
K_w= Thermal conductivity of container wall	W/mK
U= Overall heat transfer coefficient	W/m^2K
Q_t = Total steady heat transfer to container	W
M_{pcm} = Mass of PCM required	kg

Subscripts Denotes :

r : Radiative
c: Convective
o : Outside Environment
i : Inside Environment
w : Container wall

◈◈◈

Applying SMED/QCO Tool to Improve the Productivity at Screwing Station of HFR assembly – a study at Robert Bosch (i) Limited

[1]NYSTHA BAISHYA, [2]SATHISH RAO U.

[1] Manipal Institute of Technology,
Manipal, Karnataka, India
[2] Mechanical and Manufacturing Engineering,
Manipal Institute of Technology, Manipal, Karnataka, India.

ABSTRACT-Nowadays the industrial product market is increasingly demanding more customized and quality products, forcing the manufacturers to cut down the price, in order to survive in the highly competitive product market. Working on this, Robert Bosch INdia (RBIN) Limited, Bangalore Plant (BanP) designs and produces Diesel systems which make vehicles more cleaner and economical. Bosch has to manufacture products as per the demands of every customer, economically, to maintain being the world's leading manufacturer of diesel injection systems. Fuel Injection Equipment in diesel engine is the "Heart of the Engine" and plays a major role in its performance, emissions and reliability. Hot Forged Rail (HFR) finds its application in common rail fuel injection system, which stores the fuel at high pressure (1600bar). And at the same time, the pressure oscillation, which is generated due to the high pressure pump delivery and the injection of fuel are damped by the rail volume. Its design varies according to customer requirement and engine design. Therefore, BanP has to produce different types of rails to compete the diesel market in India. In order to be customer centric and productive, BOSCH follows Bosch Production Systems (BPS), the elements of BPS in Lean manufacturing are Value Stream Mapping (VSM), Value Stream Design (VSD) and Value Stream Planning (VSP). The Single Minute Exchange of Die (SMED) is one important lean manufacturing tool to reduce waste and improve production flexibility, allowing lot size reduction and manufacturing flow improvements. Quick Change over (QCO) is a set of activities (preparation, changing and adjustment) which are being carried out in between the production of two varieties to reduce changeover time and to reach the optimum production running. The proposed SMED approach was tested for screwing machines changeovers and the implementation had enabled reduction in setup time, through company's internal resources without the need for significant investment. The objective of the present study is to implement the SMED/QCO tool approach in RBIN, BanP, HFR production line at screwing station to reduce the changeover time by 90% and improve availability by >42%, thereby eliminating the possibility of investing on new production line to meet customer demand.

Key words: *Bosch Production Systems (BPS), Value Stream mapping (VSM), Value Stream Design (VSD), Value Stream Planning (VSP), Quick Change Over (QCO), Single Minute Exchange of Die (SMED), Hot Forged Rail (HFR).*

INTRODUCTION

While the market is increasingly demanding more customized products, manufacturers are under constant pressure to produce variety at low costs. Non-fulfillment of orders more frequently results in losing business to the competition. Combining these factors with the high cost of inventory and the need to increase productivity, and it becomes obvious that mastering quick changeover is essential to an organization's survival. As an organization begins a according to customer demand (takt time) while utilizing "one piece flow." For this to happen, machines need to be set up more often, highlighting the need to reduce setup time. Reducing setup time results in increased production, Single-minute exchange of dies (SMED), like other lean tools, requires a committed effort from within the organization. One of the major pitfalls organizations fall into is the desire to rush into a changeover program with very little or no upfront planning. With limited time and resources, the program is doomed for failure. The other common mistake is failure to document and standardize the process.

Quick Change over (QCO)

Quick changeover incorporates proven, simple process orientated systems and methods to reduce tools, plant or equipment changeover times to facilitate increased better quality parts and a more flexible workplace without much investment.

Single Minute Exchange of Dies

Single-Minute Exchange of Die (SMED) is one of the many lean production methods for reducing waste in a manufacturing process. It provides a rapid and efficient way of converting a manufacturing process from running the current product to running the next product. The phrase "single minute" does not mean that all changeovers and startups should take only one minute, but that they should take less than 10 minutes (in other words, "single-digit minute").

capacity, smaller batch sizes, more agility to changing demands, lower inventory and reduced lead times.

Most of the companies face this business paradigm, where they have ever increasing requests for smaller and more frequent deliveries, changing demands requested at short notice and orders for specials or

some form of uniqueness and customization of the products and services they provide and at low price. The solution is in batch size reduction, quick response and flexibility, through mastering quick changeover and standardization.
The keys to quick changeover are as follows:

1. Rethinking the idea that machines can be idle, but workers cannot be idle.
2. The ideal setup change is no setup at all or within seconds.
3. Ensuring that all tools are always ready and in perfect condition.
4. Blowing a whistle and have a team of workers respond to each changeover.
5. Establishing goals to reduce changeover times, record all changeover times and display them near the machine.
6. Distinguishing between internal and external setup activities and try to convert internal to external setup.

Basic Terms used in QCO:
The time from the last part of the old lot to the first okay part of the new lot is known as '**Loss of change over time'.**
The **'Internal change over time'** is the change over time with the plant stopped.
The loss of output due to stoppage and running (incl. Release of production) in an operating system through change over processes is known as **'Gap in Change Over'.**
Adding all internal and external change over processes gives the **'duration of change over'.**
The **'External change over time'** is the change over time when the machine is running.
The **'Change over frequency'** is the number of change over processes per unit of time.

The advantages of QCO are:

- **Reduce defect rates**
  - Quick Changeover reduces adjustments as part of setup and promotes quality on the first piece.
- **Reduce inventory costs**
  - Elimination of, or reduction in numbers of batches, and their sizes, allows for recovery of operating cash and manufacturing space.
- **Increase production flexibility**
  - Increase output and improve timeliness of response to customer orders.
- **Improve on-time delivery**
  - Quick Changeover supports the ability to meet customer demands**.**

The advantages for the employees include:

- **Easier:**
  - Easier and more transparent change over processes causes less problems (and with that less stress and hectic)
  - Uniform work load of all the employees
- **Quicker:**
  - quicker change over time gives more time for other work
- **Safer:**
  - less physical strain during change over
  - Planning safety during the Production process

Need for SMED
The customer demands in 2012 increased by ~87% (50,000 pieces of rails in 2011 and 4,00,000 pieces in 2012). Following the BPS principles, a VSM was prepared in January which depicted the current picture of the assembly line. And consequently, a VSD was also prepared predicting the future state. The gap between the two conditions was studied and a system CIP workshop was conducted.

Identification of the problem
Looking at the Takt Time Chart for the second half of 2012, the Screwing station was identified as the bottle-neck station and thus a detailed study was done. The losses were identified looking at the hourly monitoring sheet (HMS), Fig 1, which is filled up by the operators. Hourly Monitoring is done every day by the associates in the line to generate Overall Equipment Effectiveness (OEE) for each cell. Depending on 1, Cycle Time (as depicted in Fig 1) of bottle neck station in each cell, 2 (number of pieces to be produced per day) is calculated. The associates enter 3 (actual pieces produced per hour) and from there OEE of each cell is calculated.

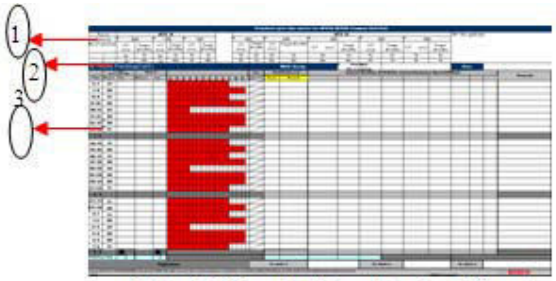

Fig. 1 Hourly Monitoring Sheet

The OEE was calculated from the HMS for CELL 2 and it looked like the following:
Fig 2. OEE Graph for Cell 2

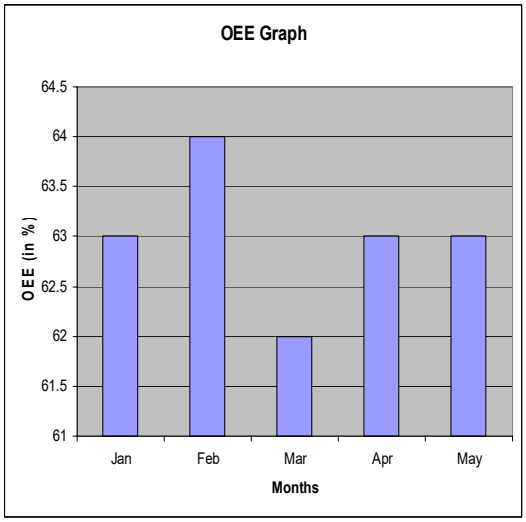

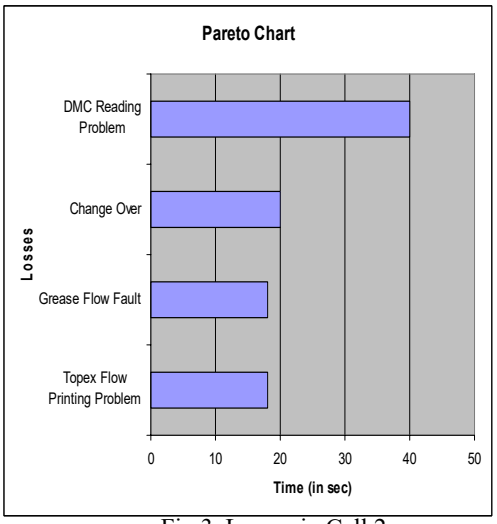

Fig 3. Losses in Cell 2

The HMS was studied carefully and the losses in Cell 2 were identified. The prominent losses are shown in Fig.3. The problem in Cell 2 was analyzed and a Quick Change Over Project was opted in Screwing Station.

Is Condition:

The Present change over matrix at Screwing Station seemed like the following:

Here, 002, 004, 007, etc are the various part numbers for rail bodies for each customer and the different types of pressure sensors (RDS), Direction Control Valves (DRV) and Screw Plugs are screwed to the rail body in this Screwing Station as a part of the assembly process.

The steps involved in the change over from the various part numbers are:

	Pressure	Direction	Screw Plug
002	0281.006.047	0281.006.200	
004	0281.006.047	0281.006.144	
007	0281.006.047	0281.006.206	
261	0281.006.937		F00R.L00.412
025	0281.006.937		F00R.L00.412
006	0281.006.937		F00R.L00.412
194	0281.006.158	0281.002.507	
224	0281.006.158	0281.002.507	
193	0281.006.158		F00R.L00.412

Screwing Station									
	002	004	007	261	025	006	194	224	193
002	-	20	20	15	15	15	20	20	20
004	20	-	20	15	15	15	20	20	20
007	20	20	-	15	15	15	20	20	20
261	15	15	15	-	8	15	20	20	20
025	15	15	15	8	-	15	20	20	20
006	15	15	15	15	15	-	20	20	20
194	20	20	20	20	20	20	-	15	20
224	20	20	20	20	20	20	15	-	20
019	20	20	20	20	20	20	20	20	-

Internal Activities as per the Programmable Logic Controller(PLC) program:

i) Start type Change.
ii) Load new data.
iii) Open doors.
iv) Unscrew Screws.
v) Close doors.
vi) Set change over cylinder to work position.
vii) Open doors.
viii) MECHANICAL CHANGEOVER- take out the fixture by unscrewing screws and disconnecting the cameras.
ix) Put the new fixture and screw it, connect the camera.
x) Close doors.
xi) Control and basic function ON.
xii) Check O-ring and low pressure Testing.
xiii) Take over new type data
xiv) Close change over cycles.

External Activities:

i) Bring the new fixture.
ii) Put back the old fixture.
iii) Bring change over tools and return it back.

Implementation of the project:

A study was done on the program of the screwing station and the various rail body part numbers.

	00	00	00	26	02	00	19	22	19
Fixture						-			
Software(PLC						-			
Station						-			
Label	x	x	x	x	x	x	X	x	x
Customer	x	x	x	x	x	x	X	x	x

✓	is similar
⬭	is similar
Δ	is similar

Table 1.5 Comparison of Parts

Thus we saw that, 004, 002 and 007 and 261 and 025 and 194, 224 and 193 have similar properties (see Table 1.4) regarding the fixture(since they had the same size and shape), Software(since the DRV, RDS/Screw Plug are the same) and the station parameters (screwing speed, torque, etc). Hence a change was done in the Progammable Logic Control(PLC) program and a few steps were skipped(from step iii to x) when changing over from the similar types. Thus, reduction was done as per the Eliminate Combine Reduce Simplify (ECRS) method and the change over time reduced from 20mins to 2 mins.

Step iii

Step x

Condition after the change

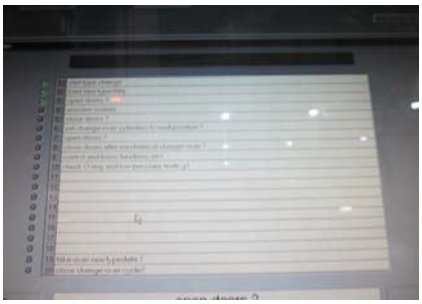

Conditions after implementation of the project:

The Change Over Matrix in the screwing Station changed to the following:

Conclusions:

We see that the change over time reduced from 20mins to 2mins, i.e by 90% and hence the availability of the machine time is increased by 42.3 %. Along with this the Every Part Every Interval (EPEI) became 1.

Screwing Station									
	002	004	007	261	025	006	194	224	193
002	-	2	2	15	15	15	20	20	20
004	2	-	2	15	15	15	20	20	20
007	2	2	-	15	15	15	20	20	20
261	15	15	15	-	2	15	20	20	20
025	15	15	15	2	-	15	20	20	20
006	15	15	15	15	15	-	20	20	20
194	20	20	20	20	20	20	-	2	2
224	20	20	20	20	20	20	2	-	2
193	20	20	20	20	20	20	2	2	-

REFERENCES

1. "Quick Change Over for Operators:", The Single Minute Exchange of Dies System Productivity Press, Portland, Oregon. ISBN: 1 - 56 327 - 125 – 7
2. A Revolution in Manufacturing: The SMED System", Shigeo Shingo; Productivity Press, Portland, Oregon. ISBN: 0 - 915 299 - 03 – 8
3. http://www.aleanjourney.com/2010/08/quickchangeover.html
4. http://en.wikipedia.org/wiki/Single_Minute_Exchange_of_ Diewikipedia.org/wiki/Single_minute_exchange of _die
5. http://world-class-manufacturing.com/smed.html
6. www.vorne.com>Learning Center
7. www.leanpresentations.com/samples/.../QuickSMED_sample.ppt\

◈◈◈

Microstructure Behaviour of Aluminium 6061 Alloy using Friction Stir Welding

SHIVAKUMAR N

Department of Mechanical Engineering
SRMUniversity
Ramapuram Campus Part-Vadapalani, Chennai

Abstract-Friction stir welding is a relatively new welding process that has significant advantages compared to the fusion process such as joining conventionally non fusion weldable alloys. Being a solid-state joining process it produces weld with reduced distortion and improved mechanical properties.

The use of aluminum alloys are widely used in different industrial applications such as ship building, aerospace and automobile industries due to their light weight, good mechanical strength and high corrosion resistance.

In this work, the main parameter considered is the heat input from the tool shoulder and tool pin. The temperature distributions of the weld at various welding speeds are obtained. The friction stir welding experiments are carried out for various transverse speeds of 0.75 mm/sec, 1.00 mm/sec, 1.25 mm/sec and 1.50 mm/sec of tool. Brinell's Hardness test, tensile test and micro structure analysis are performed on the welded material.

Keywords: *Friction; Welding; Microstructure; Temperature distribution;Friction stir welding.*

I. INTRODUCTION

Friction-stir welding (FSW) is a solid-state joining process (meaning the metal is not melted during the process) and is used for applications where the original metal characteristics must remain unchanged as far as possible. This process is primarily used on aluminium, and most often on large pieces which cannot be easily heat treated post weld to recover temper characteristics. It was invented and experimentally proven by Wayne Thomas and a team of his colleagues at the Welding InstituteUK in December 1991. TWI holds a number of patents on the process, the first being the most descriptive. In the process A rotating pin, attached to shoulder piece is translated along the joint line, causing localized plastic deformation, while frictional heating occurs due to contact between the tool and the material. Understanding and predicting the temperature distribution, active stresses developed, during the process are important.

II. LITERATURE SURVEY

Friction stir welding is a derivate of conventional friction welding. Friction stir welding is a process for joining work pieces in the solid phase, using an intermediate non-consumable tool made of a material that is harder than work piece material being welded. to maintain to the required thickness depth. According to **G.Buffaa, L. Fratini a, R. Shivpuri b [1]**,Friction stir welding (FSW) is an energy efficient and environmentally "friendly" (no fumes, noise, or sparks) welding process, during which the work piece are welded together in a solid-state joining process at a temperature below the melting point of the work piece material under a combination of extruding and forging. Significant micro structural evolution takes place during FSW: in particular continuous dynamic recrystallization (CDRX) phenomena result in a highly refined grain structure in the weld nugget and strongly affect the final joint resistance. In the paper two different analytical models aimed to the

The marked difference between the elevated temperature properties of tool and the work piece, together with suitable cyclic movement between the tool and the work piece, generates sufficient frictional heat to cause plasticized conditions in the work piece material. The work piece materials have been allowed by continuing to maintain a suitable differential between and elevated temperature properties of the tool and the hardness and elevated temperature properties of the work material. Friction stir welding can be regarded as an autogenous keyhole joining technique without the creation of liquid metal. The consolidated weld material is thus free of typical fusion welding defects. No consumable filler material or profiled edge preparation is normally necessary. In friction stir welding joints are produced with low distortion, cost effective, excellent mechanical properties have been achieved in aluminium alloys. If the travel speed is high with low spindle speed is called cold welding, and as low travel speed with high spindle speed is called hot process. FSW is a continuous hot shear process that involves solely plunging a portion of a specially shaped rotating tool between and the abutting faces of the joints. The contacting surface of the shoulder of the tool and the length of the probe below the shoulder essentially allow the probe

determination of the average grain size due to continuous dynamic recrystallization phenomena in FSW processes of AA7075-T6 aluminium alloys have been implemented in a 3D FEM model and numerical analyses of the welding processes have been performed to verify their effectiveness.

According to **M. Song, R. Kovacevic, A [2]** three-dimensional heat transfer model for friction stir welding (FSW) is presented in this paper; a moving coordinate is introduced to reduce the difficulty of modeling the moving tool. Heat input from the tool shoulder and the tool pin are considered in the model. The finite difference method was applied in solving the control equations. A non-uniform grid mesh is generated for the calculation. FSW experiments have been done to validate the calculated results. The calculated results are in good agreement with the experimental results. The calculation result also shows that preheat to the work piece is beneficial to FSW.

The paper of **A. Simar J. Lecomte-Beckers, T. Pardoenand B. de Meester [3]** says, Welding experiments on Al-6005A have been carried out using a fully instrumented milling machine. The power input was calculated from the measured torque and forces. The thermal cycles were measured at various locations close to the weld centerline. A finite element pseudo steady-state uncoupled thermal model was developed, taking into account the influence of the welding parameters on the power input. The distribution of the total power input between surface and volume heat sources was also studied. The measured and predicted thermal cycles are in good agreement when proper contact conditions between the work piece and the backing plate are introduced.

III. PRINCIPLE OF OPERATION

In FSW, a cylindrical-shouldered tool, with a profiled threaded/unthreaded probe (nib or pin) is rotated at a constant speed and fed at a constant traverse rate into the joint line between two pieces of sheet or plate material, which are butted together. The parts have to be clamped rigidly onto a backing bar in a manner that prevents the abutting joint faces from being forced apart. The length of the nib is slightly less than the weld depth required and the tool shoulder should be in intimate contact with the work surface. The nib is then moved against the work, or vice versa.

Frictional heat is generated between the wear-resistant welding tool shoulder and nib, and the material of the work pieces. This heat, along with the heat generated by the mechanical mixing process and the adiabatic heat within the material, cause the stirred materials to soften without reaching the melting point (hence cited a solid-state process), allowing the traversing of the tool along the weld line in a plasticized tubular shaft of metal. As the pin is moved in the direction of welding, the leading face of the pin, assisted by a special pin profile, forces plasticized material to the back of the pin while applying a substantial forging force to consolidate the weld metal. The welding of the material is facilitated by severe plastic deformation in the solid state, involving dynamic recrystallization of the base material. Fig: 1 shows the friction stir welding process.

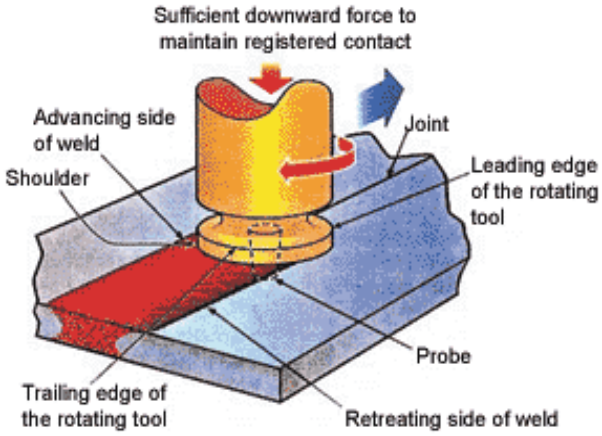

Fig: 1 FRICTION STIR WELDING PROCESS

3.1 Process Advantages

- Good mechanical properties in the as welded condition
- Improved safety due to the absence of toxic fumes or the spatter of molten material.
- No consumables - conventional steel toolscan weld over 1000m of aluminium and no filler or gas shield is required for aluminium.
- Easily automated on simple milling machines - lower setup costs and less training.
- Can operate in all positions (horizontal, vertical, etc), as there is no weld pool.
- Generally good weld appearance and minimal thickness under/over-matching, thus reducing the need for expensive machining after welding.
- Low environmental impact.
- Considerable improvement in strength, ductility, fatigue and fracture toughness

- Cost-effectiveness and ability to weld similar and dissimilar material combinations with minimal distortion is more widely appreciated.
- The thickness can vary from 1 mm to 50 mm depending on material or welding conditions.
- Since gravity has no influence on the solid-phase welding process, it can be used in many positions and geometries.
- The process has been used for the manufacture of butt welds, overlap welds, T-sections, fillet, and corner welds. For each of these joint geometries specific tool designs are required.
- Low distortion, even in long welds,
- The main advantages are that it is a rapid, clean and robust technology. One other advantage, very much appreciated by the industry, is the assured repeatability of the quality level for long periods of production
- No fume, No porosity, No spatter, Low shrinkage,
- Energy efficient,
- Non-consumable tool, One tool can typically be used for up to 1000 m of weld length in 6000 series Al alloys, No filler wire,
- No gas shielding for welding aluminium,
- No welder certification required,
- Some tolerance to imperfect weld preparations—thin oxide layers can be accepted, No grinding, brushing or pickling required in mass production, can weld aluminium and copper of >50 mm thickness in one pass.

3.2 Applications

Construction Industry

- Facade panels
- Window frames, heat exchangers and air conditioners
- Pipe fabrication
- Aluminium bridges

Land Transport Industry

- Truck bodies
- Fuel tankers
- Motorcycle and bicycle frames
- Buses and caravans
- Armor plated vehicles

Other Industries

- Aerospace - (military/civilian aircraft, rockets, fuel tanks, aircraft parts)
- Electrical - (motor housings, bus bars electrical connectors)
- Gas - (tanks and cylinders)

Automotive

- Engine and chassis cradles
- Wheel rims
- Body panels

Railway Industry

- Rolling stock, underground carriages and trams
- Railway tankers and wagons
- Container bodies
- Panels for decks, sides and bulkheads
- Aluminium extrusions
- Boat sections
- Hulls and superstructures
- Helicopter landing platforms

IV. EXPERIMENTAL STUDY

The Friction Stir Welding used to fabricate all the joints. The machine consists of a base, column, saddle, table, and vertical head. The table and vertical head is actuated by hydraulic cylinders assisted by hydraulic power pack with a pressure of 50 bars. The vertical head is provided with a 3 phase induction motor with gearbox having capacity of 11 kW. The motor speed is regulated by infinitely variable frequency control unit. Both the table and the vertical head speed can be varied infinitely with the help or hydraulic power pack and regulation valves. Thus the machine has provisions for infinitely variable speed of the spindle, horizontal feed of the table and vertical speed of the spindle. In addition to the above the vertical spindle can be actuated along Z-axis through fine feed adjustment worm and warm wheel provided in the head. The specification of the machine used in this investigation is given below

Hydraulic power pack

a). Hydraulic cylinder of Area A=0.00503 m^2

b). Feed rate of the table (Rapid) Forward direction = 70 mm/minreverse direction 55 mm/min. 2/2 solenoid operated Directional control Valve in 3 numbers and a flow control valve.

It is noteworthy that the Friction Stir Welding machine is equipped with a downward pressure measuring device to measure the downward force f capacity up to 250 KN. The Friction Stir Welding machine uses a non-consumable rotating tool to fabricate the joint. The tool consists of shank, Body, Shoulder, Tip (or) probe. Five different tool profiles such as square tool, straight cylindrical, tapered, cylindrical, threaded cylindrical and triangular tool have been used in this investigation to fabricate the joint and tool profiles are displayed in Fig. The tools are made of high speed steel and hardened for optimum hardness after machining. The steps in the welding process are shown in fig: 2 and fig: 3 show the process on FSW machine.

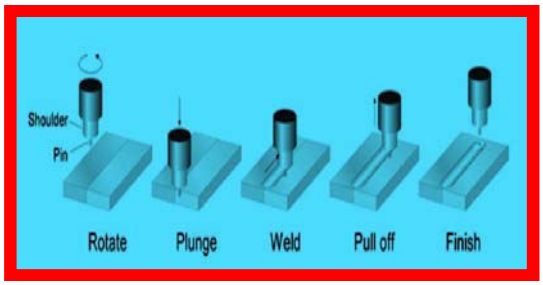

Fig: 2 Process steps

Fig: 3 Process on FSW Machine

Welded plates

Welding process

V. RESULTS AND DISCUSSION

Result for transverse speed 1.25 mm/sec

TIME IN SEC	TEMPERATURE IN °C									
0	30	30	30	30	30	30	30	30	30	30
30	281	254	227	199	172	144	117	90	62	35
60	309	280	251	222	194	165	136	107	78	49
90	324	293	263	233	203	172	142	125	82	51
120	340	315	291	266	242	218	193	169	144	120
150	363	335	315	295	268	247	217	188	162	143
180	382	358	332	320	293	261	238	215	189	160
210	406	383	360	337	314	290	267	244	221	197
240	445	401	358	314	270	227	183	139	96	52
270	536	482	427	373	318	264	209	155	100	46

Graph for transverse speed 1.25 mm/sec

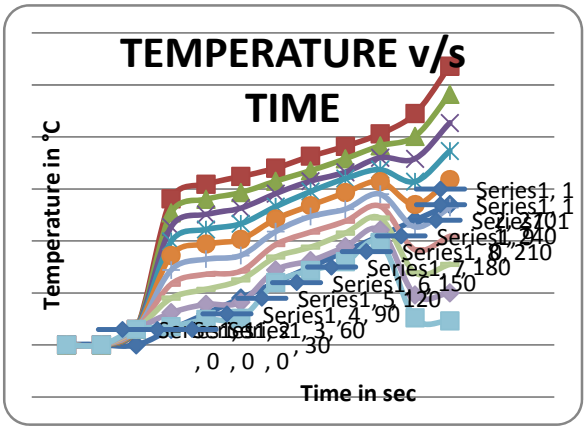

Result of Mechanical Properties Test

Transverse Speed in mm/sec	Yield Strength in MPa	Elongation in %
Base Metal	235	26.4
0.75	247	28
1.00	247	28
1.25	250	27
1.50	248	27

MICROSTRUCTURE ANALYSIS FOR VARIOUS TRANSVERSE SPEEDS

Microstructure for Transverse speed 0.75 mm/sec

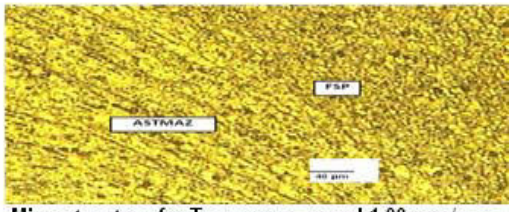

Microstructure for Transverse speed 1.00 mm/sec

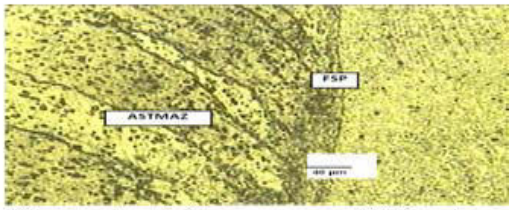

Microstructure for Transverse speed 1.25 mm/sec

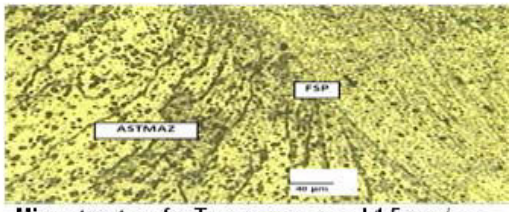

Microstructure for Transverse speed 1.5 mm/sec

CONCLUSION

From this test, the yield strength and elongation are more reliable for transverse speed of 1.25 mm/sec compared to other transverse speedsby keeping spindle speed and downward force as constant. Therefore, the suitable transverse speed for FSW of AA 6061 aluminium alloy is 1.25 mm/sec.

REFERENCES

1. G. Buffa a,., L. Fratini a, R. Shivpuri b, Feasibility of friction stir welding, *Science and technology of welding joint,* 1999, Vol. 4, No. 6, pp. 365-372.
2. M. Song, R. Kovacevic,A Aluminium Welding, *Recent developments in materials joining,* 2001, pp. 175-190.
3. A. Simar J. Lecomte-Beckers, T. Pardoenand B. de Meester, Welding of Aluminium and Aluminium alloys, *WRI journal,* 2000 Vol. 23, No. 4, pp. 5-22.
4. H.B. Cary, Modern Welding technology, Prentice-Hall, Inc., *Englewood difts*, New Jersey, 1979, pp.223.
5. K.N. Krishanan, Effect of Heat treatment state and welding parameters on the welding characteristics of friction stir welded aluminium alloys, *IWC* 2001, pp. 1024-1033.
6. C.G. Rhodes, et al, effects of friction stir welding on microstructures of 7075 aluminium, *scripta materialia*, 1997, Vol. 6, No. 3, pp. 69-75.
7. G. Liu, et al, Microstructural aspects of the friction stir welding of 6061- T6 aluminium *scripta materialia*, 2002, Vol. 37, No.3, pp. 355-361.
8. Lawrence, E. Murr, et al, Microstructures in Friction stir welded metals, *Journal of materials processing and manufacturing science*, 1998, Vol. 7, pp. 145-161.
9. L.E. Svenson, et al, Microstructure and mechanical properties of friction stir welded and AA6082, *science and technology of welding and joining*, 2000, Vol.5, No. 5, pp. 285-296.
10. K.V. Jata, et al, Continuous dynamic recrystallization during friction stir welding of high strength aluminium alloys, *scripta materialia*, 2000, Vol. 43, pp. 743-749.
11. G. Biallas, et al, Mechanical properties and corrosion behaviour of friction stir welded 2024-T6, *First international conference on Friction stir welds,* thousand oaks, CA, 1999.
12. P.L. Threadgill, Friction stir welding- state of the art, *TWI report*-678/1999.

◈◈◈

Biodiesel Engine

[1]S. V. DESHPANDE, [2]SACHIN BORSE,

[1]J.S.P.M.'S R.S.C.O.E., Tathwade.
Pune, India.
[2]Dept. of Mechanical Engg., R.S.C.O.E.,Tathwade.
Pune, India

Abstract— Biogas from anaerobic digestion of animal manure and food waste can be used as a renewable energy source for power generation. Biogas is cheaper and renewable source of energy. Hence running costs would be less.

In this study, we would construct a small biogas plant would be using the biogas produced in a single cylinder, direct-injection, compression ignition engine, which has been modified to operate under dual-fuel condition to generate electricity. The primary fuel would be biogas, which would ignited by a pilot diesel liquid injection.

Performance of the engine in terms of output power, specific fuel consumption and thermal efficiency would be evaluated over a fixed speed and varying load conditions, and compared against a conventional diesel engine.

A study would be conducted to assess the economic feasibility of the project and calculating the payback period for the biogas plant.

Keywords-*component; formatting; style; styling; insert (key words)*

1. INTRODUCTION

Energy demand in India is high and growing as a direct result from economic development and population growth. A large proportion of the country's energy imports is from foreign fossil fuels. It is important to identify alternatives for partial or total substitution of domestic, industrial and transportation fuels. Alternative energy sources must be economically feasible and environmental friendly. Among the many different types of alternative energy, biogas from the bacterial biodegradation process of animal manure waste, waste water or solid waste under anaerobic condition proves to be one of the most promising choices. Anaerobic digestion of animal manure in biogas plants for energy, fertilizer supplement and sanitation has made a significant impact for livestock production business as well as rural development. Gas engines are usually considered as prime candidates for shaft power and electricity generation. Because of its high octane number, biogas is suitable for engines with a relatively high compression ratio to maximize thermal efficiency. It was suggested that biogas/diesel dual-fuel may be applied to conventional direct-injection, compression ignition engines with minor modifications. In dual-fuel compression ignition engine operation, biogas is used mainly as a primary fuel with a 'pilot' amount of diesel fuel supplied from a normal diesel fuel injection system. In this project the present available engine (Kirloskar made, single cylinder,4 stroke) induces and compresses a mixture of gaseous fuel and intake air, which has been prepared in the venturi (external mixing device). The mixture does not auto ignite due to its high auto ignition temperature. It is ignited by energy from the combustion of the pilot diesel sprayed in.

2. OVERVIEW OF BIOGAS TECHNOLOGY

The biogas is the by product of anaerobic digestion of organic material is commonly referred as "biogas" because of the biological nature of gas production. Biogas technology refers to the production of a combustible gas called biogas and a value added fertilizer (called slurry or sludge) by the anaerobic fermentation of organic materials under certain controlled condition of temperature, pH, C/N ratio, etc. The escalating costs of fossil fuels and the decreasing availability of these sources of fuel have forced many developing countries to consider the use of renewable energy technologies (RETs) like solar, wind, and biogas based technologies such as biogas, power alcohol, and gasifiers. Of these technologies, biogas has the lowest financial inputs per kWh of output.

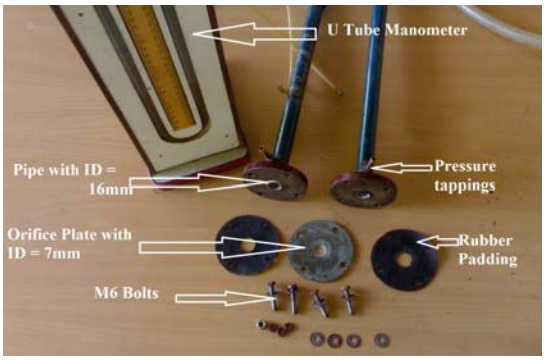

3. Flow measuring Process :-

Orifice plate **calculator** can be used for flow through orifice calculation and orifice sizing for liquids and gases. Calculator is applicable for subsonic flow and single phase fluid. Gas is considered as compressible and ideal. For gas flow, pressure ratio p_2/p_1 must be equal or greater than 0.75. **Calculator** is not for pulsating flow.

The orifice plate flow meter in our case gives a height difference of water column of about 4mm to 16mm. The results are not accurate compared with the volumetric method. It also obstructs the flow of biogas and the engine is unable to take the load because of the losses in the pipeline. Hence considering all the above prospects we concluded that the volumetric method of flow measurement is the best method and gives fairly accurate results. It is also cost effective. Moreover there is no obstruction to the flow of biogas and hence losses are minimized.

4. SECIFICATIONS:-

In the project "Development of constant speed Diesel fired biogas engine" the engine available for the project has following specifications.

4.1 **ENGINE SPECIFICATIONS:-**

Make : KIRLOSKAR
Piston diameter : 80 mm
Stroke length : 110 mm
Speed : 1500 rpm
Brake power : 5 kW
Compression ratio: 16:1
C.V. of High speed diesel : 45000 kJ/kg
Specific gravity of fuel : 0.825

GENERATOR SPECIFICATIONS :-

Power :5 h.p.
Speed :1500 rpm
Frequency : 50 Hz
A.C. generator : 6 KVA

Fig 4.1 Actual Experimental Set Up

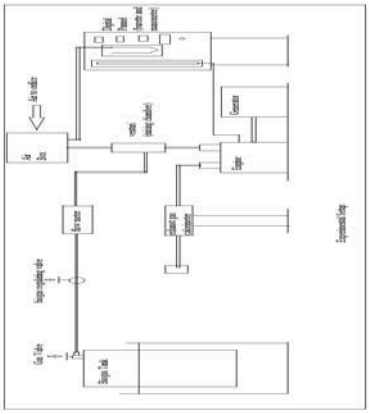

4..2 OBJECTIVE IN VENTURI DESIGN:-

1) The venturi must suck the biogas in the required quantity at all loads even when the biogas is at atmospheric pressure.
2) There must be proper mixing of air and biogas in the venture

4.3 BIOGAS PLANT CONSTRUCTIONAL DETAILS:-

For constant speed diesel fired biogas engine, the most important is supply of biogas. The question was how to bring biogas for running engine.

- Base tank = 1000 liters
- Floating tank = 750 liters
- Size ratio = 750/1000 =3/4

4.4 MATERIALS REQUIRED

SR NO	Name	Material	Qty
1	1000 litre Tank		1
2	750 litre Tank		1
3	90mm T	PVC	1
4	90mm Female Adapter	PVC	1
5	90mm Male Adapter	PVC	2
6	90mm End Cap Threaded	PVC	1
7	PVC pipe 90mm	PVC	6 feet
8	63mm Elbow	PVC	1
9	63mm Male Adapter	PVC	2
10	63mm Check Nut	PVC	1
11	63mm PVC pipe	PVC	3 feet
12	1/2 inch PVC Male Adapter	PVC	1
13	1/2 inch Elbow Metal	GI	1
14	M Seal		600gm
15	PV Seal		20ml
16	Gas Cock (1/2 inch)	Brass	1
17	50mm Gate Valve	PVC	1
18	Barrel Piece (90mm)	GI	1
19	Barrel Piece (63mm)	GI	1
20	Barrel Piece (50mm)	GI	1

Table 4.4 Materials For Biogas Plant

5. TEST PROCEDURE:-

1) device.
2) Now supply the biogas in the required quantity with the help of regulating valve, till the speed of generator shaft becomes 1500rpm.
3) Apply load by resistance bank.
4) The speed reduces.
5) Adjust the speed by regulating the biogas valve to 1500rpm.
6) Note all the readings for different loading conditions.

5.1 PARAMETERS TO BE MEASURED:-

Table 5. Parameters To Be Measured

1.	Load
2.	speed of generator shaft
3.	speed of engine
4.	Voltage
5.	Current
6.	t1 water to jacket
7.	t2 water outlet from jacket
8.	t3 water to calorimeter
9.	t4 water outlet from calorimeter
10.	t5 temp of exhaust gas inlet
11.	t6 temp of exhaust gas outlet
12.	manometer reading
13.	amt of diesel used
14.	time for diesel used
15.	height of biogas used
16.	time for biogas used
17.	time for 1lit of calorimeter water flow
18.	time for 1lit of cooling water flow

6. OBSERVATIONS FOR BIOGAS PLANT :-

RAW MATERIAL	AMOUNT	LIFT OF TANK
3 Chappati+ 300 gm Rice	1 kg	39 cm
3 Chappatis + 500gm Rice	1.4 kg	46 cm
2 Chappatis+700 gm Rice	1.3 kg	46 cm
800 gm Juice pulp	1 kg	20 cm
4 Chappatis+200 gm Egg Waste	1.2 kg	48 cm
3Chappatis+600gm Vegetable Waste	1.3 kg	43 cm
3 Chapattis	1 kg	36 cm
Bajra flour	1.5kg	58 cm

Table 6. Observations For Biogas Plant

From the above observation it can be seen that,

- Flour produces the maximum biogasRice waste also produces considerable amount of biogas.Chapatti waste & vegetable waste produces almost equal amount of biogas.Juice pulp and fibrous wastes produces least amount of biogasSurry From The Plant:-It is observed that the slurry from the biogas is excellent manure for the plants and facilitates faster growth of plants. Table 6.3.1 Readings For Dual Fuel Operation

7. FORMULAE FOR CALCULATION:-

1) Mass Flow Rate of Air, m_{diesel} = $\frac{\text{density of fuel} \times \text{amt of fuel used in cc} \times 10^{-6}}{\text{time for fuel utilisation}}$ kg/sec

Where, density of fuel= 825 kg/m^3

2) Mass Flow Rate of Water, m_w = $\frac{1}{\text{time of 1000 cc(1lit) of water}}$ lit/sec

Density of Air, ρ_a = $\frac{P}{R \times T}$ kg/m^3

Where, P= 1.013×10^5 N/m^2

R= 287 J/kg K

T= 299 K

3) Mass Flow Rate Of Air,

m_a = $C_d \times A \times \sqrt{2 \times g \times h_w \times \frac{\rho_w}{\rho_a}}$ kg/sec

Where, C_d = 0.64 (for the orifice)

$A = \frac{\pi}{4} d^2$ where d = diameter of orifice= 15mm

g = 9.81 m/s^2

ρ_w = 1000 kg/m^3

4) Mass Flow Rate Of Biogas, m_{biogas} = $\frac{\text{area of the tank} \times \text{height of biogas used}}{\text{time taken}}$

Where area of the tank = $\frac{\pi}{4} \times d^2$ where d = 0.96m

5) Heat supplied by diesel = q_{diesel} = $m_{diesel} \times C.V_{diesel}$

Where C.V. of diesel is 43890 kJ/kg

6) Heat supplied by biogas= q_{biogas} = $m_{biogas} \times C.V_{biogas}$

Where C.V of biogas is 23400kJ/kg

7) Total heat suppled = Heat supplied by biogas + Heat supplied by diesel

8) Brake Power (B.P) = $\frac{VI\eta}{\eta \times 1000}$ kW

Where, V= voltage
I = current
η = efficiency of generator

9) Brake Specific Fuel Consumption (BSFC) $= \frac{mf}{B.P}$

10) Thermal Efficiency, η_{th} = $\frac{B.P}{mf \times C.V}$

8.PERFORMANCE CHARACTERSTICS:-

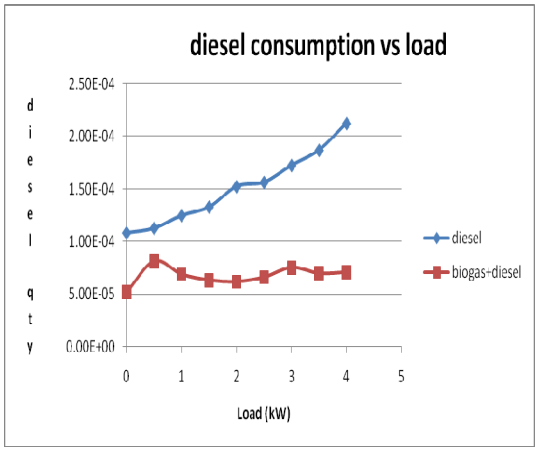

Fig 8.1 Diesel Consumption vs Load

Diesel:-

In this case it is observed that the amount of diesel consumed goes on increasing with the increase in load on the engine.

Biogas+Diesel:-

It is observed that as the rack is set a fixed position the quantity of diesel supplied at all loads in approximately the same minimum qua=

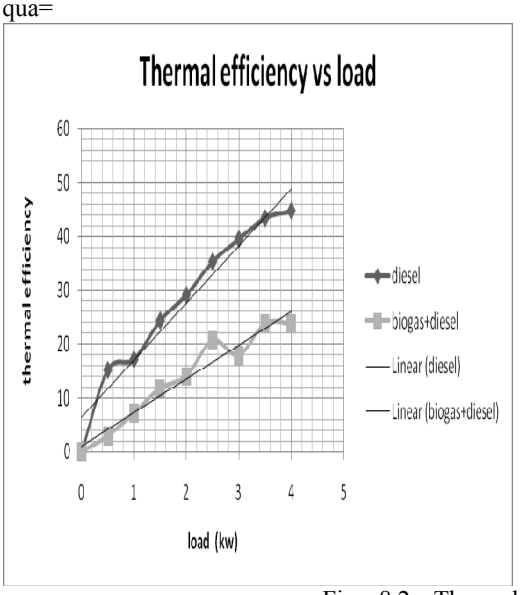

Fig 8.2 Thermal efficiency vs load

Diesel:-

It is seen that as the load increases the thermal efficiency of the engine increases.

Biogas + Diesel

It is observed that as the load increases the thermal efficiency of the engine increases.

The thermal efficiency of dual fuel operation is less than that when only diesel is used

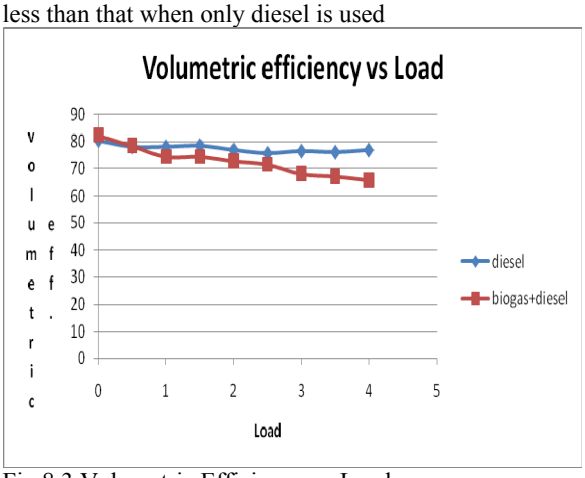

Fig 8.3 Volumetric Efficiency vs Load

Diesel:-

It is found that the volumetric almost remains constant in diesel operation.

Biogas + Diesel:-

It is seen that the volumetric efficiency reduces as the load on the engine increases.

This is because the air is substituted by the biogas in the dual fuel operaThis reduces the quantity of air taken in the engine and hence reduces it

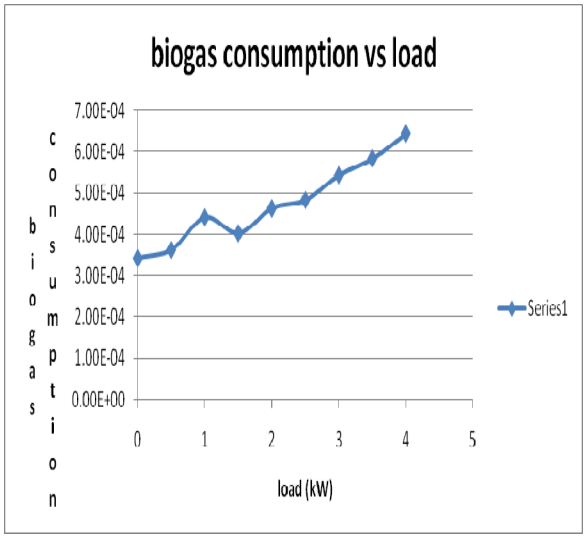

olumetric efficiencies.
Fig 8.4 Biogas Consumption vs Load

It is observed that the biogas consumption increases as the load increases.
This is because the load is taken by the biogas and the biogas flow is increased with the help of regulating valve to meet the speed requirement at different loads.

Cost of 1 litre of diesel = Rs 45
Cost of diesel for 20 mins running per day = Rs 13.91

For Dual Fuel Operation,
Amount of diesel required for 20mins of running at full load= 0.1026 litres
Cost of diesel for 20 mins running per day in dual fuel operation= Rs 4.62
Amount of diesel saved per day = Rs 9.29
Amount of Diesel saved per year = Rs 3390.85

$$\text{Payback period} = \frac{\text{cost of plant}}{\text{amount saved per year}}$$

$$= \frac{7833}{3390.85}$$

= 2years 4 months.

10. FUTURE SCOPE:-

1) The purification of biogas can be done before being sent to the engine. This will include removal of H_2S and CO_2.

2) The tests can be done on variable compression ratio engine and accurate graphs can be plotted for the same.

3) Making improvements so as to achieve about 90 per cent replacement of diesel.

4) Finding better and cost effective devices for biogas flow measurement.

It is observed that the quantity of heat supplied in case of dual fuel operation is much more than that in the diesel operation.
This may be because the calorific value of the biogas produced may be lesser than that taken from the literature survey. Secondly this might be because proper mixing of biogas does not take place as we have compromised in the velocity required at the venturi for proper mixing.

9. CALCULATION OF PAYBACK PERIOD FOR BIOGAS PLANT:-

Total Cost Of Biogas Plant = Rs 7833
Maximum amount of biogas produced in a day = 0.75 m^3/day
Maximum time for which engine would run at full load with the available biogas quantity = 20 mins/ day
As biogas is produced from waste the cost of biogas is assumed to be Rs 0.

For Diesel operation,
Amount of diesel required for 20mins of running at full load= 0.309 litres

5) The diesel engines in farms can be run on dual fuel using biogas as primary fuel. This would largely reduce the running costs.

6) The diesel generators can be operated on dual fuel using biogas as primary fuel where biogas is readily available.

11. CONCLUSION:-

In the present work, an experimental investigation has been carried out to evaluate the effect of biogas/diesel dual-fuel operation on a DI diesel engine. The engine has been modified to operate under the dual-fuel mode at high biogas/diesel replacement in order to minimise diesel consumption and maximise biogas utilisation. The results were presented in terms of power output, fuel economy, energy efficiency. From analysis of the experimental results, it was demonstrated that over 70% substitution rate by biogas can be achieved.
It is apparent that biogas/diesel dual-fuel engine operation is a promising technique for on-farm electricity generation. Significant amount of diesel can be replaced by biogas. Successful operation was demonstrated without any major drawback. Adoption of this technology will boost proportion of the farms' renewable energy usage and reduce diesel fuel cost.

REFERENCES:-

1) "Internal Combustion Engine"; M.L.Mathur, R.P.Sharma ; Dhanpat Rai Publications; Nineteenth Edition

2) "Biogas Technology"; B.T.Nijaguna; New Age International Publishers; Second Edition

3) "Long-term operation of a small biogas/diesel dual-fuel engine for on-farm electricity generation";N. Tippayawong, A. Promwungkwa, P. Rerkkriangkrai; 2007

4) "Economic assessment of biogas-to-electricity generation system with H2S removal by activated carbon in small pig farm"; Suneerat Pipatmanomai, Sommas Kaewluan, Tharapong Vitidsant; 2008

5) "Modification and tuning of diesel bus engine for biogas electricity production"; Sittiboon Siripornakarachai, Thawan Sucharitakul;2007

6) "Experimental investigations of a four-stroke single cylinder direct injection diesel engine operated on dual fuel mode with producer gas as inducted fuel and Honge oil and its methyl ester (HOME) as injected fuels"; N.R. Banapurmath, P.G. Tewaria, R.S. Hosmath; November 2007

7) "Comparative performance studies of a 4-stroke CI engine operated on dual fuel mode with producer gas and Honge oil and its methyl ester (HOME) with and without carburettor"; N.R. Banapurmath*, P.G. Tewari; 2008

◈◈◈

Life Assessment of a parabolic Spring Under Cyclic Stress & Cyclic Strain loading using finite element method

[1]J.P.KARTHIK, [2] K. L.CHAITANYA & [3] C.TARA SASANKA,

Department of Mechanical Engineering,
RVR&JC Engineering College, Guntur(Dist)-522019(A.P)

Abstract-This study presents a fatigue life prediction based on finite element analysis under non constant amplitude proportional loading. Parabolic spring is the vital component in a vehicle suspension system, commonly used in trucks. It needs to have excellent fatigue life and recently, manufacturers rely on constant loading fatigue data. The objective of this study is to simulate the non constant amplitude proportional loading for the fatigue life analysis. The finite element method (FEM) was performed on the spring model to observe the distribution of stress and damage. The fatigue life simulation was performed and analyzed for materials AISI6150, SAE1045-595-QT. when using the loading sequences is predominantly tensile in the nature; the life of mounting in Goodman approach is more conservative. When the loading is predominantly tensile in nature, the life of the component in Morrow approach is more sensitive and is therefore recommended. It can be concluded that material SAE 1045-595-QT gives constantly higher life than material AISI6150for all loading conditions under both methods.

Keywords: *Fatigue life; non constant amplitude proportional loading; parabolic spring; FEM*

1. INTRODUCTION.

A spring is an elastic object is used to store mechanical energy. Springs are usually made out of hardened steel. Originally called laminated or carriage spring, a leaf spring is a simple form of spring, commonly used for the suspension in wheeled vehicles. An advantage of a leaf spring over a helical spring is that end of the leaf spring may guided along a definite path. It takes the form of a slender arc shaped length of spring steel of rectangular cross section. The large vehicles need a good suspension system that can be deliver a good ride and handling. At the same time, that component need to be lightweight and had an excellent of fatigue life. Fatigue is one of the major issues in automotive component. It must withstand numerous numbers of cycles before it can fail, or never fail at all during the service period. From the viewpoint of engineering failure could lead to severe accidents [6]. Parabolic springs are subjected to cyclic compression and tension load when the heavy vehicle was drove on the road. In industry, manufacturer only manage to test the fatigue life of these spring using constant applications, the purpose of fatigue research consists of the prediction of fatigue life on structures, increasing fatigue life and simplifying fatigue tests [1]. In reality, the most engineering components and structures are subjected to non constant amplitude proportional loading conditions at which stress–strain cycles fluctuate with time [2]. At this condition, component tends to fail under various source of loading. Fatigue failure of mechanical components is a process of cyclic stress/strain evolutions and redistributions in the critical stressed volume [3].Using the FEM approach the fatigue life of parabolic spring is estimated for stress/strain life. Parabolic spring is widely used in automotive and one of the components of suspension system. It consists of one or more leaves [4]. As a general rule, the leaf spring must be regarded as a safety component [5] as amplitude loading. This is because non constant amplitude proportional loading fatigue test is time consuming and adding more cost. The aim of this paper is finding both stress life approach and strain life approach for different materials and mentioning

which material having maximum life and which approach is giving optimum value for stress approach and strain approach. The model of leaf spring which shown in figure1

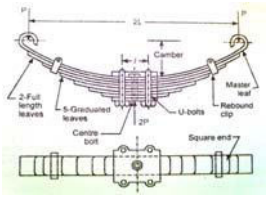

Figure 1. Model of leaf spring

2. FINITE ELEMENT BASED FATIGUE ANALYSIS.

The fatigue analysis is used to compute the fatigue life at one location in a structure. For multiple locations the process is repeated using geometry information applicable for each location. Necessary inputs for the fatigue analysis are shown in fig2. The three inputs information boxes are descriptions of the material properties, loading history and local geometry. All of these inputs are discussed following sections.

Material information-cycle or repeated data used on constant amplitude testing.

- Load histories information-measured or simulated load histories applied to a component. The term loads used to represent forces, displacements, accelerations, etc.
- Geometry information-relates the applied load histories to the local stresses and strains at the location of interest. The geometry information is usually derived from finite element (FE) results.

An integrated FE based durability analysis is considered a complete analysis of an entire component. Fatigue life can be estimated for every element in the finite element model and contour plots of life. Geometry information provided by FE results define how an applied load is provided by FE results for each load case applied independently. Data provided for the desired fatigue analysis method. The schematic diagram of the integrated finite element based fatigue life prediction analysis is shown in figure3.

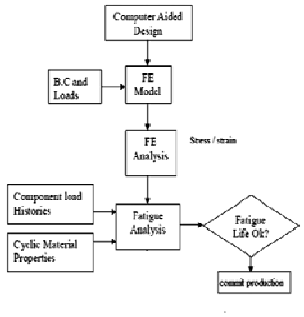

Figure 3. The finite element based fatigue analysis Cycle

The mechanical properties for the materials are mentioned in table1.

Table 1. Mechanical and cyclic properties of SAE1045-450- QT, SAE5160-825-QT &SAE1045-595-QT

Properties	Materials	
	AISI6150	SAE1045-595-QT
Yield strength(Mpa)	1550	1860.
Ultimate tensile strength(Mpa)	2070	2239
Elastic modulus(Mpa)	207000	207000
Fatigue strength coefficient(S_f)	2200	3047
Fatiguestrength exponent(b)	-0.08	-0.10
Fatigue ductility exponent(c)	-0.69	-0.79
Fatigue ductility coefficient(ε_f')	1.22	0.13
Cyclic-strainhardening exponent(n')	0.1	0.10
Cyclic strength coefficient(k')	2500	3498

2.1. Fatigue analysis methods.

Analysis of fatigue can be carried out one of three basic approaches i.e., the total life (stress-life) approach and crack propagation approach, the crack initiation approach and crack propagation approach. The total-life (stress-life) approach was first applied over a hundred years ago (Wohler, 1867) and considers nominal elastic stresses and how they are related to life. The crack-initiation (stress-life) approach considers elastic-plastic local stresses and strains. It represents more fundamental approach and is used to determine the number of cycles required to initiate a small engineering cracks. Crack-propagation or linear elastic fracture mechanics (LEFM) approach is used to predict how quickly pre-existing cracks grow and to estimate how many loading cycles are required to grow these to a critical size when catastrophic failure would occur. First two methods are used in this study and briefly discussed these two methods in the following sections. The fatigue total-life(S-N) approach is usually used for the life prediction of components subjected to high cycle fatigue, where stresses are mainly elastic. This approach emphasizes nominal stresses rather than local stresses. It uses the material stress-life curve and employs fatigue notch factors to account for stress concentrations, empirical modification factors for surface finish effects and analytical equations such as modified Goodman and Gerber equations are given by equations 1 and 2 respectively.

$$\frac{\sigma_a}{S_e} + \frac{\sigma_m}{S_u} = 1 \quad \text{-(1)} \qquad \frac{\sigma_a}{S_e} + \left(\frac{\sigma_m}{S_u}\right)^2 = 1 \quad \text{-(2)}$$

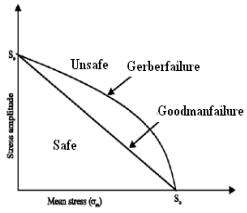

Figure 4. Representation of these mean stress correction methods

Where σ_a, Se, σ_m and S_a are the alternating stress in the presence of mean stress, alternating stress for equivalent completely reversed loading, the mean stress and the ultimate tensile strength, respectively. The typical representation of these mean stress correction method shown in fig4. The Basquin (1910) showed that alternating stress verses number of cycles to failure (S-N) in finite life region could be represented as a log-log linear relationship. Basquin equation was then used to obtain the fatigue life using the material properties listed in Table 4.. S-N approach uses to estimate the fatigue life for combined loading by determining an equivalent axial stress (Zoroufi and Fatemi, 2004) using one of the common failure criteria such as Tresca, von-mises, or maximum principal stress. The S-N equation is mathematically given by:

$$S_e = \sigma_f'(2N_f)^b$$

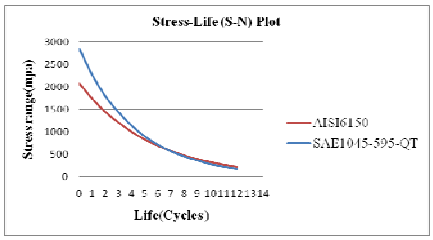

Figure 5. Stress-life (S-N) plot

Where S_e, σ_f',$2N_f$ and b are the stress amplitude, the fatigue strength coefficient, the reversals to failure and the fatigue strength exponent, respectively figure5 Shows comparison between the two materials with respect to S-N behaviour. It can be seen that these curves exhibit different life behaviour depending on the stress range experienced. From the figure, it is observed that in the long life area (high cycle fatigue), the different is lower while in the short life area (low cycle fatigue), the difference is higher. An important aspect of the fatigue process is plastic deformation. Fatigue cracks initiate from the plastic straining in localized regions. Significant localized plastic deformation is often present, total-life approach doesn't account for plastic strain. Main advantage of this method is that it accounts for changes in local mean and residual stresses. Therefore, cyclic strain-controlled fatigue method could better characterize the fatigue behaviour of materials than cyclic strain controlled fatigue particularly in notched members where the significant localized plastic deformation is often present. In the crack initiation approach the plastic strain is directly measured and quantified. The total- life approach does not account for plastic strain. One of the main advantages of this method is that it accounts for changes in local mean and residual stresses. In strain-

life when the load history contains large over loads, significant plastic deformation can exist, particularly at stress concentrations and the load sequence effects can be significant. In these cases, the crack initiation approach is generally superior to the total life approach for fatigue life prediction analysis. However, when the load levels are relatively low such that the resulting strains are mainly elastic, the crack initiation and total life approaches usually result in similar predictions. The crack initiation approach to the fatigue problem is widely used at present especially when the parabolic leaf spring are started or stopped then it is subjected to a very high stress range. The fatigue crack initiation approach involves the techniques for converting load history, geometry and material properties (monotonic and cyclic) input in to the fatigue life prediction. The operations involved in the prediction must be performed sequentially. First, the stress and strain at the critical site are estimated and rain flow cycle counting method is then used to reduce the load time history based on the peak –valley sequential. The next step is to use the finite element method to convert a reduced load time history in to a strain time history and calculate the stress and strain in the highly stressed area then the crack initiation methods are employed for predicting fatigue life. Following this, a simple linear damage hypothesis is used to accumulate the fatigue damage finally, the damage values for all cycles are summed until a critical damage some (failure criteria) is reached. In order to perform the fatigue analysis and to implement the stress strain approach in complex structures used strain life results which is simulated using the 3D models to assess fatigue damage. After the complex load history was reduced to an elastic stress history for each critical element, a Neuber plasticity correction method was used to correct for plastic behaviour. Elastic unit load analysis, using strength of material and an elastic finite element analysis model combined with a super position procedure of each load points service history was verified the local strain approach for fatigue evolution. In this study, it was observed that the local strain approach using the Smith-Watson-Topper (SWT) strain-life model is able to represent and to estimate many factors explicitly. These include mean stress effects, load sequence effects above and below the endurance limit and manufacturing process effects such as surface roughness and residual stresses.The fatigue resistance of metals can be characterized by a strain life curve. These curves are derived from the polished laboratory specimens tested under completely reversed strain control. The relationship between the total strain amplitude ($\Delta\varepsilon/2$) and reversals to failure ($2N_f$) can be expressed in following form (Coffin, 1954; Manson, 1953 [12, 13]) represents the typical total strain-life curves.

$$\frac{\Delta\varepsilon}{2} = \frac{\sigma_f'}{E}(2N_f^{\,b}) + \varepsilon_f'(2N_f^{\,c}) \quad (3)$$

Where, N_f is the fatigue life; σ'_f is the fatigue strength coefficient; E is the modules of elasticity; ε'_f is the fatigue ductility coefficient and c is fatigue ductility exponent. Morrow (1968 [14]) suggested that mean stress effects are considered by modifying the elastic term in the strain-life equation by mean stress (σ_m).

$$\varepsilon_a = \frac{\sigma_f' - \sigma_m}{E}(2N_f)^b + \varepsilon_f'(2N_f)^c \quad (4)$$

Smith (1970) was introduced another mean stress model which is called SWT mean stress correction model. It is mathematically defined

$$\sigma_{max}\varepsilon_a E = (\sigma_f')^2(2N_f)^{2b} + \sigma_f'\varepsilon_f' E(2N_f)^{b+c} \quad (5)$$

Where, σ_{max} is the maximum stress and ε_a is the strain amplitude.

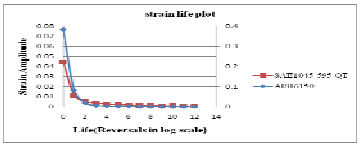

Figure 6. Strain-life (S-N) plot

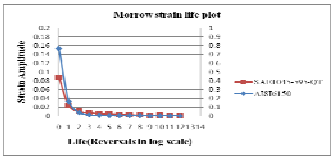

Figure 7. Morrow Strain-life (S-N) plot

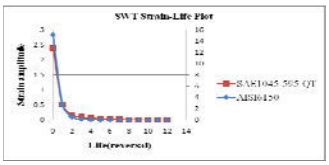

Figure 8. SWT Strain-life (S-N) plot

3.**Loading information.**

Loading is another major input for the finite element based fatigue analysis. Unlike static stress, which is analyzed with calculations for a single stress state, fatigue damage occurs when stress at a point changes over time. There are essentially four classes of fatigue loading, with the ANSYS Fatigue Module currently supporting the first three:

- Constant amplitude, proportional loading
- Constant amplitude, non-proportional loading
- Non-constant amplitude, proportional loading
- Non-constant amplitude, non-proportional loading

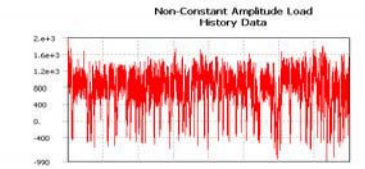

Figure 9. Non constant amplitude loading

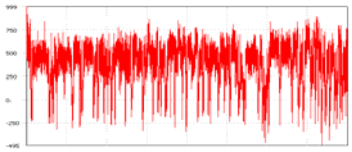

Figure 10. Transmission loading histories

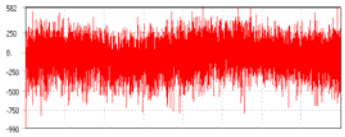

Figure 11. Bracket loading histories

Non-constant Amplitude, proportional loading within the ANSYS Fatigue Module uses a "quick counting" technique to substantially reduce runtime and memory. In quick counting, alternating and mean stresses are sorted into bins before partial damage is calculated. Without quick counting, data is not sorted into bins until after partial damages are found. The accuracy of quick counting is usually very good if a proper number of bins are used when counting. The bin size defines how many divisions the cycle counting history should be organized into for the history data loading type. Strictly speaking, bin size specifies the number of divisions of the rain flow matrix. A larger bin size has greater precision but will take longer to solve and use more memory. Bin size defaults to 32, meaning that the Rain flow Matrix is 32 x 32 in dimension. For Stress Life, another available option when conducting a variable amplitude fatigue analysis is the ability to set the value used for infinite life. In constant amplitude loading, if the alternating stress is lower than the lowest alternating stress on the fatigue curve, the fatigue tool will use the life at the last point. This provides for an added level of safety because many materials do not exhibit an endurance limit. However, in non-constant amplitude loading, cycles with very small alternating stresses may be present and may incorrectly predict too much damage if the number of the small stress cycles is high enough. To help control this, the user can set the infinite life value that will be used if the alternating stress is beyond the limit of the S-N curve. Setting a higher value will make small stress cycles less damaging if they occur many times. The Rain flow and damage matrix results can be helpful in determining the effects of small stress cycles in loading history. The component was loaded with two random time histories corresponding to typical histories for transmission and bracket components at different load levels. The detailed information about these loading histories was contained in the literature (Tucker and Bussa, 1977). These loading histories scaled to two peak strain levels and used as full length histories. Raw loading histories of the component are shown in Fig8 and 9. The terms of SAETRN, SAEBRAKT represent the loading-time history for the transmission and bracket respectively. The considered load histories are based on the SAEs profile. The abscissa uses the time in seconds.

3. FINITE ELEMENT ANALYSIS.

Numerical techniques are necessary to simulate the physical behaviour and to evaluate the structural integrity of the different designs. The objective of the current study are to calculate the fatigue life for a leaf spring of a heavy vehicle using total life and crack initiation methods, to investigate the effect of mean stress on fatigue life and the probabilistic nature of fatigue on the S-N curve via the design criteria.

4. RESULTS AND DISCUSSION.

The linear static finite element analysis was performed using ANSYS workbench finite element code. The equivalent vonmises stress contours and critical locations shown in figure 13. The eyes of

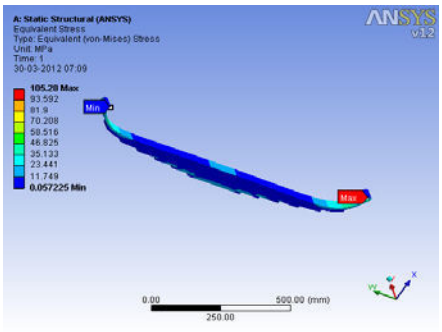

Figure 13. Stress concentration location

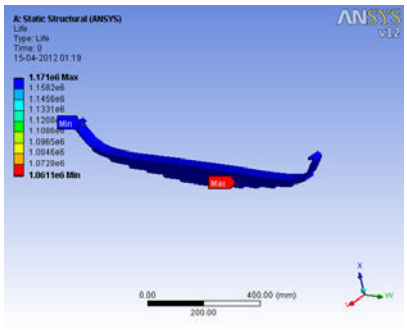

Figure 14. Life of the parabolic spring

Parabolic spring was found to be areas of high stresses. The von-mises equivalent stresses are used for subsequent fatigue life analysis and comparisons. However, in table 2, it can be seen that when using the loading sequences are predominantly tensile in the nature; the Goodman approach is more conservative. Gerber mean stress correction has been found to give conservative when the time histories predominantly zero mean.

From the table 3, it is also seen that two mean stress methods, SWT and Marrow give lives less than that achieved using no mean stress correction with the Marrow method being the most conservative for loading sequences which are predominantly tensile in nature. When using the time history has a roughly zero mean (SAEBRAKT) then two methods have been given approximately the same results. It can be also seen that SAE1045-595-QT is consistently higher life than SAE5160-825-QT, SAE1045-450-QT for all loading conditions.

Predicted life (10e5 sec)

Table 2. Predicted fatigue life using total-life approach

Loading conditions	AISI6150			SAE1045-595-QT		
	No mean	Goodman	Gerber	No mean	Goodman	Gerber
SAETRN	10.611	8.9201	9.8807	11.595	11.024	11.57
SAEBRAKT	2.4635	2.463	2.4087	3.2998	3.2996	3.2923

Table 3. Predicted fatigue life using crack-initiation approach

Loading conditions	AISI6150			SAE1045-595-QT		
	No mean	Marrow	SWT	No mean	Marrow	SWT
SAETRN	106.98	47.452	80.713	418.5	176.41	231.77
SAEBRAKT	118.19	28.864	31.694	420.81	68.072	93.29

The three-dimensional cycle histogram and corresponding damage histogram for materials using SAETRN loading histories is shown in the figures 15 and 16given below. Fig16 shows the results of the rain flow cycle count for the component It can be seen that a lot of cycles with a low stress range and fewer with a high range. The height of each tower represents the number of cycles at that particular stress range and mean. Each tower is used to obtain damage on the S-N curve and damage is summed over all towers. Figure 16.shows that lower stress ranges produced zero damage. It is also showed that the high stress ranges were found to give the most of the damage and a fairly wide damage distribution at the higher ranges which mean that it cannot point to a single event causing damage. Most realistic service situations involve nonzero mean stresses, it is, therefore, very important to know the influence that mean stress has on the fatigue process so that the fully reversed (zero mean stress) laboratory data are

usefully employed in the assignment of real situations.

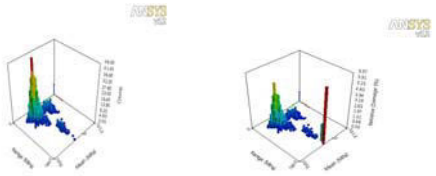

Figure 15 & Figure 16. Rain flow matrix and Damage Matrix

5. CONCLUSIONS.

A computational numerical model for the fatigue life assessment for leaf spring of the parabolic leaf spring is presented in this study. Through the study, several conclusions can be drawn with regard to the fatigue life of a component when subjected to complex variable amplitude loading conditions.

- The fatigue life was estimated based on Palmgren-Miner rule is non-conservative SWT correction and Morrows methods, and damage rule can be applied to improve the estimation. It can be seen that when using the loading sequences are predominantly tensile in the nature; the life of leaf spring in Goodman approach is 8.9201×10^5 sec which is more conservative.
- It can be seen that when using the loading sequences are predominantly zero mean (SAEBRAKT), the value of life of the leaf spring is 2.4087×10^5 sec in Gerber mean stress correction which has found to be more sensitive.
- It can be concluded that the influence of mean stress correction is more sensitive to tensile mean stress for total life approach. It is also seen that the two mean stress methods give lives less than that achieved using no mean stress correction.
- It is concluded for crack initiation approach that when the loading is predominantly tensile in nature, the life of the component in Morrow approach is 176.41×10^5sec which is more sensitive and is therefore recommended. When using the time histories has zero mean (SAEBRAKT) then all three methods have been given approximately the same results.

7. Acknowledgments.

The authors would like to thank the School of mechanical engineering, Faculty of Mechanical engineering, RVR&JC College of engineering for providing the excellent lab and library facilities and for their valuable suggestions regarding submission of this paper.

8. REFERENCES.

[1] Z. Xiulin, 2001. On some basic problems of fatigue research in engineering, *International Journal of Fatigue* 23, pp. 751–766

[2] A.Varvani-Farahani, M. Sharma, and M.R. Kianoush, 2005. Fatigue damage analysis and life assessment under variable amplitude loading conditions, *Materials Science and Engineering A* 403, pp. 42–47

[3] B. Li, L. Reis, and de Freitas, M. 2006. Simulation of cyclic stress/strain evolutions for

[4] multiaxial fatigue life prediction, *International Journal of Fatigue* 28, pp. 451–458.

[5] Leevy, G. And Cao, K. 2004. Evaluation of a Multi-Leaf Hybrid Springs for Automotive Suspensions *SAE Technical Paper Series 2004-01-0782*.

[6] Qing Li and Wei Li. 2004. A contact finite element algorithm for the multileaf spring of vehicle suspension systems. *Proc. Instn Mech. Engrs Vol. 218 Part D: J. Automobile Engineering D10802*

[7] Fischer, G., Streicher, M. and Grubisic, V. V. 1998. Durability approval of leaf spring under operational loading. *SAE paper 982839*.

[8] Fukui, H., Iwatsu, G. and Kato, J., 1974. *Leaf spring construction*, United States Patent,3814410.

[9] Grip, C.E., Hagstad, B.J. and Andersson, B.H., 1986. *Spring steel*, United States Patent,4575912.

[10] Ingvarsson, H. and Raattamaa, J-R., 1997. *Leaf spring for a rigid axle of a vehicle*, UnitedStates Patent, 5683076.

[11] SAE. *Manual on Design and application of leaf spring*, 1980. SAE HS-788. *Material Reference Materials Engineering-Mechanical Behavior Report*

[12] Lee, Yung-Li, Pan, J., Hathaway, and R., Barkey, M., 2005. *Fatigue testing and analysis, theory and practice*, UK: Elsevier Butterworth-Heinemann.

[13] Coffin, L.F. 1954. A study of the effect of cyclic thermal stresses on ductile metal, *Transaction of ASME* 79, pp. 931-950.

[14] Manson, S.S. 1956. Fatigue: a complex subject – some simple approximation. Experimental Mechanics 5, pp. 193-226.

[15] Morrow, J.D. 1968. Fatigue Properties of Metal Fatigue Design Handbook, Society of Automotive Engineers.

◈◈◈

Experimental Validation and Data Acquisition for Hyper elastic Material Models in Finite Element Analysis

[1]VENKATESH K & [2]P. L. SRINIVASA MURTHY

[1,2] Department of Mechanical Engineering ,
SVERI's College of Engineering, M.S. Ramaiaha Institute of Technology
Pandharpur, India, Bangalore, India

Abstract—This paper presents the theory, experiment setups and solution implementation of Hyperelastic Material Models in Finite Element Analysis to provide the description of material behavior that matches the conditions the product sees in real life. This can be a complex matter because the real life scenario may have the product responding simultaneously to a multiplicity of conditions such as rate, temperature and the environment. Physical testing of elastomers for the purpose of fitting material models in finite element analysis requires experiments like uniaxial tension, biaxial tension, volumetric compression in multiple states of strain under carefully considered loading conditions.

Keywords- *Finite Element Analysis, Hyperelastic Material Models, Elastomers, Volumetric compression test, Validation and Data Acquisition*

I. INTRODUCTION

Finite element analysis (FEA), including pre- and post processing, is seeing wider use despite being hampered by excessive setup time and computational requirements. 2-D applications outnumber 3-D applications due to scaling laws. Various engineers have been attributed to being the father of FEA, e.g., Courant (1943), However, the arrival of the digital computer especially in the aircraft industry led to a rapid interest in activity in the Boeing Corporation in the early 1950's. The Structural Dynamics Unit, led by M J Turner, formulated the method in 1954 and published it in 1956. The North American B-70 bomber was the first production airplane designed using FEA. The World Trade Center in New York and the John Hancock Center in Chicago were the first buildings designed on the basis of FEA.

Advances in automatic mesh generation algorithms have the potential to increase use of FEA methods by an order of magnitude. The integration of manufacturing applications into systems will be paced by software, and will be slow and incremental.

The basic concept of finite element method is discritization of a structure into finite number of elements, connected at finite number of points called nodes. The material properties and the governing relationships are considered over these elements and expressed in terms of nodal displacement at nodes. An assembly process duly considering the loading and constraints results in a set of equations governing the structural response, which are established through the application of appropriate variation principle. Solutions of these equations give the response of the structure. Selecting proper elements and subdividing the structure with large number of finite elements or by taking higher order elements can increase the accuracy of solution obtained by finite element method.

Hyperelastic models are used extensively in the finite element analysis of rubber and elastomers. These models need to be able to describe elastomeric behavior at large deformations and under different modes of deformation. In order to accomplish this daunting task, material models have been presented that can mathematically describe this behavior . There are several in common use today, notably, the Mooney-Rivlin, Ogden and ArudaBoyce.

II. HYPERELASTIC MATERIAL

Hyperelasticity refers to the materials, which can experience large elastic strain that is recoverable. Elastomer such as rubber and many other polymer materials fall in this category.

The microstructure of polymer solids consists of chain-like molecules. The chain backbone is mostly made up of the carbon atoms. The flexibility of polymer molecules allows different types of arrangement such as amorphous and semicrystalline polymers. As a result, the molecules possess a much less regular character than the metal crystals. The behavior of the elastomers are therefore very complex, on macroscopic scale, they usually behave elastically isotropic initially, and anisotropic at finite strain as the molecule chains tends to realign to loading direction.

Under essentially monotonically loading condition, however, a larger class of the elastomers can be approximated by an isotropic assumption,

which has been historically popular in the modeling of the elastomers.

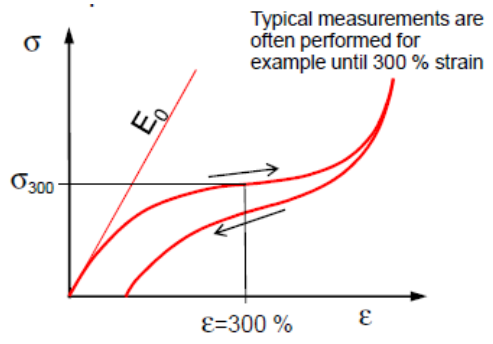

Fig. 1 Elastomer Material Behaviour

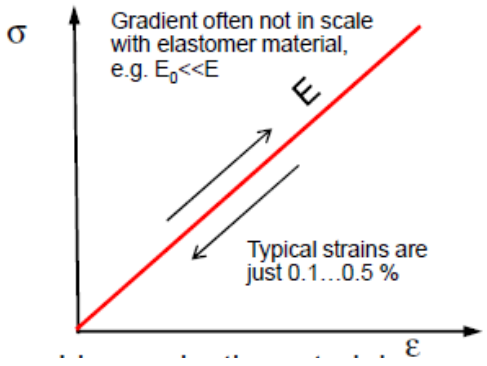

Fig. 2 Linear Elastic Material like brittle steel or ceramic

The constitutive behaviors of hyperelastic materials are usually derived from the strain energy potentials. Also, hyperelastic materials generally have very small compressibility. This is often referred to incompressibility. The hyperelastic material models assume that materials response is isothermal. This assumption allows that the strain energy potentials are expressed in terms of strain invariants or principal stretch ratios. Except as otherwise indicated, the materials are also assumed to be nearly or purely incompressible. Material thermal expansion is always assumed to be isotropic.

Elastomers are often modeled as hyperelastic. Elastomers (like rubber) typically have large strains (often some 100 %) at small loads (means a very low modulus of elasticity). The material is nearly incompressible, so the Poisson's ratio is very close to 0.5. Their loading and unloading stress-strain curve is not the same, depending on different influence factors (time, static or dynamic loading, frequency etc.). This viscous behavior is ignored if the hyperastic material model is used for description.

Force equals the spring rate times the deflection is one of the first equations an engineer meets. This equation is valid as long as the object remains linearly elastic. If one deflects the component twice as much, the force increases twice as much. If the structure yields, or large displacements occur, or the material for the spring has a non-linear stress-strain curve It may have a non-linear problem and not even know it.

III. CHOOSING A MATERIAL MODEL

The hyperelastic material models present a number of options to aid in a best fit of the material data. Mooney-Rivlin model is the by far, the most common model in use today. It presents many advantages in terms of being able to handle the different kinds of behavior seen in rubbers. The ability to increase the number of modes permits the handling of large strain behaviors with some level of dexterity. The objective of any model development effort however, is to fit the data at as low a number of modes as possible.

The effect of weathering or the presence of oil, gasoline, body fluids or other chemicals can significantly affect the behavior of a material. The consequence of the environment is often unpredictable and may improve or adversely affect the performance of the product.

A classic example may be the rubber boot of an automotive CV joint that is simultaneously seeing large deformation, temperature, cyclic loading and oil or grease. To completely describe the material behavior would require a hyperelastic model on an oil soaked boot rubber over a range of temperatures with some consideration given to rate dependency. It becomes highly impractical to attempt to model all these situations. Accordingly, one often adopts a strategy that seeks to use the simplest acceptable model that achieves a reasonable approximation of the actual scenario. This strategy may be weighted to include a more detailed modeling of the greatest potential sources of failure. Careful thought given to material modeling at the start of the FEA project results in considerable savings in time, money and effort.

The form of the Mooney-Rivlin strain energy potential is

$$U = C_{10}(\bar{I}_1 - 3) + C_{01}(\bar{I}_2 - 3) + \frac{1}{D_1}(J^{el} - 1)^2,$$

The three stretch invariants (because independent from the used coordinate system) of the characteristic equation are analog:

$$I_1 = \lambda_1^2 + \lambda_2^2 + \lambda_3^2$$
$$I_2 = \lambda_1^2\lambda_2^2 + \lambda_2^2\lambda_3^2 + \lambda_1^2\lambda_3^2$$
$$I_3 = \lambda_1^2\lambda_2^2\lambda_3^2 = 1 + \left(\frac{\Delta V}{V}\right)^2 = J^2$$

Where C10, C01 and d are material constants.

If C01 = 0, we obtain a neo-Hookean solid, a special case of a Mooney–Rivlin solid.

The nominal or engineering strain is defined as the change in length divided by the original length:

$$\varepsilon = \frac{l_1 - l_0}{l_0} = \frac{\Delta l}{l_0}$$

The stretch ratio l now is another fundamental quantity to describe material deformation. It is defined as the current length divided by the original length:

$$\lambda = \frac{l_1}{l_0} = \frac{l_1 - l_0 + l_0}{l_0} = \varepsilon + 1$$

Analog to the three principal strains, we obtain from the principal axis transformation the three principal stretch ratios

$$\lambda_1, \lambda_2, \lambda_3.$$

IV. NON-LINEAR ANALYSIS TYPES

A. *Three major types of Non-linearity:*

1) *A geometric non-linearity:* It is due to large deformations or snap-through buckling.

2) *A material non-linearity:* It is due to large strains, plasticity, hyperelasticity, creep, or viscoelasticity.

3) *A boundary non-linearity:* It is due tothe opening/closing of gaps, contact surfaces, and follower forces.

B. *Types of Material Non-linearity*

When stresses go beyond the linear elastic range, material behavior can be broadly divided into two classes:

1) Time-independent behavior:

Pasticity that is applicable to most ductile metals; non-linear elasticity that is applicable to rubber.

2) Time-dependent behavior:

creep, and visco-elasticity that are applicable to high-temperature uses; viscoelasticity that is applicable to elastomers and plastics.

IV. EXPERIMENTAL VALIDATION AND DATA ACQUISITION

The FE experiments, covering several temperatures, strain rates, material models and combinations of input test data, generated a large quantity of results. These were plotted in the form of reaction force/length versus strain (gauge extension/bond thickness) in order to qualitatively compare the results with measured data. Statistical DOE methods were considered as an option for the analysis of this data. This type of analysis would require a single value as the 'experimental' result.

The most models share common test data input requirements. In general, stress and strain data sets developed by stretching the elastomer in several modes of deformation are required and "fitted" to sufficiently define the variables in the material models. Appropriate experimental loading sequences and realistic strain levels are needed to capture the elastomer behavior that applies in the analysis.

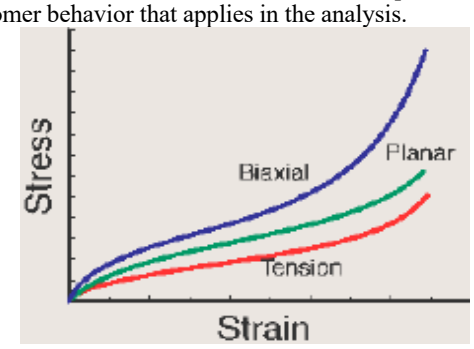

Figure.3 Final Data Set for Input into a Curve Fitter

a. *Uniaxial Tension Experiment setup*

This is the classical uniaxial tension rod mounted into a tensile testing machine. The strain must of course be measured in the thinner area of the test rod,for example by optical scanning (video extensometry); the thicker parts of the tension rod which are clamped must not be taken into account.

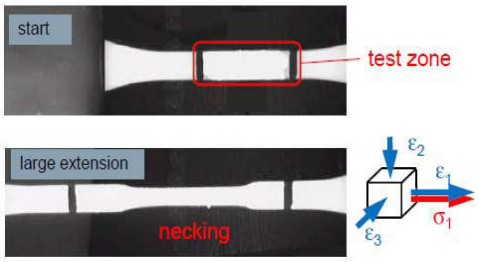

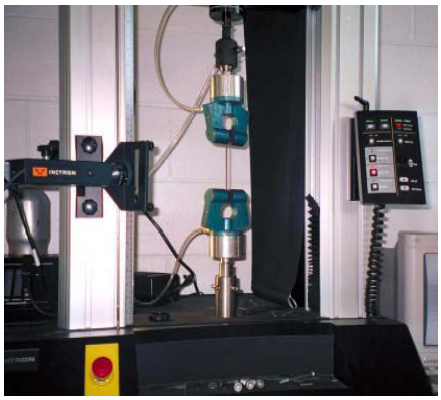

Fig.4 Uniaxial Tension rod

Fig.5 A Tension Experiment using a Video Extensometer

b. Biaxial Tension Experiment setup

This is a disk under equibiaxial tension. The specimen mounted into a "scissor" fixture for an uniaxial testing machine and the stress state may look as follows:

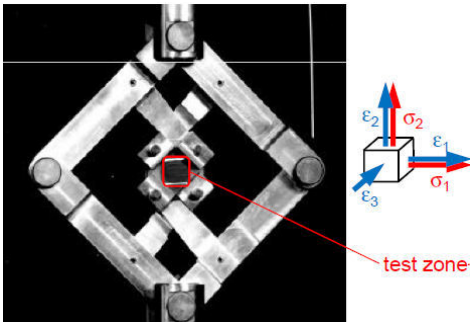

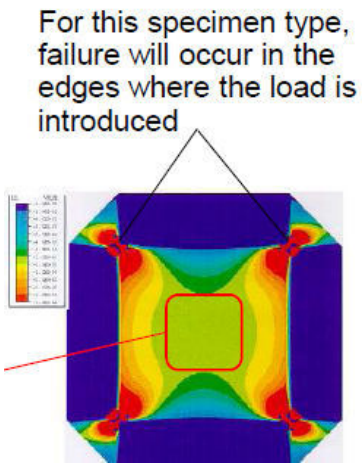

Fig.6 Biaxial Test setup and Analysis of Specimen

c. Volumetric Compression Test setup

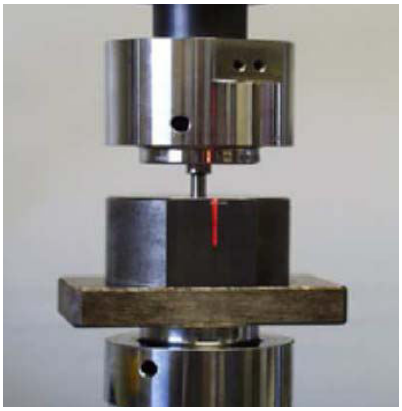

Fig.7 A Volumetric Compression Test setup

A volumetric test setup like this compresses a cylindrical elastomer specimen constrained in a stiff fixture. The actual displacement during compression is very small and great care must be taken to measure only the specimen compliance and not the stiffness of the instrument itself. The initial slope of the resulting stress-strain function is the bulk modulus. This value is typically 2-3 orders of magnitude greater than the shear modulus for dense elastomers.

d. Physical Testing and Validation

Although the experiments are performed separately and the strain states are different, data from all of the individual experiments is used as a set. This means that the specimens used for each of the experiments must be of the same material. This may seem obvious but if the specimens are specially molded to accommodate the differing instrument clamps for different experiments, it is possible that the material processing parameters may cause material variations from test to test. While it is reasonable to assume that

variation exists in the production environment and that we can never really get the exact material properties every time, it is not acceptable to have this same variation within the data set. The data represents a "snapshot" in time. If even slight variation exists between experiments, a physically impossible material model may be developed in the analysis software. The best way to avoid this problem is to cut specimens for simple tension, pure shear and equal biaxial extension from the same slab of material. The loading conditions, strain levels and straining rates should also be developed considering the inter-relationship between tests.

FEA Engineer requires support from test department for the activities namely Data acquisition for input(boundary conditions), Validation of FEA results and Field/laboratory failure reports.

e. Limitations of Hyperelastic Material Models

Most material models in commercially available finite element analysis codes allow the analyst to describe only a subset of the structural properties of elastomers. This discussion revolves around hyperelastic material models such as the Mooney-Rivlin and Ogden formulations and relates to those issues which effect testing.

- The stress strain functions in the model are stable. They do not change with repetitive loading. The material model does not differentiate between a 1stt time strain and a 100th time straining of the part under analysis.
- There is no provision to alter the stress strain description in the material model based on the maximum strains experienced.
- The stress strain function is fully reversible so that increasing strains and decreasing strains use the same stress strain function. Loading and unloading the part under analysis is the same.
- The models treat the material as perfectly elastic meaning that there is no provision for permanent strain deformation. Zero stress is always zero strain.

f. Hints for Elastomeric FEA

- Stay away from triangular elements. Elements with 2 displacement BC will have only 1 degree of freedom due to incompressibility.
- Low order elements converge easiest. 4-node brick works well.
- Sliding contact may require non-symmetric stiffness matrices for large friction coefficients.
- Watch corners for element distortion.
- u-P element formulation is most stable.
- Check for stability of material models.

V. CONCLUSION

Finite Element analysis helps in accurating design and development of products by minimising number of physical tests, there by reducing cost of prototyping and testing. Here an attempt is made to throw a light on Experimental Validation and Data Acquisition for Hyperelastic Material Models which present new challenges in automotive, aerospace, consumer goods and industrial products.

REFERENCES

[1] K.J. Bathe, "Finite Element Procedures", Prentice-Hall, 1996.

[2] W.C.Young, R.G. Budynas, "Roark's Formulas for Stress and Strains" 7th Edition, McGraw Hill.

[3] O. C. Zienkiewicz and R. L. Taylor, "The Finite Element Method" Volume 2 Solid Mechanics, 2000.

[4] Robert. D. Cook, Davis S Malkus, Michael E Pleasha, "Concepts and applications of Finite Element Analysis", 3rd Editions, John Wiley and Sons.

[5] Nitin S Gokhale, Sanjay S Deshponde "Practical Finite Element Analysis" Finite to Infinite, 2008.

[6] Gent, A.N., "Engineering with Rubber", Oxford University Press, New York, NY, 1992.

[7] Ferry, J.D. "Viscoelastic Properties of Polymers" (2nd Ed.), John Wiley & Sons, New York, NY, 1970.

[8] Wolf, D. and Miller, K. "Experimental Elastomer Analysis", Presented at a meeting of the Rubber Division, American Chemical Society, Orlando, Florida, September 21-24, 1999.

[9] Dalrymple, T., "Experimental Elastomer Analysis Course Notes", Ann Arbor, Michigan, January, 1998.

[10] Bruce Duncan, "Test Methods for Determining Hyperelastic Properties of Flexible Adhesives", Centre for Materials Measurement and Technology National Physical Laboratory paper, CMMT (MN)054 1999.

[11] Kaliske,,M., H.Rothert, "On the Finite Element Implementation of Rubber-like Materials at Finite Strains," Engineering Computations, vol.14, 1997.

◈◈◈

Core Stabilization for FRP Sandwich Composite Structure to improve Mechanical Properties

[1]SANJAY CHOUDHRY & [2]SATYA RANJAN DAS

BEE Certified Energy Auditor
CIPET-Lucknow

ABSTRACT- "A composite material is one, which is composed of at least two elements working together to produce material properties that are different to the properties of those elements on their own. In practice, most composites consist of a bulk material (the 'matrix'), and a reinforcement of some kind, added primarily to increase the strength and stiffness of the matrix". FRP (Fibre Reinforced Plastic)Sandwich structure are defined as a three layer type of construction a thick layer known as core and two thin polymer layer. For this study to minimize the component weight & to improve mechanical properties hexagonal shape aluminium honeycomb used as a core material with density of 2.4g/cc and prepreg (epoxy+carbon) used as face material.

In High strength composites utilize carbon fibre with density-1.8g/cc as reinforcement. The main purpose of FRP Sandwich Composite is to support engineering application. Mainly to reduce the weight and increases the strength without core crushing. The core crushing is nothing but it is a dimensional destruction in sandwich structure. The core crushing can be avoided by incorporating a solid PU foam which provide housing to the hexagonal honeycomb.

INTRODUCTION

A composite is comprised of two or more different materials or different phases of same material with the properties being better than that of the component materials. The properties of the new structure are dependant upon the properties of the constituent materials as well as the properties of the interface.

FRP Composite materials used in Engineering Application specially in Aerospace & automobile parts typically are produced by combining layers of carbon or glass fibres with epoxy because these materials are typically lighter and more resistant to corrosion & obtained good mechanical properties. The properties of the composite are determined by

1. The properties of the fibres.
2. The properties of the resin.
3.The ratio of fibre to resin in the composites.
4. The geometry and orientation of the fibres in the composite

Characterizations of Raw material:

Thermal Characterization:

DSC VALUE OF RAWMATERIAL

Sl No	Raw material	Onset Temp(°C)	Peak Temp(°C)
1	Carbon G801	141.70	154.23
2	Glass 120	143.52	154.44
3	FM73	123.53	154.63
4	FM 490A	140.63	153.39

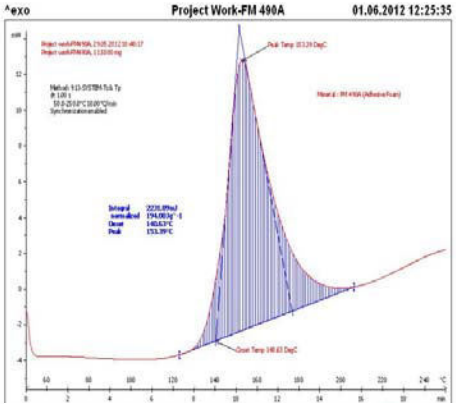

DSC OF FM490A DSC OF FM73

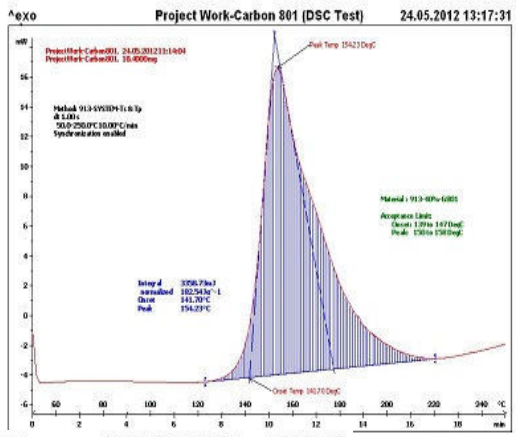

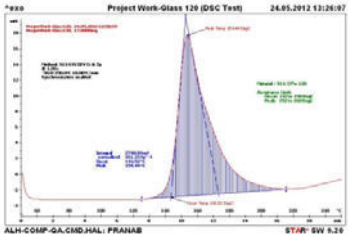

Sample no	Sample size(mm)	Bk . load(N)	Comp strength(MPa)
1	50×50×30	1793.4	0.7252
2	50×50×30	1783.6	0.71344
3	50×50×30	1803.2	0.72912
4	50×50×30	1832.6	0.74088
Avg			0.72716

DSC OF CARBON 801

DSC OF CARBON GLASS 120

Mechanical Characterization :

COMPRESSION TEST ALU HONEYCOMB

COMP STRENGTH OF PU SOLID FOAM

Experiment Details:

The Base plate(open mould) cleaned and mould releasing agent are applied on it. Then the Seven layers of prepegs (Epoxy +carbon fiber) are lay up in an orientation of 45°/ 90° on the surface of the Base plate and one layer of FM73adhesive lay up on it. In next step four pieces of solid PU foam are cut from a PU foam mat in to a desire dimension and 45°chamfer angle made . Then solid PU foam are cured in two stages by an autoclave. In first Stage cured at 75°C temperature, Heating Rate 1-2°C/Min, Pressure 1bar,Vacum0.8bar, hold on time 40min.In second stage cured at 135°C temperature, Heating rate 3-5°C/Min, pressure 2bar,vacum 0.2bar,hold on time 60min.then cooling rate follows 3-5°/Min. After curing four pieces of PU foam are joined by adhesive (special type of thermoset adhesive) to form a square shape which provide housing for hexagonal shape honeycomb. Then Pre compaction done by vacuum bag process by applying 0.8mb pressure .Special type adhesive(FM490A)

applied to the inner site area of the PU foam which bind the 25mm thickness hexagonal aluminum honeycomb. Then one layer of FM73 Adhesive and three layer of prepreg are lay up in an orientation of 45° /90° & finally a glass fiber prepreg 45°(37% epoxy+63%glass) one layer lay up on it. After completing all the sampling process,0.8 vacuum pressure is applied by vacuum bag method to remove air from the layer of prepreg. Then samples are sent to an Autoclave. In an autoclave 135°C +/- 5°C, Pressure 2bar, hold on time 65min,vaccum2br, maintain to cure the sample. Similarly same procedure followed for the second sample without PU foam

TEMPERATURE CYCLE

HEATING RATE:

1-2 ° C/ MIN

FIRST DWELL:

75 ± 5° C , 40 + 5 MIN

HEATING RATE:

1-2 ° C/ MIN

SECOND WELL:

135 ± 5° C , 60 + 5 MIN

COOLING RATE:

3-5 ° C/ MIN

PRESSURE CYCLE

A-1 BAR (Gauge Pressure)

B-2 BAR (Gauge Pressure)

VACUUM CYCLE

A'-0.8 BAR (Gauge Pressure)

B'-0.2 BAR (Gauge Pressure)

FIR

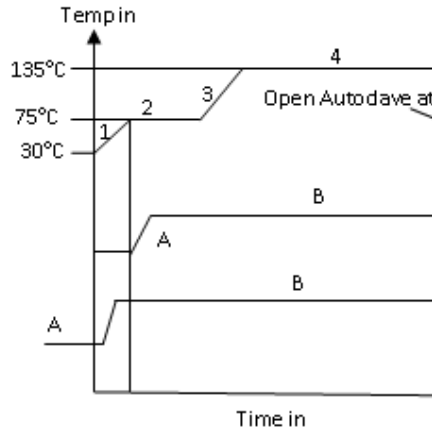

75 ± 5

Step- 1

Step -2

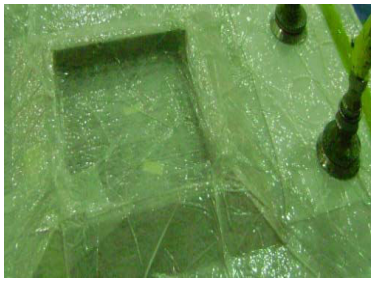

Step-3

(Prepreg layup)

(PU solid foam Assembly)

(Vacuum Bag)

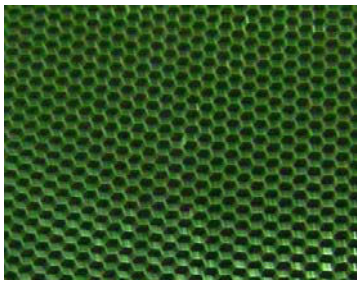

Step-4 Step -5(A)

Step -5(B)

(Aluminium Honeycomb) (Core Stabilize with PU foam) (Core Crushing)

RESULT :

UNSTABILIZED FRP SANDWICH
STABILIZED FRP SANDWICH

1.CORE CRUSHING

1. CORE CRUSHING ABSENT

2.C -SCAN
2. C-SCAN

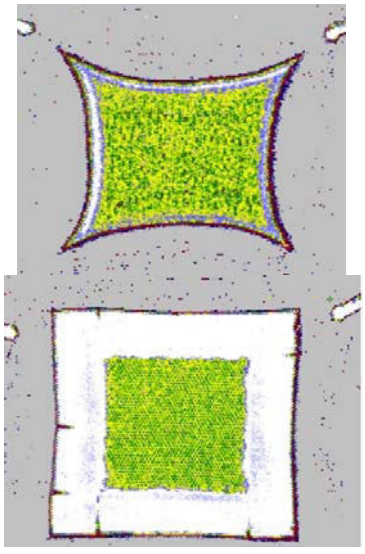

3.ILSS- 39.342MPa
3.ILSS-65.0068MP

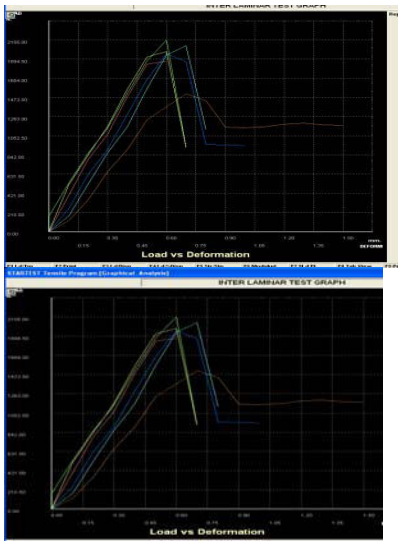

4. .FLEXURAL STRENGTH-825MPa
2-FLEXURAL STRENGTH-896 MPa

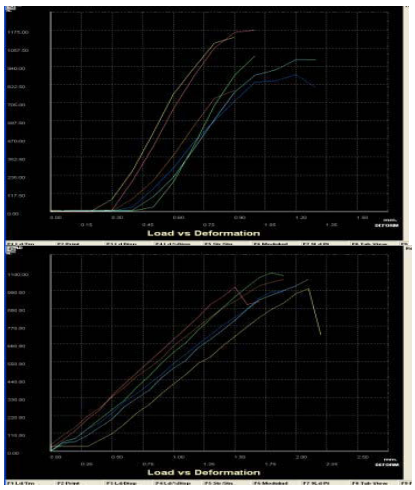

5-COMPRESSION STRENGTH-76.175 lb/sq.in
5-COMPRESSION STRENGTH-136.2lb/sq.in

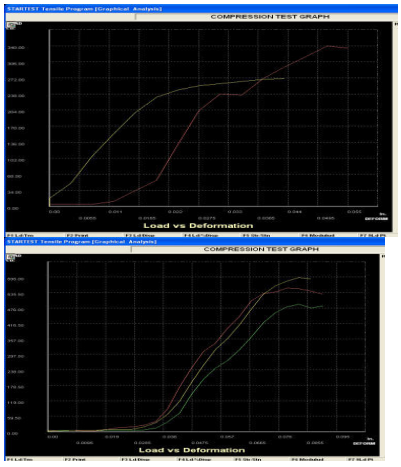

CONCLUSION :

FRP sandwich composite stabilize with PU Solid foam frame at a temperature of 135°C. By stabilizing the FRP sandwich structure the weight reduce and ILSS, Compressive Strength Increases which is suitable for Automobile, Aerospace and other Engineering Applications. From the above experiment it conclude that due to Pressure, Temperature, Vacuum with respect to Time core crushing occurred .

REFERENCE:

1. M. V. Hosur, M. Abdullah, S. Jeelani, "Manufacturing and Low-velocity impact characterization of foam filled 3-D integrated core sandwich composites with hybrid face sheets", Composite Structures, Volume 69, 2005.
2. M. V. Hosur, M. Abdullah, S. Jeelani, "Dynamic compression behaviour of integrated core sandwich composites", Materials Science and Engineering, Volume 445-446, 2007.
3. M. V. Hosur, M. Abdullah, S. Jeelani, "Manufacturing and Low-velocity impact characterization of foam filled 3-D integrated core sandwich composites with hybrid face sheets", Composite Structures, Volume 69, 2005
4. Street KN, 1971, Proc NPL Conference on *The Properties of Fibre Composites* , Nov 1971, Teddington, UK,(IPC Science & Technology Press, Guildford, Surrey), 36-46
5. Kim, H.S. and Oh, H.H. (2000). Manufacturing and impact behaviour of syntactic foam, J *Appl poly sci.*
6. Gupta, N. and Woldesenbet, E. (September, 2001). Stress concentration factor approach to analyze the deformation and fracture behaviour of particulate composites, In: *Proceedings of ASC 16th Annual Conference*. Blacksburg,
7. Mallick P.K., Composite Engineering Handbook,1997, Marcel Dekker Inc., New York, USA.
8. Noor, A. K., Burton, W. S., and Bert, C. W*., 1996.* Computational models for sandwich panels and shells, *Applied Mechanics Reviews*, Vol.49, No. 3, pp. 155-199
9. Rose, C. A., Moore D.F., Knight N. F., and Rankin C. C. 2002 Finite element modelling of the buckling response of sandwich panels, *AIAA* 2002, pp1-19.
10. Shekhar V., effect of Fibre Architecture on Properties of Pultruded Composites, M.S. Thesis, West Virginia University, Morgantown, WV 2007.
11. Summerscales J., 1998, Microstructural Characterization of Fibre-Reinforced Composites, Woodhead Publishing Ltd., Cambridge, England.
12. Vadlamani V., Strain Energy Density based Failure Criterion for GFRP Coupons under Tension and Bending, M.S. Thesis, West Virginia University, Morgantown WV 2006.
13. Vinson J.R., 1999, The Behaviour of Sandwich Structures of Isotropic and Composite Materials, Technomic Publishing Co.Inc, Pennsylvania USA
14. Yuan, W.X and Dave, D.J., 2001. Overall and local buckling of sandwich plates with laminated faceplates, Part II: Analysis, *Computer Methods in Applied Mechanics and Engineering*, Vol. 190, pp. 5215-5231.
15. Whitney J.M. and knight M., 1980, The Relationship Between Tensile Strength and Flexure Strength in Fibre-reinforced Composites, *Experimental Mechanics,*
16. Wisnom M.R., 1992, The Relationship between Tensile and Flexural Strength of Unidirectional Composites, *Journal of Composites Materials*, Vol. 26.
17. Lekhnitskii, S.G., *Elasticity of an Anisotropic Body*, p. 30.
18. Camponeschi, E.T., Jr., *Compression Response of Thick-Section Composite Materials*,DTRC-SME-90/90, August 1990.
19. Abdallah, M.G., et al., *A New Test Method for External Hydrostatic Compressive Loading ofComposites in Ring Specimens*, Fourth Annual Thick Composites in Compression WorkshopKnoxville, TN, June 27-28, 1990.
20. Bode, J.H., *A Uniaxial Compression Test Fixture for Testing Thick-Section Composites*,Fourth Annual Thick Composites in Compression Workshop, Knoxville,
21. Goeke, E.C., "Comparison of Compression Test Methods for "Thick" Composites," *CompositeMaterials; Testing and Design (Eleventh Volume), ASTM STP 1206*, ed. E.T. Camponeschi,American Society for Testing and Materials, 1993.
22. *Engineering Materials Handbook, Vol. 1, Composites*, ASM International, 1987.
23. Knight, M., "Three-Dimensional Elastic Moduli of Graphite/Epoxy Composites," *Journal ofComposite Materials*, Vol. 16, 1982, pp. 153-159.
24. Sandorf, P.E., "Transverse Shear Stiffness of T300/5208 Graphite-Epoxy in Simple Bending,"Lockheed-California Co. Report No. LR 29763, Burbank, CA, Nov.
25. Camponeschi, E.T., Jr., "Compression Response of Thick-Section Composite Materials ,"David Taylor Research Center Report No. DTRC SME-90-60, Oct. 1990.
26. Christensen, R.M. and Zywicz, E., "A Three-Dimensional Constitutive Theory for Fiber Composite Laminated Media," *Journal of Applied Mechanics*, Jan. 1990.
27. Sun, C.T. and Li, S., "Three-Dimensional Effective Elastic Constants for Thick Laminates,"*Journal of Composite Materials*, Vol. 22, No. 7, July, 1988.
28. Pagano, N.J., "Exact Moduli of Anisotropic Laminates," *Mechanics of Composite Materials*,ed. G. Sendeckyj, Academic Press, 1984, pp. 23-44.
29. Trethewey, B.R., Jr.,Wilkins,D.J.,and Gillespie,J.W.Jr."Three-Dimensional Elastic
30. Camponeschi, E.T., Jr., *Compression Response of Thick-Section Composite Materials*,DTRC-SME-90/90, August 1990.
31. Abdallah, M.G., et al., *A New Test Method for External Hydrostatic Compressive Loading of Composites in Ring Specimens*, Fourth Annual Thick Composites in Compression Workshop,Knoxville, TN, June 27-28, 1990.

◈◈◈

Efficient Cooling of Building Using Phase Change Materials Along with Coolant

[1]S. MATHANA KRISHNAN, [2]M. JOSEPH STALIN & [3]P.BARATH

Thiagarajar College of Engineering
Department of Mechanical Engineering
Madurai, India

Abstract*:* Due to upsurge in the global warming day by day, ambient temperature escalates imperceptibly and hence the residence in the tropical region experiences severe hot climate which induces the need of Air Conditioning and Refrigerants. This paper focuses on theoretical analysis on cooling of building using Phase Change Material. In existing systems, the backup time for Phase Change Material gets over by the day, so in night time it can't be used. This is the main shortcomings of this system. In order to overcome this, coolant is used to promulgate in aluminium bent shaped tube kept inside the slab of Phase Change Material in a well designed manner. In this paper, water is used as a coolant and is promulgated from the overhead water tank. In overall process, the room heat is carried away by the coolant from the overhead water tank. This leads to cool the Phase Change Material and in night time also it is possible to operate the system. The results of this paper show the time of cooling for a pondered volume of room and also its cost analysis. Factors like design, volume and selection of Phase Change Material etc., are carefully acclimatized to achieve effective forced convective heat transfer and efficacious cooling takes place. Finally this could become a great surrogate for Air conditioning.

Keywords – *Coolant; Phase Change Material; Reduce Carbon emissions; Energy efficient*

I. INTRODUCTION

As demand for Air conditioning and Refrigerants are emphatically enhanced during last decennium, it should be economically abated in order to obtain comfort cooling in buildings. During scorching summer, peak demands of electric power is escalating year by year and limited reserves of fossil fuels have led to a surge of interest with efficient energy application. Usually, day time load has become double that of the night time load. This is due to usage of Air Conditioner both in day as well as in the night. Therefore our system would be the best way to eradicate the peak demand of using electricity during night as well as day time, thereby reducing air conditioner load.

This paper focuses on cooling of building by using slabs of Phase Change Material which is very attractive because of its high thermal storage capacity. Choice of Phase Change Material plays a substantial role in addition to heat transfer mechanism in Phase Change Material. A Phase Change Material of desired operating range is picked out and when the ambient temperature is beyond the melting point of Phase Change Material, it absorbs the heat by melting since it has amble of latent heat storage. The molecules of Phase Change materials are encapsulated in a glassy substance and hence it stores the lavish amount of heat energy than in other previously existing thermal storage devices. Latent heat storage is a recent area of study and it received hefty attention during early 1970s and 1980s. In this paper, Phase Change materials are arranged in such a way that there should be air gap between each slab and mass flow rate of air was made forcefully by means of external agency and the hot air in the leeway will promulgate through the air gaps. Hence the heat is transferred to Phase Change Material which in turn heat is carried away by the water coolant from the overhead water tank. This can be made possible by passing the aluminium tubes of calculated diameter with number of bents which are made to enlarge the surface area of contact. Air is made to pass through each slabs of Phase Change Material. By this way this system extends the usage of air coolness in the night time with minimum load as possible. This system can be extended to cool the leeway within a short span of time by using a better coolant and with a proper design. In general, there will be carbon emissions due to the usage of air conditioning which could be completely eradicated by fixing this method and this could also completely abates the carbon emissions due to decrease of peak power generation supplied by oil thermal power plants. Although the initial cost for mounting of Phase Change Material and its arrangements and construction are high, it will cool the leeway to a comfort level by free of cost (by neglecting the cost of electric current consumed by the fan which induces the forced convection process).This system not only reduces the cost of electricity due to air conditioner load but also it abates the huge investments in new electricity generating plants.

II. DESCRIPTION

In India, there is scorching summer and all of us are longing of comfort cooling. This can be accomplished only by means of investing conventional energies. Alternative solutions for cooling of leeway have appeared in practice as a counterweight to expensive energy wasting conventional systems. Researchers are working for utilizing the night coolness to impart cooling effect

during day, without using enormous energy. The system is designed for absorbing night coolness and gives it back in day time. Phase change materials are used for the purpose of imparting cooling effect. These are one of the efficient thermal energy storage materials. At the beginning, Phase change materials are in idle mode when they are purchased from the chemical industry. Soon after it was incinerated to the temperature of 50 degree Celsius using water bath so as the passive crystals of PCM melts. At this moment, the Phase Change Material is made active. Then the aluminium packets are used to seal the Phase Change Material and its better conductivity is the ultimate reason for its preference.

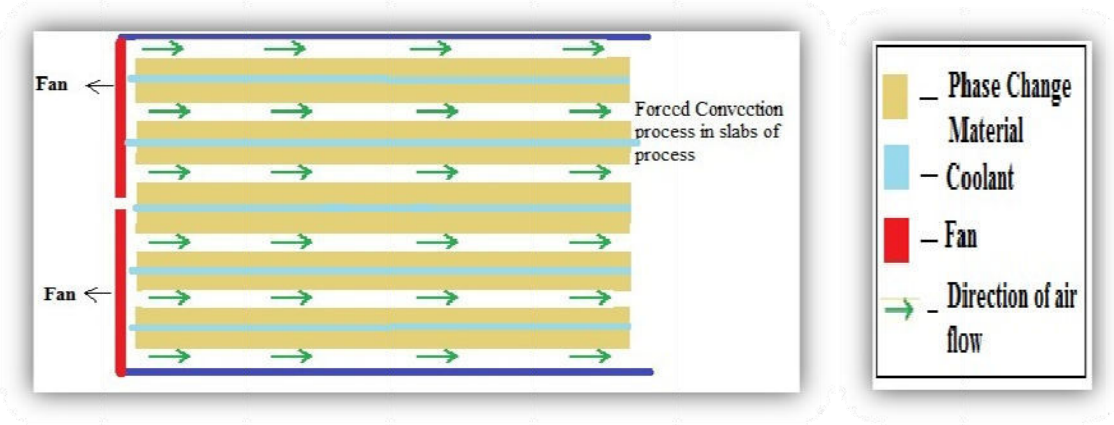

Fig1. Cooling of air using phase change materials

For example, the room size 20*20*20 ft is pondered for calculating its cooling effect. It consists of five PCM slabs with six air gaps in it. The design of the system is based on the heat load acting in the room. Various types of PCM are commercially available in the shops. Selection of PCM depends upon its latent heat and melting point since they are the major parameters for absorbing room heat. By considering several parameters, HS 29 type phase change material is selected. The property of PCM is absorption of latent heat during change of phase. The shape of the PCM slab is rectangular in cross section. The selection of this shape is for efficacious heat transfer from room to PCM slab. The dimension of one slab is 1000mm*303mm*60mm. These are calculated by using heat load of room, mass and volume of PCM. The air gap is taken as 15mm. The hot air from the leeway passes through the air gap where it transfers heat to the PCM. The maintenance of constant mass flow rate is mandatory and so we are in need of mounting fan. We are affixing one fan for every two air flow gaps. These fans regulate the mass flow rate of inlet air. The RPM of fan is calculated by considering the diameter of fan. Then the RPM is set constant for maintaining constant mass flow rate. There are five PCM slabs with four air gaps and so total height of PCM is 363mm. The required floor space for mounting the PCM is 1000mm*303mm*363mm. We are using water as a coolant for transferring heat from the PCM to outside of the room. The small aluminium tubes are fitted which has the inlet from water tank of the residence and it has the outlet to the environment. The aluminium material is selected for its good conductivity and the heat absorbed from the room by the PCM is taken away by the water from the tank. The insulated pipe is fitted from water tank to the inlet of the PCM and it is coupled with aluminium tubes which are fitted inside the PCM. Self regulating valves are fitted in the inlet of the insulated piping for controlling the mass flow rate of water. According to the prevalence of temperature in the PCM, the heat is efficaciously transferred by the water within certain time. The backup time is made infinity by installing heat exchanger. The diameter of tube is 10mm with 10 bents in one slab. The reason for bending of tube is to make contact of larger surface area with PCM for effective heat transfer. A pump is needed for recirculation of water from the tank. The tank must be insulated to maintain water at low temperature for increased efficiency. The power for pump could also be taken by installing solar panel.

III. WORKING

Overall working of the system is dependent on the effective heat transfer in the system. Five PCM slabs and six air gaps constitute the system. The PCM slabs are designed in such a way that it absorbs maximum amount of heat from the room. Imparting cooling effect to the room indicates extracting and transferring the heat from leeway to alfresco

Our ultimate aim of the system is to impart coolness to the leeway by absorbing night coolness. environment. The selected PCM has the melting point of 29 degree Celsius. Temperature of room is chosen as 34 degree Celsius. Naturally heat flows from higher temperature to lower temperature. So air from the leeway passes through the air gap and the heat is efficaciously transferred to the PCM.

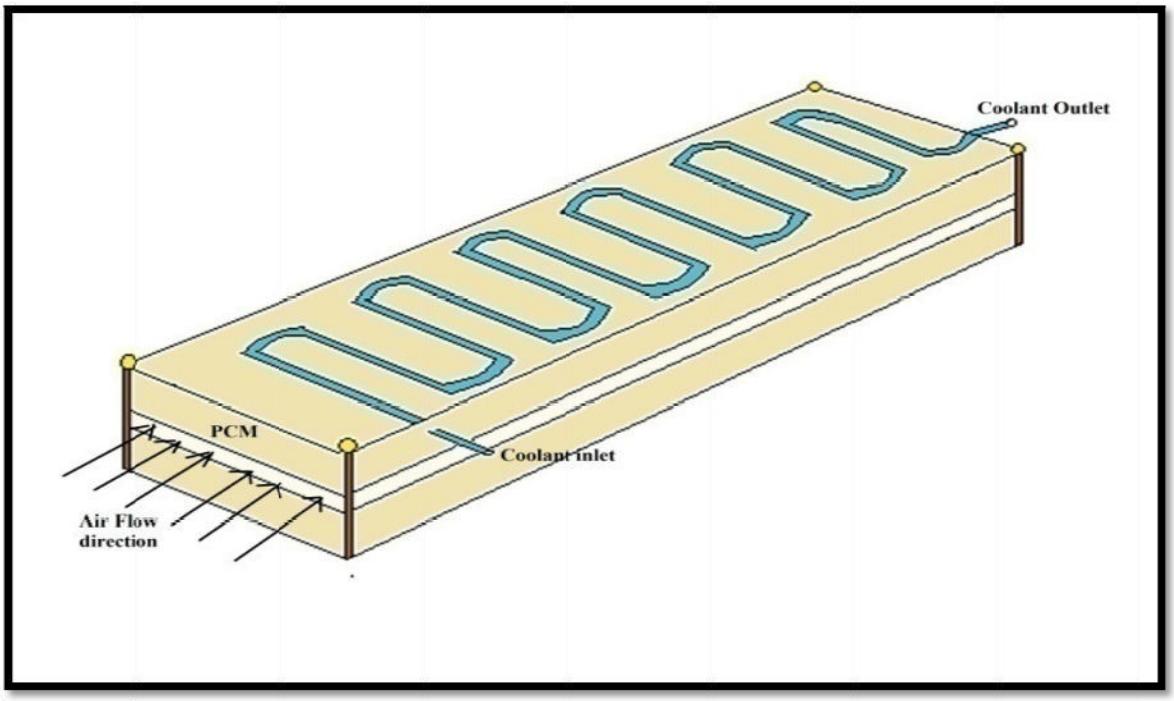

Fig2. Working of PCM along with coolant

The mass flow rate of air is kept constant for efficient heat transfer. For this purpose, a fan is mounted in the inlet of the air gap with constant RPM. Constant mass flow rate is given by the fan. The mounting of one fan is for two air gaps and the fan diameter is 90mm. Heat transfer takes place until it attains equilibrium and when the backup time is over, it emits heat in the night. This is the hefty problem in all of the existing systems. In order to avoid this problem, we are using small aluminium tube of 10mm which has 10 bents is sealed inside the PCM. The tank and the aluminium tube from the tank to the inlet of the PCM slab are well insulated. Water flows inside the tube and it carries away the heat in the PCM. The inlet to the tube is from the water tank. PCM is in high temperature and the water is in low temperature and so heat is transferred to the water. The mass flow rate of water is set constant by means of regulating Valve. A pump is required for recirculation of water in the tank. If our system should not depend on electricity, solar panels could be installed for the required power. In total, we absorb the night coolness and give it back in day time. This is one of the efficient methods of bringing cooling effect to room without spending energy.

IV. MODEL CALCULATION:

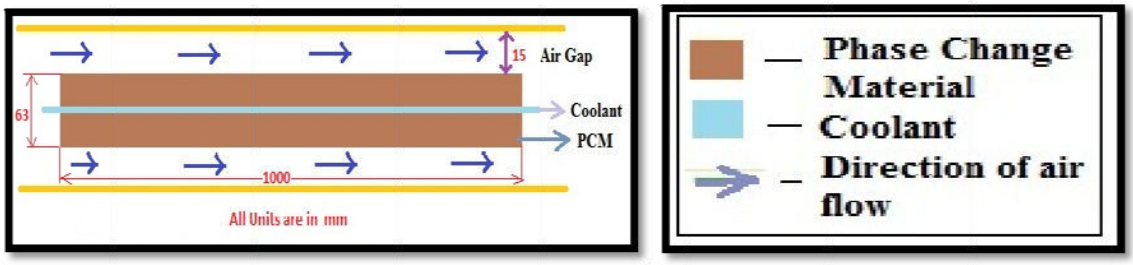

Fig3. PCM in single slab with coolant in side view

Assumptions:

- The size of the room is 20 * 20 *20 feet
- The wall of the room is made up of Brick (plastered on one side) which has a thickness of 40 cm.
- The floor of the room is made up of concrete (22 cm) with insulation (2.6 cm).
- The Ceiling of the room made of plaster (concrete).
- Room maximum temperature in daytime is chosen to be 307K (In Bangalore)
- At night time the minimum temperature is assumed to be 295K (In Bangalore)
- Bent tube circulating water is assumed to have 10 bends per slab of PCM
- Backup of 2 hours is chosen since coolant is used, there will not be any backup time and the heat will be continuously carried out by the coolant water.

Load Calculations:

- Heat transfer Coefficient Values for various materials:

Materials	U in W/m^2K
Wall Brick (plastered on one side)	1.0
Plaster Ceiling	1.15
Floor Concrete with insulation	1.0

Table1: Heat transfer coefficient for different materials.

Wall:

$Q_1 = U * A * dT$

Heat received by the wall = 2.051kW

Floor:

$Q_2 = U * A * dT$

Heat received by the Floor = 1.962kW

Ceiling:

$Q_3 = U * A * dT$

Heat comes from the ceiling = 0.601kW

- Human who rejects heat while doing light work

$Q_4 = 0.183$ kJ/s

- Heat rejected by the Equipment in the room:

Q_5 = kW * 3600 * Use factor

  - Power = 225 kW
  - Use factor = 0.68

$Q_5 = 0.153$ kW

Total heat Load = $Q_1+Q_2+Q_3+Q_4+Q_5$

Total heat Load = 3.078kW = 0.86 tons

PCM properties:

Property	Values
Name	HS 29
Melting point	29 degree Celsius
Density	1550 kg/m^3
Latent Heat	190 kJ/kg

Table2: Properties of PCM

For 2 hours backup,

Load = 1.72 ton

Load = 21776.92 kJ/day

Mass of the PCM required

m = Load / Latent heat of PCM

m = 128 kg

Density of PCM □ PCM = 1400 kg/m3

Calculate Volume of PCM **V** = 0.0914 m3

PCM slab dimensions is assumed as

Length l = 1 m

Breadth b = 0.303 m

Height h = 0.065 m

Thus we should have 5 slabs to attain the calculated volume

Mass flow rate of air

M = Load / sensitive heat (Latent heat)

M = 0.01779 kg/s

Since forced convection has to be made a fan is fitted.

For a fan diameter,

D = 93 mm

M = □ * N * D3

Rpm of the fan is calculated as

N = 1084 rpm

Heat Exchanger Calculation:

q = h * A * dT- - - - - - - - - - (1)

A = 0.5 m^2

D*π*L = A- - - - - - - - - - - (2)

The diameter of the tube is calculated as

D = 10^{-2} m [by equation (2)]

Heat transfer by the PCM = Heat absorbed by the PCM

h * A * dT = Mw * Cp * dT

The mass flow rate of water is calculated as

M_w = 0.015 kg/s

The graph plotted between Temperatures of the room Vs Time is performed by using the psychometric chart and the following equation.

m1w1 + m2w2 = m3w3

m1h1 + m2h2 = m3h3

V. RESULTS AND DISCUSSION

Results obtained by calculation are shown below in terms of graph for better and quick understanding. The ultimate goal of this work is to attain cooling effect using coolant without spending huge amount of conventional energy. In India, we are exposed to hot summer and lavish solar radiation and all of us are in need of comfort. We are presenting about the maximum and minimum temperatures prevailing in India. Average temperatures are also indicated in the graph corresponds to respective month's average temperature. The graph1 is drawn with respect to the month and corresponding temperature.

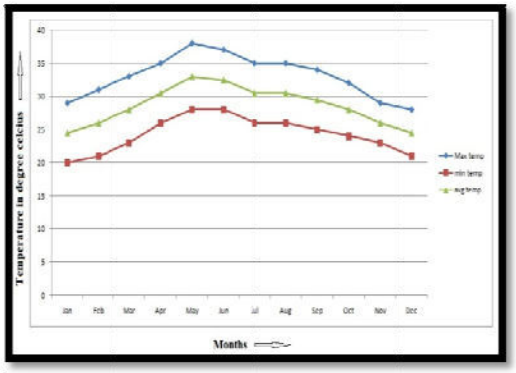

The maximum temperature in Bangalore during daytime is 307K

The minimum night time temperature in Bangalore is 295K

The difference in temperature

dT = 12 K

Convective heat transfer coefficient of water

h = 500 W/m2K.

From equation (1),

Surface area of contact of bent tube circulating water

The length of the bent tube contact with PCM is calculated as L = 15 m

Graph1. Temperature Vs Months

In order to balance the scorching summer people begins to use air conditioning system. The production and sales of AC are increased in our day to life. But AC requires lot of power consumption and it also affects the environment by releasing hazards gases. Global warming and ozone depletion are major problems caused by these kinds of equipments. The following graph2 shows that sales of AC with respect to year.

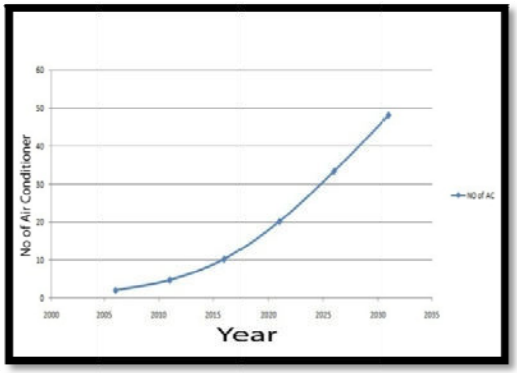

Graph2. No. of Air Conditioner Vs Year

Among all of the home appliances AC requires huge amount of power. We are collecting some information about average power consumption in home by various appliances. The graph3 & 4 given below clearly indicates that average power consumption by various equipments per year.

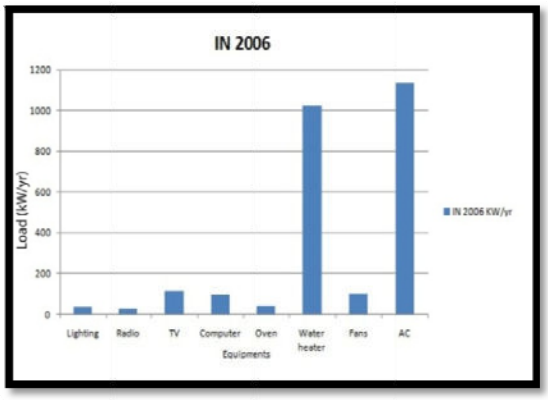

Graph3. Load Vs Equipments in 2006

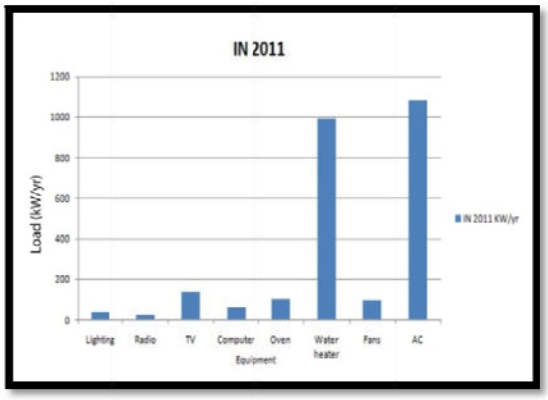

Graph4. Load Vs Equipments in 2011

But today there is a huge demand in electricity and majority of problems arising because of energy demand. Ozone depletion has to be eradicated. These are the familiar topics which are flashing in many TV channels and news papers. In order to avoid certain amount of power consumption, we have designed eco friendly and non hazardous system. The system consists of sealed PCM slabs and air gaps. The main criterion in selection of PCM is melting point and latent heat of PCM. Air from room at room temperature comes in contact with PCM at certain mass flow rate. The effective heat transfer and efficiency of the system depends on mass flow rate of air. So we have pondered the various types of PCM and calculated the corresponding mass flow rate. The graph5 are drawn with mass flow rate with respect to various types of PCM.

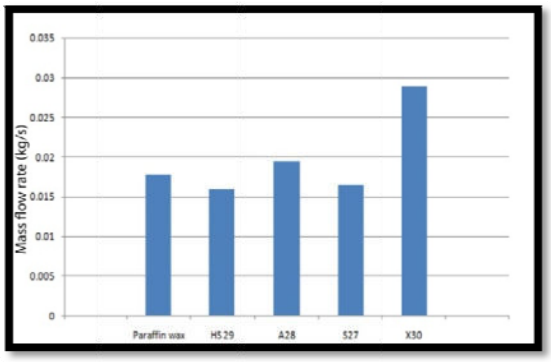

Graph5. Mass flow rate of air Vs PCM

Our goal is to maintain the room with comfort temperature. The time for various comfort temperatures are calculated. The graph6 is plotted for comfort temperature with respect to time. Finally concentration is made on cost of the system. The overall cost for our system is Rs.18200 for room size 20*20 feet. The AC cost for same room of size 20*20 feet is also analyzed.

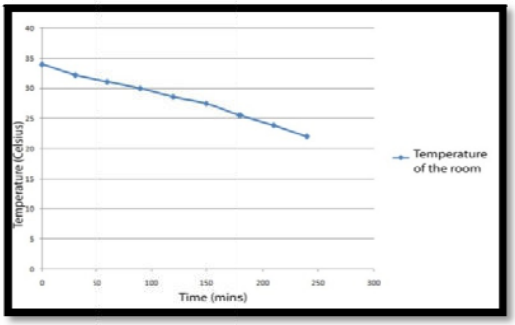

Graph6. Temperature of the room Vs Time

The graph7 & 8 plotted below shows the AC cost with and without maintenance and payback period is also indicated in the graph. By considering the cost of AC with maintenance the payback period is nearly 10 months. So in total it must be a better alternative for AC.

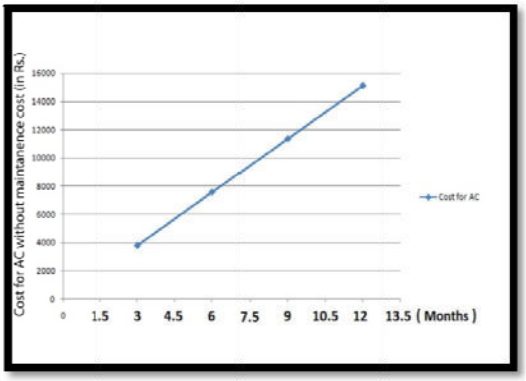

Graph7. Cost of Air Conditioner Vs Months

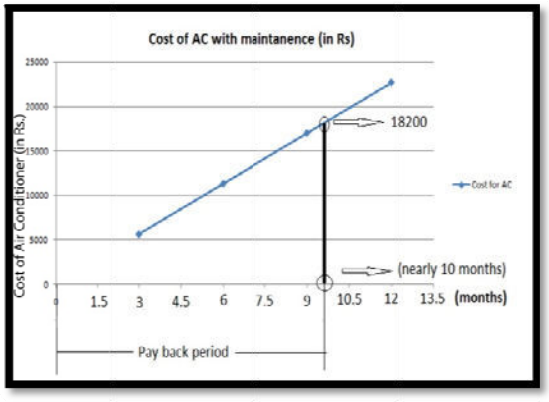

Graph8. Cost of Air Conditioner with maintenance Vs Month

VI. CONCLUSION

As our demand for Air Conditioning and Refrigeration are escalating day by day, the amount of fossil fuel will become scarce on one day. By implementing this method, it eradicates both power consumption of Air Conditioner and the carbon emissions due to Air Conditioning. The key behind this efficacious solution is the Phase Change Material. In previous papers, the overall system will work only during the daytime, but in most of the houses there will be need of Air Conditioning during night time. The usage of coolant to carry the heat energy in the PCM extends the system to work during night time. Thus this could bring extravagant changes to this hectic world. This method could greatly reduce the usage of Air Conditioning and thus saves fuel energy. Initial investment may be high in case of using Phase Change Material but maintenance cost and installation of Air Conditioner will be higher and it is also shown that within a short span of time it is able to recover the loss of initial investment of Phase Change Material. The effects of thermo physical properties of PCM, installation methodology, location of PCM are the scope for future work.

REFERENCES

[1] Cengel, Y. A. (2006). Heat and Mass Transfer: A practical approach, 3rd ed., McGraw Hill.

[2] Chen, S L, Chen,C L, Tin, C C, et al. 2000. An experimental investigation of cold storage in an encapsulated thermal storage tank, Experimental Thermal and Fluid science. Vol. 23 pp 133 144.

[3] Arkar, C. & Medved, S. (2007). Free cooling of a Building of PCM heat storage integrated into the ventilation system. Solar energy, 81(9) 1078 – 1087.

[4] Hed, G. & Bellander, R. (2006). Mathematical modeling of PCM air heat exchanger. Energy and buildings. 38, 82-89.

[5] Psychometric chart (http://en.wikipedia.org/wiki/File:PsychrometricChart-SeaLevel-SI.jpg)

[6] Incropera , F. P., Dewitt D. P. (2008). Fundamentals of heat and mass transfer, 6th edition, jhon willy & sons.

[7] J. P. Holman " A Textbook of heat and mass transfer ." Tata McGraw Hill publication.

[8] Zalba, B.; Marin J. M.; Cabeza L. F.; Mehling H.; Free cooling of building with phase change materials. Int. J. Refrig. 2004, 27, 839–849.

[9] Mohd Hafizal Mohd Isa.; Xudong Zhao.; Hiroshi Yoshino.; Preliminary Study of Passive Cooling Strategy Using a Combination of PCM and Copper Foam to Increase Thermal Heat Storage in Building Facade, Sustainability 2010, 2, 2365-2381

[10] Arkar, B. Vidrih, S. Medved, "Efficiency of free cooling using latent heat storage integrated into the ventilation system of a low energy building", International Journal of Refrigeration, Vol. 30, No. 1, 2007, p. 134-143.

[11] Residential consumption of electricity in India. (moef.nic.in/downloads/public.../Residentialpowerconsumption.pdf)

[12] Zain, Z.M; Taib, M.N.; Mohd, S.B.S. Hot and humid climate: Prospect for thermal comfort in residential building. Desalination 2007, 209, 261-268.

[13] Khudhair, A.; Farid, M. A review on energy conservation in building applications with thermal storage by latent heat using phase change materials. Energ. Conv. Manage. 2004, 45, 263-275.

[14] Temperatures in India. (http://www.whereincity.com/india/tamilnadu/)

[15] Voss, K.; Herkel, S.; Pafferott, J.; Lohrnet, G.; Wagner, A. Energy efficient office buildings with passive cooling results and experiences from a research and demonstration program. Sol. Energy 2007, 81, 424-434.

[16] Zhang, Y.; Zhou, G.; Lin, K.; Zhang, Q.; Di, H. Application of latent heat thermal energy storage in buildings: State-of-the-art and outlook. Build. Environ. 2007, 42, 2197-2209.

[17] Voelker, C.; Kornadt, O.; Ostry, M. Temperature reduction due to the application of phase change materials. Energy. Bldg. 2008, 40, 937-944.

[18] Tyagi, V.V.; Buddhi, D. PCM thermal storage in buildings: A state of art. Renew. Sustain. Energy Rev. 2007, 11, 1146-1166.

[19] Dincer I, Rosen MA. (2002).Thermal energy storage, systems and applications, John Wiley and sons, Chichester, England.

[20] Abhat.A.(1983) Low temperature latent heat thermal energy storage, Heat storage materials. solar energy 30: 313-32.

[21] Salyer IO, Sircar AK, "Phase change materials for heating and cooling of residential buildings and other applications" In: Proceedings of 25th intersociety energy conversion engineering conference.1990, pp.236– 43.

◈◈◈

Design and Experimental Analysis of Furnace for the Production of Bamboo Charcoal

[1]ARIJIT BISWAS, [2]PINAKESWAR MAHANTA

[1,2]Department of Mechanical Engineering,
Indian Institute of Technology Guwahati
Bangalore, India

Abstract—This paper presents the study of carbonization systems for the production of Bamboo Charcoal which is formed on dry distillation of raw bamboo. The paper mentions the drawbacks of the conventional practices of production of Bamboo Charcoal. Design of a new charcoal production unit is aimed at eliminating the identified drawbacks in the present methodology of production making the process of production faster and more efficient by minimizing heat loss during the production process. Designing is attempted with strong consideration for manufacture, operational cost and ease of operation of the furnace as the process finds application amongst rural people with little or no technical knowhow, making simplicity of design absolutely critical for implementation of the developed technology. Results of testing and experimentation presented in this paper describe the working prototype confirming qualitative and quantitative improvements in the bamboo charcoal being produced as compared to the conventional method of production.

Keywords- *Bamboo Charcoal, Pyrolysis, Furnace.*

I. INTRODUCTION

The production of charcoal from locally available raw material has been performed for centuries in the North East of India, China and many other parts of the world using traditional methods of production in earth pits or mud kiln [1-7]. Charcoal is formed by the pyrolysis of raw bio mass. The bio mass when heated in absence of air above a fixed temperature depending on the type of bio mass undergoing carbonization emits volatiles which are condensed to yield vinegar as a byproduct [8]. The solid residue remaining in the pyrolising chamber is called charcoal, has a porous microstructure and primarily comprises of carbon.

Even in modern times charcoal production with traditional methods is very popular amongst rural communities in developing countries [9-12] as it is used as a fuel for domestic purposes and generates income because the raw charcoal and its by product vinegar are the starting material for the manufacture of products which are in very high demand [13-14]. However the process of production is crude and inefficient, unscientific yielding poor quality of bamboo charcoal.

It takes only 3-4 years for Bamboo culms to reach adequate height and weight for commercial production of charcoal. Therefore the production of Charcoal with bamboo is very attractive as the time required to harvest the starting bio mass is lower compared to charcoal made from other sources. The process of production, usage and consumption for charcoal has a lower carbon footprint when compared to other sources of fuel and firewood [9-12]. Charcoal made from bamboo inherently has 1.5 times the calorific value as compared to wood charcoal and nearly 2-3 times the surface area of wood charcoal due to the porous microstructure of bamboo [13,18,19].

Bamboo has a number of other uses besides as a starting material in the production of charcoal, it is used in production of paper, furniture, finding usage in the handicrafts industry. Besides bamboo charcoal sticks or briquettes are used for fuel applications bamboo charcoal is used in the manufacture of activated carbon [13] which is used in clinical toxicology, manufacture of gas adsorbents, water and air filters, purification of drinking water, removal of heavy metal ions such as Lead and Cadmium, Mercury, chloramphenicol, nitrate nitrogen, air fresheners for eliminating organic impurities and smells [15-18]. Drinking water sterilized with chlorine can be treated with bamboo charcoal to remove residual chlorine and chlorides. These uses of charcoal especially bamboo charcoal is attributed to its porous microstructure and large surface area. Bamboo charcoal has the ability to act as humidifiers and as de humidifiers, it releases or absorbs moisture from the environment depending upon relative humidity therefore it is suitable for daily domestic household applications as well [18,19].

Bamboo charcoal is used in the manufacture of carbon based composites, nano rods, functional fabrics, Silicon Carbide, metal reduction and recycling. Bamboo charcoal like bamboo vinegar has beneficial medicinal properties hence used as an anti bacterial, biological preservative [18]. It is used in making herbal and medicinal soap, bamboo charcoal is also known to show beneficial effects when added in minute quantities to the diet of poultry and farm animals [18]. Here in the North Eastern part of India and in places around the world bamboo charcoal is also used in making fertilizer by addition to manure and composts.

The potential for commercial exploitation of Bamboo Charcoal is immense. The work stated in this paper was to design an efficient, low cost, simple to

operate pyrolysis unit for the production of quality bamboo charcoal capable of meeting market standards. Implementation of an improved process for production of bamboo charcoal would see increase in employment and entrepreneurship opportunities in the rural sector.

II. Field Study and Data Collection on Traditional Process for Bamboo Charcoal Production and it's Identified Drawbacks

The majority of the production of bamboo charcoal in North East India is performed with usage of a metal oil drum as a carbonizing kiln. Raw Bamboo 3-4 years old is cut to approximately 80 cm in length and loaded into the oil drum. A large amount of earth is excavated to position the oil drum horizontally and it is covered with around 1 feet of soil as shown in Fig. 1a and Fig. 1b.

Figure 1. Setting up of furnace in traditional method of production: (a) Raw Bamboo cut and loaded into tar drum in Tura. (b) Metal sheets cover opening, orifices provided for heated gas to enter into pyrolysing chamber.

The drum is loaded horizontally causing heating inside the oil drum to be non uniform, this is verified by temperature readings recorded with thermocouples inserted into the oil drum. The layer of soil provides insulation and minimizes heat loss which is crucial for carbonizing process as temperatures required for charcoal formation can be reached only with adequate insulation.

The loading end of the oil drum is closed by a metal sheet with 2 orifices. The orifices provide a passage for heated gases from combustion chamber into oil drum which is sealed with moist clay clay as shown in Fig. 1b. The combustion chamber is built by mud plastering bricks for ensuring an air tight seal as shown in Fig. 2a. The process of heating is not continuous, the unit is only fired during daylight hours as shown in Fig. 2b.

a b

Figure 2. Traditional method of producing bamboo charcoal: (a) Construction of combustion chamber with brick and mud plastering. (b) Firing of furnace during daylight hours in Tura

This extremely labour intensive process of preparing the unit manually is to be performed every time bamboo charcoal is to be produced making the process of production problematic. Also there is risk to the operator from open flames and high temperatures exposed on the outside surface of the production unit. Bamboo in the oil drum is heated convectively by burning of firewood, the process of production is carried on for 3 days.

The amount of firewood required in the process of production is high as a large fraction of the gases of combustion do not enter into the pyrolysis chamber but exit through the opening through which firewood is being provided. Poisonous gases are emitted during the production process is shown TABLE.1.

Pyrolysis involves the partial combustion of bamboo, hence one of the major products of pyrolysis is Carbon Monoxide [19]. There is no provision for proper sealing or controlled flow of gas in closed ducts therefore posing a health risk to the unit operator.

The inspection of another similar type of bamboo charcoal production unit at a different location in North East India showed noticeable variation in the sizing of the combustion chamber which is built manually. The insulation on the oil drum in this scenario was at maximum around 6". This indicated the need for standardization of the process for production of bamboo charcoal.

TABLE I. GAS CONSTITUENTS AND COMPOSITION OF EMITTED VOLATILES

Time (hh:mm)	O_2 (%)	CO_2 (%)	C0 (ppm)	C_XH_Y (ppm)	NO_X (ppm)	SO_2 (ppm)
2:00	19.22	3.48	3202	1370	57	0
4:00	7.33	10.20	2150	4600	176	103
6:00	5.28	11.61	Off limit	Off limit	7907	320
8:00	1.96	13.63	Off limit	Off limit	164	1401
11:00	6.07	11.02	Off limit	6000	195	202
12:00	5.53	11.42	5447	5910	171	488

III. Basic Conceptualization and Constructional Features

The design of the pyrolysis unit was attempted by setting of the main pyrolysis chamber vertically instead of horizontally. The combustion chamber is placed below so that flue gases from combustion of firewood rise into the pyrolysis chamber. A draft/funnel arrangement is provided on top of the pyrolysis chamber as shown in Fig.3a. Insulation has been provided with rocks and a brick lining around the pyrolyis chamber.

A uniformly perforated plate separates the pyrolysis and combustion chamber as shown in Fig.3b and Fig. 4f ensures uniform flow and heating by gas from combustion chamber into pyrolysis chamber. The firewood is loaded on a grill arrangement 3" off the ground as shown in Fig.3c, the firewood is provided into the combustion chamber through 3 duct passageways.

The ducts for providing fresh firewood are covered with movable flaps to minimize heat loss by

convection as shown in Fig.4a. Bamboo nodes are pierced to allow gases of combustion to heat the bamboo from inside as well as the outside, uniform distribution of gas is ensured by perforated distributor plate below. Grill arrangement prevents bamboo from coming in contact with the hot surface of the distributor plate as shown in Fig. 4c. The ducts have hollow passage way beneath the main opening through which firewood is loaded for entry of fresh oxygen from outside into the combustion chamber and ash formed on combustion of firewood to be pulled out from beneath as shown in Fig. 5a and Fig. 4b. The rocks are placed in the intermediate space between drum and brick lining, they serve to provide insulation as well as act as heat storage medium as shown in Fig.5b.

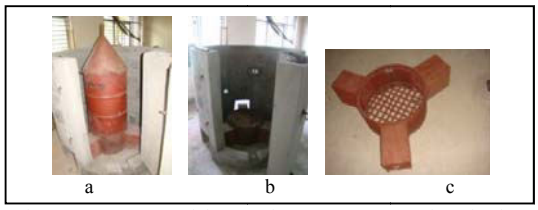

Figure 3. Features of the new furnace: (a) Setup of production unit after assembly. (b) Perforated plate separating pyrolysing chamber and combustion chamber. (c) Grill arrangement on which

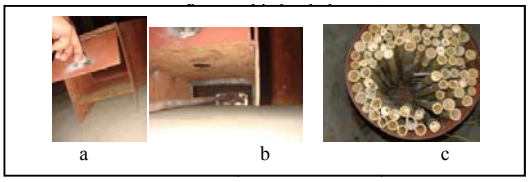

Figure 4. Feature of the new furnace which overcome the lacunas with the traditional method of Bamboo charcoal production: (a) Flaps covering entry point of combustion chamber, minimizes convective heat loss. (b) Duct passage way for entry of fresh oxygen and removal of ash from underneath the furnace. (c) Loading of the bamboo vertically in new developed production unit at IITG with perforated plate below

Figure 5. New furnace in opeation: (a) Flaps covering entry point of combustion chamber, ash formed on combustion of firewood pulled out from underneath (b) rock insulation and piping from furnace fed to condenser for bamboo vinegar production.

IV. ANALYTICAL CALCULATIONS FOR DESIGNING CHARCOAL PRODUCTION UNIT

The most critical aspect to the design of the carbonizing/pyrolysing furnace is the insulation. If the rate of heat loss from the pyrolysing chamber is high, adequate temperature required for carbonization to occur inside the chamber will not be achieved. The concept used is that the furnace is capable of providing insulation for a greater rate of heat generation than actually taking place in the production process.

The governing equating used for setting up the insulation thickness is

$$Q = Q_1 + Q_2 = \text{Net Rate of Heat Generation}$$

For safe design of furnace

$$Q = Q_1 + Q_2 = Q_{conduction} + Q_{convection}$$

Where Q is the net heat generated per second, Q_1 is the heat generated per second by burning firewood and Q_2 is the heat liberated during carbonisation of the bamboo.

$Q_1 = CV_{firewood} \times M_{firewood}/(t \times 36000) = 17681.81$ Joule/Sec and

$Q_2 = CV_{bamboo} \times M_{bamboo}/(t \times 36000) = 9479.16$ Joule/Sec

Therefore net heat generated is evaluated to be

$Q_{net\ generated} = Q_1 + Q_2 = 27160.97$ Joule/Sec

Heat Transfer due to Conduction [41] is calculated to be

$Q_{conduction} = (T_1 - T_2)/(R_1 + R_2 + R_3) = 5277.26$ Joule/Sec.

The concept of thermal resistance in a cylindrical shape is used where

$R_1 = \ln(r_2/r_1)/2\prod k_1$; $R_2 = \ln(r_3/r_2)/2\prod k_2$;

$R_3 = \ln(r_4/r_3)/2\prod k_3$

R_1, R_2, R_3 are the thermal resistance of the three layers of insulation provided on the furnace. The configuration and the parameters used to evaluate heat loss by conduction are represented in Fig.6. The total thermal resistance is given as

$R_1 + R_2 + R_3 = R_{net} = 0.05969$

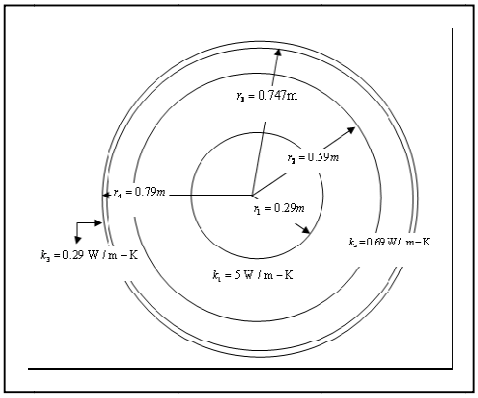

Figure 6. Schematic showing radius of insulation and thermal conductivities of various materials in furnace.

Heat Transfer due to Convection [20] is given by

$Q_{convection} = \rho \times A_c \times v \times \Delta = 23030.14$ Joule/Sec

The safe criteria for design of furnace is satisfied as $Q_{convection} + C_{onduction} >= Q_{net\ generated}$

The funnel arrangement provided at the top of the tar drum to ensure uniform continuous flow of gas by creating suitable pressure difference. The pressure difference can be calculated by use of Continuity Equation and Bernoulli's Equation as the flow velocity is low and flow is incompressible. The Continuity Equation given as

$A_1 \times V_1 = A_2 \times V_2$

Where $A_1 = 0.264 m^2$ and $A_2 = 0.00114 m^2$ represent the inlet and exit cross sectional area of the funnel shown in Fig.2a. The exit velocity $v_1 = 0.2$m/sec

therefore inlet velocity at the base of the cone represented by point 2 is calculated to be v_2=46.34m/sec using the Continuity equation and Bernoulli's Equation used for calculating pressure difference is given by

$$P_1+0.5\rho v_1^2+\rho g h_1=P_2+0.5\rho v_2^2+\rho g h_2$$

The density can be approximated to be constant over the 1 feet of flow on which the calculations are being performed without affecting the results. The height difference between the two points is also negligible. Therefore the pressure difference P_1-P_2 between the top of the funnel represented by point 1 and base of the funnel represented by point 2 is evaluated as 1500.37 Pascal. The parameters used in evaluating the above equation are represented in TABLE II.

TABLE II. PARAMTERS USED TO EVALUATE CONVECTIVE HEAT LOSS

Symbol	Description/Meaning	Value
P	Density of flowing gas	1.4 kg/m3
A_c	Area of cross section of piping	0.246m2
V	Flow velocity under natural convection	0.2 m/sec
C_p	Thermal Heat Capacity of flowing fluid	1.006 X 103 Joule/kg-K
$\Delta=T_1-T_2$	Difference between furnace interior and ambient temperature	315°C
T	Time taken for production process	11 hours
$CV_{firewood}$	Calorific Value of Firewood	18 MJ
CV_{bamboo}	Calorific Value of Bamboo	15 MJ
$M_{firewood}$	Mass of firewood	38.9 Kg
M_{bamboo}	Mass of bamboo	35 Kg

V. RESULTS AND DISCUSSIONS

The temperature distribution measured in the traditional process of production shown in Fig.7 shows large variations indicating non uniform heating of the bamboo charge inside the carbonization chamber. The standard deviation shows temperature deviation of more than 100^0C. The non uniform heating results in poor conversion of the bamboo to charcoal, leaving brands of bamboo uncarbonized or partially converted, the extremely high temperature at the firing end causes burning of the bamboo in these regions adding to the net poor yield of the process.

The orientation of the oil drum vertically, with usage of a perforated plate and adequate sealing shows improvement in the thermal profile. Points apart from the centerline it is shown in as shown in Fig.8. and points along the centerline it is shown in Fig.9.

The standard deviation in temperature observed along the centerline is a maximum of 30^0C. The sealing is improved than before, majority of the gases now enter into the pyrolysis chamber.

The process of bamboo charcoal production with the traditional process is 3 days. The yield of Bamboo charcoal is 20-30 Kg form 75-90 Kg of raw bamboo. The cycle for production with new furnace is 12-14 hours. The yield is around 13.4 Kg of completely carbonized bamboo charcoal of calorific value equivalent to the above stated or more. The amount of partially converted bamboo charcoal is around 2.8 Kg. The net yield in charcoal is around 16.2 Kg indicating conversion efficiency of 82.71%. The weight of Firewood consumed for the entire production process with the new prototype furnace is 26 Kg.

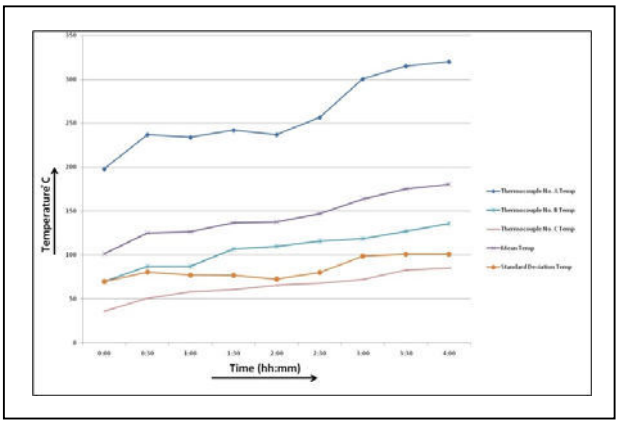

Figure 7. Thermal profile inside traditional furnace, non uniform heating with large deviations clearly indicated

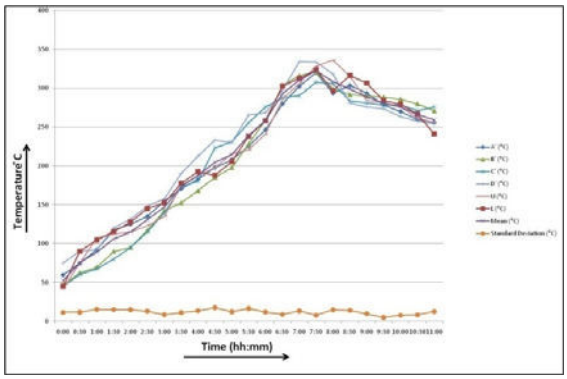

Figure 8. Thermal profile at points other than the centerline

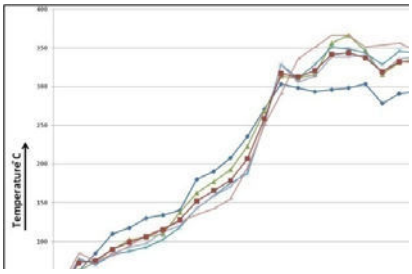

Figure 9. Thermal profile along centerline in new developed furnace

Temperature readings are taken with K-Type thermocouples oriented as shown in Fig.10 inside the pyrolyzing chamber.

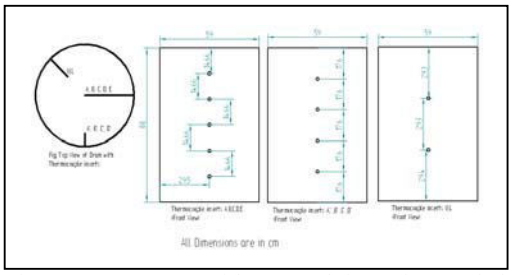

Figure 10. Arrangement of thermocouple inserts into pryolysing chamber

The calorific value of the bamboo charcoal produced with the traditional process is 6343 Kcal/Kg or lesser. The mass of firewood consumed in the traditional process is reported to be always greater than 40 Kg. The calorific value of the bamboo charcoal produced with the new method of production in Bomb Calorimeter revealed it to be 6944.23 Kcal/Kg for (Sample 1) and 6874.88 Kcal/Kg (Sample 2).

The developed process of production clearly features uniform heating, adequate insulation. The process of production of bamboo charcoal is much faster with higher conversion efficiency of raw bamboo to bamboo charcoal, The Heat loss is minimized and the process is more efficient in terms of consumption of firewood for firing. The calorific value testing of the produced bamboo charcoal clearly indicates qualitative improvements in the process of production besides the stated quantitative improvement. The temperatures recorded on the rocks used for thermal insulation show temperatures in excess of 100^{o}C; this represents a large amount of stored thermal energy that could be used for drying, cooking etc.

ACKNOWLEDGMENT

The project on design of a furnace for production of Bamboo Charcoal was performed with financial assistance from Rural Technology Action Group North East (RuTag NE). The study on Bamboo Charcoal production system was performed at the campus of Bethany Society an NGO in the North East of India.

REFERENCES

[1] J.B. Kandpal, R. C. Maheshwari, A decentralized approach for biocoal production in a mud kiln, Bioresour. Technol. 43 (1993) 99-102.

[2] J.C. Adam, Improved and more environmentally friendly charcoal production system using a low-cost retort–kiln (Eco-charcoal), Renewable Energy 34 (2009) 1923–1925.

[3] Y. Schenkel, P. Bertaux, S. vanwijnbserghe, J. Carre, An evaluation of the mound kiln carbonization technique, Biomass Bioenerg Vol. 14 Nos. 5/6, (1998) 505-516.

[4] J.-C.M. Lin, Development of a high yield and low cycle time biomass char production system, Fuel Processing Technology 87 (2006) 487–495.

[5] K.N. Patil, P.V. Ramana and R.N. singh, Performance evaluation of natural draft based agricultural residues charcoal system, Biomass and Bioenergy Vol. 18 (2000) 161-173.

[6] C. Syred, A.J. Griffiths, N. Syred, D. Beedie and D. James, A clean, efficient system for producing Charcoal, Heat and Power (CHaP), Fuel 85 (2006) 1566–1578

[7] P. Rousset, C. Aguiar, N. Labbé, J.M. Commandré, Enhancing the combustible properties of bamboo by torrefaction, Bioresour. Technol. 102 (2011) 8225–8231

[8] E. Kabir, K.H. Kim, J.W. Ahn, O.F. Hong, J.R. Sohn , Barbecue charcoal combustion as a potential source of aromatic volatile organic compounds and carbonyls, J. Hazard. Mater. 174 (2010) 492–499.

[9] O.T. Coomesa, G. J. Burt, Peasant charcoal production in the Peruvian Amazon: rainforest use and economic reliance, For. Ecol. Manage. 140 (2001) 39-50.

[10] E. Johnson, Charcoal versus LPG grilling: A carbon-footprint comparison, Environmental Impact Assessment Review, 29 (2009) 370–378.

[11] J.M.O. Scurlocka, D.C. Daytonb, B. Hames, Bamboo: an overlooked biomass resource?, Biomass Bioenerg 19 (2000) 229-244.

[12] F. Khundi , P. Jagger, G. Shively , D. Sserunkuuma, Income, poverty and charcoal production in Uganda, Forest Policy and Economics 13 (2011) 199–205.

[13] A.W.M. Ip, J.P. Barford, G. McKay, Production and comparison of high surface area bamboo derived active carbons, Bioresour. Technol. 99 (2008) 8909–8916.

[14] G. Xingzhong, Z. Lingjie, Y. Liqing, Y. Hui, Z. Lin, Preparation of silicon carbide using bamboo charcoal as carbon source, Mater Lett 64 (2010) 331–333.

[15] Z. Tan, J. Qiu, H. Zeng, H. Liu, J. Xiang, Removal of elemental mercury by bamboo charcoal impregnated with H2O2, Fuel 90 (2011) 1471–1475.

[16] H. Lalhruaitluanga, K. Jayaram, M.N.V. Prasad, K.K. Kumar, Lead(II) adsorption from aqueous solutions by raw and activated charcoals of Melocanna baccifera Roxburgh (bamboo)—A comparative study, J. Hazard. Mater. 175 (2010) 311–318.

[17] F.Y. Wang, H. Wang, J.W. Ma, Adsorption of cadmium (II) ions from aqueous solution by a new low-cost adsorbent-Bamboo charcoal, J. Hazard. Mater. 177 (2010) 300–306.

[18] JIANG Shenxue, Training Manual of Bamboo Charcoal for Producers and Consumers, Bamboo Engineering Research Center Nanjing Forestry University, May 2004. Available at : http://www.google.co.in/url?sa=t&rct=j&q=&esrc=s&source=web&cd=1&ved=0CEkQFjAA&l=http%3A%2F%2Fwww.inbar.int%2FEcono_devep%2Fdoc%2F0771%2FTraining%2520Manual.doc&ei=31zHT7fkCYe1iQfQ_fzjDg&usg=AFQjCNE_EQeZrmoi8vfRZOn2gXaMc6Dl0Q&sig2=gi5YjuEUqN5k6es36fR0AA

[19] Guan Mingjie, Manual for Bamboo Charcoal Production and Utilization, Bamboo Engineering Research Center, E. Nanjing Forestry University, May 2004. Available at :http://www.bambubrasileiro.com/arquivos/Bamboo%20Charcoal%20Production%20Manual%20-%20Nanjing%20University.pdf

[20] P.K.Nag, Heat and Mass Transfer (Second Edition, Tata McGraw-Hill Publishing Company Limited (2007).

Experimental Studies of Secondary Wick For Loop Heat pipe

[1]VINOD R, [2]JASVANTH V S & [3]U S MALLIKARJUN

Mechanical Department Siddaganga Institute of Technology
Tumkur, Karnataka Scientist-SF, Thermal System Group
ISRO Satellite Centre, Bangalore, Karnataka
Mechanical Department Siddaganga Institute of Technology
Tumkur, Karnataka

Abstract— The Loop Heat Pipe (LHP) is a passive two-phase heat transport device that is gaining importance for thermal management of high powered spacecrafts. As a part of technology development program, LHP are being developed at Thermal Systems Group, ISRO Satellite Centre. An Engineering Model LHP capable of transporting 600W has been developed under this program using porous nickel as primary wick and ammonia as working fluid. In this thesis, the issue of secondary wick in an LHP is studied experimentally. In zero gravity environment a secondary wick is necessary to supply the working fluid from the compensation chamber to the evaporator core (having the primary wick) by heat pipe action. A configuration of secondary wick encompassing three layers of wrapped SS wire mesh has been worked out for this purpose. In order to assess the performance of this secondary wick configuration, a heat pipe with same configuration is fabricated using ammonia as working fluid. In order to characterize this secondary wick configuration, the heat pipe performance tests are conducted. The heat transport capacity of this configuration is tested at various adverse tilts (evaporator above the condenser) viz., 0, 5, 10, 15, 20, 25, 50, 60 and 70mm. This configuration could transport a maximum heat load of 35W at 0mm adverse tilt. As it is difficult to simulate zero gravity environment on ground, the Engineering model LHP performance (measured in terms of heat transfer coefficient at the tooth wick interface) is studied with and without secondary wick.

Keywords-*Evaporator, Compensation Chamber, Primary Wick, Secondary Wick, Ammonia.*

I. INTRODUCTION

The present-day communication satellites electronics is making rapid progress, which primarily results in compaction of electronics. One of the consequences of such advancement is a sharp rise in heat flux from the electronic packages, which poses a major challenge in their thermal management. It is expected that internal thermal dissipation in the near future communication spacecrafts will be of the order of 10 to 15kW. Efficient thermal management system is required to collect the concentrated heat dissipations from the electronic packages and its distribution over the spacecraft radiators. Two-phase heat transfer technologies have the potential to transport large amounts of heat over long distances with minimal temperature drops. As these systems employ the latent heat of fluids they are light in mass. The two-phase thermal management systems for spacecraft application can be broadly classified as:

With the ever increasing number of payloads and electronic components on a satellite and with advances in compaction of electronic packaging, the radiating area on the satellite body would be insufficient to maintain the components within their operating temperature limits. These conditions demand use of deployable radiator. These radiators are in the stowed (folded) condition at the time of the launch and are deployed once the spacecraft reaches its designated orbit, thereby increasing the available radiating area. The heat generated in the satellite bus can be transmitted to the deployable radiator by means of LHPs. Compared to heat pipes LHPs are less sensitive to adverse elevation in 1-g operation. LHPs exhibit both high reliability and high heat transport capacity.

II. WORKING PRINCIPLE

The loop heat pipe (LHP) is a passive two-phase heat transport device that operates on a closed two-phase fluid-flow cycle, sustained by a capillary medium in the evaporator. It consists of an evaporator, transport lines, and a condenser. Smooth tubes (carrying liquid and vapor) connect the capillary evaporator and the condenser. A two-phase reservoir called the compensation chamber (CC) is located adjacent to the evaporator. It exchanges liquid with the rest of the loop depending on the heat load. The operating principle of an LHP (discussed in detail later) is similar to that of a conventional heat pipe. In contrast to the distributed capillary structure in a heat pipe, the capillary structure in an LHP is limited to the evaporator. This results in considerably lower pressure drop within the wick, which translates into higher heat transport efficiency (in terms of both magnitude of heat transfer and distance over which it is transferred).

Following paragraphs explains the LHP operating principle with the aid of a pressure–temperature (P-T) diagram (Figure 2). An LHP operates in a two-phase fluid flow cycle in which the working fluid gains heat in the evaporator zone while heat is lost in the condenser to the sink. Figure 3 pictorially depicts heat transfer in the evaporator. The heat that is supplied to the evaporator (Q_{load}) is primarily used in heating (including evaporation) the fluid in the

evaporator (Q_{evap}). Some portion of the applied heat is lost to the ambient ($Q_{evap-\infty}$) and the compensation chamber (Q_{Lr}). Thus the heat balance in the evaporator heater plate (or evaporator envelope) can be given by

$$Q_{evap} = Q_{load} - Q_{Lr} - Q_{evap-\infty} \quad (1)$$

Q_{evap} is the heat that is transferred to the fluid in the evaporator. The vapor generated in the evaporator wick is sensibly heated ($Q_{evap-sh}$) in the vapor grooves as the evaporator envelope is at a temperature higher than the fluid saturation temperature. Pressure drop, due to friction, occurs as the fluid flows through various loop components on its way back to the evaporator core from the evaporator exit. As a result, the pressure in the core (point 5) is lower than that above the wick meniscus (point 0). Since the core and the CC are in a saturated two-phase state, the temperature of the fluid in the core will be lower than on the outer surface of the wick. This temperature difference across the wick causes some heat leak into the core (Q_{Lc}, often termed back conduction). Thus, the energy balance in the evaporator is

$$Q_{evap} = \underbrace{mh_{fg,0}}_{\text{Vaporization}} + Q_{Lc} + Q_{evap-sh} \quad (2)$$

The vapor leaving the evaporator (point 1) is superheated. The degree of superheat varies with the working fluid. Working fluids with lower evaporation heat transfer coefficient result in higher evaporator temperature. This leads to increased sensible heating in the vapor grooves, resulting in higher vapor superheat at the evaporator exit. The superheated vapor is transported along the vapor line, wherein heat exchange and pressure drop occur (point 2). The flow in the vapor line is normally turbulent, even at low heat loads; thus, significant pressure drop occurs in the vapor line, often leading to superheated vapor at the exit (depending on heat exchange and pressure drop in the vapor line). The fluid looses heat (Q_{sink}) in the condenser by sensible cooling of the vapor followed by latent heat removal and finally sensible cooling of the liquid. Fluid flow in the condenser tube is also associated with significant pressure drop. The fluid leaving the condenser exchanges heat with the surroundings, as it traverses the liquid line. Some pressure drop also occurs in the liquid line; however, it is significantly lower than the total loop pressure drop. The fluid leaving the liquid line is generally subcooled. The subcooling associated with the returning liquid balances the heat leaks in the core and CC together. The heat balance in the evaporator core is given by

$$Q_{Lr} + Q_{Lc} + x_4\, h_{fg,5} = \underbrace{A_r U_{r-\infty}(T_r - T_\infty)}_{\text{loss to ambient}} + \underbrace{\dot{m}\, C_{p,54}(T_5 - T_4)}_{\text{sensible heating}} \quad (3)$$

The compensation chamber temperature is dictated by an energy balance between the cool liquid line working fluid, heat leaks from the evaporator, and possible thermal interaction with the surroundings [1]. The fluid in the CC is saturated up to moderate heat loads. Beyond a certain heat load (Q_{hf}) the CC may hardfill i.e., the CC is full of subcooled liquid. This condition is encountered if the LHP fluid inventory is high. Often the CC is charged such that it never hard-fills and the fluid in the CC is always saturated (point 5).

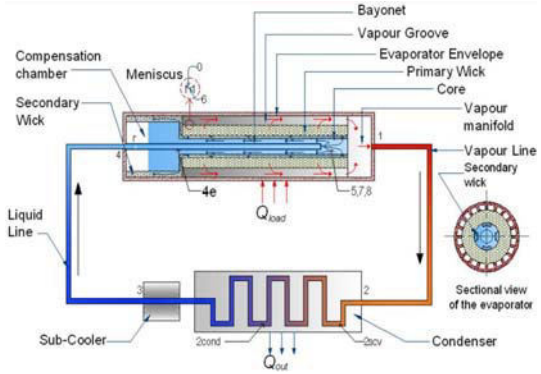

Figure 1. Schematic of Loop Heat Pipe.

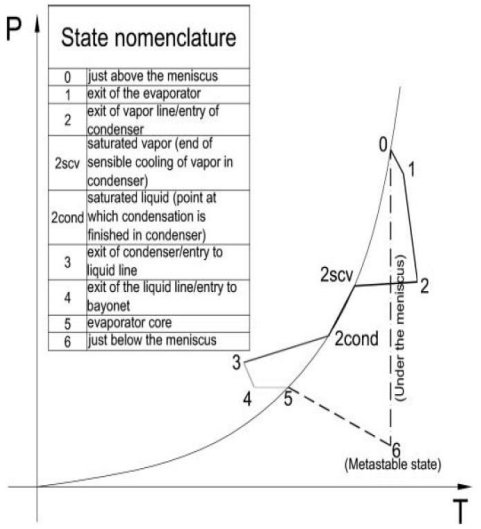

Figure 2. Depiction of States of the Fluid at the Entry and Exit of Various Components

If the CC hardfills, then the state of the fluid in the CC is subcooled and thus point 5 would lie left of the saturation curve. The fluid, in the core, migrates radially outward through the wick where it undergoes sensible heating. The fluid in the wick is superheated liquid. Just below the meniscus (point 6) the pressure of the liquid is lowest in the entire loop, while the temperature is almost the same as that of the vapor above the meniscus. The fluid in the wick does not undergo boiling/evaporation as the incipient superheat is not exceeded. It may be noted that the fluid, as it traverses in the wick to the meniscus (processes in segments 5–6 and 6–0 in Figure 1.2), is

not in an equilibrium state; rather, it traverses through a series of non equilibrium states and hence cannot be represented on a P-T diagram; therefore, processes 5–6 and 6–0 are represented with dashed lines.

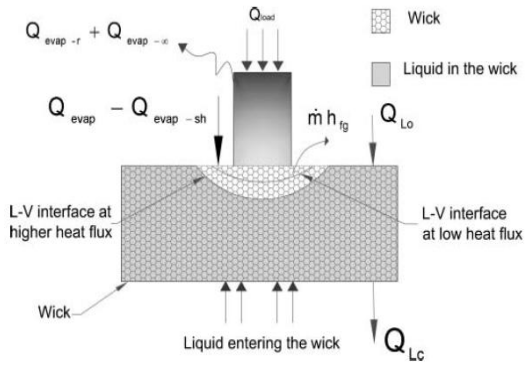

Figure 3. Heat and Mass Flow in the Evaporator of an LHP

The surface tension in the meniscus help sustains the flow around the loop. Circulation of working fluid in the loop is possible if and only if the total loop pressure drop does not exceed the maximum possible capillary pressure (capillary limit) permissible across the meniscus located at the liquid–vapor interface in the wick. This is expressed by the inequality

$$\Delta P_{mcp} \geq P_0 - P_6 = \Delta P_{12} + \Delta P_{23} + \Delta P_{34} + \Delta P_{56} \qquad (4)$$

Where the maximum capillary pressure (ΔPmcp) is given by the Laplace–Young equation

$$P_{mcp} = 2\sigma \cos(\theta) / r_{wp} \qquad (5)$$

Where r_{wp} is the pore radius of the wick and θ is the contact angle. When heat is applied on the evaporator, evaporation occurs on the outer surface of the wick. For the fluid flow in the loop to initiate, it is necessary that a favorable pressure difference is established across the wick. Since the fluid on either side of the wick is saturated, the pressure difference is related to the temperature difference across the wick by the Clausius–Clapeyron relation (also possible to obtain from equation of state [6]. If the total pressure drop in the loop ($P_0 – P_6$) exceeds maximum capillary pressure (ΔPmcp) the loop deprimes. Other operating limits (namely, viscous limit, sonic limit, etc.) have been discussed in references [4].

It may be noted that the total pressure drop in the loop is much smaller than the absolute pressure in the loop; hence the saturation temperature anywhere in the loop differs by a small value ($T_0 – T_5 \approx 1$ K or less). Thus, the saturation temperature in the loop (T_0) is a unique temperature for a given operating condition and is often called the operating temperature (T_0). Often the temperature in the CC is taken as the operating temperature (generally measured on the top surface of the CC under terrestrial condition where falling film condensation may occur due to minor heat losses to the ambient). The direct measurement of the CC temperature might not always be a true representative of the operating temperature, as the wall temperature will be influenced by:

(i) The cooling of the CC liquid by the cold liquid returning from the condenser.

(ii) The heat transfer along the CC wall due to heating from the evaporator envelope.

Another condition when direct measurement of the CC temperature fails to represent the operating temperature is when the CC is hard-filled. It is noteworthy that the small saturation temperature difference between the evaporator and condenser ($T_0 – T_{2cond}$) results in very high thermal conductance within the loop.

An important component of the LHP in microgravity applications (i.e. space) is the Secondary wick. It serves a number of purposes:

(i) Ensures that the primary wick stays wet during heat load transients

(ii)Under steady state, it isothermalizes the core of the evaporator and the compensation chamber by a mechanism analogous to heat pipe action.

(iii)In terrestrial applications it ensures the wick is wetted when the LHP evaporator has an adverse tilt (i.e. evaporator above compensation chamber). Thus in terrestrial applications, the primary wick determines the adverse elevation capacity (i.e. height of evaporator above condenser) whereas the secondary wick determines the adverse tilt capacity.

This study seeks to understand some aspects of the operation of a secondary wick in an LHP.

III. EXPERIMENTAL OBJECTIVE

The objective of this thesis was to study a secondary wick configuration for loop heat pipe constructed at ISRO Satellite Centre. This study was carried out in two phases:

(i) In order to evaluate the secondary wick heat transport capability, the secondary wick configuration working as a heat pipe was fabricated. This configuration of (SS316L, 3rolls wire mesh) performance was characterized for heat transport capability under different adverse tilts of heat pipe.

(ii) In order to study the performance of secondary wick (to determine if it reduces the evaporative heat transfer coefficient) in the Engineering model LHP, tests were conducted with and without secondary wick in the LHP fabricated at ISAC.

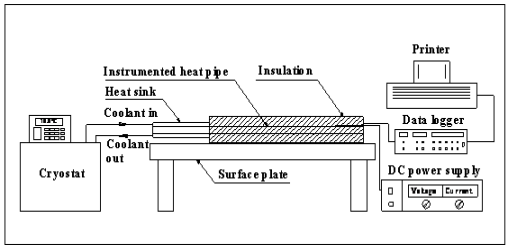

Figure 4. Schematic of Heat Pipe Test Set up

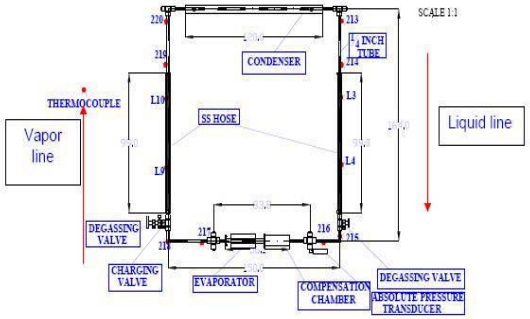

Figure 5. Schematic of LHP Test Set up

TABLE I

Vapor Line	Liquid Line	Reservoir
Outer diameter: 6.35mm	Outer diameter: 6.35mm	Outer diameter: 40mm
Inner diameter: 4.5mm	Inner diameter: 4.5mm	Inner diameter: 35mm
Length: 2354mm	Length: 2598mm	Length: 120mm
Material: SS316L	Material: SS316L	Material: SS304
Volume: 29cc	Volume: 36cc	Volume: 115cc

Evaporator	Nickel Wick
Active Area = 27960mm2	Size: Tubular (OD=24.5mm, ID=11mm, Length=200mm)
Groove Dimensions : Trapezoidal (Base=2.66mm, Top=5.79mm, Height=5mm)	Pore Size: 7-12µm
	Porosity: 35%
No of Grooves: 10	Volume of Vapor manifold: 33cc
Contact area with wick: 10000mm2	Volume of Vapor Groove: 43cc
Secondary Wick	
Material	SS mesh
Length	200mm
Outer	11mm
Inner	10.4mm
Pore Size	<100µm
No of Layers	3

IV. RESULTS AND DISCUSSION

The performance of secondary wick configuration, while operating as a heat pipe (heat pipe performance test) is presented first. Subsequently, the LHP experimental performance test with and without secondary wick are presented.

The fabricated heat pipe contains ammonia as working-fluid and a wick structure (3 rolls of ss wire mesh) enclosed in an evacuated hermetically sealed envelope. The fluid absorbs heat energy and becomes vapor due to latent heat of vaporization. The vapor carries this heat energy and rejects by condensation on the radiator and the condensate liquid returns back due to capillary action of the wick in order to maintain continuous transfer of heat energy. Therefore, heat transport capability of a heat pipe is limited mainly due to **capillary pressure** generated in the wick i.e., the axial grooves in axially grooved heat pipe. For the heat pipe to function satisfactorily, the capillary pressure developed by the grooves should be capable of providing enough mass flow rate of the working fluid to carry the heat from the evaporator to condenser, while overcoming maximum pressure drop in the liquid and vapor flow paths. Hence, the capillary pressure should overcome all the pressure losses occurring in the liquid and vapor flow paths including any pressure drop due to **adverse gravity** condition (adverse tilt).

The heat pipe of length 600 mm (typical length of an LHP) was selected for the determination of heat transport capability. The heat pipe was divided into three zones, namely, heat input / evaporator zone (**150** mm long), heat removal / condenser zone (**150** mm long) and heat transport / adiabatic zone (**250** mm long). The heat pipe was instrumented with an electrical heater of capacity 100 W at evaporator end and T-type thermocouples (30 AWG) at various locations on both the channels for axial temperature measurements. The evaporator and adiabatic zones of the heat pipe were insulated with ceramic wool and foam. The condenser end of the heat pipe was mounted with a heat sink connected to a cryostat set at **10ºC** for all the cases of adverse tilts. Near zero gravity condition can be simulated in the laboratory by keeping heat pipe horizontal.

Therefore, instrumented heat pipe was kept on a leveled surface plate through suitable support fixture, which has a provision for adverse gravity tilt adjustments. After each test, the adverse elevation was varied and experiments were conducted for obtaining the capillary burn out.

Heat input was given to the heat pipe through the heater and increased in steps till dryout which represents maximum heat load a heat pipe can transfer, while maintaining the required operating temperature, defined as the average adiabatic temperature of the heat pipe, by adjusting the set temperature of cryostat. **Dry out** (when the return liquid is not able to reach the evaporator) in a heat pipe is easily observed by a sudden rise in the evaporator temperature with a small additional heat load increase.

The same procedure was followed for determination of maximum heat transport of the heat pipe at different adverse tilts also.

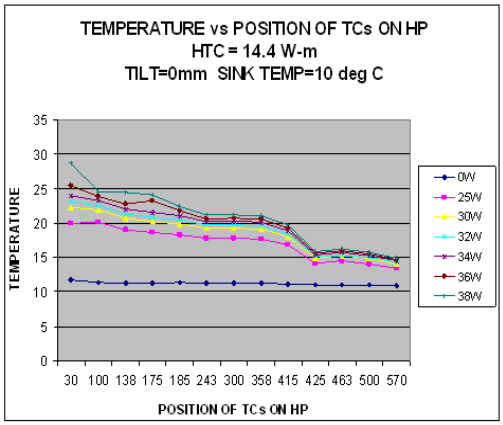

Figure 6. 0mm Tilt, Temperature vs Position of Thermocouples

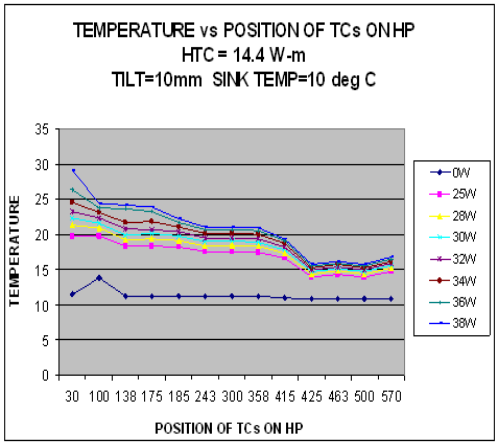

Figure 7. 10mm Tilt, Temperature vs Position of Thermocouples

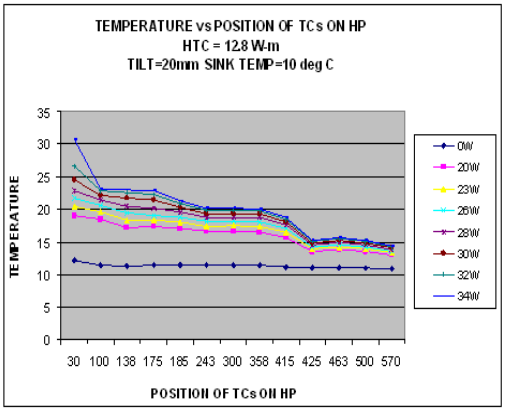

Figure 8. 20mm Tilt, Temperature vs Position of Thermocouples

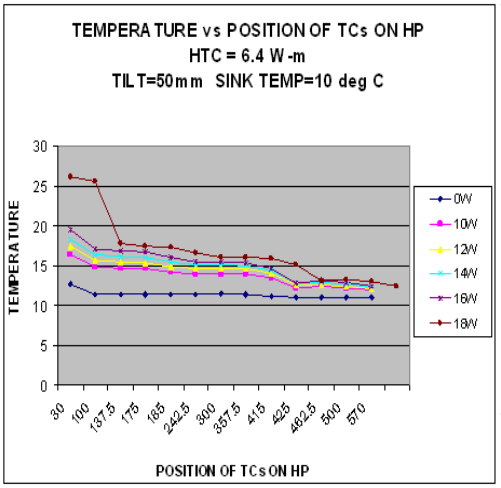

Figure 9. 50mm Tilt, Temperature vs Position of Thermocouples

The heat pipe experimental test data are summarized in the table 5.1 and Fig. 5.10. The heat transport capability at different adverse tilts is given therein. It is observed that a maximum of **36** W was transported at **0** tilt and about **10 W** at **60** mm adverse tilt. Thus the configuration with 3 wraps of SS wire mesh can handle the design requirement of 25 W at an operating temperature of **20ºC**.

TABLE II

TILT mm	SINK TEMP °C	EFFECTIVE LENGTH m	BURN OUT HEAT LOAD	EXPERIMENTAL HEAT TRANSPORT CAPABILITY W-m
0	10	0.4	36	14.4
5	10	0.4	36	14.4
10	10	0.4	36	14.4
15	10	0.4	34	13.6
20	10	0.4	32	12.8
25	10	0.4	30	12
50	10	0.4	16	6.4
60	10	0.4	10	4
70	10	0.4	4	1.6

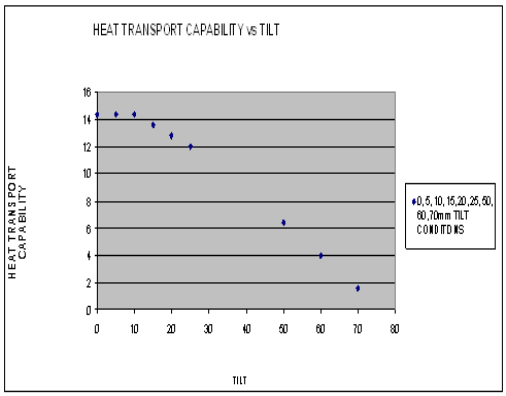

Figure 10. Heat Transport Capability vs Tilt

The LHP fabricated at ISAC was tested with and with out the secondary wick with ammonia as working fluid and Nickel wick. The goal of this test is to see if the secondary wick blocks the liquid flow to the primary wick. The LHP was tested at 0 mm adverse elevation at a heat load of about 600W in both the cases. The steady state temperatures (defined as < 0.1 deg C/ hr) obtained at the heat load of 600 W with and without the secondary wick.

The goal of this test was to see if the secondary wick blocks the liquid flow to the primary wick. The heat transfer coefficient with no secondary wick is 30117.0 W/m^2K where as with the secondary wick the heat transfer coefficient is 19115.92 W/m^2K. While this represents a 30% degradation in the heat transfer coefficient, the heat transfer coefficient is well above the requirement of 8000 W/m^2K. Thus the test concluded that this secondary wick configuration is adequate and it can transport 36W at 5mm adverse tilt.

V. CONCLUSION

From this study, the proposed configuration of secondary wick is adequate based on two criteria outlined below:

1) Heat transport capability (36 W at 5mm adverse tilt).

2) Blockage of wick: While there is significant blocking of wick, it is concluded that the heat transfer coefficient is still adequately large enough to allow fluid flow to the primary wick.

Thus the future generation of LHP at ISAC may use this secondary wick configuration.

ACKNOWLEDGMENT

The authors would like to acknowledge Thermal System Department of Indian Space Research Organization, Bangalore, Karnataka, for their support to this project, and valuable guidance

REFERENCES

[1] Adoni, A. A., Ambirajan, A., Jasvanth, V. S., Kumar,D., Dutta, P., and Srinivasan, K., Thermohydraulic Modeling of Capillary Pumped Loop and Loop Heat Pipe, Journal of Thermophysics and Heat Transfer, vol. 21, no. 2, pp. 410–421, 2007.

[2] Jasvanth, V. S., Adoni, A. A., Ambirajan, A., and Kumar, D., Results of Experimental and Theoretical Study of Ammonia Based Loop Heat Pipe, Journal of Spacecraft Technology, vol. 19, pp. 18–31, January, 2009.

[3] Singh, R., Akbarzadeh, A., Dixon, C.,Mochizuki,M., and Riehl, R. R., Miniature Loop Heat Pipe With flat Evaporator for Cooling Computer CPU, IEEE Transactions on Components and Packaging Technologies, vol. 30, no. 1, pp. 42–49, 2007.

[4] Launay, S., Satre, V., and Bonjour, J., Parametric Analysis Of Loop Heat Pipe Operation: A Literature Review, International Journal of Thermal Sciences, vol. 46, pp. 621–636, 2007.

[5] Adoni, A. A., Ambirajan, A., Jasvanth, V. S., Kumar, D., and Dutta, P., Effects ofMass of Charge on Loop Heat Pipe Operational Characteristics, Journal of Thermophysics and Heat Transfer, vol. 23, no. 2, pp. 346–355, 2009.

[6] Adoni, A. A., Ambirajan, A., Jasvanth, V. S., Kumar, D., and Dutta, P., Theoretical and Experimental Studies on an Ammonia-Based Loop Heat Pipe With a flat Evaporator, IEEE Transactions on Components and Packaging Technologies, vol. 33, no. 2, pp. 478–487, 2010.

[7] Adoni, A. A., Ambirajan, A., Jasvanth, V. S., Kumar, D., and Dutta, P., Theoretical Studies of Hard filling in Loop Heat Pipes, Journal of Thermophysics and Heat Transfer, vol. 24, no. 1, pp. 173–183, 2010.

[8] Adoni, A. A., Ambirajan, A., Jasvanth, V. S., Kumar, D., Badarinarayan, K., and Dutta, P., Evaporation Heat Transfer Coefficient in a Capillary Pumped Loop and Loop Heat Pipe for DifferentWorking fluids, Heat Transfer Engineering, vol. 33, 2012 (in press).

[9] Launay, S., Sartre, V., and Bonjour, J., Analytical Model for Characterization of Loop Heat Pipes, Journal of Thermophysics and Heat Transfer, vol. 22, no. 4, pp. 623–631, 2008.

[10] S W Chi, "Heat Pipe Theory" Vol 1, 1971

[11] W G Anderson, P M Dussinger, S D Garner, D B Saraff, "Loop Heat Pipe Design, Manufacturing and Testing", Heat Transfer Summer Conference, San Francisco, 2009.

[12] Teirm T Hoang, "Mathematical Modeling of Loop Heat Pipe-Part 2, Secondary Wick Analysis," 5th International Energy Conversion Engineering Conference and Exhibit, USA, 2007

◈◈◈

Thermal Analysis of an Electronic Package using TAMS and TNETFA

[1]NATARAJ K A, [2]S GANESAN & [3]K V SREENIVASA RAO

[1] Mechanical Department Siddaganga Institute of Technology Tumkur, Karnataka
[2] Thermal System Group ISRO Satellite Centre Bangalore, Karnataka
[3] Mechanical Department Siddaganga Institute of Technology Tumkur, Karnataka

Abstract— A typical electronics package is verified using the lumped modeling methodology using the FORTRAN code TNETFA and TAMS available in academic literature. TAMS stand for Thermal Analyzer for Multilayer Structures (TAMS) and TNETFA stands for Transient Network Thermal Analyzer (TNETFA). Electronics packages constitute dissipation heat sources of components located on multi - layered boards (PCB). Protecting the components from thermal damage which comes from careful selection of layout, dissipation levels and thermal control methods. Code implementation, code verification, academic benchmarks and board level validations has been made to validate the applicability of TAMS and TNETFA codes for PCB thermal analysis. A review of compact thermal modeling method to package electronics problem is studied. Results of the thermal analysis are compared with standard benchmarks in available literature. While considering the strong conduction and radiation modes under typical operating environments, improvements in the temperature levels of the cards were observed with changes in Location of chips, Operational sequence of cards and Re-arrangements of cards within the package. Based on the results of thermal analysis changes are suggested to improve thermal performance of the electronic package.

Keywords-*TAMS, TNETFA, Electronic package, PCB, Chip,* lumped modeling

I. INTRODUCTION

Power dissipation is an important issue in present day PCB design. Power dissipation will result in temperature difference and pose a thermal problem to a chip. In addition to the issue of reliability, excess heat will also negatively affect electrical performance and safety.

Circuit boards are often called printed circuit boards or PCB's. The modern manufacturing process is however based on etching not printing. The simplest PCB has one or two layers of copper. They are typically used in low cost home electronics. High performance products require more complex layer structures. The only areas where copper has been etched away are where via holes connect signals from one layer to another. A PCB usually serves three functions.

1. Provides the necessary mechanical support for the components in the circuit.
2. Necessary electrical interconnections.
3. Bears some heat load from all the components which it carries.

Various components are placed on the PCB with different power sources. Many different types of components are involved covering various shapes and electrical lead wire arrangements. Generally used components are discussed below. Dual inline packages (DIP'S), large scale integrated circuits (LSIC's), hybrids and most recently the micro processes have been replacing the discrete resistors, capacitors, transistors and diodes. No matter which groups of components are used for an electronic system, the mounting techniques must provide sufficient cooling to permit the device to operate effectively in its environment. The best method of determining the effectiveness of any cooling system appears to be in the **measurement of the case and junction temperatures** of the individual electronic components. Experience has shown that it is not a good practice to exceed the case temperature of **100 degree centigrade** for long period on electrically operating equipment's with any of the components mentioned above, or the failure rates show a large increase when the electronic components are to be cooled only by conduction. A good heat flow path must be provided from each component to the ultimate heat sink. The ultimate heat sink may simply be the outside ambient air, or it may also be a sophisticated liquid cooled heat exchanger. Each segment along the heat flow path must be examined in detail to ensure that the thermal resistance is low enough for the proper cooling.

SCOPE OF WORK

The existing literature on PCB thermal analysis suggests lumped thermal model development and open source codes like TAMS and TNETFA can help the user to solve academic and reasonably sized board level thermal problems.

In this work, the source codes of TAMS and TNETFA have been made use of to create, validate a series of problems and also understand its results with the commercially available tools like TAK, PC-Analyze and FEAP software's.

II. TAMS AND TNETFA

TAMS is written in FORTRAN IV in a manner that permits the program to be run on most computing systems with at least 30,000(decimal) words of memory. The equations derived for sources and resistances at various levels within the multilayer structure have been included with present values of depth that meet the requirements of most practical problems.

Application of TAMS requires the user to select from one of six possible cases, any of which may use anisotropic thermal conductivity.

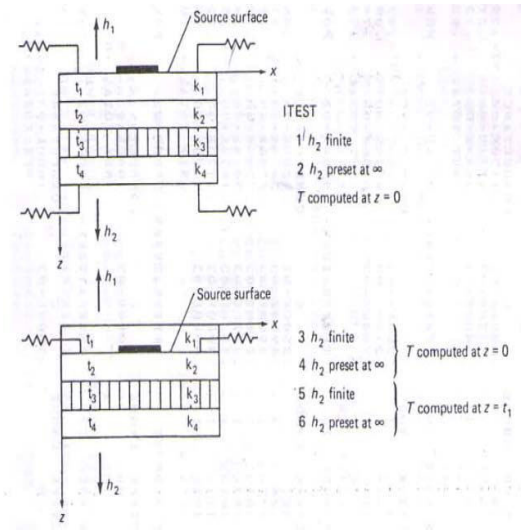

Fig 1. Problem cases for TAMS

The above figure emphasizes the multilayer aspect. Cases 1, 3 and 5 are concerned with Newton's law cooling from both the surfaces, whereas cases 2, 4 and 6 assume an isothermal surface (T_A) at the base. In all the cases except 3 and 4, the temperatures are calculated at the source centers and in the same plane as the sources. The two exceptions, cases 3 and 4, still provide the temperature calculations at the x, y centers of the source, but displayed in the z-direction to the top surface (z = 0). The use of resistances attached to the bottom surface (z = C4) is limited to case 1, sufficient for most problems.

TAMS PROGRAM ACCURACY

The accuracy of a particular solution is dependent upon at least three factors.

- The first is the extent to which the physical problems and TAMS model have one to one correspondence. Certainly this is difficult to assess quantitatively.
- Second, the basic physical parameters, thermal conductivity and heat transfer coefficients, are very often known to no better than +_ 20%.
- A third element addressed is the error obtained by truncating the Fourier-series to a finite number of terms.

TAMS does not have a self-contained series truncation system, but rather the user resorts to a program option that outputs a single-source plot of temperature vs number of terms.

TNETFA is a general purpose steady state and transient thermal analysis program that may be used to predict temperature pressure and airflow. Although the program is not difficult to use, the engineer or designer will have to spend some time to develop familiarity we basic input rules and features peculiar to this program.

A thermal network analysis requires a theoretical model that provides a one to one correspondence between the physical and mathematical models. As in all simulation techniques, the theoretical model is in reality an approximation of physical model. A successful thermal analysis requires the correct identification of significant aspects of the physical system that must be individually incorporated into theoretical model as conductance elements. The geometry of some heat transfer and air flow problems is sufficiently complex that the analyst may be able to include only the most significant flow paths.

Each element of the thermal model must be quantitatively specified. In a conduction problem a path length, cross sectional area and thermal conductivity are required to complete specify a single element. A convectively cooled surface must be described by a surface element area and a heat transfer coefficient. Accurate values of heat transfer coefficients are particularly difficult to obtain because complex and irregular shapes give rise to airflow and heat transfer characteristics that are often quite different often what is predicted using classical heat transfer criteria.

A few comments are in order concerning airflow predictions. Two techniques are indicated in this book. The first uses classical methods to predict pressure and airflow distribution within an electronic enclosure. TNETFA permit solutions of pressure network problems to o complex for scientific calculator solutions. Occasionally it is necessary to have both laminar and turbulent flow resistances in a single network and TNETFA will accumulate this kind of problem.

A second analytical tool available for airflow characterization uses two-dimensional laminar flow theory. Air velocity and temperature rise may be computed from streamline computations. This method is most valid for forced airflow, and accuracy of the results dependent upon the extent to which the actual airflow is of streamline nature. There are very few data at present to indicate the accuracy of this method other than qualitative-type indications of potential trouble spots.

THEORITICAL BASICS OF TAMS AND TNETFA

The equation requiring a solution is the differential equation for steady state heat conduction with an anisotropic thermal conductivity K_{xi}, K_{yi}, K_{zi} independent of x, y, and z respectively within each layer.

$$K_{xi} (\Delta^2T/ \Delta x^2) + K_{yi} (\Delta^2T/ \Delta y^2) + K_{zi} (\Delta^2T/ \Delta z^2) = -Q$$

BOUNDARY CONDITIONS:

The most applicable edge boundary conditions on T(r) assume negligible heat loss across these usually small areas:

$$\Delta T/ \Delta x = 0; x=0, A$$

$$\Delta T/ \Delta y = 0; y=0, B$$

Radiation and convection from either or both of the substrate surfaces are accounted by:

$$K_z \Delta T/ \Delta z - h_1 T = 0; Z = 0$$

$$Kx \Delta T/ \Delta z + h_2 T = 0; Z = C4$$

Where, h_1 and h_2 are the appropriate heat transfer co-efficient. As isothermal at Z= C4 is obtained in the final solution by letting h_2 approach infinity. Note that the surface flux density is written as having linear temperature dependence.

SOLUTIONS FOR MULTI SOURCES

The theoretical considerations of extending the single-source solution to the significantly more practical problem of a multi-source, multiple lumped resistance application are accomplished by super position of the single source solutions.

$$T(r_i) = \sum_{j=1}^{NS} Q_j A_{ij}(r_i, r_j) - \sum_{k=1}^{NR} F_k A_{ik}(r_i, r_k) + T_A$$

Multi-source, multi resistance temperature

The A_{ij} and A_{ik} are solution for single source magnitude; i.e., A_{ij} is the temperature $T(r_i)$ at r_i due to a unit source at r_j for zero ambient temperature. Q_j is the heat into the system at r_j and F_k is the heat out of the system at r_k and through a lumped parameter thermal resistance R_k.

III. PROBLEM DEFINITION AND ENCLOSURE DETAILS

The current package consists of a PCB with number of components having different level of heat dissipations. Each PCB is conductively and radiatively coupled for heat transfer. With the modes of heat transfer being conduction, convection and radiation. The aim of the present work is predicting the steady state temperature of a PCB. Effects due to various thermal parameters of the components are studied and analyzed.

The enclosure and board properties in detail required to carry out the problem. A printed circuit board is 9.0inX9.0in in dimension and 0.5in thick. A realistic problem with 34 components with a total power dissipation of 19.37W is taken, solved and analyzed. The component details are given in the table below. Both one resistor and two resistor models are solved using TNETFA tool.

BOARD PROPERTIES

Name: sample card
Type: PCB
Material: FR4
Thermal conductivity: 0.00686W/in deg C
Board emissivity: 0.9
Total power: 19.57W
Length: 9.0 in
Width: 9.0 in
Thickness: 0.5 in
Node size: 10X 10
Initial temperature: 51 deg C
Natural convection dimensional parameter: 1.6667
Resistor type: 1 and 2 resistor.
Component style: Dual inline package (DIP)
Number of leads: 8.
Lead cross section area: 4.52 X E-4 in^2.
Lead length: 2.04E-1 in
Lead material: Kovar.
Lead thermal conductivity: 3.95E-1

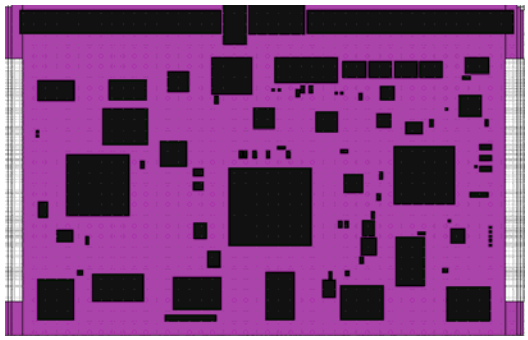

Fig2. PCB with components

ENCLOSURE PROPERTIES

Type: Hallow tray type
Total power: 0W
Length: 10in
Width: 10in
Height: 10in
Temperature: 51°C
Thermal conductivity: 0.26021W/in^0C
Wall thickness: 0.5 in

Fig 3. PCB in an enclosure

COMPONENTS DETAILS

SOURCE	POWER (W)	X-PCB (in)	Y-PCB (in)	LENGTH (in)	WIDTH (in)	HEIGHT (in)	R_{jb} (^{0}C/W)	R_{jc} (^{0}C/W)
1	4.0	2.413	7.086	1.1328	1.137	0.16	1.2	1.2
2	2.3	1.833	3.82	1.47	1.48	0.16	12.1	0.19
3	2.0	3.33	6.05	0.487	0.487	0.16	17.6	7.34
4	1.83	2.61	1.239	1.1036	1.092	0.16	17.4	7.8
5	0.825	1.082	1.78	0.9296	0.5232	0.16	82	18
6	0.75	3.98	3.34	0.386	0.3912	0.16	20.9	20.5
7	0.75	4.05	4.475	0.386	0.3912	0.16	20.9	20.5
8	0.75	4.75	6.014	0.3830	0.386	0.16	20.9	20.5
9	0.75	0.7927	7.75	0.518	0.9144	0.16	95	20
10	0.75	0.7927	6.837	0.518	0.9144	0.16	95	20
11	0.75	0.4366	4.119	0.9144	0.5232	0.16	95	20
12	0.6	0.4165	0.607	0.607	0.650	0.16	50	50
13	0.45	0.4368	2.529	2.5296	0.645	0.16	50	50
14	0.45	0.4368	8.087	8.087	0.7747	0.16	50	50
15	0.396	3.7388	7.625	7.625	0.6654	0.16	82	18
16	0.396	3.7388	6.76	6.7612	0.6908	0.16	82	18
17	0.33	4.26	0.762	0.762	0.4064	0.16	53.3	24.7
18	0.315	4.582	2.324	2.324	0.264	0.16	52	4
19	0.26	3.688	5.354	5.354	0.264	0.16	52	4
20	0.26	3.56	5.74	5.74	0.264	0.16	52	4
21	0.167	0.167	5.436	5.436	0.6146	0.16	84.04	18.2
22	0.165	3.952	1.818	1.818	0.2214	0.16	104	38
23	0.16	4.064	2.38	2.38	0.264	0.16	52	4
24	0.033	4.582	6.78	6.78	0.3911	0.16	104	38
25	0.033	4.582	7.457	7.4572	0.3911	0.16	104	38
26	0.033	4.572	8.74	0.3911	0.6704	0.16	104	38
27	0.033	4.572	8.07	0.3911	0.6704	0.16	104	38
28	0.017	1.442	5.45	0.3048	0.232	0.16	113	46.6
29	0.033	2.89	5.76	0.142	0.1828	0.16	206	86
30	0.033	3.147	5.76	0.1472	0.1828	0.16	206	86
31	0.033	5.01	2.37	0.3073	0.4267	0.16	73	24
32	0.033	5.01	1.46	0.3073	0.4242	0.16	73	24
33	0.033	5.01	1.91	0.3073	0.4216	0.16	73	24
34	0.033	5.01	2.83	0.3073	0.4318	0.16	73	24

CASE 1: ONE RESISTOR MODEL RESULTS FROM TNETFA vs TAK

COMPONENT (DIP-8 PINS)	TNETFA (Deg C)	TAK (Deg C)	COMPONENT (DIP-8 PINS)	TNETFA (Deg C)	TAK (Deg C)
1	90.0	92.33	18	81.07	83.2
2	68.71	71.15	19	82.67	84.2
3	140.5	142.0	20	82.71	82.07
4	74.0	76.34	21	45.52	46.04
5	76.98	78.26	22	68.05	70.17
6	74.86	76.2	23	73.33	75.4
7	88.51	90.99	24	66.68	69.86
8	74.96	77.6	25	60.96	62.43
9	68.6	70.0	26	51.61	50.82
10	87.80	90.42	27	36.12	36.41
11	88.16	90.08	28	57.92	59.70
12	60.73	61.55	29	70.72	70.21
13	63.87	65.0	30	75.55	76.06
14	63.67	65.7	31	43.78	44.78
15	78.64	80.2	32	42.19	43.09
16	88.56	90.12	33	42.25	43.20
17	60.81	61.55	34	42.99	44.03

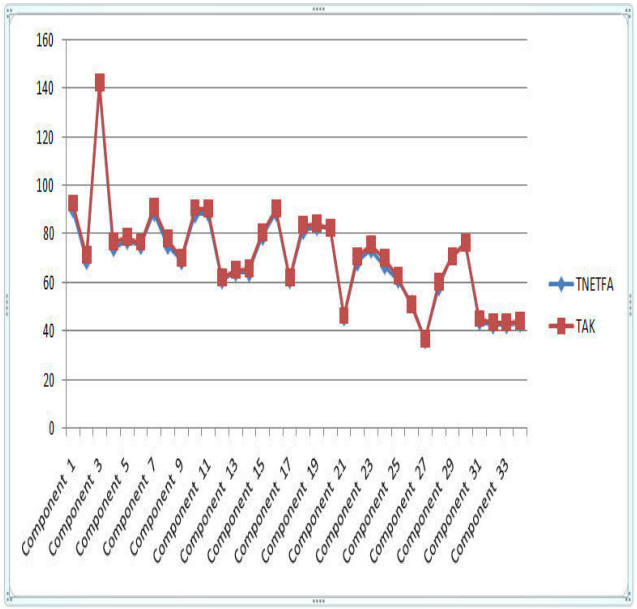

Fig 4 Graph plot for 1-resistor model, TNETFA vs TAK

CASE 2: TWO RESISTOR MODEL RESULTS FROM TNETFA vs TAK

COMPONENT (DIP-8 PINS)	TNETFA (Deg C)	TAK (Deg C)	COMPONENT (DIP-8 PINS)	TNETFA (Deg C)	TAK (Deg C)
1	86.21	88.16	18	78.25	80.18
2	65.23	67.25	19	78.73	80.79
3	133.5	135.98	20	78.77	80.09
4	70.30	72.00	21	43.62	44.186
5	72.94	74.95	22	65.40	67.23
6	71.97	72.3	23	70.64	72.53
7	85.57	87.7	24	62.16	64.93
8	72.06	74.2	25	56.73	57.85
9	65.64	66.66	26	48.18	47.8
10	81.47	82.33	27	35.51	35.7
11	81.75	83.00	28	55.05	56.4
12	57.54	59.08	29	67.19	69.25
13	59.92	61.00	30	71.52	73.6
14	60.48	62.21	31	42.59	43.46
15	73.27	75.04	32	41.17	41.95
16	80.73	82.79	33	41.27	42.09
17	59.02	60.45	34	41.99	42.87

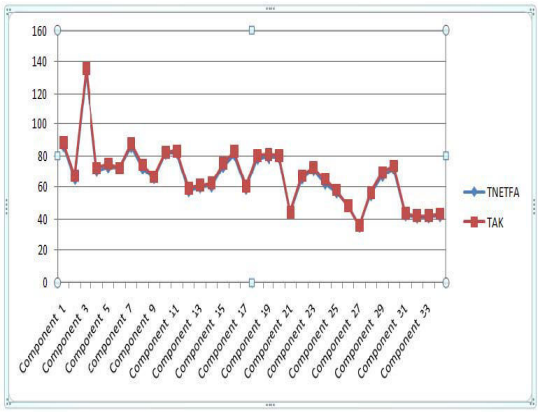

Fig 5 Graph plot for 2-resistor model, TNETFA vs TAK

IV. CONCLUSION

An effective thermal modeling and analysis solver can provide considerable ease in thermal analysis of an electronic package and its components. Such solver can provide the analyst a mean to evaluate design alternatives towards evolving better thermal management schemes. Thermal performance levels in terms of temperatures can be accessed under different operating conditions and safe operating levels can be specified for operation of any electronic package.

The open source codes of TAMS and TNETFA were compiled and tested with a series of verification problems. The difficulty in using them from manually prepared data files was realized while solving larger problems. So, suitable GUI interfaces with data validation were developed as a part of this study. An enclosure housing a typical PCB with several components was thermally analyzed using the above tools. Their results from a commercial tool like TAK were also compared. A good match in results was noticed for the problems attempted in this project. The analysis carried out using TAMS and TNETFA could provide useful insight into the thermal behavior of an electronic package.

ACKNOWLEDGMENT

The authors would like to acknowledge Thermal System Department of Indian Space Research Organization, Bangalore, Karnataka, for their support to this project, and valuable guidance

REFERENCES

[1] Lee, C.C. "Thermal analysis of integrated circuit devices and packages" **Volume:** 12, 701 – 709, Dec 1989

[2] Da-Guang Liu "Asymptotic thermal analysis of electronic packages and printed-circuit boards", **Volume:** 18, 781 – 787, Dec 1995

[3] Ellison, G.N. "Extensions of the closed form method for substrate thermal analyzers to include thermal resistances from source-to-substrate and source-to-ambient" **Volume:** 15, 658 – 666, Oct 1992

[4] Ellison, G.N, "Thermal analysis of circuit boards and microelectronic components using an analytical solution to the heat conduction equation" Int. Heat Transfer, 144 – 150, 5-7 Mar 1996

[5] Gordon Ellison "Thermal Computations for Electronic Equipments" Von Nostrand press.

[6] Dean L. Monthei, et al., Package Electrical Modeling, Thermal Modeling, and Processing for GaAs Wireless Applications, Kluwer Academic Publishers, 1999.

[7] Chin, J. H., Panczak, T. D. and Fried, L., 1992, Spacecraft thermal modeling, Int. J. Numer.Methods Eng., vol. 35, pp.641-653.

[8] Ellison, G. N., The effect of some composite structures on the thermal resistance of substrates and integrated circuit chips. IEEE Trans. Electron Devices, March, 1973, ED-20, 233-8.

[9] Ellison, G. N., The thermal design of an LSI single chip package. IEEE Trans. Parts, Hybrids, and Packaging, December, 1976, PHP-12, 371-8.

[10] Ellison, G. N., Thermal analysis of micro electric packages and printed circuit boards using an analytical solution to the heat conduction equation. Advances in engineering software, Elsevier Science Limited.

◈◈◈

Plc Based Automated System in Process Industry Using PLC and SCADA – A Study at FLSMIDTH (I) Private Limited

SHAHID FAIZEE

Manipal Institute of Technology,
Manipal, Karnataka, India

ABSTRACT-Modern PLCs can be programmed in a variety of ways, from ladder logic to more traditional programming languages such as BASIC and C. Another method is State Logic, a very high level programming language designed to program PLCs based on state transition diagrams. SCADA (SUPERVIOSRY CONTROL AND DATA ACCQUISATION) is a system used to monitor a plant from a central location. It is widely used in water treatment plants and lately it has been used in chlorination and pumping station, cement manufacturing process, power, steel, etc.Automation is the use of machines, control systems and information technologies to optimize productivity in the production of goods and delivery services. The correct incentive for applying automation is to increase productivity, and/or quality beyond that possible with current human labor levels so as to realize economies of scale, and/or realize predictable quality levels. FLSMIDTH Automation has been supplying modern process and quality control technology since the early 1970s.The objective of Expert Control System (ECS) which is Supervisory Control And Data Acquisition (SCADA) is to interpret the automation process in a graphical form.A SCADA (ECS or any other) system usually consists of the following subsystems: A human–machine interface or HMI is the apparatus or device which presents process data to a human operator, and through this, the human operator monitors and controls the process. A supervisory (computer) system, gathering (acquiring) data on the process and sending commands (control) to the a process. Remote Terminal Units (RTUs) connecting to sensors in the process, converting sensor signals to digital data and sending digital data to the supervisory system. Programmable logic controller (PLCs) used as field devices because they are more economical, versatile, flexible, and configurable than special-purpose RTUs.PLC Logics have been developed in PLC Software SIEMENS STEP7 (S7).These PLC logics are then used to develop Motor Blocks. These developed logics are then used in simulating applications in PLC system. The SIEMENS PLC will then be communicated with Expert Control System (ECS) SCADA through communication ports. This SCADA is a product of FLSMIDTH. The Inputs and Outputs defined in the PLC SIEMENS Software are available as buttons when the Motor Blocks developed and downloaded into the PLC Hardware are integrated with ECS SCADA. The buttons can be operated from the SCADA Software itself and thus any process industry such as CementPlant, Mineral Industry, etc. can be automated.

Key words: *FLSMIDTH Automation, Expert Control System (ECS), Supervisory Control and Data Acquisition System (SCADA), Programmable Logic Controller (PLC).*

INTRODUCTION

The old focus on using PLC automation simply to increase productivity and reduce costs was seen to be short-sighted, because it is also necessary to provide a skilled workforce who can make repairs and manage the machinery. Moreover, the initial costs of automation were high and often could not be recovered by the time entirely new manufacturing processes replaced the old. (Japan's "robot junkyards" were once world famous in the manufacturing industry.)

FLSMIDTH Automation is now often applied primarily to increase quality in the manufacturing process such as Cement Plant, where automation can increasethequality substantiallyby reducing the labor cost and increasing the efficiency of the cement plant by making every process automated.

Expert Control System (ECS)

ECS/Process Expert is a high-level control and optimization solution for complex process such as pyro processes. Pyro processing is a process in which materials are subjected to high temperatures (typically over 800°C) in order to bring about a chemical or physical change. Pyro processing includes such terms as ore-roasting, calcination and sintering. Equipment for pyroprocessing includes kilns, electric arc furnaces and reverberator furnaces.
Cement manufacturing is a very common example of pyro processing. The raw material mix (raw meal) is fed to a kiln where pyroprocessing takes place. As withmost industries, pyro processing is the most energy-intensive part of the industrial process.Control optimization is performed using the ECS/Process Expert advanced capabilities that are specifically tailored to meet the individual user requirements. The control and optimization system is based on the well-known industrial platform ECS (Expert Control & Supervision) system specially developed for supervisory control, monitoring and reporting functions.

Benefits of Expert Control System (ECS)

- ECS/Process Expert helps plant management to meet and adapt production goals, and to compete effectively in increasing market demands.
- Combination of the know-how from plant engineers and operators with ECS/Process Expert and FLSmidth Automation's extensive expertise results in the creation of

the best possible high-level process control system.

- Improved process stability is done through continuous, accurate and consistent process evaluation and control actions. Rapid control and suppression of process upsets. Lower operating costs through energy and maintenance savings.
- Better, more uniform end-product quality. Better utilization of human, capital and material resources. Minimized emissions and environmental effects. Release of operators from routine control actions.

Problem Statement

Development of Faceplates (Faceplates contains information about inputs and outputs of PLC logics) in SCADA ECS (Expert Control System) Software based on:

- Development of ladder logics in Siemens Step 7 (S7) PLC Software.
- Development of Motor Block using the developed logics.

Motor Block

Motor Block is a block diagram made from a number of logics developed in SIEMENS PLC Software.

In development of Motor Block, following INPUTS were used: Motor Ready (RDY), Run Feedback (RFB), Local Stop (LSP), Local Start (LST), Safety Interlock (SAF), Sequential Interlock (SQI), Process Interlock (PRO), Start Interlock (STI), and Overload (OVL).

And the OUTPUTS used in Motor Block were: Motor Okay (MOK), Command 2 (COM2), Motor Run (MRN), Command 1 (COM1), Trip (TRIP), and Motor Run Delay (MRD).

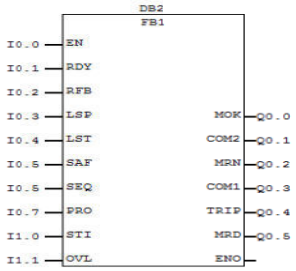

Figure 1 Motor Block Diagram

INPUTS	SYMBOLS	ABBREV.
ENABLE	I0.0	EN
READY	I0.1	RDY
RUN FEEDBACK	I0.2	RFB
LOCAL STOP	I0.3	LSP
LOCAL START	I0.4	LST
SAFETY INTERLOCK	I0.5	SAF
SEQUENTIAL INTERLOCK	I0.6	SEQ
PROCESS INTERLOCK	I0.7	PRO
START INTERLOCK	I1.0	STI
OVERLOAD	I1.1	OVL

OUTPUTS	SYMBOLS	ABBREV.
MOTOR OKAY	Q0.0	MOK
COMMAND 2	Q0.1	COM1
MOTOR RUN	Q0.2	MRN
TRIP	Q0.3	TRIP
MOTOR RUN DELAY	Q0.4	MRD

I0.0, I0.1, I0.2, I0.3, I0.4, I0.5, I0.6, I0.7, I1.1 are the inputs of Motor Block.

Q0.0 Q0.1, Q0.2, Q0.3, Q0.4 are the outputs of Motor Block.

Terms Related to Motor Block

The Motor Block and Group Control Block have number of features in terms of interlocks present. There are four different types of interlocks. They are:

Safety Interlock: The function of this interlock is to provide the safe operation of the unidirectional motor.

Sequential Interlock: Its function is to provide the sequential operation of a number of motors. If any motor in the sequence fails, it will give a return error.

Process Interlock: The function of this Interlock is to provide smooth operation of the number of processes taking place in the individual unidirectional motor.

Start Interlock: The function of this interlock is to provide the proper starting of the unidirectional motor(s).

The Advantages for Motor Block is:

- The Motor Block has individual signals to stop and start the motor.
- The Motor Block also has a response signal from the motor to indicate that the motor is running.
- In the Motor Block, the time between sending the signal to activate the motor andreceiving the response signal is calculated. If nosignal is received in this time, themotor must be switched off**.**

Integrating the Motor Block (PLC Logics) with SCADA

After the development of Motor Block and Group Control Block in SIEMENS S7 Software and downloading the block logics into the PLC Hardware, faceplates are designed for motor blocks and group control block. To develop the Faceplates, it is necessary to create Submods. Submods are the parts of faceplates. For a Motor Block and Group Control Block, total six Submods were created.

The Submods consists of the following:

INPUTS defined for the Motor Block Group Control Block in SIMATIC S7 Software. OUTPUTS defined for the Motor Block Group Control Block in SIMATIC S7Software. The Modes i.e. the Local Mode and Auto Mode and Startand Stop Buttons will also be present in a submod.

The Screenshots showing how a submod is designed is as shown below:

Motor Block:

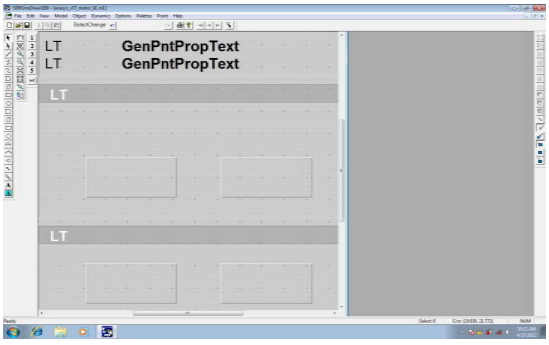

Figure 2 Start and Stop (Auto and Local Mode)

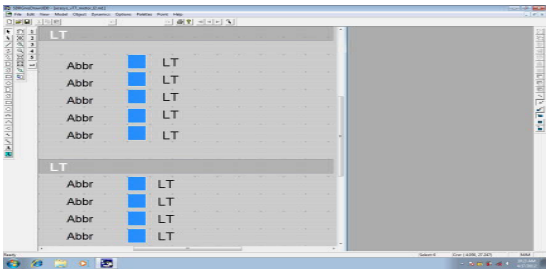

Figure 3 Submod for Inputs

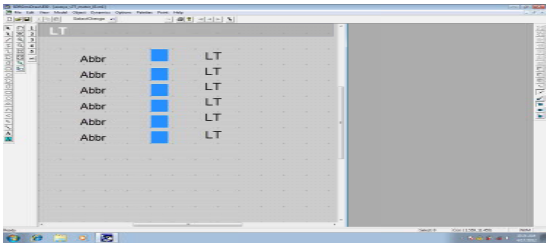

Figure 4 Submod for Outputs

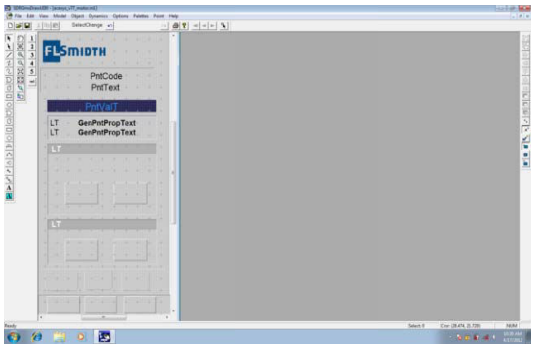

Figure 5 Faceplate for Motor Block

Figure 6A Typical Layout for Crusher in Cement Plant (Run-Time Mode)

Implementation of PLC and SCADA Software and Hardware

The PC in which the logics (Motor Block and Group Control Block) are created is connected to the PLC Hardware through an Ethernet Cable. The Program i.e. the logics are transferred through this Ethernet module from the PLC Software to PLC Hardware. The SCADA and PLC Hardware are then made to communicate with each other through Ethernet Communication Protocol. The Crusher section created in the ECS software is then converted from

editor mode to run time mode. In this run time mode, the buttons present on the faceplates for the crusher section can be operated and thus, the crusher (section) of a cement plant can be automated.

Result Analysis

The ECS SCADA has the capability of displaying the trends.Whenthe informationgathered is displayed graphically and the SCADA system shows the developing problems and helps the management in taking the corrective measures by showing the problems in Hunman Machine Interface device such as Computer Screen in graphical form.

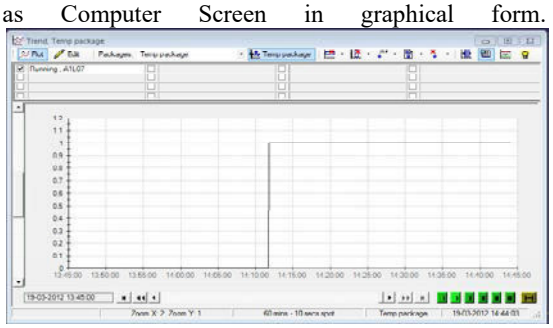

Figure 7 Graphical Interpretation by Expert Control System (ECS) SCADAthrough Human Machine Interface (HMI)

CONCLUSION

- One typical part is Crusher, which is used to crush the raw materials brought from quarry mines by quarry trucks and the raw material are then crushed into the crusher. The function of Crusher is to crush the raw materials such as limestone into tiny balls
- With the development of this project, it will significantly reduce the labor cost and improves the performance of plant in the manufacturing industry.
- Management can save time as well because information is gathered by SCADA at a central location so that personnel do not have to go and wander about on site.
- It has the capability of displaying the trends. When information gathered is displayed graphically, the system shows the developing problems and helps the management in taking the corrective measures.
- It will be the one system that will keep running everything perfectly, smoothly and fast.
- The Automated System developed can be used in various parts of a Cement Plant such as Crusher, Kiln, Preheater, and even for logistics purposes.
- The main focus of this project is controlling a unidirectional motor used in a Crusher section of a Cement Plant using Siemens PLC controller Hardware. The unidirectional Motor thus can be used to control or run different parts of a Cement Plant.

REFERENCES

[1] "SIEMENS STEP 7(S7) ACESYS-Reference Manual", PEPPERL+FUCHSPublisher (Germany), Edition 2008, Part No. 194576 08 /10 05

[2] "SENSORS FOR FACTORY AUTOMATION", PEPPERL+FUCHS Publisher(Germany), Edition 2008, Part No. 193679 04/08 01

[3] PLC Basics and Communication Protocols, www.plcmanual.com

[4] Expert Control System (ECS) SCADA Software, www.flsmidth.com/automation

[5] SIEMENS SIMATIC STEP7 (S7) Software, www.automation.siemens.com

[6] http://en.wikipedia.org/wiki/Automation

[7]http://www.flsmidth.com/en-US/Products/Product+Index/All+Products/Process+Control/Advanced+Process+Control/ProcessExpert+Cement

◈◈◈

Air conditioning of Motor Vehicles using Liquid Nitrogen

[1]M. JAIVIGNESH, [2]B. VIJAYA RAMNATH

Department of Mechanical Engineering,
Sri Sai Ram Engineering College
Chennai, Tamil Nadu, India.

Abstract— Cryogenics is a branch of physics that studies the production of very low temperatures (below 123K) and the behaviour of materials at those temperatures. It is frequently applied to low temperature refrigeration applications such as in the liquefaction of gases and in the study of physical phenomena of materials at temperature approaching absolute zero. Liquefied gases, such as liquid nitrogen and liquid helium are used in many cryogenic applications. Using liquid nitrogen as a refrigerant reduces chloro-fluorocarbon (CFC) emission in atmosphere and it is an eco-friendly technique. This paper deals with usage of liquid nitrogen in air conditioning of motor vehicles. First the preparation of liquid nitrogen is discussed, followed by its storage and working as a refrigerant in air conditioning system. This is followed by its advantages and draw - backs.

I. INTRODUCTION

Air conditioning is a process by which air is cooled and dehumidified. An air conditioner especially operates on refrigeration at near ambient temperatures. There are many physical principles that relate to air conditioning. Basically, most air conditioning systems operate on the principle of evaporation and condensation of a refrigerant.
In the past, a chloro-fluorocarbon (CFC), R-12, used to be employed as a refrigerant for air conditioning in cars. As CFC is detrimental to the earth's ozone layer, a more environmental-friendly refrigerant, R-134A, has been mostly used since 1996. Additionally, to make sure existing CFC-12 is used as much as possible, rather than being wasted and released to the atmosphere, EPA (Environmental Protection Agency) issued regulations under section 609 of the 'Clean Air Act' to require that shop technicians use machines to recycle CFC-12. If an environmental friendly refrigerant like liquid nitrogen is used, it will not cause pollution of atmosphere. Air-conditioning of automobiles using cryogens like liquid nitrogen is an eco-friendly technique.

II. LITERATURE REVIEW

1. W. Peschka and C. Carpetis (1980) gave a short report on the design and test of a semi-automatic liquid hydrogen refueling station for automobiles.

2. Gustav Lorentzen and Jostein Pettersen (1993) suggested that the use of the old refrigerant carbon dioxide offers a key to the complete solution of the environmental problems in many areas of refrigeration usage.

3. Gustav Lorentzen (1994) presented some examples of how carbon dioxide can be used as a refrigerant.

4. Srinivasan et al (2003) presented exergy charts for carbon dioxide (CO_2) based on the new fundamental equation of state and the results of a thermodynamic analysis of conventional and trans-critical vapour compression refrigeration cycles using the data thereof.

5. Andy Pearson (2008) assessed the reasons why ammonia is so popular in industrial systems, the reasons why it is deemed less suitable for other applications and the possible benefits at local, national and international levels that might be gained by more general acceptance of ammonia as a refrigerant.

6. James M. Calm (2008) reviewed the progression of refrigerants, from early uses to the present, and then addresses future directions and candidates.
7. S.A. Tassou et al (2009) presented review on current approaches in road food transport refrigeration, estimates of their environmental impacts, and research on the development and application of alternative technologies to vapour compression refrigeration systems that have the potential to reduce the overall energy consumption and environmental impacts.

8. T.S. Ravikumar and D. Mohan Lal (2009) showed that a new mixture R134a/R600a/R290 can be a promising substitute for the existing R12 systems and it can eliminate the use of hygroscopic PAG oil.

9. Mohammad Omar Abdullah et al (2011) presented a comprehensive review on the past efforts in the field of adsorption air-conditioning systems for automobile. This work also aims to investigate the physicochemical properties of oil palm shell-based activated carbon and its feasibility for application in adsorption air-conditioning system.

10. Hamid Khayyam et al (2012) concluded that proposed intelligent energy management Control (IEMC) System developed based on Fuzzy Air

Conditioning Controller with Look-Ahead (FAC-LA) method is a more efficient controller for vehicle air conditioning system than the previously developed Coordinated Energy Management Systems (CEMS).

III. CRYOGENIC AIR SEPARATION AND LIQUIFIER SYSTEMS

Cryogenic air separation processes are routinely used in medium to large scale plants to produce nitrogen, oxygen, and argon as gases and (or) liquid products. Cryogenic air separation is the preferred technology for producing very high purity oxygen and nitrogen. It is the most cost effective technology for high production rate plants. All plants producing liquefied industrial gas products utilize cryogenic technology. The complexity of the cryogenic air separation process, the physical sizes of equipment, and the energy required to operate the process all vary with the number of gaseous and liquid products, required product purities, and required delivery pressures. Nitrogen-only production plants are less complex and require less power to operate than an oxygen-only plant making the same amount of product. Co-production of both products, when both are needed, increases capital and energy efficiency. Making these products in liquid form requires additional equipment and it doubles the amount of power required per unit of delivered product.

IV. GENERAL PROCESS DESCRIPTION OF CRYOGENIC AIR SEPARATION

There are numerous variations in air separation cycles used to make industrial gas products. Design variations arise from differences in user requirements. Process cycles are somewhat different depending upon how many products are desired (either nitrogen or oxygen; both oxygen and nitrogen; or nitrogen, oxygen and argon); the required product purities; the gaseous product delivery pressures desired; and whether one or more products will be produced and stored in liquid form.

Figure 1. Cryogenic air-separation process

All cryogenic air separation processes consist of a similar series of steps. Variations in selected process configuration and pressure levels reflect the desired product mix (or mixes) and the priorities/ evaluation criteria of the user. Some process cycles minimize capital cost, some minimize energy usage, some maximize product recovery, and some allow maximum operating flexibility.

V. CRYOGENIC LIQUID STORAGE

A. Dewars:

The typical container used to store and handle cryogenic fluids is the dewar. The dewar is multi-walled designed with a vacuum jacket for insulation and pressure relief valves to protect against over-pressurization. Cryogens normally are stored at low pressures. Liquid nitrogen dewars have one pressure relief valve set at 22 psig.

B. Cryotank:

The universal cryotank division of UIG offers a full line of cryogenic liquid storage tanks for liquid oxygen (LOX), liquid nitrogen (LN, LIN), liquid argon (LAR) and liquid carbon dioxide service, plus LNG and Ethylene storage tanks.

VI. CRYOGENIC AIR CONDITIONING SYSTEM IN AN MOTOR VEHICLE:

Water feels cold on our skin because it takes away heat (540 cal/gram) as it evaporates. Water vapour from our breath fogs and warms a cold glass as liquid water beads condense on the cold surface. The air conditioning unit repeats these phase transitions, evaporation of liquid to gas and condensation of gas to liquid, in a continuous cycle to carry heat from an evaporator inside a compartment to be released at a condenser outside.

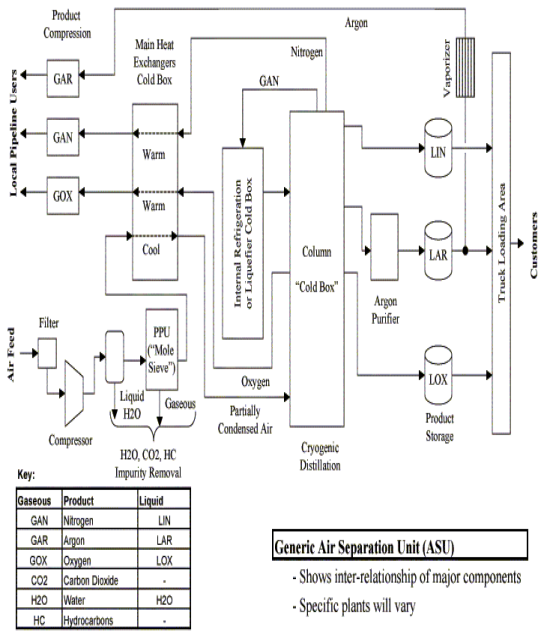

VII. WORKING OF AIR CONDITIOING SYSTEM USING LIQUID NITROGEN AS REFRIGERANT:

Air conditioning like it says 'conditions' the air. It not only cools it down, but also reduces the moisture content, or humidity. A number of people do not realize that turning on the air conditioning actually reduces the number of miles per gallon of a car. There is energy used in removing the heat and moisture from the air in the car, and this consumes

petrol because of the extra engine load. Air conditioning's main principles are

- Evaporation
- Condensation,
- Compression
- Expansion.

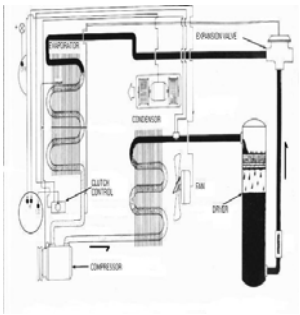

Figure 2. An automotive air-conditioning system

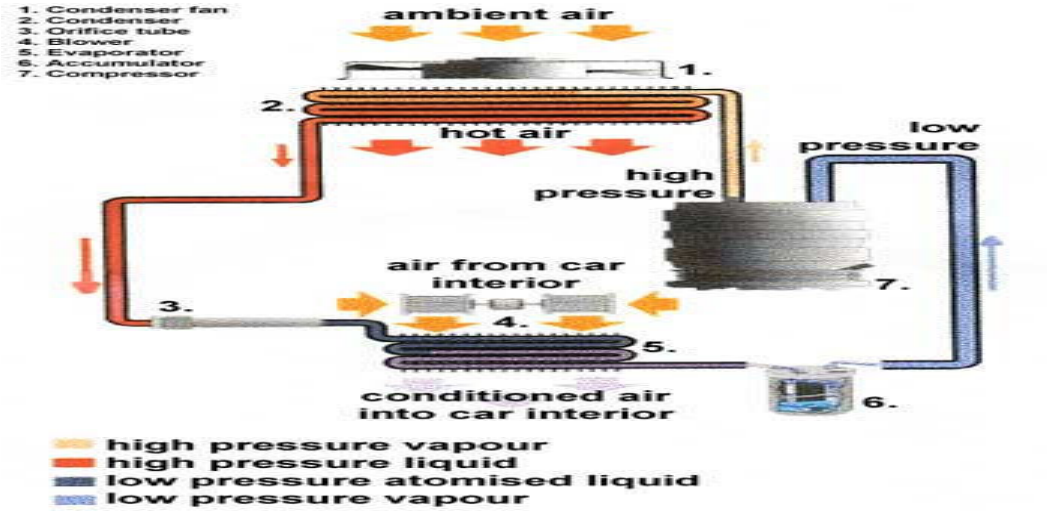

Figure 3. Air conditioning system using liquid nitrogen

Below discussed are the various components of an air conditioning system using liquid nitrogen.

A. Compressor:

The compressor is the work horse of the air conditioning system, powered by a drive belt connected to the crankshaft of the engine. When the air conditioning system is turned on, the compressor pumps nitrogen vapour under high pressure to the condenser.

B. Condenser:

The condenser is a device used to change the high-pressure nitrogen vapour to a liquid. It is mounted in front of the engine's radiator, and it looks very similar to a radiator. The vapour is condensed to a liquid because of the high pressure that is driving it in, and this generates great deal of heat. The heat is then in turn removed from the condenser by air flowing through the condenser on the outside.

C. Receiver:

Now the liquid nitrogen moves to the receiver-dryer. This is a small reservoir vessel for the liquid nitrogen, and removes any moisture that may have leaked into the nitrogen. Moisture in the system causes havoc, with ice crystals causing blockages and mechanical damage.

D. Expansion Valve:

The pressurized nitrogen flows from the receiver-drier to the expansion valve. The valve removes pressure from the
liquid nitrogen so that it can expand and become nitrogen vapour in the evaporator.

VIII. ADVANTAGES OF USING LIQUID NITROGEN IN AIR CONDITIONING

1. It is an eco-friendly technique. It does not release harmful pollutants to the atmosphere.
2. There is not risk of global warming & depletion of ozone layer.

3. As there is no release of carbon dioxide, green house effect can be avoided.
4. No lung or other respiratory related problems are caused due to the breathing of cooled air from a cryogenic air conditioner.
5. Due to the non-emission of carbon monoxide, it does not contribute to the air pollution as well as acid rain.
6. Liquid nitrogen being the cheapest most widely produced and most common cryogenic liquid, serves as an excellent refrigerant.
7. The temperature it puts out inside the vehicle is consistent and stable.

IX. SAFE HANDLING AND USAGE

Liquid Nitrogen can be hazardous to personnel if not handled properly. By reviewing this fact sheet, one will become aware of the conditions that increase the risk of accidents and injuries that can occur when working with cryogenic liquids.

X. DISADVANTAGES

1. Cold Embrittlement
   At cryogenic temperatures, many materials such as rubber, plastic and carbon steel can become so brittle that very little stress can break the material. Hence, for storing liquid nitrogen there is a necessity to use a material that will withstand cryogenic temperature.

2. Pressure buildup and Explosions
   Without adequate venting or pressure-relief devices on the containers, enormous pressures can build up on cryogen evaporation. A pressure relief vessel or a venting lid should be used in the liquid nitrogen storage containers to protect against pressure build-up.

3. Oxygen Enrichment
   Nitrogen, which has a low boiling point than oxygen will evaporate first. This can leave an oxygen-enriched condensate on the surface that can increase flammability of materials near the system creating potentially explosive conditions.

XI. CONCLUSION

Cryogenic air conditioning in automobiles is an eco-friendly technique. There is no emission of CFC's and hence damage to the ozone layer is prevented. Due to the non-emission of carbon monoxide, it does not contribute to the air pollution as well as acid rain. There is no risk of green house effect as there is no emission of carbon dioxide. It is relatively cheaper and can maintain constant and stable temperatures inside the vehicle. There are no respiratory problems created due to the breathing of air from cryogenic air conditioners. Thus it is a new and effective technique that can be implemented in all vehicles.

REFERENCES

[1] W. Peschka and C. Carpetis, "Cryogenic hydrogen storage and refueling for automobiles", International Journal of Hydrogen Energy, Volume 5, Issue 6, 1980, Pages 619-625.

[2] Gustav Lorentzen and Jostein Pettersen, "A new, efficient and environmentally benign system for car air conditioning", International Journal of Refrigeration, Volume 16, Issue 1, 1993, Pages 4-12.

[3] Gustav Lorentzen, "Revival of carbon dioxide as a refrigerant", International Journal of Refrigeration, Volume 17, Issue 5, 1994, Pages 292-301.

[4] Srinivasan, Y.K. Lim, J.C. Ho and N.E. Wijeysundera, "Exergetic analysis of carbon dioxide vapour compression refrigeration cycle using the new fundamental equation of state", Energy Conversion and Management, Volume 44, Issue 20, December 2003, Pages 3267-3278.

[5] Andy Pearson, "Refrigeration with ammonia", International Journal of Refrigeration, Volume 31, Issue 4, June 2008, Pages 545-551.

[6] James M. Calm, "The next generation of refrigerants – Historical review, considerations, and outlook", International Journal of Refrigeration, Volume 31, Issue 7, November 2008, Pages 1123-1133.

[7] S.A. Tassou, G. De-Lille and Y.T. Ge, "Food transport refrigeration – Approaches to reduce energy consumption and environmental impacts of road transport", Applied Thermal Engineering, Volume 29, Issues 8-9, June 2009, Pages 1467-1477.

[8] T.S. Ravikumar and D. Mohan Lal, "On-road performance analysis of R134a/R600a/R290 refrigerant mixture in an automobileair-conditioning system with mineral oil as lubricant", Energy Conversion and Management, Volume 50, Issue 8, August 2009, Pages 1891-1901.

[9] Mohammad Omar Abdullah, Ivy Ai Wei Tan and Leo Sing Lim, "Automobile adsorption air-conditioning system using oil palm biomass-based activated carbon: A review", Renewable and sustainable energy reviews, Volume 15, Issue 4, May 2011, Pages 2061-2072.

[10] Hamid Khayyam, Jemal Abawajy and Reza N. Jazar, "Intelligent energy management Control System", Applied Thermal Engineering, Volume 48, 15 December 2012, Pages 211-224.

[11] Dr. Mamata Mukhopadhyay, "Fundamentals of Cryogenic Engineering", Eastern Economy Editions, 2011.

"Stereo lithography" Effective Technique for Hearing AID Manufacturing

[1]PRANAV R. BIRAJDAR, [2]SHRUTI S. BAMMANI & [3]SHRINIWAS S METAN

[1,2,3] Dept. of Mechanical Engg. Nagesh Karajagi Orchid College of Engineering and Technology Solapur, Maharashtra, India.

Abstract— Rapid Prototyping (RP) Technologies are able to generate a 3D object directly from a CAD file, which is opposite to the conventional machining processes. Generally, conventional machining removes the raw materials layer by layer but in Rapid Prototyping material is added layer by layer. Stereolithography (SLA) remains one of the most powerful and versatile of all RP techniques. It has the highest fabrication accuracy and an increasing number of materials, that can be processed, are becoming available. A hearing aid is a small electronic device that the user wears in or behind his/her ear. It amplifies sound to provide speech information to listeners with a hearing loss. A hearing aid has three basic parts: a microphone, an amplifier, and a speaker which are assembled in a shell. Every shell like their respective ear cavities are unique as fingerprints, with the left cavity differing from the right one, for each individual. The current process of manufacturing customized hearing aids consists of many manual steps, all of which require expert knowledge and a very skilled labor. This paper gives an overview regarding the conventional shell manufacturing and presents a more effective solution: the Rapid Prototyping Method which is a more sophisticated and advanced process can be used to manufacture hearing aid effectively. It primarily includes three stages: impression scanning, virtual modeling and shell manufacturing.

Keywords- *Rapid Prototyping Technologies; CAD; Additive manufacturing; Stereolithography; Hearing Aids.*

I. INTRODUCTION

Rapid prototyping technologies are additive processes that fabricate parts layer-by-layer called Layer Manufacturing (LM).They are capable of creating parts with small internal cavities and complex geometries. The process for rapid prototyping and manufacturing (RP&M) basically consists of three steps: form the cross sections of the object to be manufactured, lay the cross sections layer by layer, and combine the layers [1].

RP&M method was first presented at the AUTOFACT show in Detroit (US) in November 1987, by a company called 3D Systems, Inc. At that time, the process was very inaccurate and the choice of materials was limited. Over about twenty years, many RP processes have been developed to produce various parts , for instance Laminated Object Manufacturing (LOM) , Fused Deposition Modeling (FDM) , Ink Jet Printing , Three Dimensional Printing (3DP) , Selective Laser Sintering (SLS) , Solid Ground Curing (SGC) and Stereolithography (SLA)[2], [3].

A. 3-D Printing Process

Although several rapid prototyping techniques exist, all employ the same basic five-step process. The steps are:

1. Create a CAD model of the design.
2. Convert the CAD model to STL (Standard Triangular Language) format.
3. Slice the STL file into thin cross-sectional layers.
4. Construct the model one layer atop another.
5. Clean and finish the model.

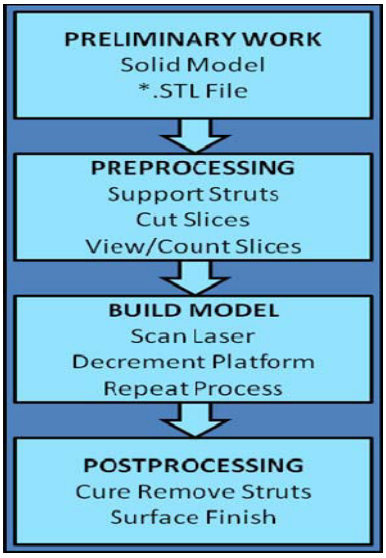

Fig 1: Rapid Manufacturing Process

1. *CAD Model Creation:* First, the object to be built is modeled using a Computer-Aided Design (CAD) software package (Pro/ENGINEER, Solid Works).
2. *Conversion to STL Format:* The various CAD packages use a number of different algorithms to represent solid objects. The industry standard exchange format for additive manufacturing is the STL (Stereolithography or Standard Triangulation Language) file. Basically, it is a file that replaces the original surface of solid, surface or scanned model with a mesh of

triangulated surface segments. Almost all of today's CAD systems are capable of producing a STL file. Because STL files use planar elements, they cannot represent curved surfaces exactly. Since the STL format is universal, this process is identical for all of the RP build techniques.

3. *Slice the STL File:* In the third step, a pre-processing program prepares the STL file to be built. Several programs are available, and most allow the user to adjust the size, location and orientation of the model. The pre-processing software slices the STL model into a number of layers from 0.01 mm to 0.7 mm thick, depending on the build technique. The program may also generate an auxiliary structure to support the model during the build. Supports are useful for delicate features such as overhangs, internal cavities, and thin-walled sections. Each RP machine manufacturer supplies their own proprietary pre-processing software.
4. *Layer by Layer Construction:* The fourth step is the actual construction of the part. Using one of several techniques RP machines build one layer at a time from polymers, paper, or powdered metal.
5. *Clean and Finish:* The final step is post-processing. This involves removing the prototype from the machine and detaching any supports. Some photosensitive materials need to be fully cured before use. Prototypes may also require minor cleaning and surface treatment. Sanding, sealing, and/or painting the model will improve its appearance and durability [4], [5], [6].

B. *The Need of Hearing Aids*

According to the latest scientific statistics, the percentage of the population with hearing problems is about 10%: a considerable figure which would mean about 70 million people in Europe and 30 million in North America while, at a global level, this would reach an alarming total of 500 million people [7].

In the United States of America approximately 17 in 1,000 children under age 18 have hearing impairment which steeply increases to 314 in 1,000 people over age 65 [8]. Hearing loss costs Australia almost $12 billion a year, with almost 160,000 people not working because they can't hear well enough [9].

Total world production of hearing aids is less than one tenth of global need; 75% of the annual production is distributed to North America and Europe and the rest 25% to the rest of the world. Thus it is important to accurately determine the extent of need of hearing aids in various countries [10].

C. *Stereolithography*

The Stereolithography apparatus is the first commercial RP process which was invented by Charles Hull in 1987 by 3D systems, Inc. The Stereolithography is an additive manufacturing process in which a liquid photo curable resin acryl-ate material is used. The process begins with the vat filled with the photo-curable liquid resin and the elevator table set just below the surface of the liquid resin. A laser beam then traces a single layer cross-section onto the surface of a vat of liquid polymer vectorizing first in one direction and then in the orthogonal direction and undergoing the photo polymerization Process (linking small molecules known as monomers into chain-like larger molecules known as polymers) which causes the polymer to harden precisely at the point where the ultraviolet light hits the surface.

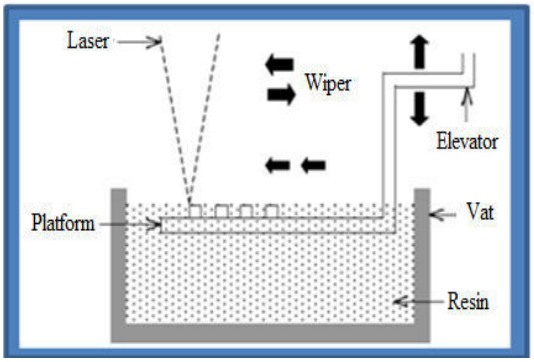

Fig 2: Schematic of SLA process

The UV laser is controlled by a galvanometer driven mirrors to generate X–Y motion. After a pattern has been traced, the SLA's elevator platform descends by a single layer thickness, typically 0.05 mm to 0.15 mm. Then, a resin-filled blade sweeps across the part cross section, re-coating it with fresh material. On this new liquid surface, the subsequent layer pattern is traced; adhering to the previous layer, in this way, the model is built layer by layer from bottom to top. When all layers are completed, the prototype is about 95% cured. Afterward, the solid part is removed from the vat and rinsed clean of excess liquid supports are broken off and the model is then placed in an ultraviolet oven for complete curing.

D. *Types Of Hearing Aids*

A hearing aid is basically a public-address system. Its key components are microphone, amplifier, receiver and a battery. Hearing aids can be categorized in many ways. The simplest way to categorize them is by the place in which they are worn, which also implies the size of the hearing aid.

1) Behind The Ear (BTE): Suitable for every type of hearing loss from mild to severe, the ear mould is custom made to fit any ear shape and the main components are housed externally. Companies manufacturing this style of aid have made significant improvements in recent years by decreasing the size whilst maintaining the quality of sound.

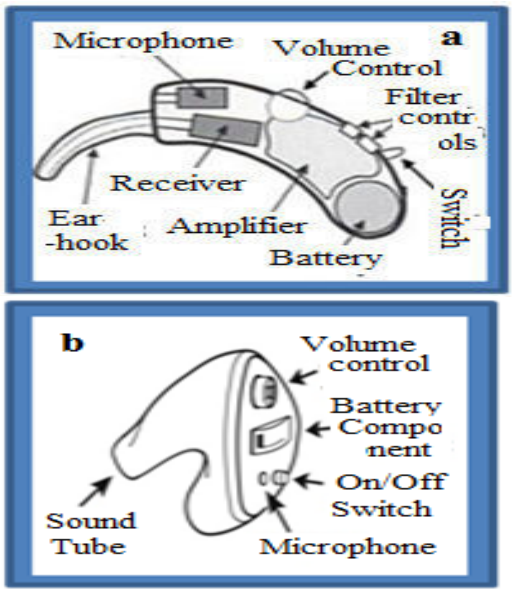

Fig 3: (a) Behind the Ear (b) In the Ear

2) In The Ear (ITE): This style is suitable for most degrees of hearing loss. The aid is smaller and so easier to use than the BTE types. These hearing aids fit comfortably and securely in the ear. Clients report that they can be more comfortable than most 'Behind-The-Ear' (BTE) aids [14], [15].

II. MANUFACTURING OF HEARING AIDS

Manufacturing of hearing aids is a very accurate and precise process with no room for error. Basically, there are two most prominent manufacturing techniques. Both these techniques are explained in detail below.

A. Conventional Shell Manufacturing

There are 10 steps that are followed by most companies when producing a hearing aid shell using the conventional approach. Although slight differences occur between manufacturers, the same 10 steps need to be completed regardless of the style of the custom product.

1. *Cast***:** A cast is a record of the ear impression made directly from the ear (Fig 4a). The Oto-block is removed and the lateral process is cut to make a base. Silicon material is poured over the ear impression to make this cast which, when completed, is called the investment.

2. *Trim:* The impression is then cut down to an appropriate size for the model ordered (Fig 4b). It is also tapered and detailed so that the finished shell can be easily inserted into the wearer's ear.

3. *Wax:* The trimmed impression is now dipped into hot wax (Fig 4c). The number of times it is dipped and the temperature of the wax determine the thickness of the wax on the impression. In general, the severity of the hearing loss and the dispenser's request for shell tightness will determine the amount of wax buildup. The skill of the technician is extremely important in ensuring an even coating of wax on the impression.

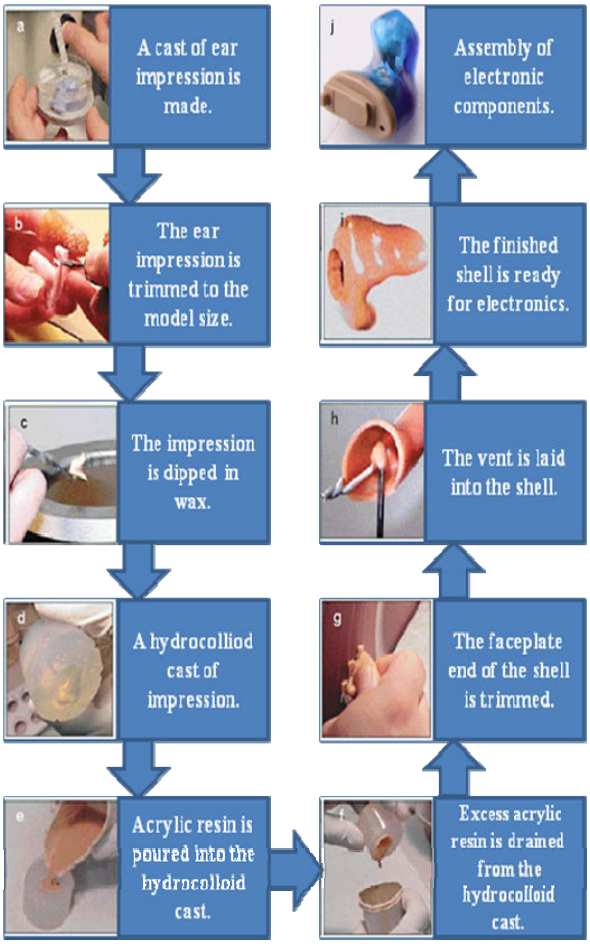

Fig 4(a- j): 10 steps of conventional shell manufacturing.

4. *Cast #2:* The trimmed and waxed impression is now cast in hydrocolloid (Fig 4d).This natural jell-like material is solid at room temperature, but liquefies when heated slightly. The hydrocolloid liquid will not melt the wax on the impression, and once it has hardened, an accurate casting of the impression is formed.

5. *Pouring of Shell Material:* Room-temperature cured (RTC) or UV-cured acrylic is poured into the hydrocolloid cast to make the shell (Fig 4e). The color of the acrylic is selected before pouring. The acrylic is allowed to cure slightly. The curing process starts from the outside and progresses towards the core of the shell.

6. *Drain/Drip:* With the acrylic hardening on the outside and the liquid acrylic still on the inside, the cast is turned over in order to drip the excess liquid acrylic out (Fig 4f). This creates a hollow shell that is a replica of the trimmed impression.

7. *Trim #2:* The shell that has just been formed will have excess acrylic on its lateral (usually faceplate) end from the dripping out of the hydrocolloid cast. This end must be flattened before the faceplate can be attached (Fig 4g).The amount of trimming determines the final profile of hearing aid.

8. *Vent:* The vent is now installed (Fig 4h). The vast majority of vents are internal channel vents. The diameter of the vent is determined by the hearing loss, available space, and the dispenser's request. The technician drills a hole in the shell at the receiver end, and then runs a wire of the desired diameter through the shell at the target location. Liquid acrylic is poured over the wire to make the channel vent. Once the acrylic has cured, the wire is removed and the vent is ready.

9. *Attaching Faceplate and Buffing Shell:* The technician aligns the faceplate over the shell, glues it in place, and then trims and rounds out any sharp corners in the faceplate. Once glued and assembled, the shell is buffed using a mild abrasive. The shell is now ready for electronics (Fig 4i).

10. *Assemble Electronics***:** The internal cavity of the shell is examined by the technician and excess acrylic is excavated using burrs. This step is necessary in order to give the technician room to properly position the receiver in order to minimize the risk of internal feedback. Installation of a wax guard system in the shell may require additional acrylic onto the shell. Once the electronic module and the battery/microphone assembly are installed, the custom hearing aid is ready for quality assurance testing (Fig 4j) [16], [17]

B. *Additive Manufacturing Method*

*1. The Impression***:** The process begins with an impression. The impression-taking process remains the same at this time as conventional method mentioned above (Fig 5a).

2. 3-D Modeling: Modeling is the process where the technician modifies the virtual impression with 3D modeling software and creates a virtual hearing aid shell (Fig 5d).An accurate ear impression is necessary to create a properly fitting ear shell. There are a number of operations that the modeler performs with the virtual impression to create the virtual shell (Fig 5e).

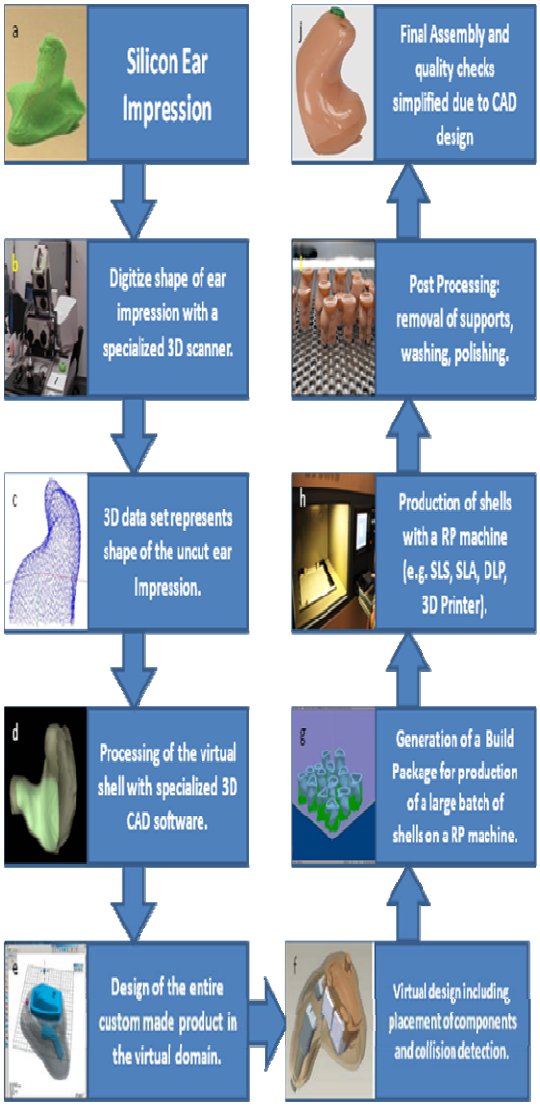

Fig 5(a-j): The 10 steps of shell manufacturing by Rapid Prototyping

3. 3-D Laser Scanning: The digital processing starts with the scanning of the shape of the ear impression. Using advanced laser-scanning methods, it is possible to produce an extremely accurate three-dimensional replica of the ear impression (Fig5b).The ear impression is scanned using lasers with specially created high-end optics that scan the impression, taking up to 100,000 data points, with precision on the level of microns. The resulting data file, called a "point cloud," is the virtual image of the impression. This image is an exact electronic duplicate of the impression, and its accuracy is designed to far exceed traditional physical methods for making the impression investment (Fig 5c).

4. Virtual Modeling: In virtual modeling, the technician experiments with the size of the shell

and different placements of the virtual components into the virtual shell until the best possible placement are achieved. The image of the virtual impression is used throughout the modeling as a virtual control mold. This allows the modeler to see the extent of the modifications performed and the anticipated fit of the finished hearing aid in the patient's ear.

In addition, all changes including the exact amount of material added or removed from the virtual impression are recorded in the computer for later retrieval and analysis. Virtual modeling of one hearing aid shell takes approximately 5 to 10 minutes (Fig 5f). Virtual modeling also plays an important role in generation of a build package for production of a large batch of shells on a SLA machine (Fig 5g).

5. Printing: Printing is the term used for the actual production of the shell. It is so called because the instructions generated during the modeling stage are now "printed" onto the material that is used to make the shell. In the Stereo Lithographic Apparatuses (SLA), a photo-sensitive acrylic resin is used as the materials to make shells. Because this material is very similar to the UV-cured acrylic material used today for conventional shells, it has the advantage that the resulting shells may be modified and treated like any other acrylic shells.

During the printing process, the SLA printer uses a laser (that has a spectrum that includes the UV range) to harden the photosensitive resin into shells that have been modeled during the modeling stage. The laser outlines the shell according to the instructions specified during the modeling stage. Very thin layers of material (1/10 mm thickness) are hardened to form the shell. For example, a CIC shell that is 20 mm in total length will require 200 layers of material to be hardened. This will take approximately 2-8 hours to complete depending on the number and styles of hearing aids being made. To optimize the process, anywhere from 40 to 80 different shells can be printed at the same time in a production run (Fig 5h).

6. Post processing and Installation: After the shells are collected, the supports are removed. They are cleaned and cured a final time in an UV oven before they are sent to have the faceplates and electronics assembled (Fig 5i).

The surface of the shell is matted to provide a skin-like texture. This textured finish provides a firm, comfortable fit with suitable retention in the ear. Yet, the material is not porous and it is designed for easy cleaning. Installation process includes aligning of faceplate and electronics module interface to the exact position specified during the modeling stage (Fig 5j) [18, 19, 20, 21].

III. DISCUSSION

Additive manufacturing is particularly well suited to the hearing industry because of the need to fit each user's ear with a custom appliance for maximum performance. Furthermore, it integrates all record-keeping within the computer database, negating the need to store processed ear impressions or the need to request new impressions for remakes. For the wearers, shells made with digital technology are more comfortable to wear and may allow the wearers to use more of the available gain from the hearing aids. Many renowned manufacturers such as Siemens, Starkey, Phonak, Unitron and Widex are making use of various rapid prototyping techniques for manufacturing of hearing aid. Widex, onr of the world's largest manufacturer of hearing aids uses Stereolithography for shell production.

Stereolithography process is basically selected because of its highest fabrication accuracy which eventually makes the hearing aid more comfortable and a better fitting device. The shells are made from a hypoallergenic, medical-grade plastic. Its textured surface is designed to increase wearer comfort and to reduce slippage. This method is comparatively cheaper if the shells are manufactured in a batch.

This type of shell-making technology holds some fascinating possibilities for the not-too-distant future. As software algorithms are improved, additional refinements of the virtual shell will allow for an even more accurate fit of the hearing instrument. Software algorithms will allow for simulations of insertion and removal, as well as simulations of the dynamics of the ear canal during jaw movement when speaking or chewing.

Research efforts are underway to eliminate the ear impression completely and scanning the ear directly as a means to create a virtual impression instead. It may be possible in the future to eliminate the physical impression, transferring all the necessary patient data directly to the manufacturer via the Internet.

IV. CONCLUSION

RP technology is elaborated in brief and a comparative study between conventional manufacturing and manufacturing using Stereolithography (SLA) is explained in detail with hearing aid example. As Stereolithography is fast and effective, saves time and money, allows speed delivery therefore it is one of the better alternatives for hearing aid manufacturing. In medical applications tolerances in manufacturing is one of the important aspects and by SLA we can control tolerances within 0.005mm/mm. Especially for products that require very high precision or surface finish stereo lithography system is one of the best

option. The description of various stages of ear shell manufacturing by both of these methods proves that SLA method is more effective for hearing aid manufacturing. A successful attempt has been made to include some important factors which prove the RP technique to be more efficient and accurate than the conventional method.

REFERENCES

[1] Terry Wohlers; New Developments and Trends in Product Design, Prototyping, Tooling, and Reverse Engineering, Wohlers Associates, Inc, 2000. Colorado, USA.

[2] Y. Abouliatim, T. Chartier; Fabrication of ceramics by stereolithography; RTejournal - Forum für Rapid Technologie, 2007; pp 1. (http://www.rtejournal.de/ausgabe4/1163/index html #Bandyopadhyay)

[3] Dr.A. Dolenc;An Overview Of Rapid Prototyping Technologies In Manufacturing; pp 5. (Institute of Industrial Automation Helsinki University Of Technology).

[4] Miltiades A. Boboulos; CAD-CAM & Rapid Prototyping Application Evaluation; Copyright 2010 Miltiades A. Boboulos, Ph.D. & Ventus Publishing ApS; ISBN 978-87-7681-676-6; pp 134-135.

[5] Mr.Sanjay C.Kumawat, Mrs.A.L.Gawali; APPLICATION OF CAD IN RAPID PROTOTYPING TECHNOLOGY; Journal of Engineering Research and Studies; E-ISSN 0976-7916; pp 3.

[6] Muhammad Enamul Hoque; Rapid Prototyping Technology- Principles and Functional Requirements; copyright 2011 InTech Publishers; pp 2.

[7] NIDCD; Statistics about Hearing Disorders, Ear Infections, and Deafness; 2006, National Institute on Deafness and Other Communication Disorders.

[8] Cox R, Alexander G.; (1995) The Abbreviated Profile of Hearing Aid Benefit. Ear Hear; 16:176-186.

[9] *Hearing loss in Australia - Australian* Hearing; p1; (www.hearing.com.au/upload/media.../Hearing-loss-in-Australia.pdf).

[10] Guidelines for hearing aids and services for developing countries (2nd edition); September 2004; copyright World Health Organization; ISBN 92-4-159243-5; pp 10.

[11] Vineet Kumar Vashishtha, Neeraj Mehla, Rahul Makade; ADVANCEMENT OF RAPID PROTOTYPING IN AEROSPACE INDUSTRY-A Review; ISSN: 0975-5462 Vol. 3 No. 3 March 2011.

[12] http://www.curbellplastics.com/prototyping-tooling sla-resins.html

[13] http://www.3dproparts.com/technologies/ stereolithography-sla

[14] Harvey Dillon; Hearing Aids; THIEME PUBLISHING GROUP 2001; pp 10-11.

[15] http: //www.countyhearing.co.uk/hearing-aids/

[16] Richard Cortez; Nick Dinulescu; Klavs Skafte; Brian Olson ; Denise Keenan; Francis Kuk, PhD; Changing with the Times: Applying Digital Technology to Hearing Aid Shell Manufacturing; Hearing Review, Vol. 11, No. 3, pp. 30-38; Publication Date: March 2004.

[17] William Lesiecki ; Shell Technology: The Shape of Things to Come in E-business; Hearing Review - October 2002.

[18] Paul Darkes and Laura Voll; Shaping the Future of Shell Technology with Digital Mechanics; Hearing Review-April 2002.

[19] Chester Pirzanski; Earmolds and Hearing Aid Shells: A Tutorial; Hearing Review -Septenber 2006.

[20] William Lesiecki; Does the In-Office Electronic Scanning of Impressions Really Change Everything; Hearing Review -January 2006.

[21] Massimo Martorelli; Virtual Prototyping in the Development Process of Customised Hearing Aid Shells; VIMation Journal; Issue 1, 2010; pp 34-35.

◈◈◈

Thermal analysis of a Gas Turbine Rotor Blade by using Ansys

G.NARENDRANATH(M.TECH)[1], S.SURESH M.TECH (ASSOC. PROFF)[2] & PUNNA RAO PAMARTI (M.TECH)[3]

[1,2]Siddharth Institute of Engineering and Technology
Puttur, Chittoor Dist, India
[3]Department of Mechanical Engineering
Mic College of Technology, Kanchikacherla
Vijayawada, Krishna Dist, Andhra Pradesh, India

Abstract— In the present work, the first stage rotor blade off the gas turbine has been analyzed using ANSYS 9.0 for the mechanical and radial elongations resulting from the tangential, axial and centrifugal forces. The gas forces namely tangential, axial were determined by constructing velocity triangles at inlet and exist of rotor blades. The material of the blade was specified as N155. This material is an iron based super alloy and structural and thermal properties at gas room and room temperatures The turbine blade along with the groove blade is modeled with the 3D-Solid Brick element. The geometric model of the blade profile is generated with splines and extruded to get a solid model in CATIAV5R15. The first stage rotor blade of a two stage gas turbine has been analyzed for structural, thermal and modal analysis using ANSYS 9.0 Finite Element Analysis software. The gas turbine rotor blade model is meshed in HYPERMESH 7.0, meshing software. The thermal boundary condition such as convection and operating temperatures on the rotor blade is obtained by theoretical modeling. Analytical approach is used to estimate the tangential, radial and centrifugal forces. The results obtained are discussed and reported.

Keywords-*ANSYS, CATIA V5R15, HYPERMESH 7.0*

I. INTRODUCTION

The purpose of turbine technology are to extract the maximum quantity of energy from the working fluid to convert it into useful work with maximum efficiency by means of a plant having maximum reliability, minimum cost, minimum supervision and minimum starting time.

The gas turbine obtains its power by utilizing the energy of burnt gases and the air which is at high temperature and pressure by expanding through the several ring of fixed and moving blades. Mikio Oi, Mariko Suzuki Natsuko Matsuura some of the experiments done on the structural analysis and shape optimization in turbocharger development(1) In this comparison between conventional method and computer aided engineering is done. It is essential to incorporate the Computer Aided Engineering in the turbocharger development and design process. Structural analysis of there component parts has been made so far mainly on the automotive and marine turbochargers, centrifugal compressors. We have made analysis of the stress caused by external force and pressure, analysis of thermal stress caused by heat and analysis of vibrations caused by natural frequency in the compressor impeller, turbine impellers and rotors as rotary parts., Sanford Fleeter, were done on the Fatigue life prediction of turbomachine blading(2), T.Madhusudhan, Need for analysis of stress concentration factor in inclined cutouts of gas turbine blades (3), M.Pradeep, Naveen Babu Chandu, Influence of taper, twist and thickness in rotor blades using Finite Element Analysis(4), Stuart Moffaty, Li He Blade forced Response prediction fro industrial gas turbines(5), M.Venkatarama Reddy, additional Director CVRaman nagar, Bangalore (6) describes the influence of taper, twist, thickness in rotor blade using Finite element analysis. Turbo machine rotor blades are subjected to different types of loading such as fluid or gas forces, inertia loads and centrifugal forces, Dr. K. Ramachandra**,** Director, Gas Turbine Research Establishment, Bangalore, (7) describes need for analysis of stress concentration factor in inclined cutouts of gas turbine blades, aero engine gas turbine blades are aerofoil in cross section and are twisted mounted on annular plate, which in turn is fixed to rotating disc. Blades operate at very high speed and temperature leading to induction of respective stresses. For air-cooling purpose, blades are provided with number of minute cooling holes (0.5 to 0.8 mm) on the hollow walls of the blades through which pressurized air is ejected. Holes are oblique, oriented at compound angles and are stress raisers and lower the resistance of the blade to thermal and mechanical fatigue.

II .WORKING OF THE GAS TURBINE

A gas turbine is an engine where fuel is continuously burnt with compressed air to produce a steam of hot, fast moving gas. This gas stream is used to power the compressor that supplies the air to the engine as well as providing excess energy that may be used to do other work. Turbine compressor usually sits at the front of the engine. There are two main types of

compressor, the centrifugal compressor and the axial compressor. The compressor will draw in air and compress it before it is fed into the combustion chamber. In both types, the compressor rotates and it is driven by a shaft that passes through the middle of the engine and is attached to the turbine as shown in fig 1.1

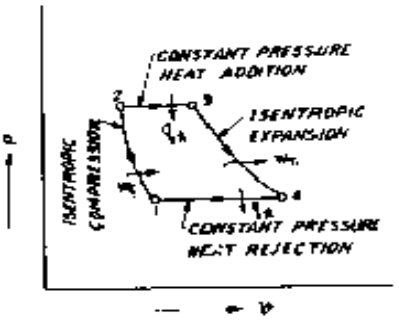

Fig 1.1 Indicator diagram of gas turbine

A. CONSTRUCTION OF TURBINE ROTOR BLADES AND THEIR COMPONENTS

Knowing the fluid conditions at exit of the gas generators, a value of static pressure was assumed at the turbine outlet. From this, the corresponding enthalpy drop required in the power turbine was calculated. The limitation in fixing the velocity triangles come from the peripheral speed of rotor and flow velocities. It is preferable to keep the both in reasonable range so as to minimize the losses.

After the primary fixing of velocity triangles between the axial gaps of the turbine blade rows, the blade profile is selected. In blade section there are two approaches, the direct and indirect approach. The blade profile selected should yield the flow angle required to give the desirable enthalpy drop. Also the pressure distribution at the end of stage should be uniform. If it is not so the blade angles are changed to match these requirements.

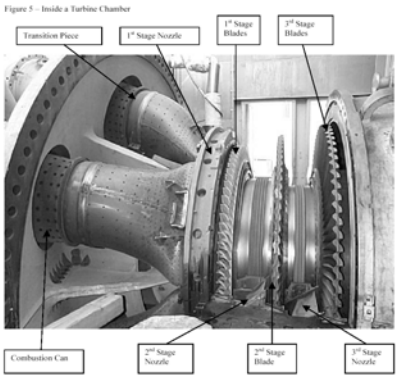

Fig 1.2 Construction of Turbine Rotor And Their Components

The gas turbine have been taken from the preliminary design of a power turbine. As the temperature has a significant effect on the overall stresses in the rotor blade, it has been felt that a detailed study can be carried out on the temperature effects to have a clear understanding of the combined mechanical and thermal stresses.

B. VIBRATION OF BLADES

If a blade of an assembly of blade is acted upon by an instantaneous force free vibrations are setup because of the inherent resilience of the blade or blade assembly. The frequency of these vibrations depends on the dimensions of the blade or blade assembly as well as their method of mounting on the discs. Moving blades in turbine are subjected to time variable loads in addition to the static loads.

C. PRODUCTION OF BLADES: -

Blades may be considered to be the heart of turbine and all other member exist for the sake of the blades. Without blading there would be no power and the slightest fault in blading would mean a reduction in efficiency and costly repairs.

D.TURBINE BLADE ATTACHMENT: -

The attachment of the turbine blade to the rotor is the most critical aspect of gas turbine.design.All the forces are transmitted through the attachment to the rotor. Especially at the low-pressure end of turbine of large output, the attachment has to bear relatively large forces due to high speed; the centrifugal force on the blade is many times its mass. It is therefore necessary to estimate the stresses in the attachment, but sometimes it is very difficult to get the exact values.

There is always the possibility of stress concentration at the sharp corners. Therefore selection of material is very important which can be safeguard from this stress concentration.

E. BRAYTON CYCLE COMPONENTS:

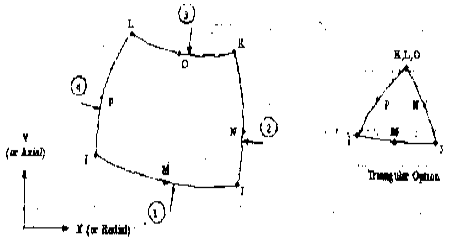

Gas turbines usually operate on an open cycle, as shown in Figure 1. Fresh air at ambient conditions is drawn into the compressor, where its temperature and pressure are raised. The high-

pressure air proceeds into the combustion chamber, where the fuel is burned at constant pressure.

Figure 1 – An Open Cycle Gas-Turbine Engine

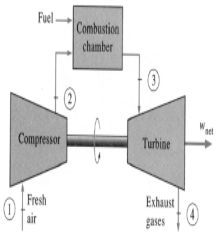

Figure 2 – A Closed Cycle Gas-Turbine Engine

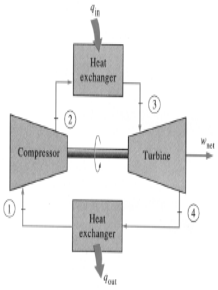

Fig: 1.3 Open & Closed Cycle of Gas Turbine

III. FINITE ELEMENT METHOD FORMULATION

D. FINITE ELEMENT METHOD

The finite element method is a numerical analysis technique for obtaining approximate solutions to a wide variety of engineering problems. Although originally developed to study stresses in complex airframe structures, it has since been extended and applied to the broad field of continuum mechanics.

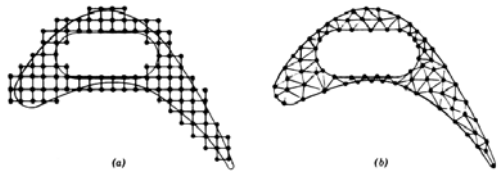

Fig: 1.4 Discretizations Of Turbine Blade Profile

E. Plane 82type 2-D 8-Node Structural Solid Element

Plane 82 is a higher order version of the two dimensional four-node element. It provides more accurate results for mixed (quadratic-triangular) automatic meshes

Fig: 1.6 plane 82 2-d structural solid

and can tolerate irregular shapes without as much loss of accuracy.

Element Name	Plane 82
Nodes	I, J, K, L, M, N, O, P
Degrees of Freedom	UX, UY
Real constants	none
MaterialProperties	EX,EY,EZ PRXY,PRYZ,PRXZ NUXY,NUYZ,NUXZ) ALPX,ALPY,ALPZ,DENS
Surface loads	Pressure
Body loads	Temperatures
Special features	Plasticity, creep, stress stiffening, large deflection, and large strain.

F. SOLID 95 3D 20-NODE STRUCTURAL SOLID ELEMENT

Solid 95 is higher order version of the 3-D 8-node solid element. It can tolerate irregular shapes without as much loss of accuracy. Solid 95 elements have compatible displacement shapes and are well suited to model curved boundaries The element is defined by 20 nodes having three degrees of freedom per node, translations in the nodal x, y, and z directions.

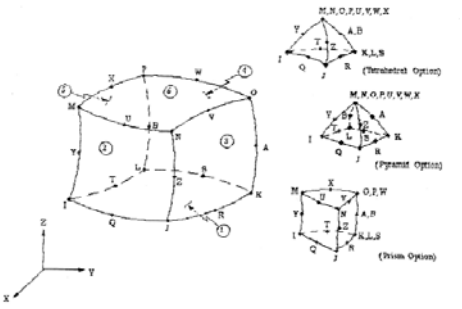

Fig:1.6 Solid 95 3-D structural solid

SOLID 95 INPUT SUMMARY

Element Name	Solid 95
Nodes	I, J, K, L, M, N, O, P,Q,R,S,T,U,V,V,W,X,Y,Z,A,B
Degrees of Freedom	UX,UY,UZ
Real constants	None
Material Properties	EX,EY,EZ(PRXY,PRYZ,PRXZ NUXY,NUYZ,NUXZ) ALPX,ALPY,ALPZ,DENS
Surface loads	Pressure
Body loads	Temperatures
Special features	Plasticity, creep, stress stiffening, large deflection, and large strain.

IV. EVALUATION OF GAS FORCE ON THE ROTOR BLADES

Gas forces acting on the blades of the rotor in general have two components namely tangential (Ft) and axial (Fa). These forces result from the gas momentum changes and from pressure differences across the blades. These gas forces are evaluated by constructing velocity triangles at inlet and outlet of the rotor blades.

A. EVALUATION OF GAS FORCES ON THE FIRST STAGE ROTOR BLADE

At the inlet of the first stage rotor blades,

Absolute flow angle $\alpha 2 = 23.850$

Absolute velocity V2 = 462.21 m/s
The velocity triangles at inlet of first stage rotor blades were constructed

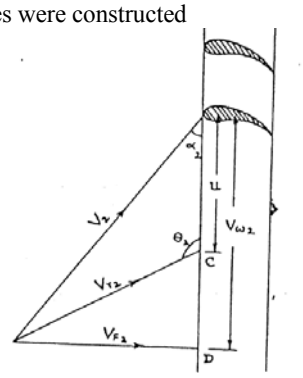

Fig: 1.7 Inlet velocity triangles of I-stage rotor blades

Diameter of blade midspan D = 1.3085 mt.
Design speed of turbine N = 3426 r.p.m.
Peripheral speed of rotor blade at its midspan U = πDN/60
From the velocity triangles in fig we get,
Whirl velocity Vw2 = 422.74 m/s
Flow Velocit, Vf2 = 186.89 m/s
Relative velocity, Vr2 = 265.09 m/s
Blade angle at inlet, θ2 = 135.017 0
At the exit of first stage rotor blades,
Flow velocity, Vr3 = 180.42 m/s
Relative flow angle, θ2 = 37.88 0

B. EVALUATION OF GAS FORCES ON SECOND STAGE ROTOR BLADES

The gas forces and power developed in second stage rotor blades were evaluated using the same procedure and similar equations that were used for first stage rotor blades

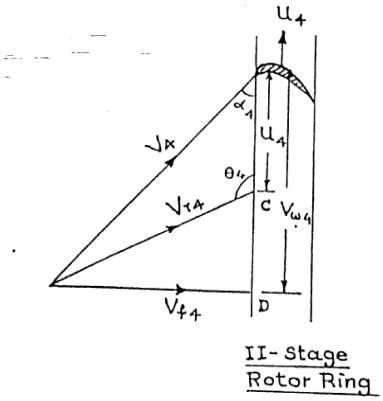

Fig: 1.8 Inlet Velocity Triangles Of Ii-Stage Rotor Blades

Tangential force	Ft = 244.49 Newtons
Axial force	Fa = 0.944 Newtons
Power developed	P = 13.972 Mega Watts

C. ANALYSIS OF FIRST STAGE ROTOR BLADE ON ANSYS 9.0

The structural, thermal, modal modules of ANSYS 9.0 were used for the analysis of the rotor blade. The rotor blade was analyzed for mechanical stresses, temperature distribution, combined mechanical and thermal stresses and radial elongations, natural frequencies and mode shapes.
Element Type 1: 8 node quadrilateral element
Element type 2: 20 node Brick solid element.
The following material properties were defined in the material property table named as material type 1.
Young's Modulus of Elasticity (E) = 2e5 N/mm2
Density (ρ) = 7136.52 e-9 T/mm3
Coefficient of thermal expansion (α) = 6.12e-6 /0C
The aerofoil profile of the rotor blade was generated on the XY plane with the help of key points defined by the coordinates as given below. Then a number of splines were fitted through the keypoints. A rectangle of dimensions 49*27 mm

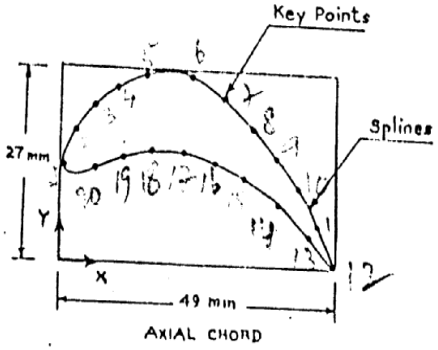

Fig 1.9 Boundary of aerofoil section

LIST OF SELECTED KEYPOINTS

NO	X	Y LOCATION (Z=0)
1.	0.00	0.00
2.	2.6	17.3
3.	5.85	21
4	10	25
5	14.8	26.6
6	22.9	25.3
7	28	22.2
8	33.4	18.5
9	38	14.4
10	42	10.9
11	45.5	5.70
12	49.00	0.00
13	6.18	12.4
14	11.2	14.4
15	16.18	15.5
16	21.1	14.9
17	26	13.6
18	38.2	8.77
19	45	3.95
20	49	0.00
21	49	27.00
22	0.00	27.00
23	19.8	0.00
24	1.00	13.6
25	29.2	0.00
26	29.2	27.00
27	19.8	27.00
28	15.2	27.00

29	18.08	27.00
30	49.00	0.27E-1
31	48.90	0.288E-1
32	29.2	12.49
33	19.8	26.62
34	19.8	15.12
35	29.2	21.25
36	0.00	0.30E-1

Using splines and lines 9 different areas were generated which was shown

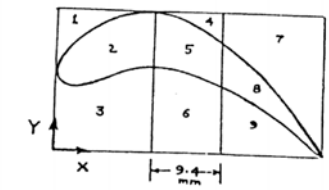

Fig:2. Areas of turbine rotor blade

By using these points ,created the blade modal in CATIAV5 R15 with the help of commands like spline,extrude,add etc.after that export this modal into HYPERMESH7.0 and mesh it by using commands like automesh, tetmesh etc and exported into ANSYS9.0.

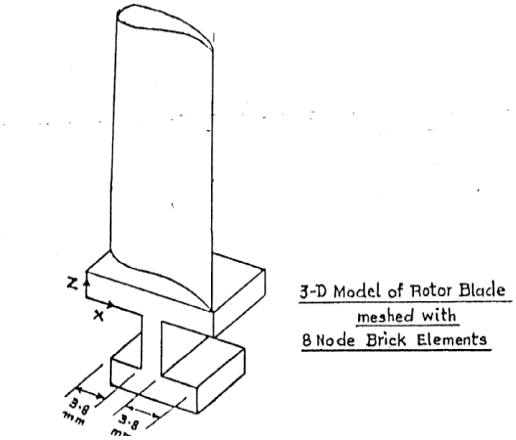

Fig: 2.1 3-D model of rotor blade

V . STRUCTURAL BOUNDARY CONDITIONS TO BE APPLIED ON THE ROTOR BLADE MODEL

Two structural boundary conditions namely displacement and force were applied on the rotor blade model. The solution part of ANSYS was opened and the displacement constraints (U) were imposed on the areas shaded and numbered.

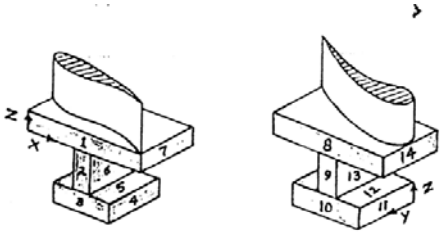

Fig 2.2 Structural boundary conditions on rotor blade

Ux = 0 for areas 4,5,6,7 and 11,12,13,14

Uy = 0 for areas 1,2,3 and 8,9,10

Uz = 0 for areas 5 and 12

U represents displacement and suffix X, Y, Z represents the direction in which the displacement was constrained.

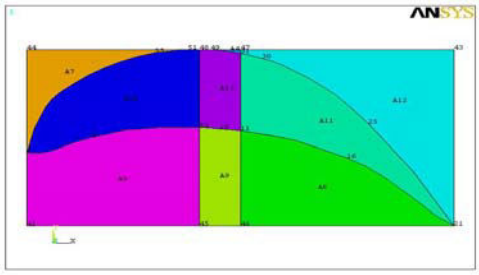

Fig: 2.3 Area Diagram of gas turbine rotor blade

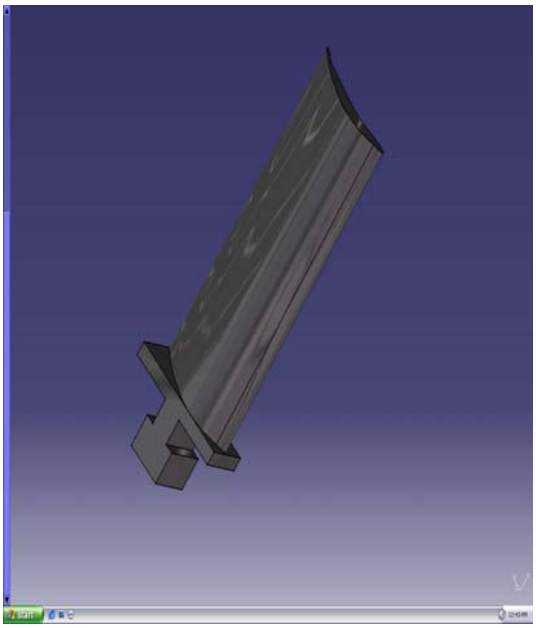

FIG:2.4 GEOMETRIC MODEL OF GAS TURBINE ROTOR BLADE

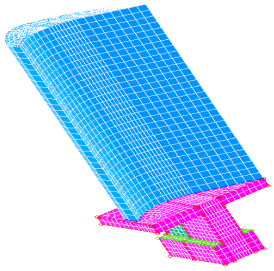

Fig:2.5 Brick mesh gas turbine rotor blade using hypermesh.

V RESULTS

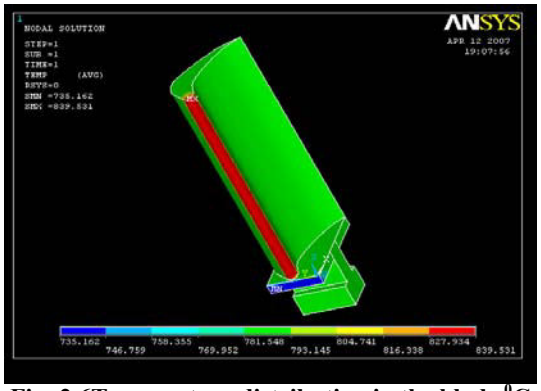

Fig: 2.6Temperature distribution in the blade, ^{0}C

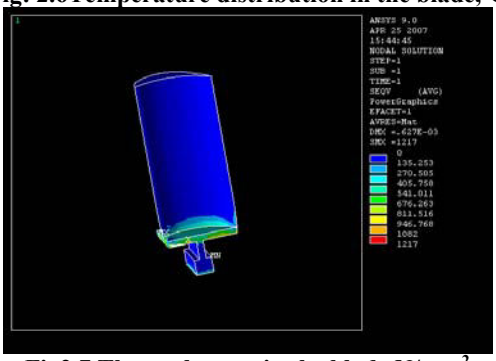

Fig2.7 Thermal stress in the blade,N/mm^2

VI .CONCLUSION

It is observed that the temperature variations from leading edge to the trailing edge on the blade profile is varying from 839.5310C to 735.1620C at the tip of the blade and the variation is linear along the path from both inside and outside of the blade.

Considerable changes are not observed from the first 6 mm length from the leading edge and from there to next 36 mm length of blade the temperature is gradually decreasing and reaching to a temperature of 781.5480C and for another 4 mm length it is almost constant.., it is observed that the maximum thermal stress is 1217.and the minimum thermal stress is.the maximum thermal stress is less than the yield strength value i.e, 1450.so, based on these values

REFERENCES

[1] Mikio Oi, Mariko Suzuki Natsuko Matsuura,Ishikawajima-Harima heavy industries Company Ltd," structural analysis and shape optimization in turbocharger development", 2nd MSC Worldwide Automotive User Conference, 1999.

[2] Sanford Fleeter, Chenn Zhou, Elias Houstis, John rice Purdue University, Indiana,"Fatigue life prediction of turbomachine blading", Advanced strategic alliance programme, July 1998.

[3] T.Madhusudhan, Dr.H.Maheshappa, Dr.K.Ramchandra,"Need for analysis of stress concentration factor in inclined cutouts of gas turbine blades," Proceeding of Advances in Mechanical Engineering, Jawaharlal Nehru National College of Engineering Shimoga, Karnataka, India, 2004.

[4] M.Pradeep, Naveen Babu Chandu, Rajan Bhardwaj, K.Kumar,"Influence of taper, twist and thickness in rotor blades using Finite Element Analysis", National Conference on Emerging trends in Engineering, Technology and Maanagement, 8-9 Sep.2003, ISTE Chapter, Adhiyamaan Engineering Collge, Hosur, Tamilnadu India.

[5] Stuart Moffaty, Li He," Blade forced Response prediction fro industrial gas turbines", Proceeding of ASME Turboexpo 2003,International gas turbine and aeroengine Congress and Exhibition, June 16-19 2003,Atlanta Georgia, U.S.A.

[6] Dr. K. Ramachandra, Director, Gas Turbine Research Establishment, Bangalore,

[7] T.Madhusudhan,Dr.H.Maheshappa, Dr.K.Ramchandra,"Need for analysis of stress concentration factor in inclined cutouts of gas turbine blades," Proceeding of Advances in Mechanical Engineering, Jawaharlal Nehru National College of Engineering Shimoga, Karnataka, India, 2004..

◈◈◈

Analysis of the influence of WEDM parameters on Surface roughness And Material removal rate of Tungsten Carbide*

P.PURNASURESH[1] , S.RAVI KUMAR[2], DR.M.VENKATESWARA RAO[3]

[1] Department of Mechanical Engineering, Bapatla Enggineering College, Bapatla, Guntur, India
[2] Department of Mechanical Engineering, Bapatla Enggineering College, Bapatla, Guntur, India
[3] Mechanical Department, Bapatla Enggineering College, Bapatla, Guntur, India

Abstract-Wire electrical discharge machining (WEDM) is a specialized thermal machining process capable of accurately machining parts with varying hardness or complex shapes, which have sharp edges that are very difficult to be machined by the main stream machining processes. The practical technology of the WEDM process is based on the conventional EDM sparking phenomenon utilizing the widely accepted noncontact technique of material removal. In this project, the effects of various process parameters of WEDM like pulse on time (T_{ON}), pulse off time (T_{OFF}), servo voltage (SV), peak current (IP) have been investigated to reveal their impact on surface roughness and material removal rate of Tungsten carbide using one variable at a time approach. The optimal set of process parameters has also been predicted to minimize the surface roughness and maximize the material removal rate. It is followed by optimizing the machining condition for confirmation test purposes. Then, the conformation test needed to evaluate the error margin between predicted result by software and confirmation result by experiment in terms of the machining characteristics. The effectiveness of WEDM process with tungsten carbide (WC) is evaluated in terms of the material removal rate, surface roughness of the work piece produced. It is observed that brass is most suitable for use as the tool electrode in WEDM of WC. Better machining performance is obtained generally with the electrode as the cathode and the work piece as an anode. The experimental studies were performed on ELECTRONICA SPRINTCUT 734 WEDM machine. Surface roughness (Ra) and Material removal rate (MRR) in this experiment was calculated by using mathematical method. The result of the experiment then was collected and analyzed using DESIGN EXPERT (DOE) software. This was done by using the TWO LEVEL FULL FACTORIAL technique and ANOVA analysis.

Key words: *WEDM, T_{ON}, T_{OFF}, SV, IP, Ra, MRR, DOE, Two Level Full Factorial and ANOVA.*

Introduction and Problem Statement

1.1 Introduction Of Wire Edm (Wedm)

Accompanying the development of echanical industry, the demands for alloy materials having high hardness, toughness and impact esistance are increasing. Nevertheless, such materials are difficult to be machined by traditional machining methods. Hence, non-traditional machining methods including electrochemical machining, ultrasonic machining, electrical discharging machine (EDM) etc. are applied to machine such difficult to machine materials. WEDM process with a thin wire as an electrode transforms electrical energy to thermal energy for cutting materials. With this process, alloy steel, conductive ceramics and aerospace materials can be machined irrespective to their hardness and toughness. Furthermore, WEDM is capable of producing a fine, precise, corrosion and wear resistant surface.

WEDM is considered as a unique adoption of the conventional EDM process, which uses an electrode to initialize the sparking process. However, WEDM utilizes a continuously travelling wire electrode made of thin copper, brass or tungsten of diameter 0.05-0.30 mm, which is capable of achieving very small corner radii. The wire is kept in tension using a mechanical tensioning device reducing the tendency of producing inaccurate parts. During the WEDM process, the material is eroded ahead of the wire and there is no direct contact between the work piece and the wire, eliminating the mechanical stresses during machining.

Importance Of Wedm Process In Present Day Manufacturing

Wire electrical discharge machining (WEDM) technology has grown tremendously since it was first applied more than 30 years ago. In 1974, D.H. Dulebohn applied the optical-line follower system to automatically control the shape of the components to be machined by the WEDM process. By 1975, its popularity rapidly increased, as the process and its capabilities were better understood by the industry. It was only towards the end of the 1970s, when computer numerical control (CNC) system was initiated into WEDM, which brought about a major evolution of the machining process (Ho et. al., 2004).

Its broad capabilities have allowed it to encompass the production, aerospace and automotive industries and virtually all areas of conductive material machining. This is because WEDM provides the best alternative or sometimes the only alternative for machining conductive, exotic, high strength and temperature resistive materials, conductive

engineering ceramics with the scope of generating intricate shapes and profiles (Kozak et.al., 2004 and Lok and Lee, 1997).

WEDM has tremendous potential in its applicability in the present day metal cutting industry for achieving a considerable dimensional accuracy, surface finish and contour generation features of products or parts. Moreover, the cost of wire contributes only 10% of operating cost of WEDM process. The difficulties encountered in the die sinking EDM are avoided by WEDM, because complex design tool is replaced by moving conductive wire and relative movement of wire guides.

Basic Principle Of Wedm Process

The WEDM machine tool comprises of a main worktable (X-Y) on which the work piece is clamped; an auxiliary table (U-V) and wire drive mechanism. The main table moves along X and Y-axis and it is driven by the D.C servo motors. The travelling wire is continuously fed from wire feed spool and collected on take up spool which moves though the work piece and is supported under tension between a pair of wire guides located at the opposite sides of the work piece. The lower wire guide is stationary where as the upper wire guide, supported by the U-V table, can be displaced transversely along U and V-axis with respect to lower wire guide. The upper wire guide can also be positioned vertically along Z-axis by moving the quill.

A series of electrical pulses generated by the pulse generator unit is applied between the work piece and the travelling wire electrode, to cause the electro erosion of the work piece material. As the process proceeds, the X-Y controller displaces the worktable carrying the work piece transversely along a predetermined path programmed in the controller. While the machining operation is continuous, the machining zone is continuously flushed with water passing through the nozzle on both sides of work piece. Since water is used as a dielectric medium, it is very important that water does not ionize. Therefore, in order to prevent the ionization of water, an ion exchange resin is used in the dielectric distribution system to maintain the conductivity of water.

In order to produce taper machining, the wire electrode has to be tilted. This is achieved by displacing the upper wire guide (along U-V axis) with respect to the lower wire guide. The desired taper angle is achieved by simultaneous control of the movement of X-Y table and U-V table along their respective predetermined paths stored in the controller. The path information of X-Y table and U-V table is given to the controller in terms of linear and circular elements via NC program. Figure 1.1 exhibits the schematic diagram of the basic principle of WEDM process (Tosun et.al., 2004).

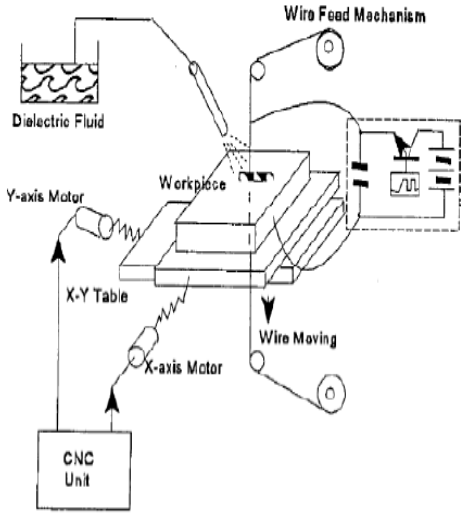

Figure 1.1: Schematic Diagram of the Basic Principle of WEDM Process

1.4 Mechanism Of Material Removal In Wedm Process

The mechanism of metal removal in wire electrical discharge machining mainly involves the removal of material due to melting and vaporization caused by the electric spark discharge generated by a pulsating direct current power supply between the electrodes. In WEDM, negative electrode is a continuously moving wire and the positive electrode is the work piece. The sparks will generate between two closely spaced electrodes under the influence of dielectric liquid. Water is used as dielectric in WEDM, because of its low viscosity and rapid cooling rate(Lok and Lee, 1997).

No conclusive theory has been established for the complex machining process. However, empirical evidence suggests that the applied voltage creates an ionized channel between the nearest points of the work piece and the wire electrodes in the initial stage. In the next stage the actual discharge takes place with heavy flow of current and the resistance of the ionized channel gradually decreases. The high intensity of current continues to further ionize the channel and a powerful magnetic filed is generated. This magnetic field compresses the ionized channel and results in localized heating. Even with sparks of very short duration, the temperature of electrodes can locally rise to very high value which is more than the melting point of the work material due to transformation of the kinetic energy of electrons into heat. The high energy density erodes a part of material from both the wire and work piece by locally

melting and vaporizing and thus it is the dominant thermal erosion process

1.5 Advantages Of Wedm Process (Benedict G.F., 1987)

As continuously travelling wire is used as the negative electrode, so electrode fabrication is not required as in EDM.

- There is no direct contact between the work piece and the wire, eliminating the mechanical stresses during machining.
- WEDM process can be applied to all electrically conducting metals and alloys irrespective of their melting points, hardness, toughness or brittleness.
- Users can run their work pieces over night or over the weekend unattended.

1.6 Disadvantages Of Wedm Process (Benedict G.F., 1987)

- High capital cost is required for WEDM process.
- WEDM process exhibits very slow cutting rate.
- It is not applicable to very large work piece

1.7 Applications Of Wedm Process

The present application of WEDM process includes automotive, aerospace, mould, tool and die making industries. WEDM applications can also be found in the medical, optical, dental, jewellery industries, and in the automotive and aerospace R & D areas (Ho et. al., 2004).

The machine's ability to operate unattended for hours or even days further increases the attractiveness of the process. Machining thick sections of material, as thick as 200 mm, in addition to using computer to accurately scale the size of the part, make this process especially valuable for the fabrication of dies of various types. The machining of press stamping dies is simplified because the punch, die, punch plate and stripper, all can be machined from a common CNC program. Without WEDM, the fabrication process requires many hours of electrodes fabrication for the conventional EDM technique, as well as many hours of manual grinding and polishing. With WEDM the overall fabrication time is reduced by 37%, however, the processing time is reduced by 66%. Another popular application for WEDM is the machining of extrusion dies and dies for powder metal (PM) compaction (Benedict G.F., 1987).

PROBLEM STATEMENT

To investigate Optimal set of process parameters(Ton and Toff ,SV and IP) for various Machining characteristics (Ra and MRR) using DOE Two level Full Factorial experiment methodology.Here design expert software (DOE) automatically suggesting optimal machining parameters. So the suggested parameters should be verified experimentally by conducting confirmation test.

OBJECTIVE

- To determine significant parameters that influences the machining responses during WEDM of Tungsten Carbide.
- To establish a mathematical model for surface finish and material removal rate during WEDM of Tungsten Carbide.
- Full factorial method from DOE used in order to analyze and determine global solutions for optimal cutting parameters of WEDM.

SCOPE

The scope of this project consist of

- Wire electro discharge machining (WEDM) – ELEKTRA SPRINTCUT 734 will be employed.
- Tungsten Carbide will be used as a work material.
- Brass wire of diameter 0.25mm used as electrode.
- Process parameters to be studied include Pulse on time (Ton), Pulse off time(Toff) ,Peak current(IP), servo voltage(SV).
- The classical DOE and analysis of variance (ANOVA) method will be processed using Design Expert software version 8.0.7.1.

EXPERIMENTAL DESIGN METHODOLOGY

A scientific approach to plan the experiments is a necessity for efficient conduct of experiments. By the statistical design of experiments the process of planning the experiment is carried out, so that appropriate data will be collected and analyzed by statistical methods resulting in valid and objective conclusions. When the problem involves data that are subjected to experimental error, statistical methodology is the only objective approach to analysis. Thus, there are two aspects of an experimental problem: the design of the experiments and the statistical analysis of the data. These two points are closely related since the method of analysis depends directly on the design of experiments employed. The advantages of design of experiments are as follows:

- ✓ Important decision variables which control and improve the performance of the product or the process can be identified.
- ✓ Experimental error can be estimated.
- ✓ Inference regarding the effect of parameters on the characteristics of the process can be made.

CONFIRMATION EXPERIMENT

The confirmation experiment is a final step in verifying the conclusions from the previous round of experimentation. The optimum conditions are set for the significant parameters (the insignificant parameters are set at economic levels) and a selected number of tests are run under specified conditions. The average of the confirmation experiment results is compared with the anticipated average based on the parameters and levels tested. The confirmation experiment is a crucial step and is highly recommended to verify the experimental conclusion.

CONCLUSION

1. The effects of process parameters viz. Ton, Toff, SV, IP on machining characteristics viz. Ra and MRR were observed.

2. Optimal set of process parameters were obtained for various machining characteristics using DOE Two level Full Factorial experiment methodology.

3. Two Level Full Factorial experiment methodology was applied for developing the mathematical models for Ra and MRR.

4. Pulse on time (Ton) and servo voltage (SV) was found to be most significant factor in both the machining characteristics (Ra and MRR).

5. Process parameters vs Machining characteristics

Process Parameters	Machining characteristics	
	Surface Roughness	Material Removal Rate
Ton increases	Increases	Increases
Toff increases	Almost constant	Decreases
SV increases	Decreases	Decreases
IP increases	Increases	Increases

REFERENCES

1. H. Singh*, R. Garg(january2009). "*Effects of process parameters on material removal rate in WEDM*" Journal of achievements in material manufacturing. Vol.32 and Issue1.
2. S.H.Tomadi, M.A.Hassan, Z. Hamedon, *Member, IAENG R.Daud, A.G.Khalid(IMES2009). "Analysis of the Influence of EDM Parameters on Surface Quality, Material Removal Rate and Electrode Wear of Tungsten Carbide*" Vol .2.
3. Kamal Jangraa*, Sandeep Grovera and Aman Aggarwalb (2009), "*Simultaneous optimization of material removal rate and surface roughness for WEDM of WC-Co composite using grey relational analysis along with Taguchi method*" YMCA University *of Science and Technology, Faridabad, India* in International Journal of industrial engineering pg no.479-490.
4. I.Puertas∗, C.J. Luis,L.ALVAREZ,(2009)"*Analysis of the influence of EDM parameters on surface quality, MRR and*
5. *EW of WC–Co" Public University of Navarre (Spain)* (journal of material processing technology) pg.no153-154 .
6. M. N. Islam, N. H. Rafai, and S. S. Subramanian,(july2 2010)"An Investigation into Dimensional Accuracy Achievable in Wire-cut Electrical Discharge Machining" in proceedings of the world congress on engineering Vo III.
7. Mohd Syafiq Bin Dzulkapli,"Study the Effect of Wire-EDM Parameters on Surface Roughness for Machining Die-Steel"(University Teknikal MalaysiaMelaka for the Bachelor Degree of Manufacturing Engineering in Manufacturing Process).
8. Koona Ramji and pujari srinivasarao "*Effect of wedm conditions on surface roughness: a prapmetric optimisation using taguchi method"* (IJAEST) Gitam University, Mechanical engineering department, vishkapatanam , Vol 6 pg,no.42-48.
9. K.h.ho.newman, S.Rahimifard , R D Allen " *State of the art in wire electrical discharge machining (WEDM)* in international journal of machine tool and manufacturing pg no.1247 -1259 *)*(Volume24(oct2004)).
10. U.Esme , A.Sagbas and F.Kahraman(2009) " *Prediction of surface roughness in WEDM using DOE and Neural etworks"* International Journal of science & Technology ,Vol.33 pg.no 231-240.

◈◈◈

Experimental Investigation on Diesel Engine Using Fish oil Methyl Ester as Alternative Fuel

[1]KEERTHI B L, [2]DR R SURESH & [3]K V YATHISH

[1,2] Mechanical Department
Siddaganga Institute of Technology
Tumkur, Karnataka
[3]District Bio-fuel Information & Demonstration Center
Tumkur, Karnataka

Abstract— Biodiesel is reliable, renewable and bio-degradable and recognized as a clean alternative fuel to reduce pollutant emissions from combustion equipment. Because cultivated land is too limited to grow seed oil plants sufficient to produce both food and biodiesel. In this study, mainly concentrates on preparing biodiesel from fish oil using trans-esterification and comparing fuel properties with neat diesel. Experimental studies were made using fish oil biodiesel blends with diesel in a single cylinder engine with different injection pressure. The test showed that there is no major deviations in the engine performance and fish biodiesel shows good combustion properties.

Keywords- Biodiesel, Fish Oil, Transeterification, Engine Performance

I. INTRODUCTION

Energy is considered as a critical factor for economic growth, social development and human welfare. Since their exploration, the fossil fuels continued as the major conventional energy source with increasing trend of modernization and industrialization, the world energy demand is also growing at faster rate. To cope up the increasing energy demand, majority of the developing countries import crude oil apart from their indigenous production. This puts extra burden on their home economy. Hence, it is utmost important that the options for substitution of petroleum fuels be explored to control the burden of import bill.

There are limited reserves of the fossil fuels and the world has already faced the energy crisis of seventies concerning uncertainties in their supply. Fossil fuels are currently the dominant global source of CO_2 emissions and their combustion is stronger threat to clean environment. Increasing industrialization, growing energy demand, limited reserves of fossil fuels and increasing environmental pollution have jointly necessitating the exploring of some alternative to the conventional liquid fuels, vegetable oils have been considered as appropriate alternatives to the conventional liquid fuels, vegetable oils have been considered as appropriate alternative due to their prevalent fuel properties. It was thought of as feasible option quite earlier. However despite the technical feasibility, vegetable oils as fuel could not get acceptance, as they were more expensive than petroleum fuels. This led to the retardation in scientific efforts to investigate the further acceptability of vegetable oils as alternate fuels. Later, due to numerous factors as stated above created resumed interest of researchers in vegetable oils as substitute fuel for diesel engines. In view of the potential properties, large number of investigation has been carried out internationally in the area of vegetable oils as alternate fuels. Some of the vegetable oils from farm and forest origin have been identified. The most predominantly sunflower, soybean, cottonseed, canola, jatropha, peanut oil etc. have been reported as appropriate substitute of petroleum based fuels. The vegetables oils can be used in diesel engines by various techniques such as fuel modification by transesterification, diesel-vegetable blends, vegetable oil heating etc.

II. METHODOLGY

A. Preparation Of Fish Oil Methyl Ester

Several methods are available to produce biodiesel, such as transesterification, catalysis pyrolysis, amidation with diethylmine, Of these transesterification is most widely used in biodiesel production. The general equation for transesterification of vegetable oils containing triglycerides as fallows.

The raw fish oil was transestified with methanol to produce biodiesel. An electro-magnetic stirrer is used to stir methanol with base catalyst sodium hydroxide. The process flow chart of biodiesel extraction is as shown below.

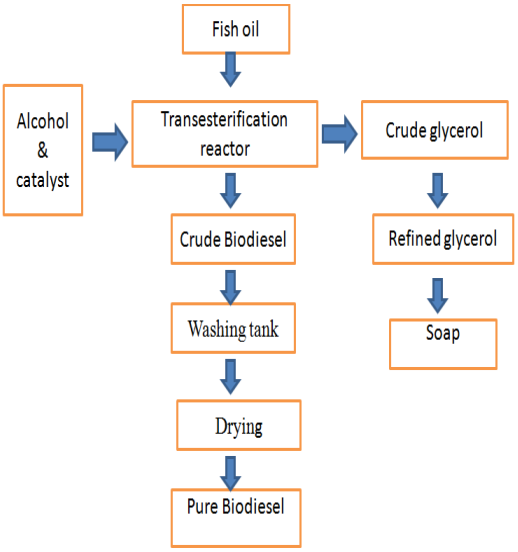

Figure1. Process Flow Chart

Figure2: Pictorial representation of Biodiesel Extraction

Finally 890ml of biodiesel and 110ml of glycerin was obtained from 1litre of fish oil.

B. Fuel Charecteristics of The Tested Fuels

Characteristics	Fish oil biodiesel	Diesel
Specific Gravity	0.885	0.83
Flash Point ^{0}C	165	5
Fire Point ^{0}C	174	59
Kinematic Viscosity at 40^{0}C (mm^2/s)	4.3	2.2
Calorific value (kJ/kg)	36804	42800

Table1: Fuel Properties of the Tested Fuels

C. Experimental setup

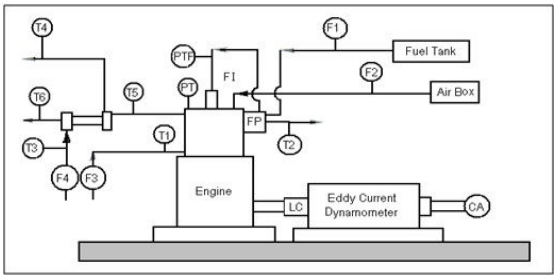

Figure 2: Schematic Diagram of the Experimental Set-up

PTF : Fuel Injection Pressure Sensor
PT : Combustion Chamber Pressure Sensor
FI : Fuel Injector
FP : Fuel Pump
T1 : Jacket Water Inlet Temperature
T2 : Jacket Water Outlet Temperature
T3 : Inlet Water Temperature at Calorimeter
T4 : Outlet Water Temperature at Calorimeter
T5 : Exhaust Gas Temperature before Calorimeter
F1 : Liquid fuel flow rate
F2 : Air Flow Rate
F3 : Jacket water flow rate
F4 : Calorimeter water flow rate
LC : Load Cell
CA : Crank Angle Encoder
EGC : Exhaust Gas Calorimeter
T6 : Exhaust Gas Temperature after Calorimeter

The Schematic diagram of the engine test rig is shown in Fig. The engine test was conducted on four-stroke single cylinder direct injection water cooled compression ignition engine connected to eddy current dynamometer loading. The engine was always operated at a rated speed of 1500 rev/min. The engine was having a conventional fuel injection system. The injection nozzle had three holes of 0.3 mm diameter with a spray angle of 120º. A piezoelectric pressure transducer was mounted with cylinder head surface to measure the cylinder pressure. It is also provided with temperature sensors for the measurement of jacket water, calorimeter water, and calorimeter exhaust gas inlet and outlet temperatures. An encoder is fixed for

crank angle record. The provision is also made for the measurement of volumetric fuel flow. The built in program in the system calculates brake power, thermal efficiency and brake specific fuel consumption..

III. RESULTS AND DISCUSSION

The experiments were conducted on a direct injection compression ignition engine for various loads and various blends of biodiesels. Analysis of performance parameters and emission characteristics like brake power, brake specific fuel consumption, brake thermal efficiency, hydrocarbon, carbon monoxide, nitrogen dioxide and exhaust gas temperatures are evaluated.

A. Performance characteristics:

1. Brake thermal efficiency (BTE): This is defined as the ratio between the brake power output and the energy of the fuel combustion.

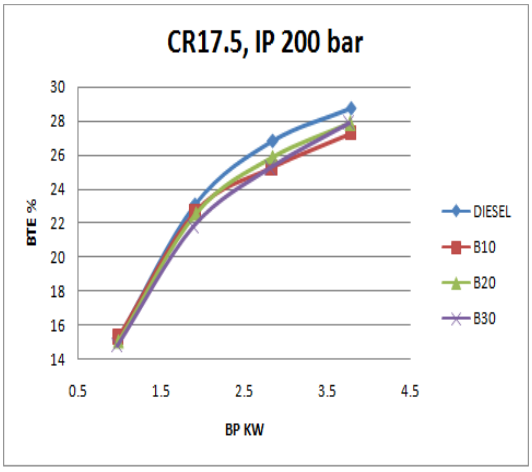

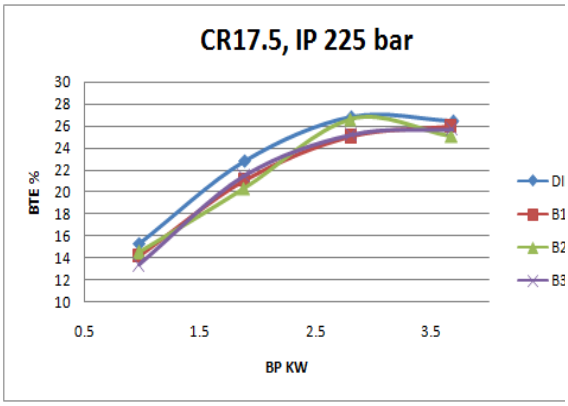

Figure 4: Brake Power v/s Brake thermal efficiency.

Figure4 shows the variation of brake thermal efficiency with load for different diesel–biodiesel blends & neat diesel at compression ratio of 17.5:1 and injection pressure of 200 bars and 225bars. The brake thermal efficiency is highest with B30 in all loads which are nearer diesel for IP 200bar. B20 shows the minimum efficiency for IP 225 bar. Injection Pressure 200bar shows higher brake thermal efficiency compare to injection pressure 225bar.

2. Brake fuel consumption (BSFC)

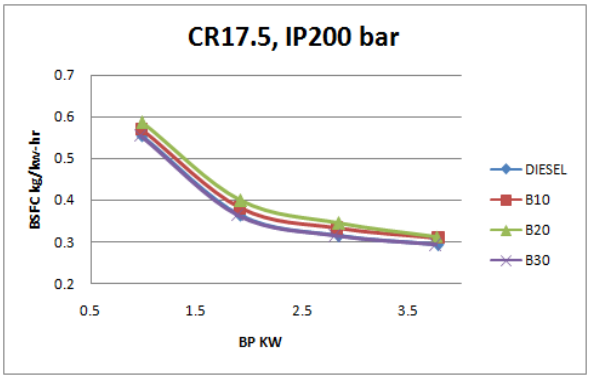

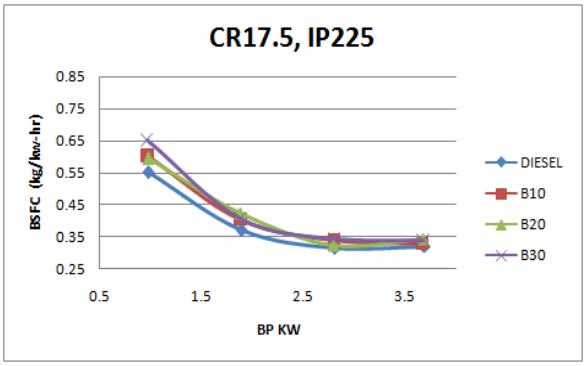

Figure 5: Brake Power v/s Brake fuel consumption

Figure5 shows the variation of brake specific fuel consumption (BSFC) with BP for different diesel–biodiesel blends & neat diesel at compression ratio of 17.5:1 and injection pressure of 200 bars and 225bars. As the load increases, BSFC decreases for all fuel blends. At full load B30 shows the lowest fuel consumption compare other blends.

3. Exhaust gas temperature (EGT)

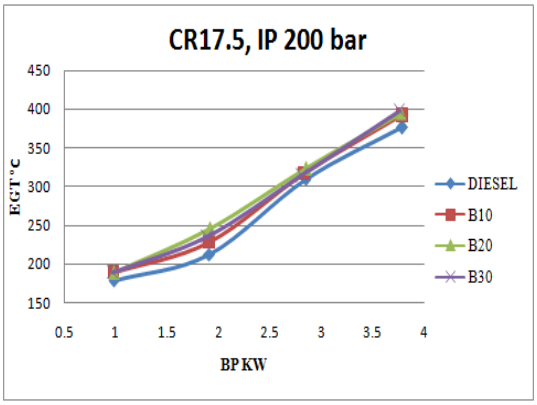

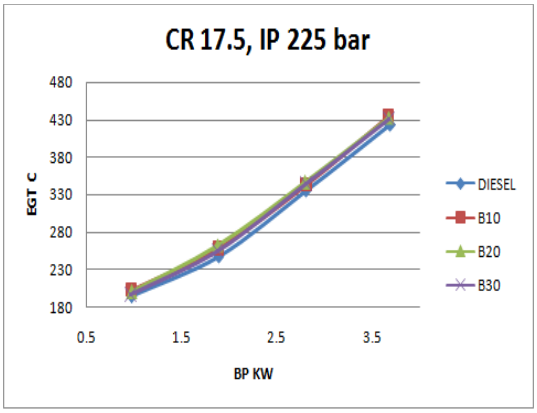

Figure 6: Brake power v/s Exhaust gas temperature

The results show that the exhaust gas temperature increases with increase in load for all blends & diesel. At all loads, diesel was found to have the lowest temperature and the temperatures for various blends show an upward trend with increasing concentration of Fish oil biodiesel in the blends. The EGT of all the blends and diesel are higher at injection pressure of 225 bar compared to 220 bar. The biodiesel contains oxygen which enables the combustion process and hence the exhaust gas temperatures are higher.

B. Engine Exhaust Results.

1. Hydrocarbon (HC)

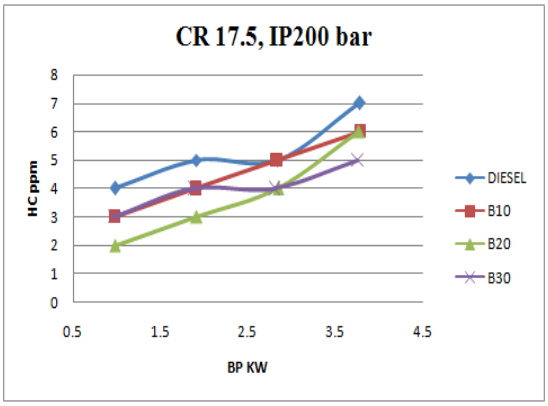

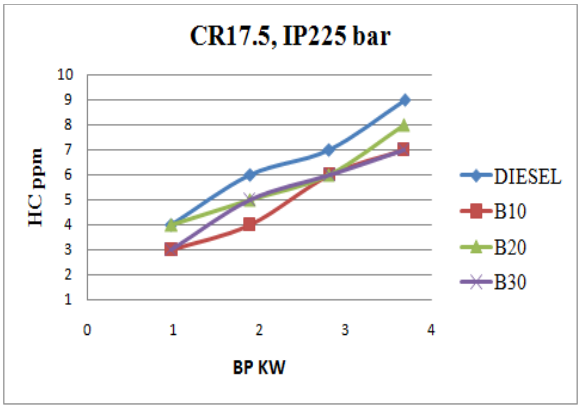

Figure 7: Brake Power v/s Hydrocarbon

Unburnt hydro carbons emission is the direct result of incomplete combustion Graph shows the variation of hydro carbon emission with brake power for different diesel–biodiesel blends & neat diesel at compression ratio of 17.5:1 and injection pressure of 200 bars and 225bars. The HC emission for all the blends and neat diesel goes on increases as load increases for both injection pressures. B30 shows the lower HC emission compared to neat diesel at full load. A reason for the reduction of HC emissions with biodiesel is the oxygen content in the biodiesel molecule, which leads to more complete and cleaner combustion.

2. Oxides of Nitrogen (NOx):

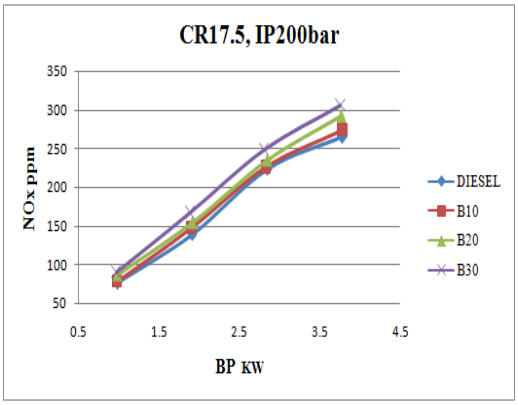

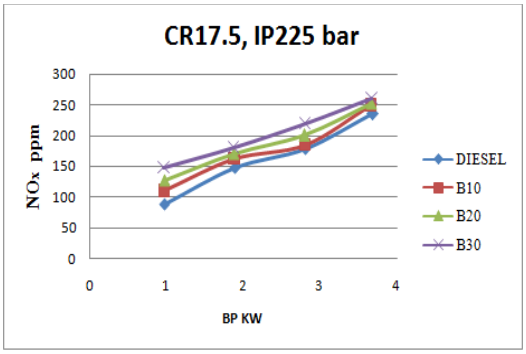

Figure 8: Brake Power v/s Oxides of Nitrogen

Figure 8 shows the variation of NO_x emissions with BP for different diesel–biodiesel blends & neat diesel at compression ratio of 17.5:1 and injection pressure of 200 bars and 225bars.The NOx emission for all the blends and neat diesel goes on increases as load increases for both injection pressures. Biodiesel shows the higher NO_x emission compared to diesel at all loads for both injection pressures. From this curve, two observations can be made. First, NO_x emissions are a direct function of engine loading. This is expected because with increasing load, the temperature prevailing inside the combustion chamber increases and NO_x formation is a strongly temperature dependant phenomenon. Injection pressure 200bar shows less NO_x emission compare to injection pressure 225bars.

3. Carbon Monoxide (CO)

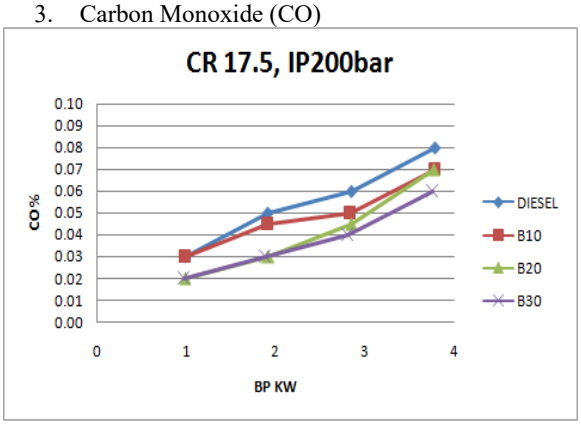

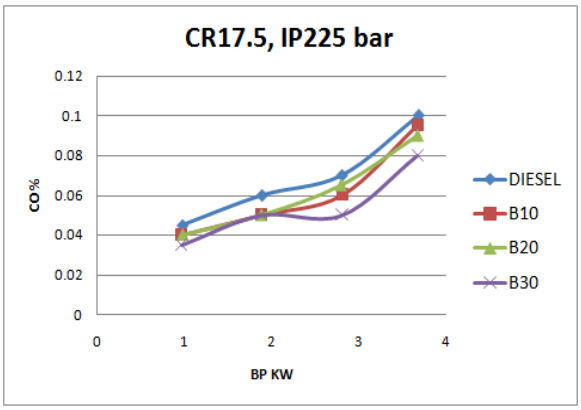

Figure9: Brake Power v/s Carbon monoxide

CO is a byproduct of combustion if combustion does not take place, carbon monoxide will not be created. Based on this premise, when a misfire occurs, the carbon monoxide that would have normally been produced during the production. Generally speaking, on fuel injected vehicles, high CO means too much fuel is being delivered to the engine for the amount of air entering the intake manifold. Figure 9 shows the variation of CO emissions with load for different diesel–biodiesel blends & neat diesel at compression ratio of 17.5:1 and injection pressure of 200 bars and 225bars. The CO emission for all the blends and neat diesel goes on increases as load increases for both injection pressures. B30 shows the lower CO emission compared to neat diesel at all loads. A reason for the reduction of CO emissions with biodiesel is the oxygen content in the fuel, which enhances a complete combustion of fuel, thus reducing CO emissions.

IV.CONCLUSION

1. Engine performance with biodiesel does not differ greatly with neat diesel. B30 shows good results compare with other blends. A little more fuel consumption is often encountered due to lower calorific value and comparing with 225bar injection pressure 200bar shows higher brake thermal efficiency and less fuel consumption.

2. Most of the major exhaust pollutants such as HC, and CO are reduced with the use of blends of biodiesel as compared to neat diesel. The major drawback of biodiesel is NOx emissions which increase diesel–biodiesel fuel blends as compared to conventional diesel fuel.

3. Among biodiesel blends with diesel, B30 shows better performance end emission characteristics

4. In terms of fuel properties and exhaust emission characteristics, fish oil biodiesel is regarded as a alternative fuel

REFERENCES

[1] F.Halek, A.Kavousi, and M. Banifatemi, "Biodiesel as an alternative fuel for Diesel Engines," World Academy of Science, Engineering and Technology.

[2] Cherung-Yuan Lin**,** Rong-ji Li, "Engine performance and emission characteristics of marine fish-oil biodiesel produced from the discarded parts of marine fish" fuel processing technology 90 (2009) 883-888

[3] Rasim Behçet, "Performance and emission study of waste anchovy fish biodiesel in a diesel engine" fuel processing technology 92 (2011) 1187-1194

[4] GVNSR Ratnakara Rao, H.W Wang, H.Y. Chen, L.B. Zhou and D.m Jiang, "study of combustion characteristics of a compression ignition engine with dimethyl ether," Proc Instn Mech engrs*,* vol 213, pp. 1877-1884, 2009

[5] Sharanappa Godiganur, C.H. Suryanarayana Murthy, and Rana Prathap Reddy, "6BTA 5.9 G-1 Cummins engine performance and emission tests usimg methyl ester mahua oil/diesel blends," Renewable energy, pp.2172-2177, 2009

[6] Cherng-Yuan Lin**,** Tsan-Huang Huang, "Cost–benefit evaluation of using biodiesel as an alternative fuel for fishing boats in Taiwan," Marine policy 36(2012) 103-10

[7] Metin Gumus, Cenk Sayin, Mustafa Canakci, "The impact of fuel injection pressure on the exhaust emissions of a direct injection diesel engine fueled with biodiesel–diesel fuel blends" , Fuel 95 (2012) 486–494

[8] Sukumar Puhan, n. vedaraman, Boppana V.B. Ram, G. Sankarnarayanan and K. Jeychandran, "Mahua oil methyl ester as bio diesel-prearation and emission characterstics," *biomass and Bioenergy,* vol 28, pp. 87-93, 2005

[9] Rosca Radu, "Exhaust Emission & Performance of Diesel Engines with Bio Diesel as Fuef," Fuel 1998, 77, pp 1389-1391

[10] Sharanappa Godiganur, Ch. Suryanarayana Murthy, Rana Prathap Reddy "Performance and emission characteristics of a Kirloskar HA394 diesel engine operated on fish oil methyl esters" Renewable Energy 35 (2010) 355–359

◈◈◈

Experimental Determination of Heat Transfer Coefficient by Natural Convection for a Commercially Available Heat Sink Used for Cooling of Electronic Chips

[1]SUNIL HIREHOLI, [2]K.S. SHASHISHEKHAR & [3]S. GEORGE MILTON

[1,2,3]Dept. of Mechanical Engineering
Siddaganga Institute of Technology
Tumkur, Karnataka, India..

Abstract-Measurements have been conducted for experimentally determining the heat transfer co-efficient of a commercially available heat sink employed in electronic circuits. For determining the heat transfer coefficient the chip is replaced with a heating coil. The power input to the heating coil is obtained by measuring the input voltage and current. Temperature measurement for varying heat inputs is done using RTD thermocouples. Heat transfer co-efficient is computed from the measured data. This is done for different configurations of the heat sink.

Keywords*: electronic circuits, heat sink, heat transfer co-efficient, RTD thermocouples.*

I. INTRODUCTION

Electronic circuits are used in diverse fields such as aircraft, locomotives, space applications, ships, submarines, communication systems defence applications, etc. These electronic circuits generate heat that must be dissipated while keeping chip temperature inside cabinet within safe limits for optimum performance. The miniaturization of electronic devices has put a lot of constraints on the heat dissipation pattern of the circuit boards. Heat dissipation is achieved in many circuits by employing a suitable heat sink. So study of heat transfer co-efficient of heat sink becomes important.

Heat sinks are devices capable of removing heat from the system with which they are in direct contact by exchanging the extracted heat with another fluid or its surroundings. This is normally achieved by either increasing surface area of heat sink significantly or by increasing heat transfer coefficient.

Today, heat sinks are usually applied to thermal management of electronic devices and systems. In the past decade, tight packing and rapid development of integrated circuit technology have increased thermal management requirements of electronic devices. Moore's law predicts that the number of transistors in an integrated circuit will double every 18 months due to lowering of minimum manufacturing cost per component each year. These come with problem of effective heat removal for these systems to operate without failure, as the reliability of semi-conductor devices is inversely proportional to square of its change in temperature [1].

Extensive literature information exists relating to the study of natural convection flows with shrouded fins of varying fin tip clearance. For example, Patankar and his colleagues [Zhang and Patankar, 1984]; Karki and Patankar, [1985,1987] have carried numerical simulations of the enhancing effects of shrouded fins.[2]

II. EXPERIMENTATION

Fig. 1 shows the heat sink with the heating coil of about 34 ohms fixed to it for conducting measurements. The location and the size of the heating coil are selected so that it occupies the same place as that of the chip to which the heat sink is attached. The heating coil is fixed in such a way that one side of the heating coil heats the metallic surface of the heat sink while the other side is insulated using a strip of asbestos just covering the heating coil alone leaving the rest of the heat sink surface for heat transfer through natural convection. Later while calculating the effective area available for heat transfer the surface area covered by the heating coil and the asbestos strip is subtracted from the total surface area of the heat sink. In all, three RTD thermocouples have been fixed at three different locations as indicated in Fig. 1. Average of all the three temperatures measured by these thermocouples is used in calculating the heat transfer coefficient as discussed later.

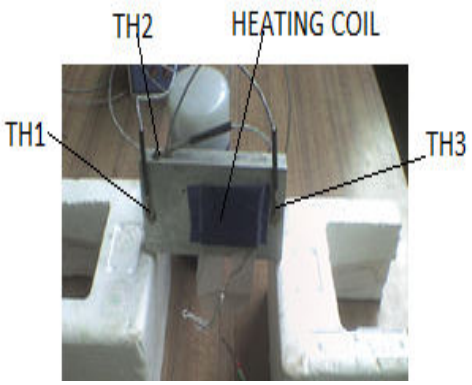

Fig. 1 Photograph of the heat sink with the heating coil and thermocouples denoted as TH1, TH2 & TH3.

A. Heat sink kept in the open air

Fig. 2 shows a photograph of the experimental set-up used for measurements. For the measurements described in this section the heat sink is kept at a height from the surface of the table to enable free flow of air from the bottom of the sink. Alternating current from mains is supplied to the heating coil attached to the heat sink through a dimmerstat as seen in the photograph (Fig.2). Voltage across the heating coil is measured using a voltmeter and current is measured using an ammeter. Heat dissipated and the associated heat transfer co-efficient are calculated using the following basic equations [2], [3].

$$Q = V I \qquad (1)$$

$$T = \frac{T1+T2+T3}{3} \qquad (2)$$

$$h = \frac{Q}{A(T-Ta)} \qquad (3)$$

where,
Q = Heat generated by the heating coil, W
V = Voltmeter reading, V
I = Ammeter reading, A
T_1, T_2, T_3 = Temperature readings of thermocouples, ^oC
T = Average temperature of heat sink, ^oC
h = Heat transfer coefficient, W/m^2K
A = Effective area of the heat sink
$= 21.705 \times 10^{-3}\ m^2$
Ta = Room Temperature, ^oC

The results from measurement are tabulated in Table 1.

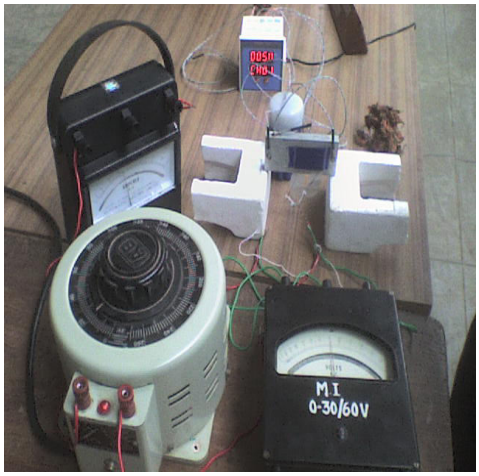

Fig. 2 Experimental setup with heat sink kept in the open air

Table-1. Experimental results for heat transfer coefficient for heat sink kept in open air

Sl.No	V((V)	I(A)	Q(W)	T(^oC))	Ta(^oC))	h(W/m^2K)
1	13.4	0.375	5.025	43.33	32	20.43
2	16.6	0.58	9.628	52.67	32	21.46
3	18.4	0.64	11.78	57.33	32	21.42

B. Heat sink kept in Amplifier box without top cover

As shown in Fig. 3, heat sink is kept in Amplifier box with top cover removed. Current is supplied from dimmerstat to the heating coil attached to the heat sink. The heating coil gets heated and transfers heat to the sink, increasing the heat sink temperature. Voltmeter and ammeter are used to measure voltage and current respectively. Heat dissipated and heat transfer co-efficient are calculated using Eq. (1),(2),(3). The results from measurement are tabulated in Table 2.

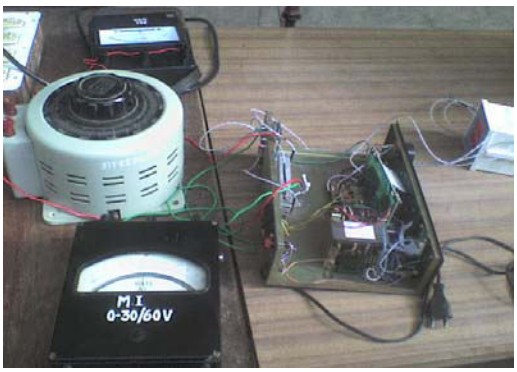

Fig. 3 Heat sink kept in the box with open top.

Table-2. Experimental results for heat transfer coefficient for heat sink kept in amplifier box without top cover

Sl.No	V((V)	I(A)	Q(W)	T(°C))	Ta(°C))	h(W/m^{2}K)
1	13.2	0.445	5.874	48.66	32	16.24
2	15.5	0.515	7.98	52.66	32	17.79
3	17.2	0.575	9.89	55.66	32	19.25

C. *Heat Sink kept in Amplifier box with top cover*

As shown in Fig.4, heat sink is kept in closed amplifier box. Current is supplied from dimmerstat to the heating coil attached to the heat sink. The heating coil gets heated and transfers heat to the sink, increasing the heat sink temperature. Voltmeter and ammeter are used to measure voltage and current respectively. Heat dissipated and heat transfer co-efficient are calculated using Eq. (1),(2),(3). The results from measurement are tabulated in Table 3. The results for all the three cases are plotted in Fig. 5.

Fig. 4 Heat sink kept in the box with top closed

Table-3. Experimental results for heat transfer coefficient for heat sink kept in amplifier box with top cover

Sl.No	V((V)	I(A)	Q(W)	T(°C))	Ta(°C))	h(W/m^{2}K)
1	12.2	0.32	3.904	41.33	28	13.49
2	16.2	0.45	7.29	53	30	14.6
3	18.5	0.53	9.805	58.67	30	15.76

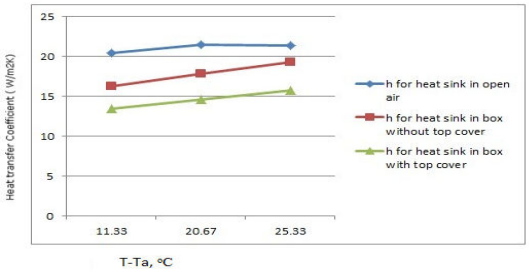

Fig. 5 Variation of heat transfer coefficient with temperature difference

III. CONCLUSION

The heat transfer coefficient is obtained experimentally for a commercially available heat sink at different configurations – in open air, in amplifier box without top cover, in amplifier box with top cover. It is found that heat transfer coefficient is lowest when heat sink is kept in Amplifier box. The measured values of the heat transfer coefficient can be used to test the various correlations used for theoretical prediction of the heat transfer coefficient within the range of measurement employed here.

ACKNOWLEDGMENT

Authors thank their colleagues for their support and encouragement for the present project work.

REFERENCES

[1] P.Teertstra. J.R. Culham and M.M. Yovanovich," Analytical model for simulating the thermal behaviour of Microelectronic Systems", ASME 1995.

[2] M. P. GARCIA,M. R. COSLEY," Experimental and computational studies on the thermal management of electronics enclosures using natural convection",Eurotherm seminar No. 5

[3] Rajput, "Heat and mass transfer", S. Chand and Company Ltd.,2010

[4] Ozisik, "Heat transfer: a basic approach", McGraw-Hill, 1985

◈◈◈

Extraction of Bio-Diesel from the Thevetia peruviana oil and conducting a performance and emission tests with SC5D additive at different injection pressures

[1]SUNIL.B.LAKKUNDI, [2]DR.G.S.SHIVASHANKAR &[3] DR.L.K SRIPATHI

[1,2]Mechanical Department
Siddaganga Institute of Technology Tumkur, Karnataka
[3]Mechaical department
J.N.N.College of engineering, Tumkur, Karnataka

Abstract— The world is confronted with the twin crises of fossil fuel depletion and environmental degradation. The indiscriminate extraction and consumption of fossil fuels have led to a reduction in petroleum Reserves. Petroleum based fuels are obtained from limited reserves. These finite reserves are highly concentrated in certain region of the world. Therefore, those countries not having these resources are facing a foreign exchange crisis, mainly due to the import of crude petroleum oil. Hence it is necessary to look for alternative fuels, and the best available alternative is Biodiesels. In this direction, it has already been proved that thevetia peruviana seed oil can be a good alternative fuel for CI engine Tests are conducted on single cylinder four stroke water cooled compression ignition engine to evaluate the feasibility of blends of Thevetia peruviana methyl ester with SC5D Additive. Our studies indicate that 20 % blend of Thevetia peruviana with SC5D Additive is the best blend among all other blends. The performances of 20 % blend of Thevetia peruviana methyl ester with SC5D Additive shows highest break thermal efficiency. As the amount of Thevetia peruviana methyl ester blend with SC5D Additive increases the HC, CO in exhaust decreases.

Keywords- *Diesel engine, Biodiesel, performance, Emissions, Thevetia Peruvian Methyl Ester, SC5D Additive.*

I. INTRODUCTION

The World energy crisis has become the foremost crucial topic in this new era. Unstable price of petroleum fuel in the world market and recent environmental concerns on gas emission during combustion have led to intensive search for alternative energy sources that are not only renewable but sustainable. Without doubt, one of the most important evolutions in the renewable energy sector is the development of biodiesel.

Biodiesel has better properties than that of petroleum diesel such as renewable, biodegradable, non-toxic, and essentially free of sulfur and aromatics. Biodiesel fuel has the potential to reduce the level of

Pollutants and the level of potential or probable carcinogens stated that Biodiesel has become more attractive recently because of its environmental benefits and fact that it is made from renewable resource.

However, the bottleneck to produce biodiesel in commercial scale is the high cost of edible virgin oil, in which account for more than 70% of the overall biodiesel production cost. In addition, using edible virgin oil such as rapeseed, sun flower, soybean and palm oil in biodiesel production has raised the concern of food versus fuel debate. Thus, recent biodiesel development has shifted to use non-edible and waste oil as a new and sustainable feedstock for long term production. It is strongly believed that using these oils will help in improving economical feasibility of biodiesel and minimize the hurdle of food versus fuel phenomena

II. PREPARATION OF THEVETIA PERUVIANA BIODIESEL

Thevetia peruviana plant seed is a non edible oil seed .The plants grow very quickly and not much maintenance is required. The main advantage of this plant is, it yields almost throughout the year and seeds contain 35 to 40% of oil. Thevetia peruviana seed oil is converted in to biodiesel by transesterficaton process. The free fatty acid (FFA) content in the raw oil calculated first and depending on the FFA, the amount of NAOH to be added is determined. The NAOH is dissolved in the methanol in a proper ratio and the mixture is added to raw oil which is heated at 65ºc for 2 hours. The methanol reacts with the raw oil and separates the glycerin from the raw oil. The glycerin is layer is separated from the biodiesel and biodiesel is washed for removing the traces of NAOH and glycerin and finally dried to remove the water traces. After drying the bio diesel is ready to use. The Fig1.shows the process flow chart for the preparation of Thevetia peruviana biodiesel

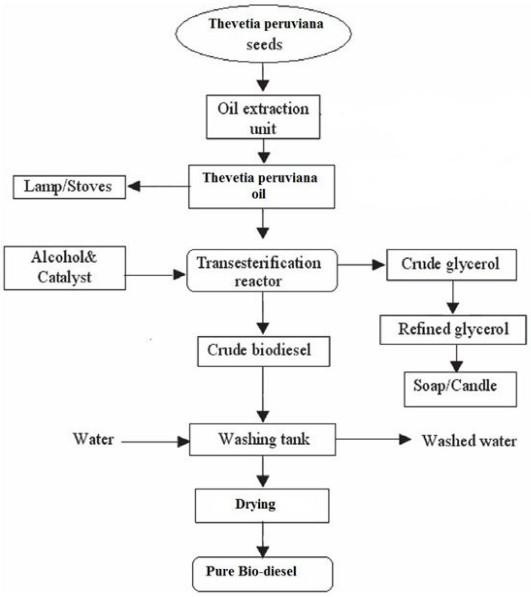

Fig 1 Process Flow Chart

TABLE 1

Properties of Thevetia peruviana Bio-diesel.

Characteristics	TPME	Diesel
Specific Gravity	0.875	0.82
Flash Point ^{0}C	170	56
Fire Point ^{0}C	186	58
Kinematic Viscosity at 40^{0}C (mm^2/s)	5.34	1.83
Calorific value (kJ/kg)	39950	42250

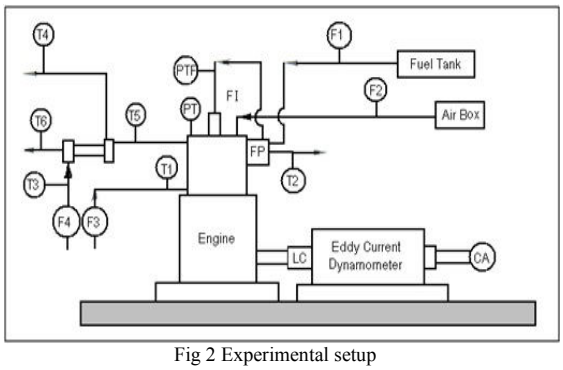

Fig 2 Experimental setup

PTF : Fuel Injection Pressure Sensor
PT : Combustion Chamber Pressure Sensor
FI : Fuel Injector
FP : Fuel Pump
T1 : Jacket Water Inlet Temperature
T2 : Jacket Water Outlet Temperature
T3 : Inlet Water Temperature at Calorimeter
T4 : Outlet Water Temperature at Calorimeter
T5 : Exhaust Gas Temperature before Calorimeter
F1 : Liquid fuel flow rate
F2 : Air Flow Rate
F3 : Jacket water flow rate
F4 : Calorimeter water flow rate
LC : Load Cell
CA : Crank Angle Encoder
EGC: Exhaust Gas Calorimeter
T6 : Exhaust Gas Temperature after Calorimeter

The Schematic diagram of the engine test rig is shown in Fig.2 The engine test was conducted on four-stroke single cylinder direct injection water cooled compression ignition engine connected to eddy current dynamometer loading. The engine was always operated at a rated speed of 1500 rev/min. The engine was having a conventional fuel injection system. The injection nozzle had three holes of 0.3 mm diameter with a spray angle of 120º. A piezoelectric pressure transducer was mounted with cylinder head surface to measure the cylinder pressure. It is also provided with temperature sensors for the measurement of jacket water, calorimeter water, and calorimeter exhaust gas inlet and outlet temperatures. An encoder is fixed for crank angle record. The provision is also made for the measurement of volumetric fuel flow. The built in program in the system calculates brake power, thermal efficiency and brake specific fuel consumption. The software package is fully configurable and averaged P-Θ diagram, P-V plot and liquid fuel injection pressure diagram can be obtained for various operating conditions. The Exhaust emissions are measured with the help of a exhaust gas analyzer

III. RESULTS AND DISCUSSION

This paper compares specific fuel consumption, brake thermal efficiency and exhaust emissions of blends of TPME and SC5D Additive with those of diesel.

Performance characteristics:

Engine performance characteristics are the major criterion that governs the suitability of a fuel. This study is concerned with the evaluation of Brake Specific fuel Consumption (BSFC) and Brake Thermal Efficiency (BTE) of the blends of TPME and SC5D Additive with diesel

1. BRAKE THERMAL EFFICIENCY (BTE)

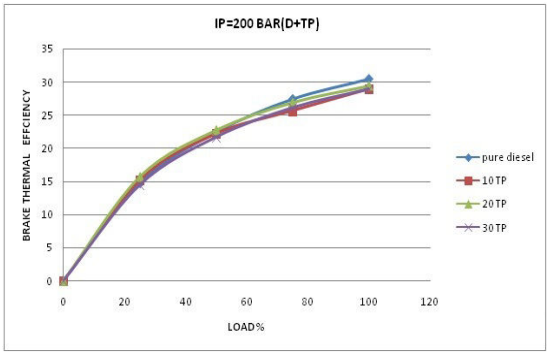

Fig.1 Variation of BTE with load for different percentages
Of TPME in Diesel

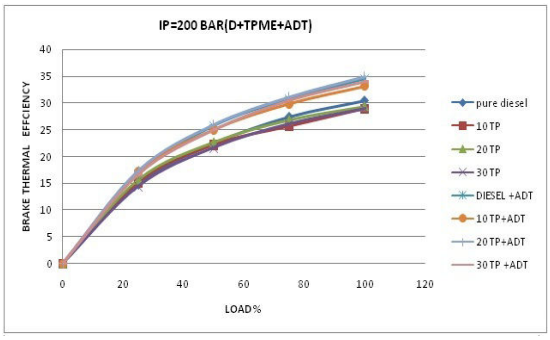

Fig.2 Variation of BTE with load for different percentages
Of TPME and SC5D additive in Diesel

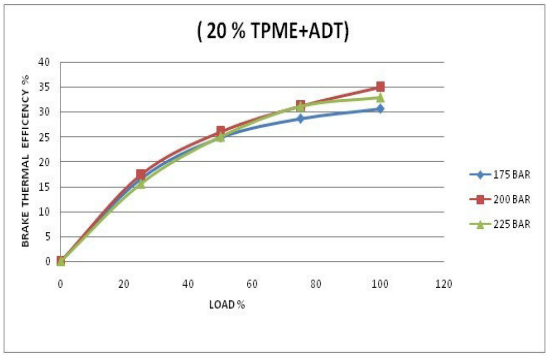

Fig 3. Variation of BTE with load for 20%TPME
and SC5D Additive at different Injection Pressures

Fig1.Shows that Brake Thermal Efficiency is slightly higher than that of diesel and BTE increases with load for TPME blends and fig 2.Shows again it increases by adding SC5D Additive to TPME blends. And from fig3. It is seen that as the injection pressure increases BTE also increases up to 200 bar and decreases for further increase in injection pressure.

2. BRAKE SPECIFIC FUEL CONSUMPTION (BSFC)

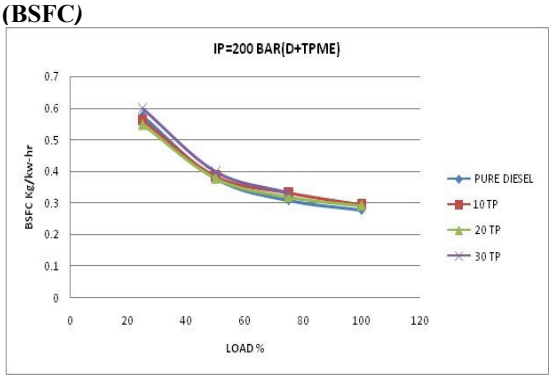

Fig.4 Variation of BSFC with load for different percentages
Of TPME in Diesel

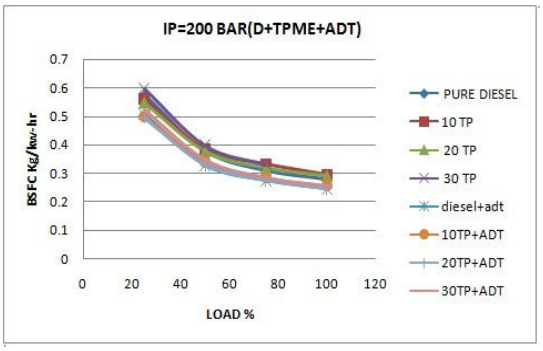

Fig.5 Variation of BSFC with load for different percentages
Of TPME and SC5D additive in Diesel

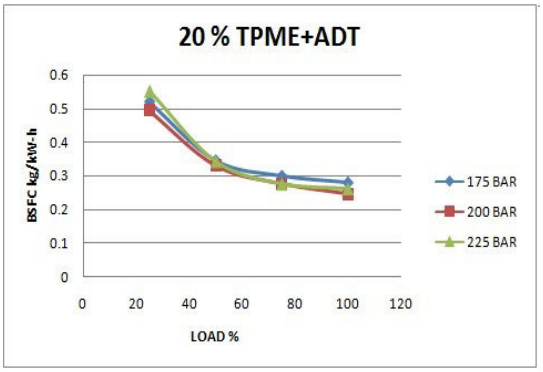

Fig 6. Variation of BSFC with load for 20%TPME
and SC5D Additive at different Injection Pressures

TPME has lower calorific value than that of diesel. Hence Brake Specific Energy Consumption is slightly higher than that of the diesel. From fig 4. It is seen that the BSFC decreases with load for TPME blends, fig 5. Shows BSFC still more decreases by adding SC5D Additive to TPME blends. And also from fig 6. It is also seen that as the injection pressure increases BSFC decreases up to 200 bar and increases for further increase in injection pressure

3. EXHAUST GAS TEMPERATURE (EGT)

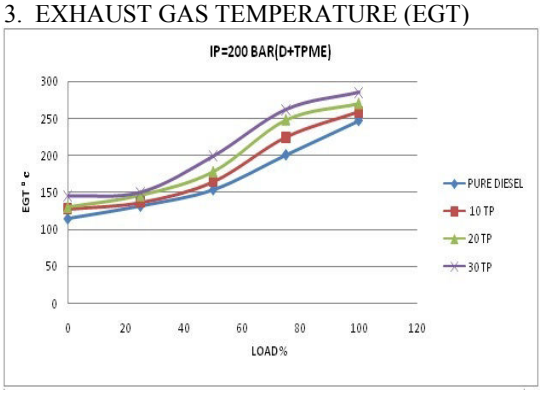

Fig 7.Variation of Exhaust Gas Temperature with load

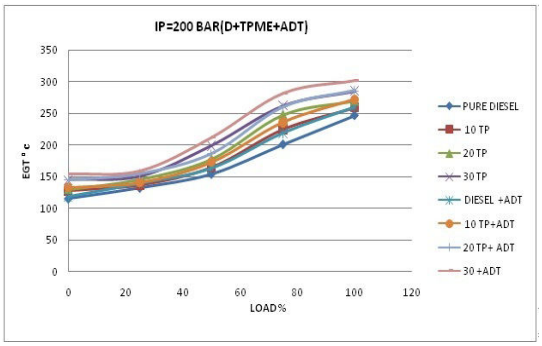

Fig 8.Variation of Exhaust Gas Temperature with load for different percentages of TPME and TPME with SC5D Additive in diesel

Fig 9. Variation of EGT with load for 20%TPME and SC5D Additive at different Injection Pressures

It is observed that from fig 7. EGT increases with load because more fuel is burnt at higher loads to meet the power requirement and also observed that EGT increases with percentage of TPME blends and fig 8. Shows again it increases by adding SC5D Additive in the test fuel for all loads. This may be due to the oxygen content of the TPME and SC5DAdditive, which improves combustion and thus may increase the EGT. From fig 9.It is seen that as injection pressure increases Exhaust Gas Temperature also increases.

4. OXIDES OF NITROGEN (NOx)

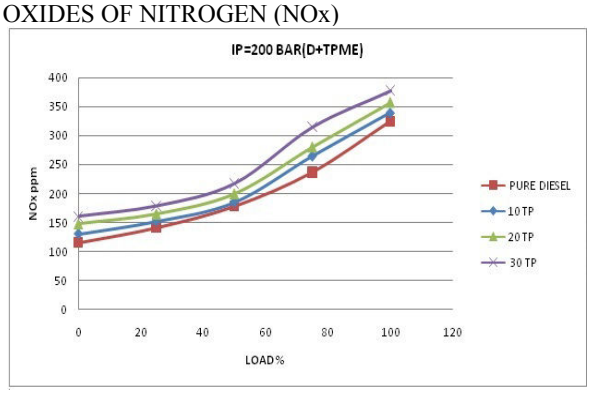

Fig 10.Variation of NOx Temperature with load

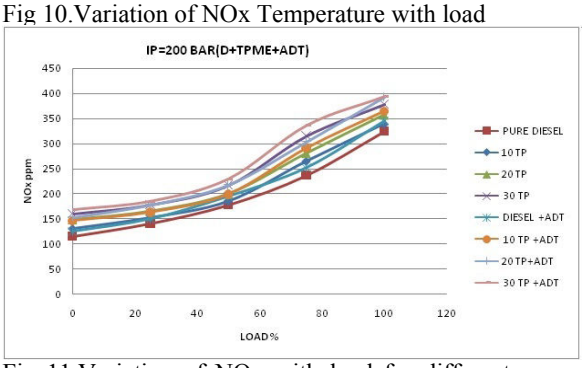

Fig 11.Variation of NOx with load for different percentages of TPME and TPME with SC5D Additive in diesel

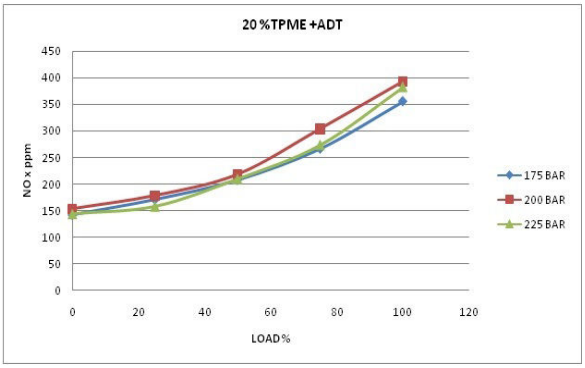

Fig12.Variation of NOx with load for 20%TPME and SC5D Additive at different Injection Pressures

Fig 10.Shows gradual increase in the emission of nitrogen oxides (NO_x) with increase in percentage of TPME blends and again fig 11.Shows it also increases by adding SC5D Additive in the fuel. The NO_x increases for TPME may be associated with the oxygen content of TPME, since the oxygen present in the fuel may provide additional oxygen for NO_x formation And from fig 12.It is seen that as the injection pressure increases NO_x emission also increases.

5. UNBURNT HYDROCARBON (HC)

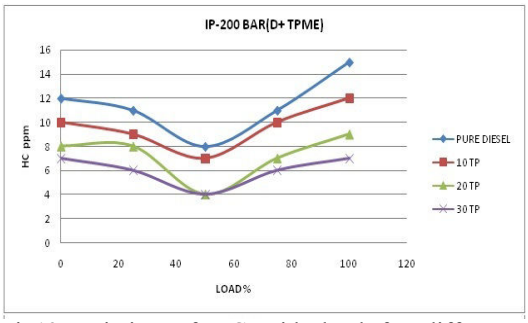

Fig13.Variation of HC with load for different percentages Of TPME in Diesel

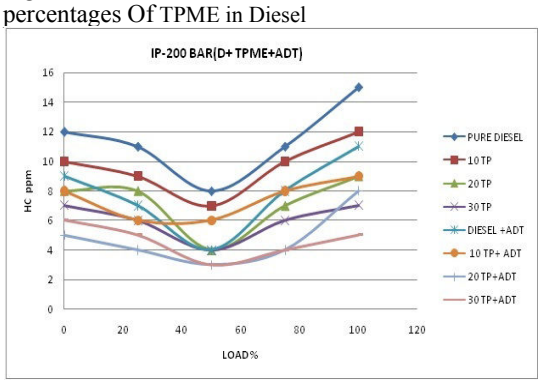

Fig 14. Variation of HC with load for different percentages of TPME and JME with SC5D Additive in Diesel

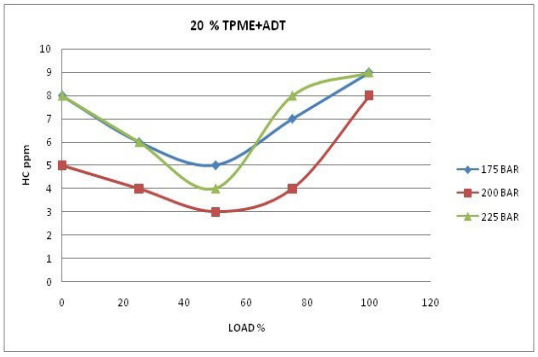

Fig 15. Variation of HC with load for 20%JME and SC5D Additive at different injection pressures

From fig 13. it is observed that hydrocarbon emission increases with load and as the percentage of TPME blends increases hyrocarbon emission is reduced and again from fig 14 it is seen that by adding SC5D Additive to TPME blends the emission is reduced more. And fig 15. Shows that as the injection pressure increases hydrocarbon emission is reduced.

6. CARBON MONOXIDE (CO)

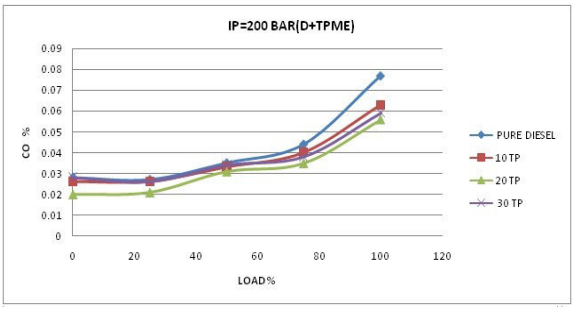

Fig 16. Variation of CO with load for different percentages Of TPME in Diesel

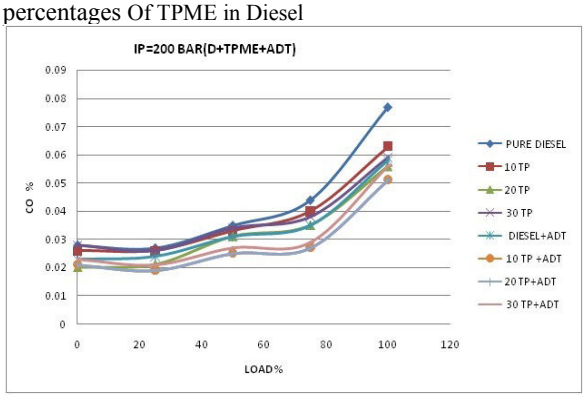

Fig 17. Variation of CO with load for different percentages of TPME and TPME with SC5D Additive in Diesel

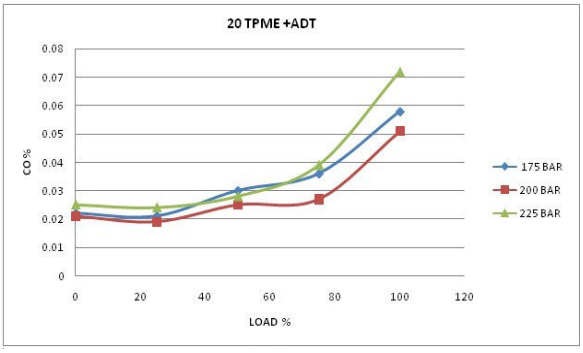

Fig 18. Variation of CO with load for 20%TPME and SC5D Additive at different injection pressures

From fig 16. it is observed that carbon monoxide emission is lesser at light loads and increases suddenly at higher loads because of the Presence of fuel rich mixture at higher loads and as the percentage of TPME blends increases carbon monoxide is reduced and again from fig 14 it is seen that by adding SC5D Additive to TPME blends the emission is reduced more. And fig 15. Shows that as the injection pressure increases carbon monoxide emission is reduced.

CONCLUSIONS

- Brake thermal efficiency increases with the increase in injection pressure and best efficiency occurs for the 20% blend of TPME with SC5D Additive and diesel at full load. Thus an improvement of 4% of Brake thermal efficiency is achieved.
- NOx emission is found to be marginally increases with the addition of more and more TPME with SC5D Additive to diesel.
- HC emissions decrease with TPME blends and with SC5D Additive.
- CO emissions decrease with TPME blends and with SC5D additive.
- It is also observed that the exhaust gas temperature increases with percentage of TPME in the test fuel for all the loads.
- TPME with SC5D Additive satisfies the important fuel properties as per ASTM specification of Biodiesel and improves the performance and emission characteristics of engine significantly.

REFERENCES

[1] T Baluswamy ,Marappan,"Perforamance evaluation of direct injection diesel engine with blends of thevetia peruvaina seed oil and diesel". Journal of scientific and industrial research. Volume 66, december 2007,PP. 1035-1040.

[2] C.V. Mahesh, Dr. E.T. Puttaiah, Swetha.S, "Effect of injection pressure on the performance and emission characteristics of c i engine using jatropha curcus as bio-diesel with sc5d additive" International Journal of Engineering Research and Applications. ISSN: 2248-9622. Vol. 2, Issue 3, May-Jun 2012, pp.2282-2287

[3] K. Kannan ,M. Udayakumar, "Experimental study of the effect of fuel injection pressure on diesel engine performance and emission". ARPN Journal of Engineering and Applied Sciences. VOL. 5, NO. 5, MAY 2010, ISSN 1819-6608.

[5] Y.V.Hanumantha Rao, Ram Sudheer Voleti , A.V.Sitaram Raju and P.Nageswara Reddy, "Experimental investigations on jatropha biodiesel and additive in diesel engine", Indian Journal of Science and Technology Vol.2 No 4 (Apr. 2009) ISSN: 0974- 6846

[4] Venkata hanumantha rao yarrapathruni, ram sudheer voleti, nageswara reddy pereddy, and venkata sitarama raju alluru,"jatropha oil methyl ester and its blends used as an alternative fuel in diesel engine", original scientific paper udc: 621.43.041.6:662.756.3 doi:10.2298/tsc i0903207y

[6] Vijittra Chalatlon, Murari Mohon Roy, Animesh Dutta3 and Sivanappan Kumar, "Jatropha oil production and an experimental investigation of its use as an alternative fuel in a DI diesel engine", B2N 5E3, N1G 2W1.

[7] Doddayaraganalu Amasegoda DHANANJAYA, Chitrapady Visweswara SUDHIR, and Padmanbha MOHANAN, "combustion characteristics of diesel engine operating on jatropha oil methyl ester", Original scientific paper UDC: 621.43.041.6:662.756.3 DOI: 10.2298/TSCI1004965D.

[8] J.Sadhik Basha and R.B. Anand, "Role of nanoadditive blended biodiesel emulsion fuel on the working characteristics of a diesel engine", JOURNAL OF RENEWABLE AND SUSTAINABLE ENERGY 3, 023106 (2011).

[9] F.K. Forson _,E.K. Oduro, E. Hammond-Donkoh, "Performance of jatropha oil blends in a diesel engine", Renewable Energy 29 (2004) 1135–1145.

[10] Emil Akbar, Zahira Yaakob, Siti Kartom Kamarudin, Manal Ismail, Jumat Salimon, "Characteristic and Composition of Jatropha Curcas Oil Seed from Malaysia and its Potential as Biodiesel Feedstock Feedstock" , European Journal of Scientific Research ISSN 1450-216X Vol.29 No.3 (2009), pp.396-403

◈◈◈

Pneumatic Actuator Modeling For Optimization OF Mechatronic Systems

D.SOWJANYA JESSY[1], K.RAJA SEKHAR BABU[2], DR.M.VENKATESWARA RAO[3]

[1]Mechanical Engineering, Bapatla Engineering College, Bapatla, Guntur Dt, A.P, India
[2] Department of Mechanical Engineering, Bapatla Engineering College, Bapatla, Guntur Dt, A.P, India
[3] Mechanical Department, Bapatla Engineering College, Bapatla, Guntur Dt, A.P, India

Abstract: The possibility of coupling between different elements comprising a mechatronic system and mechanical systems (mechanisms or structures) at an early stage of the design procedure becomes a significant issue in a number of applications. To this end, it can become very useful to analyze the actuator performance as a function of the size, design parameters and physical limitations. Since there a broad range of actuator technologies has boosted a number of research works focusing on general criteria for actuator comparison and selection for different applications, actuator selection criteria must be used to choose the most suitable actuator for different applications. The present work deals with the formulation of model-based design rules to be used in the conception of optimized mechatronic systems employing linear pneumatic actuators. The main contribution of this project is the application of new methodology to pneumatic actuators. It expands the results obtained in Gomis-Bellmunt et al. (Gomis-Bellmunt O, Galceran-Arellano S, Sudrià-Andreu A, Montesinos-Miracle D, Campanile LF. Linear electromagnetic actuator modeling for optimization of mechatronic systems. Mechatronics 2007; 17(2–3):153–63) where the methodology is presented and applied to linear electromagnetic actuators.

1. INTRODUCTION:

1.1 Actuators:

Actuators are one of the principal elements employed in all the industries. Actuators can be defined as energy converters which transform energy from an external source into mechanical energy in a controllable way. They are operated by a source of energy, usually in the form of an electric current, hydraulic fluid pressure or pneumatic pressure, and convert that energy into some kind of motion. That motion can be in virtually any form, such as blocking, clamping, ejecting or many other types of motion. Actuators typically are used in manufacturing or industrial applications and might be used in devices such as motors, pumps, switches and valves. Actuators are the final elements in a control system. can also be analyzed as energy converters, focusing on robot applications. Several reported works provide rules and charts for actuators selection and others focus on the study of different actuator classes.

The present work is based on the methodology presented in [1] for electromagnetic actuators, where a detailed analysis of linear electromagnetic actuators following general procedure and oriented towards improving the actuator design has been presented. In [1], a new methodology to analyze linear electromagnetic actuators by modeling their maximum output mechanical quantities (force, work and stroke) as functions of the geometry and material properties is necessary to be developed. The motivation to undertake such a work stems from the need for light and volume reduced structures and systems, which are to be integrated in the design procedure as early as possible. Hence, the geometric relationships, Actuators can be found as system component in nearly every controlled system to move or steer particular parts to control the overall process of the system.Ashby and Cebon in [2] presented an actuator selection criterium to be used in software to choose most suitable actuator for different applications. Another suitable selection and classification criterion has introduced in [3] by comparing different actuators available in the market. Huber et al. [5] introduced a comparison of different actuators based on their performance regarding stress, strain, energy and precision. The performance of different solid state actuators available in the market was analyzed in [6]. Different magnetic actuators focusing on their applications were investigated in [7]. An actuator

aspect ratios and material properties that maximize the actuator output quantities with a certain limited volume or weight, along with their scalability for the integration in structures are studied in this paper. The main contribution of the present paper is the application of methodology developed in [1] to pneumatic actuators. A validation of the results is done by comparing numerical results with industrial actuator data.

1.2 Types of Actuators:

The actuator input quantity may be the current or the charge or the voltage or the fluid pressure or the temperature. The output quantities are the force, the work and the stroke.

Based on the type of input quantity, the actuators may be grouped in number of ways:

- Electro-magnetic Actuators

- Piezoelectric Actuators
- Magnetostrictive Actuators
- Fluid power Actuators
- Thermal Expansion Actuators

Electro-magnetic Actuators input is a power-less electrical signal and their output an electrical power or mechanical energy, which is commonly a torque for motors or a thrust for translational movements. They are used in automotive start motors, electric door locks, appliances, hydraulic valves, speaker/voice coils, power relays and pinball machines.

Piezoelectric actuators are devices that produce a small displacement with a high force capability when voltage is applied. There are many applications where a piezoelectric actuator may be used, such as ultra-precise positioning and in the generation and handling of high forces or pressures in static or in dynamic situations.

Magnetostrictive materials undergo a deformation when a magnetic field is present. The Magnetostrictive Actuators are solid state magnetic actuators. A current driven coil surrounding the magnetostrictive rod generates the expansion of the rod. Magnetostrictive Actuators are in strong competition with the standard piezoelectric actuators. They find applications as sound generators (sonars), proportional valves, high forces generators or low voltage actuators (it can be less than 12V). They are used in machine tools, gas & petroleum industry, and are considered for medical, military and space industries.

Fluid power actuators receive fluid from a pump (typically driven by an electric motor). After the fluid has been pressure, flow, and directionally controlled, the actuator converts its energy into rotary or linear motion to do useful work. The term fluid power refers to energy that is transmitted via a fluid under pressure. With hydraulics, that fluid is a liquid such as oil or water. With pneumatics, the fluid is typically compressed air or inert gas. Fluid power is used in a diverse range of applications from mobile construction and aerospace equipment to powering industrial machinery.

Thermal expansion Actuators refer to actuators based on thermal expansion of a solid. Thermal expansion of a solid, results in a small volume change but a large force. These actuators are so precise they can be engineered to move within several thousandths of an inch, and work in any temperature range from 30F to 300F. These devices are being used by many industries such as aerospace, automotive, agricultural, and solar and HVAC.

2. METHODOLOGY:

The new methodology described in [1] is applied to pneumatic actuators. The main steps are:

Step-1: **Design parameters:**

In order to obtain clear design parameterization geometrical factors, aspect ratios and filling factors are presented. Study of the geometry and materials of the actuators introducing the geometrical factors k_i which define the ratio between any geometrical dimension l_i and a reference geometrical dimension l in the same axis as $k_{i=} l_i \div l \rightarrow l_i = k_i .l$, and aspect ratios $\eta = r \div l$. Study of filling factor which provides information about the portion of usable cross section surface when electric wires are concerned.

Step-2: **Force-stroke and work-stroke characterization:**

Analysis of the force, stroke and work production of the actuators assuming the quasi-static behavior is to be done. That means a general expression of the output quantities as a function of all the input quantities involved is developed in second step. In this work an ideal power supply with no losses will be considered, it implies that the load will not change the supplied pressure and it can be assumed with no loss of generality if the power of the power supply is larger than the nominal power consumed by the actuator.

Step-3: **Limiting quantities:**

Discussion of the limiting quantities involved in the output quantities expressions. The output quantities developed by an actuator can be controlled by modifying the input quantities. Some physical limits like maximum allowed temperature, mechanical resistance etc. do not allow the actuator output quantities to be increased indefinitely. Therefore, all the other quantities must be expressed as functions of the mentioned quantities.

Step-4: **Maximum force for a given size:**

Study of the limit force, stroke and work of the actuator is to be done. The quantities involved in the force, stroke and work expressions developed in the second step are substituted in the fourth step in order to express them depending on the limiting values and design parameters. The analysis of a given output quantity, for a given class of actuators, as a function of the design variables, shows (as a rule) a monotonic dependence on certain size variables.

Step-5: **Scalability:**

Analysis of the scalability of the actuator. In the fifth step the actuator performance as a function of the size is analyzed and the scalability and application range are discussed.

Step-6: **Comparison:**

Comparison between the theoretical results and the industrial actuator quantities. Actuators from different manufacturers need to be compared, taking into account their dimensions, maximum allowed pressures, strokes etc.

3. PNEUMATIC ACTUATORS:

Fluid power actuators use the fluid power to provide mechanical work. The pressure is the input quantity, performing the same function as the current in electromechanical actuators. The difference between the pressures **P** in two different chambers results in a relative pressure which produces a force **F** in a given surface **S** which yields **F = P.S**. The fluid actuators employed in the industry are mainly divided by the state of the fluid employed: hydraulic actuators employ an incompressible liquid (usually oil), while pneumatic actuators employ a compressible gas (air).

Pneumatic actuators are commonly used in many engineering fields. They present good force and work densities even though not as high as the hydraulic actuators. They can perform strokes as long as needed like their hydraulic counterparts. They are easily controllable and the power source providing the energy can be placed far away from the actuator. However, they cannot work with pressures as high as the hydraulic actuators because of the problems derived from the high compressibility of the gases. Nevertheless, the pneumatic systems can work at higher environment temperatures. The main disadvantages of Hydraulic Actuators are the safety problems generated by the high pressures needed (the same fact that provides the advantages), the leakage flow (that can become an important problem for actuator performance, safety conditions and environmental issues) and the hardly inflammability of the oil employed.

Therefore, in any pneumatic circuit, the required mechanical motion is obtained from actuators that form the last and important limb in the circuit. The required motion may be either linear or rotary. Based on the type of motion, the actuators can be classified as *Pneumatic cylinders* and *Pneumatic motors*. The actuators used to get the linear motion are called the *pneumatic cylinders*. The actuators used to get the rotary motion are known as *pneumatic motors*.

A pneumatic cylinder is a device, which converts fluid power into linear mechanical force and motion. It usually consists of a movable element, a piston and a piston rod operating within a cylindrical bore.

3.1. Step 1: Design Parameters

In Figure 1, a Pneumatic Actuator is sketched. For x=0, both orifices are completely closed, when x>0 follows $P_1>P_2$ since $P_s>P_r$, and the plunger moves forward, when $x < 0$ follows $P_2 < P_1$ and it moves backward. The sections can be written as $A_1=\pi D_1^2/4$ and $A_2=\pi (D_1^2-D_2^{2)}/4$ where D_1 is the diameter of the cylinder and D_2 is the diameter of the rod which guides the plunger. The geometry of hydraulic cylindrical actuators is shown in Figure 2.

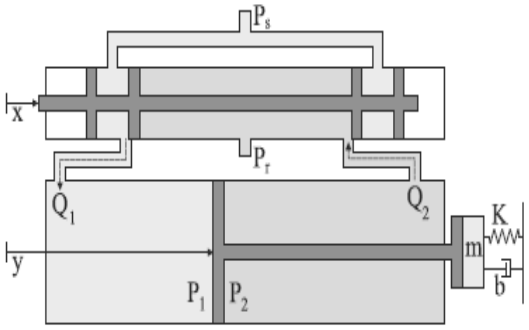

Fig. 1. Hydraulic actuator.

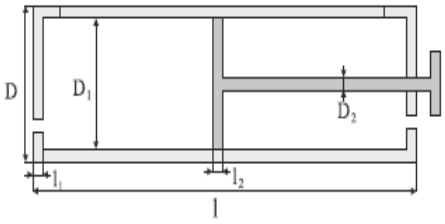

Fig. 2. Geometry of a hydraulic actuator.

3.2. Step 2: Force-stroke and work-stroke characteristic

The cylinder force can be expressed as $F=P_1A_1- P_2A_2$ where P_i is the pressure in the chamber i and A_i is the effective section of the piston. It can be expressed as:

$$F=P_1\pi D_1^2/4- P_2\pi (D_1^2-D_2^{2)}/4 \quad \text{------ (1)}$$

The force performed by the cylinder in steady-state conditions depends on whether the movement is done forward or backward, since the section is different.

Assuming $P_2=P_r=0$ and $P_1=P_s$, the forward force can be expressed as:

$$F_f= P_s\pi D_1^2/4 \text{ ---------- (2)}$$

Concerning the backward force, $P_2=P_s$ and $P_1=P_r=0$. The force yields:

$$F_b= P_s\pi (D_1^2-D_2^{2)}/4 \text{ ---------- (3)}$$

Assuming quasi static behavior the work can be obtained assuming the force is constant during the time and therefore multiplying the force times the displacement.

3.3. Step 3: Limiting quantities

The maximum allowed shear stress is the main quantity limiting the available mechanical force and work. It can be expressed using the Mohr circle

as half the difference between the radial and tangential stresses. The radial stress in a thick walled cylinder can be written as a function of the position **r** in the wall as follows:

$\sigma_{rr}=\frac{PD_1^2}{D^2-D_1^2}\left(1-\frac{D^2}{4r^2}\right)$ ---------- (4)

The tangential stress in a thick walled cylinder yields:

$\sigma_{tt}=\frac{PD_1^2}{D^2-D_1^2}\left(1+\frac{D^2}{4r^2}\right)$ ---------- (5)

The equivalent shear stress can be derived from (4) and (5) as:

$\sigma_{eq}=(\sigma_{rr}-\sigma_{tt})/2=\frac{PD_1^2}{D^2-D_1^2}\left(\frac{D^2}{4r^2}\right)$ ---------- (6)

From Equation (6), it can be clearly seen that the maximum shear stress is produced for the minimum value of r, i.e. $r=D_1/2$. Using the defined geometric relationships the maximum shear stress yields:

$\sigma_{eq}=\frac{P}{1-K_{D1}^2}$ ---------- (7)

Hence, to not overcome the shear stress threshold, the maximum pressure must be established as:

$P_{L1}=\sigma_{eq}(1-K_{D1}^2)$ ---------- (8)

For backward motion, there arises another fact: there exists a maximum axial stress σ_{aa} in the rod attaching the load. It implies another pressure limitation:

$P_{L2}=\sigma_{aa}K_{D2}^2$ ---------- (9)

Then, the maximum pressure for backward motion P_{Lb} can be written as:

$P_{Lb}=\min\{P_{L1},P_{L2}\}=\min\{\sigma_{eq}(1-K_{D1}^2),\sigma_{aa}K_{D2}^2\}$ ---------- (10)

Defining $\alpha=\sigma_{aa}/\sigma_{eq}$, $\alpha>0$, it may be expressed as:

Analyzing the expression (16), the maximum design factor may be found by using $1-K_{D1}^2=\emptyset K_{D2}^2$ or its equivalent formulation

In such a case:

$q_f=(1-K_{D1}^2)(K_{D1}^2-1+K_{D1}^2/\emptyset)$ ---------- (17)

It can be expressed as:

$q_f=-\frac{\emptyset+1}{\emptyset}K_{D1}^4+\frac{2\emptyset+1}{\emptyset}K_{D1}^2-1$ ---------- (18)

$P_{Lb}=\sigma_{eq}\min\{(1-K_{D1}^2),\alpha K_{D2}^2\}$ ---------- (11)

3.4. Step 4: Maximum Force, stroke and work

3.4.1 Forward Motion

Using equations (8) and (2), the maximum available force per cross-section can be expressed for the forward motion as:

$\frac{F_f}{\pi D^2/4}=\sigma_{eq}(1-K_{D1}^2)K_{D1}^2$ ---------- (12)

The design factor q_f can be defined as:

$q_f=(1-K_{D1}^2)K_{D1}^2$ ---------- (13)

and is the factor to be maximized in the design. Analyzing the latter expression, it can be seen that for a given size the forward force is maximized for $K_{D1}=1/\sqrt{2}$ performing a force per cross-section of $\sigma_{eq}/4$ with a design factor $q_f=1/4$.

3.4.2. Backward motion

Using Equations (11) and (3), the maximum available force per cross-section can be expressed for the backward motion as:

$\frac{F_f}{\pi D^2/4}=\sigma_{eq}\min\{(1-K_{D1}^2),\ \emptyset\alpha K_{D2}^2\}\ (K_{D1}^2-K_{D2}^2)$ ---------- (14)

An alternative formulation yields:

$$\frac{F_f}{\pi D^2/4}=\begin{cases}\tau_{eq}\left(1-k_{D1}^2\right)\left(k_{D1}^2-k_{D2}^2\right) & 1-k_{D1}^2<\varphi k_{D2}^2\\ \tau_{eq}\varphi k_{D2}^2\left(k_{D1}^2-k_{D2}^2\right) & 1-k_{D1}^2\geqslant\varphi k_{D2}^2\end{cases}$$

---------- (15)

The design factor $q_f=4F_f/\sigma_{eq}\pi D^2$ may be defined as:

$$q_f=\begin{cases}\left(1-k_{D1}^2\right)\left(k_{D1}^2-k_{D2}^2\right) & 1-k_{D1}^2<\varphi k_{D2}^2\\ \varphi k_{D2}^2\left(k_{D1}^2-k_{D2}^2\right) & 1-k_{D1}^2\geqslant\varphi k_{D2}^2\end{cases}$$

---------- (16)

$K_{D2}=\sqrt{(1-K_{D1}^2)/\emptyset}$

To obtain the maximum design factor: $\frac{dq_f}{dK_{D1}}=0$ ---------- (19)

Then the maximum K_{D1} i.e. K_{D1max} yields:

$K_{D1max}=\sqrt{\frac{2\emptyset+1}{2\emptyset+2}}$ ---------- (20)

It can be demonstrated that it is maximum, since $\ddot{q_f}(K_{D1max})<0$ where $\alpha>0$. The maximum design factor yields:

$q_{fmax} = \frac{1}{4}\frac{1}{\emptyset^2+1}$ --------- (21)

And $K_{D2max}=\sqrt{\frac{1}{2\emptyset(\emptyset+1)}}$ ---------- (22)

Then for □=1, $K_{D1max}=\sqrt{3}/2$ and the maximum design factor $q_f=1/8$ for $K_{D2}=1/2$. It can be noted that the maximum design factor is half the value of the one found for forward motion.

3.4.3 Considering forward and backward motion

In practical cases, both forward motion and backward motion are used. If the average force including forward motion and backward motion are considered:

$\frac{F_{fb}}{\pi D^2/4} = \frac{\tau_{eq}}{4}[min\{(1-K_{D1}^2), \emptyset K_{D2}^2\}(K_{D1}^2 - K_{D2}^2) + (1-K_{D1}^2)K_{D1}^2]$ --- (23)

An alternative formulation yields:

$$\frac{F_f}{\pi D^2/4} = \tau_{eq}\left(1-k_{D1}^2\right)k_{D1}^2 + \begin{cases} \left(1-k_{D1}^2\right)\left(k_{D1}^2-k_{D2}^2\right) & 1-k_{D1}^2 < \varphi k_{D2}^2 \\ \varphi k_{D2}^2\left(k_{D1}^2-k_{D2}^2\right) & 1-k_{D1}^2 \geq \varphi k_{D2}^2 \end{cases}$$ ------ (24)

A detailed analysis show that the maximum can be derived from (24), by differentiating against K_{D1} and K_{D2} and equaling to zero. The following system of equations is obtained:

$K_{D2} - K_{D1}\frac{1}{\sqrt{2}} = 0 \quad and \quad \emptyset K_{D2}^2 - 2K_{D1}^2 = -1$ -------- (25)

Solving, the maximum is obtained as: (Taking □=1)

3.5. Step 5: Scalability

Regarding the scalability, the static behavior of hydraulic actuators does not have the dependence on size-dependant numbers such as the Nusselt

3.6. Step 6: Industrial Actuators

The results obtained analytically are compared with industrial actuators in the present section. Actuators from ARO Pneumatic Actuators have been studied, taking into account their dimensions, maximum allowed pressures, strokes, etc. The models and theoretical expressions developed in the previous steps match remarkably well with industrial actuator data

$K_{D1max} = \sqrt{\frac{2}{4-\emptyset}} \quad and \quad K_{D2max} = \sqrt{\frac{1}{4-\emptyset}}$ ----- (26)

3.4.4 Stroke and Work

From Figure 2, Stroke is given by $l-2l_1-l_2$. For the sake of simplicity, l_1 can be considered equal to $l_1= l_2= (D-D_1)/2$, since there correspond to the wall thickness. The stroke is then

$l- 3l_1=l-(3/2)\ D\ (1-K_{D1}) = l(1-3\eta(1-K_{D1}))$

It will be maximized for η=0, which is clearly not possible, due to the fact that no force would be performed for such an aspect ratio. In this case, the force criterium would be dominant, while trying to obtain the smaller the better aspect ratio η for stroke maximization purposes.

Similar conclusions can be extracted analyzing the work. The maximum forward work per volume can be expressed as:

$\frac{W_f}{\pi l D^2/4} = \tau_{eq}(1-K_{D1}^2)K_{D1}^2(1-3\eta(1-K_{D1}))$ ------ (27)

The work is maximized for η=0. Concerning the dependence on K_{D1}, the maximum volumetric work can be found as the solution K_{D1} of the above equation whose solution is omitted because of its length. For η=0, it yields:

$K_{D1max}=\frac{\sqrt{2}}{2}$ ------- (29)

It can be noted that only the forward motion has been addressed. Similar effects to those observed with the force when dealing with backward and averaged forward and backward motion appear with the work as well.

number (as happened with electromagnetic actuators in [1]). Hence, as long as the static behavior is concerned the scalability criterium applies for the usual industrial range of dimensions.

The comparison between the inner-output diameter ratio of the analyzed actuators and the optimum extracted analytically from the equations show that the matching is remarkable. It can be seen in Figure 3, where the relationship between the inner and outer diameter for different industrial actuators is plotted. It can be noted that the real actuator data regression lies between the optimum for forward ($K_{D1max}=1/\sqrt{2}=0.7071$) and backward motion (dotted lines with $K_{D1max}=\sqrt{3}/2=0.866$). It

can be noted, that it is placed very close to the backward motion optimum.

Static behavior of hydraulic actuators does not have the dependance on size-dependant numbers such as the Nusselt number (as happened with electromagnetic actuators in [1]). The relevant limiting design quantity is the maximum allowed shear stress, which determines the required thickness of the cylinder walls for a given pressure or determines the maximum cylinder pressure for a given thickness.

The force-cross-section relationship analyzed in Section 3.4 has proven to apply for the real actuators as well. In Figure 4, it can be noted that the real actuator performance for different actuators (shown in thin lines for different families of industrial actuators) is below the maximum threshold (shown in the bolder line for steel G10100 HR). The regression analysis of each class of actuator shows that the quotient between the force and the cross-section can be found as the considered operating pressure. Depending on the type of steel or material used, the maximum allowed shear stress can be increased, allowing higher pressures in the cylinder for a given geometric factor K_{D1}.

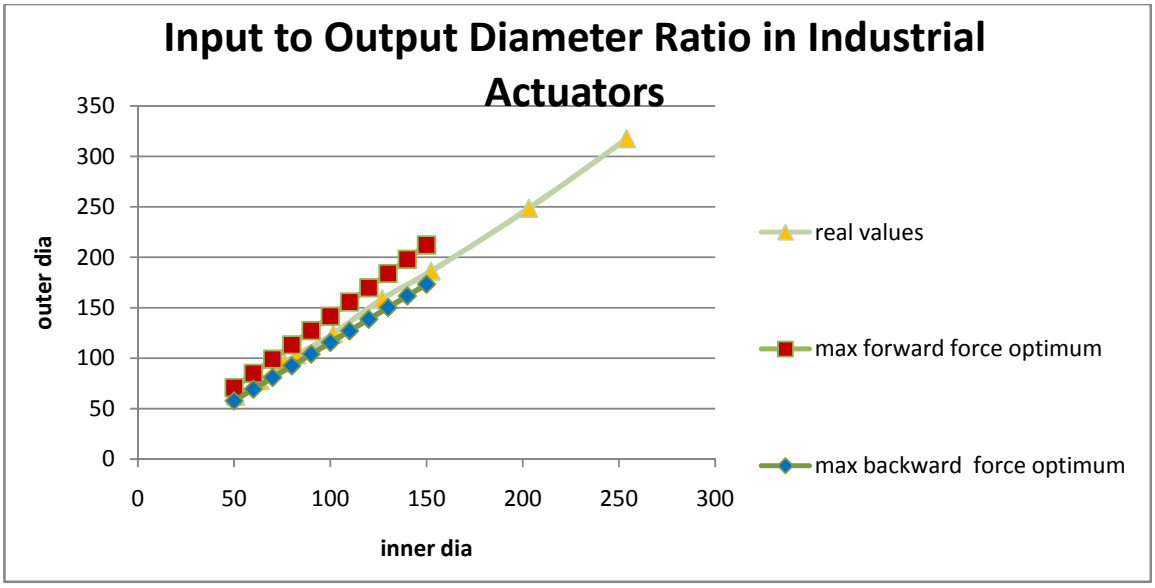

Figure 3: Comparison between the input to output diameter ratio existing in Industrial Actuators and the results of present work

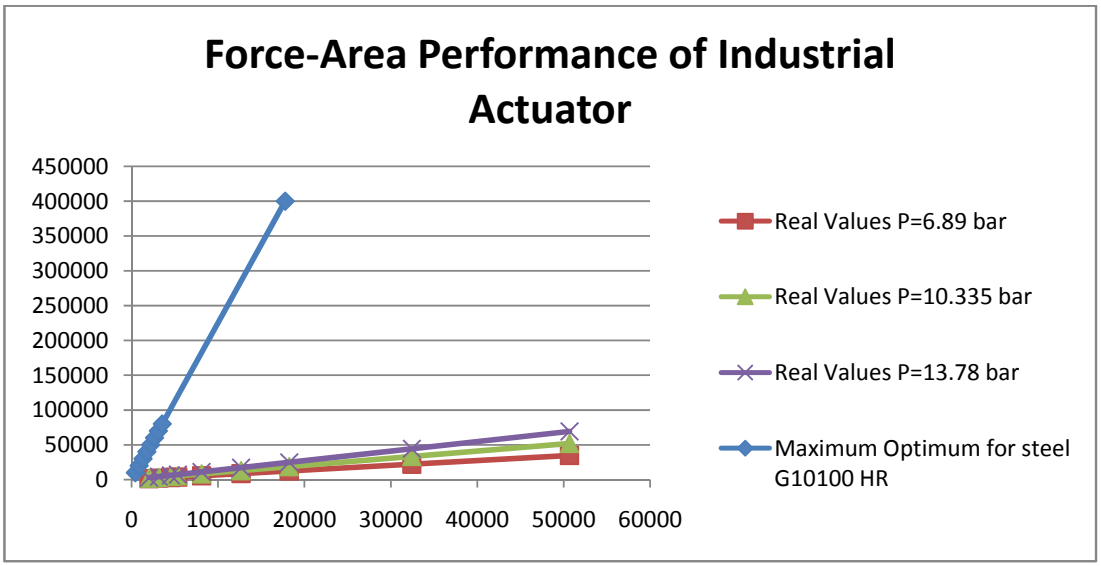

Figure 4: Industrial Pneumatic Actuator force- area performance

4. CONCLUSIONS:

The present work has dealt with the optimization of linear pneumatic actuators. The procedure presented in [1] has been employed to obtain the maximum force in a given volume, weight or cross-section. The scalability of the analyzed actuators has been also discussed.

The limit output quantities have been found for certain aspect ratios and geometric relationships. The results have been compared with the performance of industrial actuators and it has been noted that the industrial actuators behave as expected

REFERENCES:

[1]Gomis-Bellmunt O, Galceran-Arellano S, Sudrià-Andreu A, Montesinos-Miracle D, Campanile LF. Linear electromagnetic actuator modeling for optimization of mechatronic and adaptronic systems. Mechatronics 2007; 17(2–3): 153–63.

[2]Ashby MF, Cebon D. Material selection in mechanical design. In: Troisieme Conference Europeenne sur les Materiaux et les Procedes Avances, Euromat'93, Paris, June 8–10, 1993.

[3]Zupan M, Ashby MF, Fleck NA. Actuator classification and selection – the development of a database. Adv Eng Mater 2002; 4(12):933–40.

[4]Huber JE, Fleck NA, Ashby MF. The selection of mechanical actuators based on performance indices. Proc R Soc Lond A 1997; 453:2185–205.

[5]Giurgiutiu V, Rogers CA, Chaudhry Z. Energy based comparison of solid state induced strain actuators. J Intell Mater Syst Struct 1996; 7(1):4–14.

[6]Howe D. Magnetic actuators. Sensors and Actuators 2000; 81: 268–74.

◈◈◈

Innovative Techniques in the field of Metrology with the Aid of Data Acquisition

[1]S.SUGANTHAN, [2]B.R. GIRINATH

Department of Mechanical engineering, Adhiparasakthi engineering college,
Melmaruvathur, Tamil nadu, India.

ABSTRACT-The aim of this paper is to design a miniature vane anemometer in a alternative way which has some great significances than the conventional one. This anemometer removes the usage of sophisticated devices like sensors in the conventional one, so obviously it is more cost effective. The construction of this instrument is done by utilizing the back emf of electric motor and is then calibrated with the aid of data acquisition techniques. LabVIEW software is utilized for performing data acquisition techniques.

INTRODUCTION

In this paper we are going to explain about the several innovative techniques in the field of metrology with the aid of data acquisition systems. By implementing this system we can eliminate the various sophisticated instruments in measuring devices
and also the device can be manufactured in a cost effective manner.

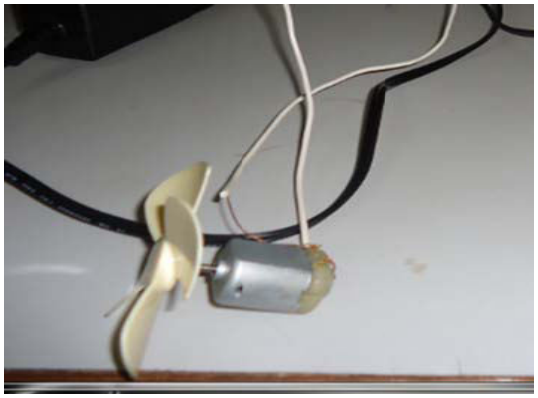

Fig 1 – Fan attached with electric motor

The calibration setup consists of a fan which is capable of rotating even at low values of air velocities. This fan is attached to a electric motor. To make the device compact a mini motor is employed for this purpose which has a maximum speed of about 20,000rpm.

Fig 2 – Hot Wire Anemometer

The other important device for designing a successful calibration setup is a standard instrument. For this purpose a hot wire anemometer is chosen as a standard instrument.

Hot wire anemometer senses the value of air velocity by temperature changes when air passes through it.

To explain this technique we have provided an example by calibrating a vane anemometer with the technique of data acquisition, with the help of the software called LabVIEW.

The process of calibrating the vane anemometer are discussed as follows.

THE CALIBRATION SETUP

This experimental setup consists of the following components.

MEASURMENT OF VOLTAGE

When air passes over the fan which is attached to a electric motor the fan begins to rotate, since the fan is attached to a electric motor it generates a back emf which is to be sensed.

To sense the values of the voltage generated due to the back emf of the electric motor the motor is connected to a DAQ (Data acquisition) board as shown in figure 3.

The DAQ board maintains a interface with a computer with the aid of a software called Lab VIEW.

The purpose of selecting this method is to increase the accuracy of the system. Since the voltage is a variable factor with respect to time the software

takes 20K acquisitions per second and the mean value is then calculated.

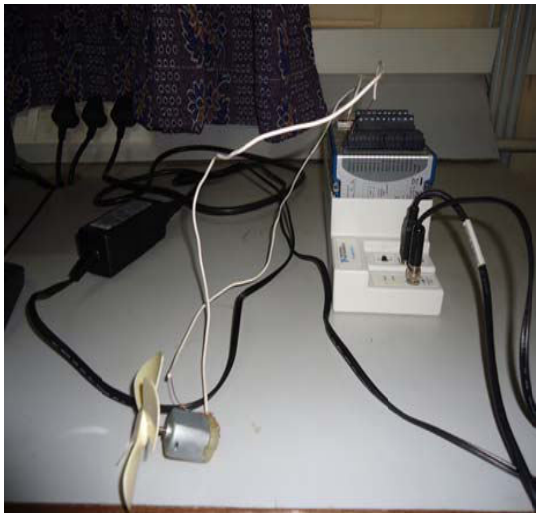

Fig 3 – Measurement of voltage

This process only determines and influences the accuracy of our system, So we provided a great concern in this process of acquisition of voltage from electric motor. The mean value of the total acquised values is then noted as the final value of voltage for that corresponding air velocity.

Fig 4. Shows the varying value of voltage with respect to time while working on LabVIEW.

.

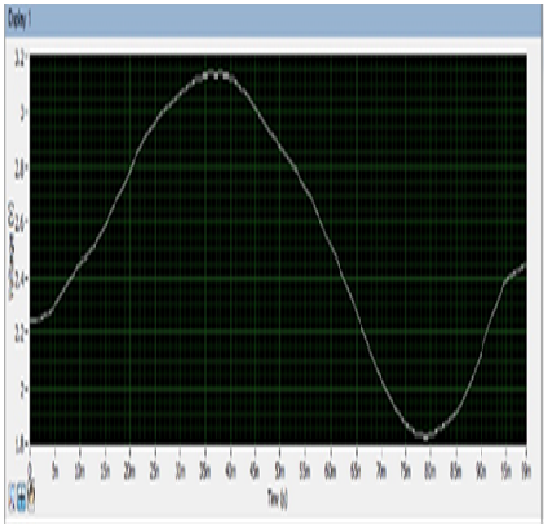

Fig 4 – voltage vs. time

MEASURMENT OF AIR VELOCITY

The velocity of the air which causes the fluctuation of the value of voltage is to be measured. Hot wire anemometer is used for this purpose of measurement of air velocity.

For the different value of voltage the corresponding values of air velocities are to be noted simultaneously.

Fig 5- measurement of air velocity by hot wire anemometer

PROCESS OF CALIBRATION

The process of calibration involves the measurement of different values of voltage generated for different values of air velocities which is also measured.

For this process a blower is taken which is capable of generating a high value of air velocity. A rheostat is also connected to the blower to control the velocity of air coming out of the blower so that different values of air velocities can be generated by that blower.

Fig 6- blower used during calibration

First the rheostat is kept in a state such that it offers high value of resistance to the input current of blower and is shown to the fan which is attached to the electric motor which is further to the DAQ board.

When the fan rotates due to changes in value ok voltage the graph in LabVIEW fluctuates. The average value of the fluctuations in that graph is noted and the velocity of the air which caused the fluctuation in voltage is also measured using the hot wire anemometer.

The same procedure is repeated for different positions of rheostat so that variable speeds in blower

can be attained and the values of the air velocity and voltage are measured and are tabulated as shown below.

VOLTAGE (V)	Air velocity (m/s)
0.636	0.07
2	0.85
30	7.3
29	5.2
12	3.5
11	1.7
9.2	1.3
8.1	1.2

Table 1 – Respective values of voltage and air velocity

GRAPH REPRESENTING VOLTAGE VS. AIR VELOCITY

From the values in that table a graph is plotted as shown below, which is useful to find the value of air velocity for the corresponding voltage which is generated by the back emf of the electric motor.

METHOD OF MEASUREMENT OF AIR VELOCITY

To measure the velocity of the unknown air first the motor is exposed to the air which is to be measured, so that the fan rotates which leads to production of back emf. The value of voltage thus produced is noted.

The value of voltage noted is marked as a point in the voltage (**blue**) curve and a straight line in downward direction is drawn until it meets the air velocity (**red)** curve. The point where it meets the red curve is marked. The value at the Y-axis which is parallel to the marking at the red curve gives the value of air velocity of that unknown air.

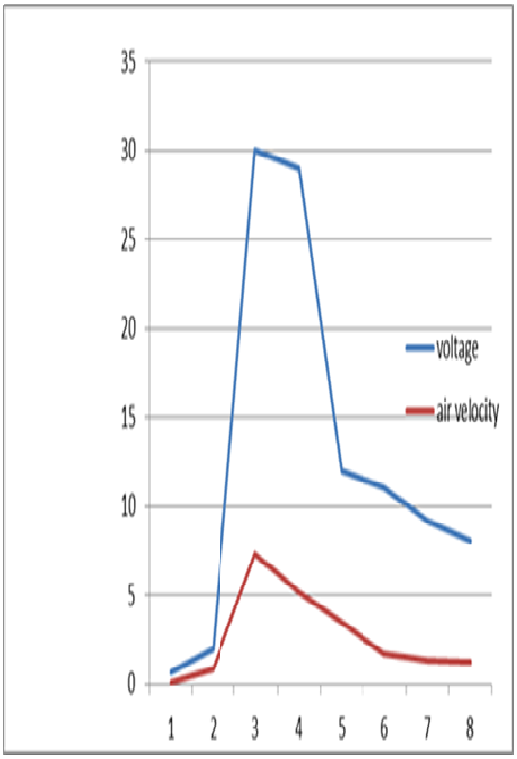

Fig 6 – voltage vs. air velocity

Fig 6 represents the graph of voltage vs. air velocity, from which the corresponding air velocities for the obtained voltages are calculated.

CONCLUSION

A successful instrument is thus designed and calibrated which can be used at any circumstance for measuring the air velocities.

REFRENCES

[1] Walt Boyes . Instrumentation reference book
[2] Micheal Tabolt smith. Audio engineers reference book.
[3] LabVIEW developer. National instruments books and publications.
[4] Chest of books.com. Basics of anemometers.
[5] R.K.Jain. engineering metrology

◈◈◈

Elephant Grass-Glass Fiber Hybrid Composites

M.MAHESH[1] , K.POORNIMA[2], DR.M.VENKATESWARA RAO[3]

[1]Department of Mechanical Engineering, Bapatla Engineering College, Bapatla, Guntur, India
[2] Department of Mechanical Engineering, Bapatla Engineering College, Bapatla, Guntur, India
[3] Mechanical Department, Bapatla Engineering College, Bapatla, Guntur, India

Abstract: An attempt has been made in the present work to explore and the possible use of variety of cultivated/wild grown fiber in the development of elephant grass–glass fiber reinforced polyester hybrid composites. The fiber is extracted from retting and manual method, and the test specimens are prepared as per "ASTM"standards. Five different contents are incorporated in the specimen, with each fiber content five identical specimens are prepared. Elephant grass–glass fiber reinforced polyester hybrid composites, are prepared by incorporating up to (40/0%,30/10%,20/20%,10/30%,0/40%) by mass.. It is observed clearly (40/0%) only mass of fiber compare with (30/10%) of hybrid composites. There is tensile strength, tensile modulus, flexural strength, flexural modulus; impact strength is 65.415Mpa,68.635Mpa,123035Mpa,1536.3Mpa, 257.305j/m, 2282.85 j/m respectively. There is increases the percentage of natural fiber to the glass fiber content increase the tensile strength ,tensile modulus, flexural strength, flexural modulus, impact strength, respectively.

The effect of NaOH treatment of the Elephant grass fibers on these properties was also studied. It was observed that hybrid composite increase with glass fiber content. These properties were found to be higher when NaOH Elephant grass fiber were used in the hybrid composites. The elimination of amorphous hemi-cellulose with NaOH leading to higher crystallinity of the Elephant grass fibers with NaOH treatment may be responsible for these observations.

INTRODUCTION

The word "composite" means two or more distinct parts physically bounded together". Thus, a material having two more distinct constituent materials or phases may be considered a composite material. Fiber-reinforced composite materials consist of fiber of high strength and modulus embedded in or bonded to a matrix with distinct interfaces (boundary) between them. In this form, both fiber and matrix retain their physical and chemical identities, yet they produce a combination of properties that cannot be dependent behavior, thermal insulation, thermal conductivity, acoustical insulation and electrical insulation. Naturally, neither all of the properties are improved at the same time nor is there usually Their beginnings are unknown, but all recorded history contains references to some form of composite material. For example, straw was used by the Israelites to strengthen mud bricks. Plywood was used by the ancient Egyptians when they realized that wood could be rearranged to achieve superior strength and resistance to thermal expansion as well as to swelling owing to the presence of moisture.. More recently, fiber reinforced resin composites that have high strength-to-weight and stiffness-to- weight ratios have become important in weight-sensitive applications such as aircraft and space vehicles achieved with either of the constituents acting alone. In general, fiber are the principal load-carrying members, while the surrounding matrix keeps them in the desired location and orientation, acts as a load transfer medium between them, and protects them from environmental damages due to elevated temperatures and humidity etc. The properties that can be improved by forming a composite material include strength, stiffness, corrosion resistance, wear resistance, attractiveness, weight, fatigue life, temperature-

any requirement to do so. Composite materials have a long history of usage.

CLASSIFICATION OF COMPOSITES:

The commonly accepted classification of composites is:

1) fibrous composites,
2) laminated composites,
3) Particulate composites.

1) The fibrous composite:

The fibrous composites are formed by embedding and binding together of fibbers by a continuous matrix. According to the definition fibre is a material in an elongated form such that it has a minimum length to a maximum average transverse dimension of 10:1, a maximum cross-sectional area of 5.2 x 10^{-4} cm^2 and a maximum transverse dimension of 0.0254 cm. A fiber is inherently much stiffer and stronger than the same material in bulk form, because of its perfect structure. Commercially available fibres are of glass, boron, Kevlar and graphite. The matrix is meant for bonding the fibrous so that they act in concert. The purpose of the matrix is manifold, namely to support, to protect and to transfer stress among the fibers. The matrix is usually of much lower strength, stiffness and density and is tougher than the fibres. It would not withstand itself high stresses. Resins are widely used as matrix materials. The composite, resulting from the combination of fibers and matrix, possesses higher specific stiffness and specific strength, and is lighter than conventional engineering materials.

2) Laminated Composites:

Bonding layers of different materials or same materials makes laminated composites. In this class of composites, discontinuous matrix or mechanical fasteners are used at times to keep the layers together. Depending upon the ways of fabrication, behavior, or constituent materials of laminates, laminated composites are commonly called as bimetal, clad-metals, laminated or safety glass, plastic based laminates, laminated fibrous or hybrid composites and sandwiches.

3) Particulate composites:

Suspending particles of one or more materials in a matrix of another material produces particulate composites. The particles and matrix can be either metallic or non-metallic. The commonly used particulate composites are concrete, solid rocket propellants, carbides etc.

.

RESEARCH NEEDS:

Natural fibers have played a significant role in human civilization since prehistoric times, with humans having depended on them for garments and other simple domestic uses as well as complex uses such as land dwellings and reed-built sailing craft. Modern technological innovations producing synthetic fibers with a wide selection of desirable properties by manipulations of the condensation of short-or-long-chain polymers compete with and in some cases, surpass the production of vegetable fibers in many countries.

In a tropical country like India, there are large varieties of regenerative plants and trees with fiber content. Some of them are cultivated over the generation and some are wild plants, trees, and creepers that grow in forests and woods. It is an established fact that any material in its fibrous form is stronger than in bulk form. Using the fact, these strong fibers are used to reinforce the weak materials. Bamboo, country Date, Jute, Sisal, Banana and Palms available freely in the countryside has been used in their crude form. Over the last four decades, composites of synthetic fibers have been developed adopting the knowledge of naturally available vegetative organs of bamboo, palm trees, sisal, etc. It is concerned with the reduction of weight of space vehicles and aircraft for optimum pay load. The constituents of these exotic composites are of high-cost: they are cost effective only in high-tech fields. They do not meet the needs of common person. The depleted natural resources of construction materials necessitate the research for cost-effective substitutes. There comes the knowledge of synthetic composites to develop new substitutes by proper conglomeration of cheap vegetative and waste materials.

For the past decades, very small contribution of research work was found towards the design and fabrication of composite materials using natural fibers. The proposed research work is intended to exploit the advantages of using natural fibers as reinforcement material in composites.

Under the proposed research work, the following aspects of natural fibers and composites are studied.

i) Identification of natural fibers
ii) Identification of matrix material
iii) Extraction of various natural fibers
iv) Preparation of natural fiber reinforced plastic specimens for Bending test
v) Bending test of natural fiber composites

ASPECTS OF THE PROPOSED RESEARCH WORK:

The proposed research work is intended to exploit the advantages of using natural fibers as reinforcement material in composites. The work provides basic understanding of the

behavior and response of new natural fibres and lightweight materials. Under the proposed research work the following aspects of natural fibres and composites have been studied.

1. Preparation of natural fiber -glass fiber reinforced hybrid composite specimens as per ASTM standards.
2. Tensile properties of natural fiber -glass fiber reinforced hybrid composite at various weight percentages.
3. Flexural properties of natural fiber -glass fiber reinforced hybrid composite at various weight percentages
4. Impact properties of natural fiber -glass fiber reinforced hybrid composite at various weight percentages

RESULTS

Specific weight **:** It is the ratio of weight (N) of the specimen to the volume (m^3) of the specimen.
Ultimate bending strength **:** It is the ratio of ultimate load at failure to the cross sectional area of the specimen.
Flexural modulus **:** It is the ratio, within the elastic limit of stress to corresponding strain.
Specific bending strength **:** It is the ratio of ultimate bending strength (N/m^2) to the specific weight (N/m^3) of the composite.
Specific flexural modulus **:** It is the ratio of flexural modulus (N/m^2) to specific weight (N/m^3) of the specimen.

CONCLUSIONS

1. Being the density of untreated Elephant grass is less than (1.01)times compared to treated Elephant grass fibre.
2. In tensile testing of fiber composites, the tensile strength ,modulus and weight percentage calumns observed that there is increases the weight percentages of glass to the natural fiber percentage containt (30/10% to 10/30%)there is increases the tensile strength and modulus compare (10/30%)of EGRP hybrid composites only mass of glass fiber there is less strength and modulus (0/40%)at 1.50,1.22 times respectively. Is an untreated fiber composites.and treated there is 1.35,1.10 times respectively.
3. The curve drawn between load Vs deflections there is (40/0%) of EFRP is less strength at (1.02) times compared to the (30/10%) of EGRP. Is an untreated fiber composites.
4. The curve drawn between load Vs deflections there is (40/0%) of EFRP is less strength at (1.11) times compared to the (30/10%) of EGRP. Is an treated fiber composites.
5. The load deflection curves are shown in fig no 1. For only mass of fibre curve shows (40/0 %) .An increases the glass fiber content at(30/10 %)increasing the load defflections at 1.06 times respectively . Similarly with NaOH treatment of fibercomposites (40/0%), to the glass fiber hybrid composites(30/10 %) an 1.12 times increases as shown in (fig 2).
6. From (figure 3and 4). drawn between weight percentage on x-axis and flexural strength modulus, on y-axis, it is observed that flexural strength,modulus of (40/0%) of EFRP composites compare EGRP hybrid (30/10%) composites less than 1.056,1.04 times respectively, in without any treatment.
7. A graph is drawn by taking percentage of weight fraction on X-axis and Impact energy(J/m) is taken on Y-axis shown fig (9).it is observed that with out treatment of EFRP composites (40/0%) .compare with NaOH treatment of EGRP hybrid composites (40/0%) is less than 1.78 times respectively.An increases the weight percentages of glass fiber to the Elephant grass fiber increases the strength.

SCOPE FOR FUTURE WORK

For the total understanding of the behavior of the Elephant grass –Glass fiber reinforced hybrid composites; further study in many aspect is needed.

The present work can be extended in the following directions.

1. Other surface treatment for the fiber for better interface bonding.

2. The expected life of elephant grass- Glass fiber reinforced hybrid composites in view of biodegradability.
3. Effect of moisture and other environments on the biodegradability of the elephant grass- Glass fiber reinforced hybrid composites.
4. Easier and cheaper method of extraction and process of elephant grass fibers.
5. Fabrication techniques for mass production.
6. study of thermal and acoustic properties of elephant grass- Glass fiber reinforced hybrid composites.

REFERENCES

1. "S. Mishra[a], A. K. Mohanty [b], L. T. Drzal[b], M. Misra[b], S. Parija[c], S. K. Nayak[c] and S. S. Tripathy[c]" Studies on mechanical performance of biofibre/glass reinforced polyester hybrid composites : Composites Science and Technology
   Volume 63, Issue 10, August 2003, Pages 1377-1385
2. . P.NOORUNNISA, KHANAM, M.MOHAN REDDY, K.RAGHU, K.JOHN AND S.VENKATA NAIDU 'Tensile, flexural and compasive properties of sisal/silk hybrid composites" published in journal of thermo plastic composites materials VOL 26-NO 10/2007 PP 1065-1070.
3. KC.MANI KANDAN NAIR AND SABU THAMOSE "Effect of ageing on the mechanical properties of short sisal fiber reinforced polystyrene composites" published in journal of thermo plastic composites materials VOL 16-MAY/2003 PP 249-271.

Hydrogen Enriched Compressed Natural Gas as a Fuel To Increase IC Engine Performance with Control of Emissions

[1]KAUSTUBH R KAPADANI, [2]KAVITA R KAPADNI, [3]SHYAM S DAREWAR,[4]RAVINDRA F DUNDE & [5]CHUNILAL K GOSAVI

[1,3,4,5]Mechanical Engineering Department
[1,3,4,5]PES Modern COE, Pune University
Pune, India
[2]Mechanical Engineering Department
[2]MES COE, Pune University
Pune, India

Abstract — Main drivers for introducing Hydrogen Enriched Compressed Natural Gas Blended Fuel for automobiles are to increase IC engine performance and reduction of both local pollutants and emission gases from nvironments. Air pollution is fast becoming a serious global problem with increasing population and its subsequent demands. This has resulted in increased usage of hydrogen as fuel for internal combustion engines. Hydrogen resources are vast and it is considered as one of the most promising fuel for automotive sector. As the required hydrogen infrastructure and refueling stations are not meeting the demand, widespread introduction of hydrogen vehicles is not possible in the near future. One of the solutions for this hurdle is to blend hydrogen with methane. Such types of blends take benefit of the unique combustion properties of hydrogen and at the same time reduce the demand for pure hydrogen. Enriching natural gas with hydrogen could be a potential alternative to common hydrocarbon fuels for internal combustion engine applications. Many researchers are working on this for the last few years and work is now focused on how to use this kind of fuel to its maximum extent.With increasing concern about energy shortage and environmental protection, research on reducing exhaust emissions, reducing fuel consumption, reducing engine noise and increasing engine performance has become the major researching aspect included in this study research paper.

Keywords — *HCNG; NOx; Pollutants; Emission Control; Engine Performance.*

I. INTRODUCTION

Probably in this century it is believe that crude oil and petroleum products will become very scare and costly to find and produce. Probably continue to be improved and increase in number of automobiles dictates that there will be a great demand for alternative fuels in the near future. Alternative fuels availability, use must, and will become more common in the coming decades. The engines used for alternative fuels such as Hydrogen, blend of H-CNG, compressed Natural gas, LPG, alcohols etc. are modified engines which were originally designed for gasoline fuelling has started appearing on the market in India which use dual fuel by using conversion kit.

The use of H-CNG blended fuel in automobiles is very costly at present. This is often because of the quantity used. H-CNG will cost much less if the amount of their usage gets to the same order of magnitude as gasoline and diesel.

A) Previous work & Indian Government Policy

India's Standing Committee on Emission Regulation, part of the Ministry of Shipping, Road Transport and Highways, approved 20% hydrogen & 80% CNG blend for use in vehicles.

Accordingly changes are being made in Central Motor Vehicle Rules (CMVR), Gas Cylinder Rules, Motor vehicle Act, Government has also constituted a committee to frame, regulations for HCNG blends above 20 % Hydrogen. Work in progress to frame regulations ISO standards for HCNG and Hydrogen kit component testing are being framed in ISO TC 22 SC 25.

Similar process will be followed by Bureau of Indian Standards (BIS). The project, involving Ashok Leyland, Bajaj Auto, Eicher Motors, Mahindra & Mahindra and Tata Motors, began as an attempt to control the emission of NO_x from poorly-maintained CNG vehicles. At 20 percent, hydrogen mixes well with CNG and does not reduce the power output of engines significantly. The new fuel will be made part of the Central Motor Vehicle Rules, which govern the automotive industry in the country. The five automotive majors will collaborate in developing HCNG engines.

B) CNG as automobile fuel

CNG is considered as an important fuel with potential to substitute the conventional liquid petroleum fuel to significant extent to a significant extent in foreseeable future. CNG is a much clean burning fuel having methane as its main constituent which is highly knock resistance. It has narrower flammability limits (5 -15 % by volume). Therefore, it is safe fuel to work upon. It is observed that working with CNG gives substantially low exhaust emissions, low exhaust smoke and substantial reduction in noise levels. Since the exhaust emissions have vital importance to us, the CNG has become as

important vehicular fuel. It is being used in vehicles in Delhi, Mumbai, and Pune etc.

C) Hydrogen as automobile fuel

The most attractive feature of hydrogen as an IC Engine fuel are that it can be produced from a potentially available raw material, water, and the main product of its combustion again is water. Hydrogen has very low density both as gas and as liquid. Hence, in spite of its high calorific value on mass basis its energy density as a liquid is only one fourth that of gasoline.

Hydrogen has extremely wide ignition limits. This allows a spark ignition engine to operate on hydrogen with very little throttling, a decided advantage. Stoichiometry hydrogen air mixture burns seven times as fast as the corresponding gasoline air mixture. This too is a great advantage in IC engines, leading to higher engine speeds and greater thermal efficiency. Hydrogen has a high self-ignition temperature but requires very little energy to ignite it. Hence, it is highly prone to pre-igniton and back flash in SI Engines.

Hydrogen can be used in IC Engines by three methods:
1) By manifold induction 2) By direct introduction of hydrogen into the cylinder 3) By supplementing gasoline

D) Blend of Hydrogen with CNG as automobile fuel

By adding hydrogen to CNG, the properties of the fuel changes in several ways. The most important factors are:

1) Lower ignition energy and fast burning rate of HCNG makes it less resistant to knocks than CNG at constant equivalence ratio.
2) It improves Lower heating value & higher consumption in terms of Nm^3 / km.
3) HCNG have Lower compressibility factor, fewer Nm^3 in a tank at 200 bars compared to CNG.
4) Higher flame speed & faster combustion compared to CNG. So engine efficiency is higher.

Hydrogen enrichment have focused on natural gas utilizing lean-burn, spark-ignited (SI) engines. H-CNG mixtures with 5, 15, and 30 vol% hydrogen gives greater performance characteristics as compare to SI and CI Engines. The H-CNG blends up to 30 vol% hydrogen enabled very lean operation and NOx emission reductions with some penalty in total hydrocarbon (THC) emissions.

Brake-mean effective pressure (BMEP) is the work performed by the engine per cycle divided by the cylinder volume displaced per cycle. 30 vol% H-CNG fuel mixtures shows better results on actual and theoretical BMEP diagram relative to CNG. Despite its low energy density, hydrogen can improve engine performance at very lean engine operation because it releases more energy per unit oxygen consumed. Moreover, the increased flame speed and lean combustion ability of hydrogen increase the combustion efficiency significantly.

II. Hydrogen Percentage In H-CNG And Its Physical Compatibility With Modified Engine Components

Due to the small proportion of hydrogen in the mixture (H-CNG blends up to 30 percent by volume or 5 percent by mass hydrogen were considered) the physical properties of the fuel mixture are close to the baseline natural gas fuel and do not impact components such as piping, valves, and storage tanks. The potential for hydrogen embrittlement is expected to be quite low because component materials found in the fuel system are carbon steels, stainless steels, aluminium alloys, copper, and copper alloys, which are acceptable for gaseous hydrogen at ambient temperatures.

The fuel flow rate sensor uses thermal conductivity of the gaseous fuel used to measure the fuel flow rate. At similar conditions, hydrogen has over six times higher thermal conductivity compared to natural gas. Thus, the H-CNG mixture will have higher thermal conductivity and will saturate the output of the fuel flow rate sensor towards the maximum flow rate conditions.

TABLE I
CHANGE IN NATURAL GAS AND H-CNG FUEL PROPERTIES WITH INCREASE of H_2 %

	Natural Gas	**HCNG (10%)**	**HCNG (20%)**	**HCNG (30%)**
H_2 [% Vol]	0	10	20	30
H_2 [% energy]	0	3.2	7.0	14.4
LHV[MJ/Kg]	45.3	46.2	46.7	48.5
LHV[MJ/Nm^3]	36.9	34.3	31.7	29.2
AFR_{stoich}	15.6	15.8	16.1	16.4
$LHV_{stoich, mix}$ [MJ/Nm3]	3.375	3.367	3.358	3.349

TABLE II
COMPARISON OF PROPERTIES OF HYDROGEN, CNG, HCNG AND GASOLINE.

A comparison of properties of Hydrogen, CNG, HCNG blend and Gasoline is given in Table II, It is to be noted that the properties of H-CNG lie in between those of Hydrogen and CNG.

III. H-CNG ENGINE DEVELOPMENT WITH CONTROL OF NO_X EMISSIONS

This literature review was conducted to uncover existing research on H-CNG mixtures used for lean-burn spark-ignited engines. Previous studies indicate that H-CNG mixtures with hydrogen content in the range of 20 to 30 volume percent (vol %) are optimum in terms of performance and emissions benefits, while still providing operation within the limits of the existing engine hardware.

A) Engine Development Constraints

- Maintain or improve horsepower and torque relative to the natural gas engine with minimum engine modifications.
- Total hydrocarbon emissions should not increase relative to the natural gas engine.
- Maximize the NOx reduction benefit relative to the baseline natural gas engine with minimum engine modifications.
- Maintain or improve Performance of the engine relative to the natural gas engine with minimum engine modification.

The optimization strategy used for the H-CNG calibration is to lean the air/fuel mixture and retard the spark timing (relative to the CNG) in order to optimize NOx reduction while maintaining torque, fuel efficiency, and other emissions similar to the CNG baseline.

H-CNG reduced engine out NOx and non-methane hydrocarbons (NMHC) emissions by 50% and 58%, respectively, as shown below in Table III. Engine out methane and THC emissions were reduced by 16% and 23%, respectively. There is no significant change in fuel efficiency. A short drivability study using a chassis dynamometer test cycle is useful to maintain the desired speed and torque capability under H-CNG fuelling of the engine.

TABLE III
ENGINE OUT EMISSIONS (RESULTS of TRIAL ON CUMMINS B GAS 5.9L ENGINE, 37 hp @ 2,800 rpm, 500 lb-ft @ 1,800 rpm)

Engine out Emissions [g/bhp-hr]	CNG	H/CNG (20 – 30) vol [%]	Difference [%]
Nox	2.0	1.0	-50%
NMHC	0.24	0.10	-58%
NOx +NMHC	2.24	1.10	-51%
CH_4	3.0	2.5	-16%
THC	3.4	2.6	-23%
CO	2.3	2.1	-9%

Properties	H_2	CNG	H-CNG	Gasoline
Stoichiometric composition in air, Vol [%]	29.53	9.48	22.8	1.76
Auto ignition temperature [^{0}C]	858	813	825	501-744
Limits of flammability in air, vol. [%]	4-75	5-15	5-35	1.0-7.6
Minimum energy for ignition in air [mJ]	0.02	0.29	0.21	0.24
Burning Velocity in NTP air [cm s^{-1}]	325	45	110	37-43
Quenching gap in NTP air [cm]	0.064	0.203	0.152	0.2
Diffusivity in air [cm^2 s^{-1}]	0.63	0.2	0.31	0.0817-25
Percentage of thermal energy radiated [%]	17-25	23-33	20-28	30-42
Normalized flame emissivity	1.00	1.7	1.5	1.7
Equivalence ratio	0.1-7.1	0.7-4	0.5-5.4	0.7-3.8

Early research on hydrogen enrichment was focused on fuels such as gasoline and isooctane. Later studies of hydrogen enrichment have focused on natural gas utilizing lean-burn, spark-ignited (SI) engines. These experiments shows that the H-CNG blends up to 30 vol% hydrogen enabled very lean operation and NOx emission reductions with some penalty in total hydrocarbon (THC) emissions.

Brake-mean effective pressure (BMEP) is the work performed by the engine per cycle divided by the cylinder volume displaced per cycle. BMEP is an accepted metric to assess an engine's ability to do work and is independent of engine size. Figure 1 shows the theoretical and actual BMEP difference of a 30 vol% H-CNG fuel mixture relative to CNG. Despite its low energy density, hydrogen can improve engine performance at very lean engine operation because it releases more energy per unit oxygen consumed. Moreover, the increased flame speed and lean combustion ability of hydrogen increase the combustion efficiency significantly.

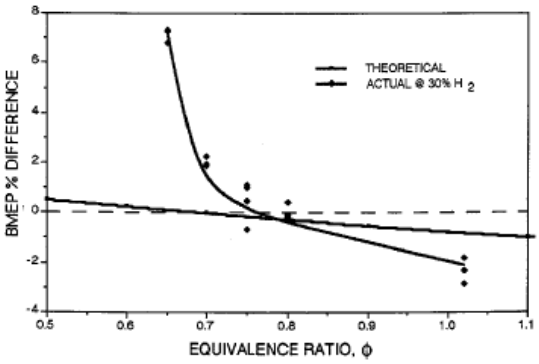

Fig. 1. Comparison between theoretical and actual BMEP change with 30 vol% hydrogen in methane.

B) Spark Timing

Optimizing spark timing can be used as a strategy to avoid knocking and to avoid exceeding the limit of maximum cylinder pressure when operating under lean burn conditions. An effective way to reduce NOx emission is to retard the spark timing. This is due to the combustion stability and the elevated flame temperature in the cylinder. For lower engine speed such as 900 rpm it is found that the NOx emissions also increase slightly when the spark timing becomes closer to TDC beginning around 5 degrees CA BTDC. This is because of the increased engine power loss when the ignition timing is set too close to TDC because the fuel cannot burn completely and the combustion process mainly takes place in the expansion stroke with a relatively low-pressure environment. So the thermal efficiency is greatly affected by the spark timing. It rises as the spark timing is advanced. This is due to the decrease in temperature due to the early ignition timing.

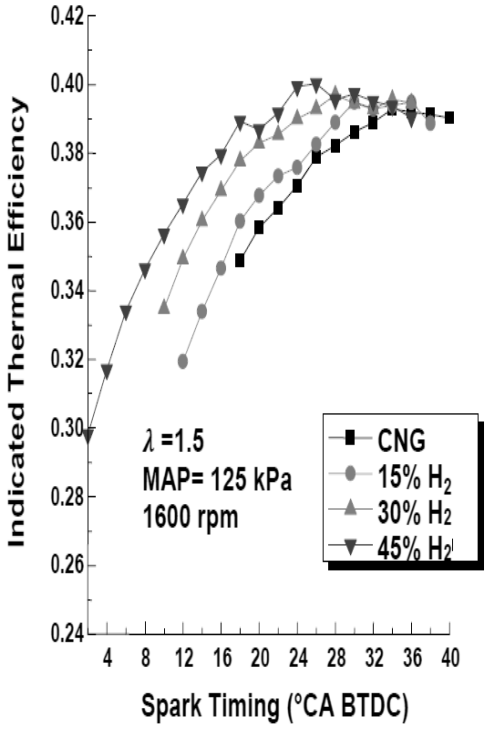

Fig. 2. Indicated thermal efficiency at different spark timings

As shown in fig. Below, the engine efficiency can be increased fuelling the engine by H-CNG blends. The available data shows that a performance of an engine increases with increase of the hydrogen quantity in the blend. Furthermore, depending on the relative air/fuel ratio values associated to the combustion of the blends, an overall environmental benefit can be noticed as higher than 1.The increase in efficiency with the hydrogen addition is due to the reduction in the equivalence ratio.

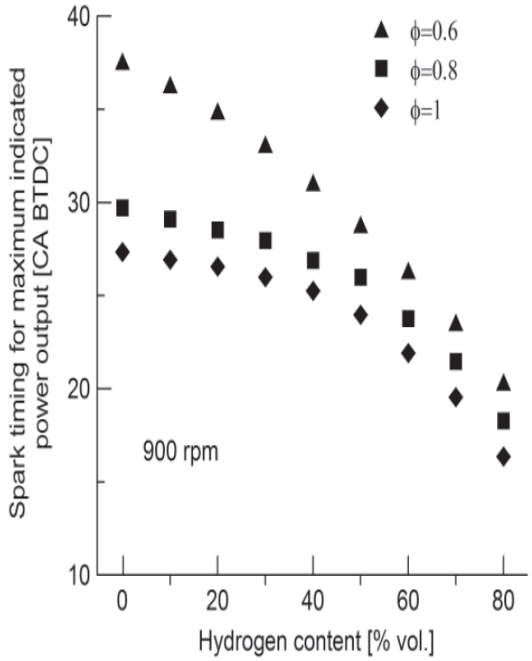

Fig.3. Spark timing for maximum indicated power output versus hydrogen content (simulation)

C) Compression Ratio

Because both natural gas and hydrogen are gaseous fuels, they are able to with-stand a higher compression ratio which allows for increased efficiency. Although the studies on the effect of an increased compression ratio on the performance and emission of the fuel are not plentiful, it has been proven to be an effective method to increase performance. According to NRG Tech Report (2002), by completing tests on an H-CNG engine with compression ratio ranged from 9.1 to 15.0, it was concluded that a desirable compression ratio ranges between 12 and 15. However, care must be taken to avoid engine knock.

IV. HYDROGEN - CNG MIXING AND SUPPLY SYSTEM

Mixing system is required to blend desired amount of hydrogen with natural gas in a pressure stabilizing tank just before entering the engine. The tank is divided into two chambers with a damping line used to improve the mixture uniformity. A schematic of the fuel supply system is shown in figure 4. The flow rate of natural gas and hydrogen can be measure using a fuel flow transmitter and flow control valve is used to adjust the flow rate of the hydrogen according to the flow rate of CNG and obtain the target hydrogen fraction.

The layout of the system is shown in Fig. 4. The fuel is delivered to the engine through a venturi, which is supplied with the fuel mixture at a slight over pressure. The richness is controlled using a control valve in the supply line.

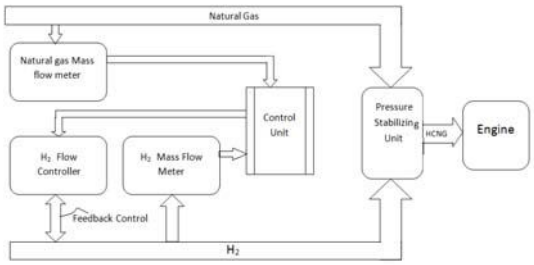

Fig. 4. Schematic of the fuel preparation system

Pure hydrogen and natural gas, as well as mixtures of these fuels can be used with this system. The hydrogen can be store in steel cylinders. The pressure required is 200 bars; the natural gas can be obtained from the city gas station at 30 mbar over pressure. Measurement of the fuel flow rate is made using mass flow meters in both of the supply lines. If hythane is used, the hydrogen flow can be control by a mass flow controller (the same device is used as mass flow meter for pure hydrogen). From the measured natural gas flow the necessary hydrogen flow is computed and supplied as input signal to the mass flow controller. This will results in constant hydrogen content, independent of engine speed and load. The hydrogen concentration is given in volume % (the term mass flow meter/controller only means that the measurement is automatically compensated for temperature and pressure changes, the reading are in Nm^3/h. Alternatively, hythane (or any other fuel) from a high pressure tank (200 bar) can be used for short runs: it contains a very limited amount of hythane and freezing problems can occur. By putting this tank on a scale fuel consumption can be measured. The system described as above is only able to provide mixtures with up to 65 % hydrogen, due to limitations in the control unit. For higher hydrogen content the mass flow controller has to be regulated independently of the natural gas flow or opened completely.

V. Engine Performance

Performance plays an important role in the choice of a fuel. H-CNG has many advantages when it comes to performance because of the high octane number of hydrogen, the engine performance generally increases with the addition of hydrogen.

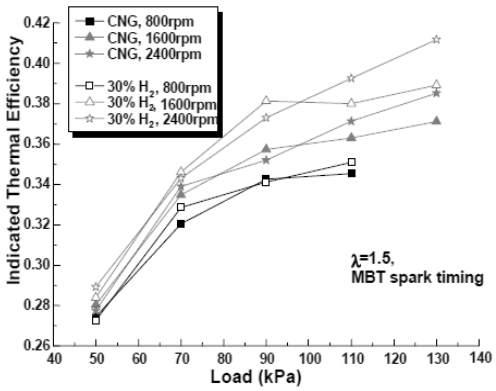

Fig. 5. Indicated Thermal efficiency Vs. Load for variable speed and different hydrogen percentage values

The thermal efficiency of both natural gas and H-CNG increases with increasing load, which makes it an ideal fuel for high load applications and heavy-duty vehicles, this relationship can be seen in figure 5. It is clearly seen in figure 5 that in nearly every case, the H-CNG fuel has a higher thermal efficiency than pure natural gas.

Engine performance is verified by comparing the torque curves for each fuel. The torque curve demonstrates the capability of the engine to maintain full load under H-CNG fuelling. As shown in Figure 6 comparing full torque achieved under natural gas and H-CNG fuelling. As seen from the NREL H-CNG transits bus engine test results, the H-CNG torque is either equal to or slightly higher than the torque generated with natural gas. The engine achieves a peak torque of 697 Nm at 1600 rpm and a rated torque of 596 Nm at 2800 rpm. Corresponding results for the engine power at full torque are also shown in Figure 6. The engine achieves a rated power of 237 HP at 2800 rpm under H-CNG fuelling.

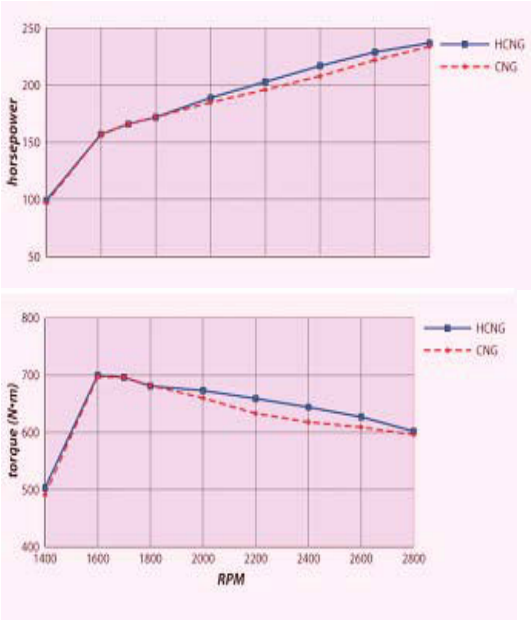

Fig. 6. Comparison between CNG and H-CNG full torque

Methane has a slow flame speed while hydrogen has a flame speed about eight times higher than methane as shown in Figure 7; therefore at the stoichiometry condition, when the equivalence ratio is higher; the combustion of methane is not as stable as with H-CNG.

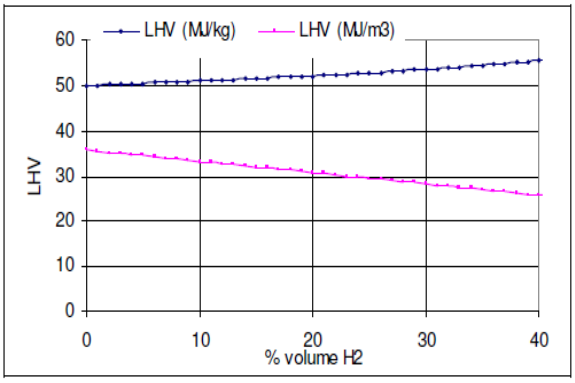

Fig. 7. Flame laminar speed for methane and HCNG

As a consequence of the addition of hydrogen to natural gas an overall better combustion had been verified, even in a wide range of operating conditions (equivalence ratio, compression ratio, etc.), finding the following main benefits:

• A higher efficiency • Lower CO2 production and emissions

Because of chemical and physical properties of hydrogen, H-CNG, despite its higher LHV per kg, has a lower LHV per Nm^3, shown in Figure 8, depending on the hydrogen content. Therefore, a natural gas engine, when fuelled with H-CNG, shows a lower power output, while maintaining its better efficiency.

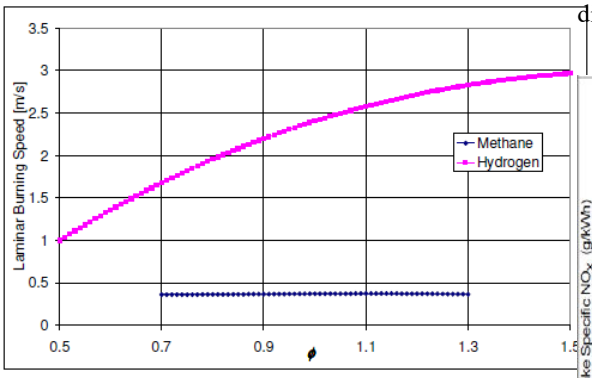

Fig. 8. LHV for different percentage of Hydrogen

To restore a good value of power output, especially for lean burn mixtures (for equivalence ratio =1.4 the engine loses are 50% of its power), a good solution could be represented by a turbocharged engine with a higher charging pressure.

Hydrogen leverage is defined as the ratio:

(% Emissions Reduction)/(% Energy Supplied as Hydrogen).

The increased efficiency makes this value higher than 1. An obvious benefit of the leverage effect is that a CO2 reduction is possible even if the hydrogen used is produced by natural gas without any sequestration of CO2.

VI. The Impact Of H-CNG Blends On Engine Exhaust Emissions

Considering emissions, when H-CNG fuel is compared with gasoline and diesel it appears to be a very appealing alternative fuel. When compared to gasoline, it produces significantly less nitrous oxide, carbon monoxide, carbon dioxide and non-methane emissions. And when compared with diesel, it nearly eliminates the particulate matter which is often of great concern. Compared to pure natural gas, it has been concluded that the addition of hydrogen increases the NOx emissions while reducing the HC emissions. The combustion stability is also improved by the addition of hydrogen which plays a part in reducing the un-burnt hydrocarbon emissions.

Hydrogen Enriched Compressed Natural Gas(H-CNG) has recently attracted attention as a fuel for internal combustion engines enabling extremely low NOx emissions without after-treatment. Because of the favourable combustion characteristics of hydrogen, HCNG allows engines to utilize high charge dilution (fuel lean or high exhaust gas recirculation operation) which can significantly increase engine efficiency with the simultaneous benefit of low NOx level. Figure 9 representing the level of NOx output for various hydrogen concentration and equivalence ratio. Higher concentrations allow further reductions in NOx but diminishing overall benefits because of the difficulties of storing the hydrogen fuel.

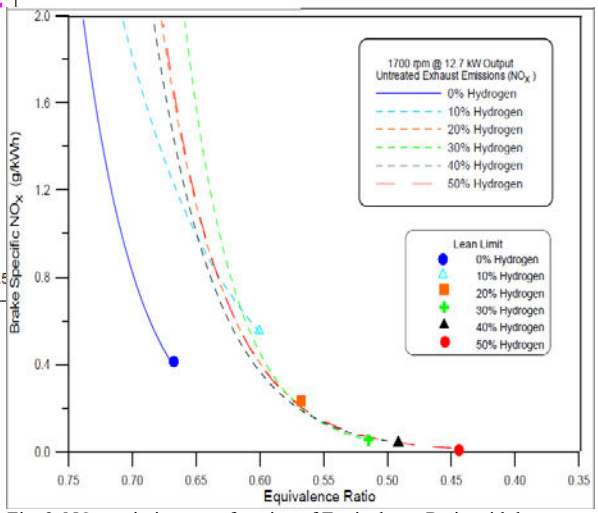

Fig. 9. NOx emissions as a function of Equivalence Ratio with lean limits for various H-CNG blends

The largest amount of NOx is produced where the air/fuel ratio is slightly lean of stoichiometry and is denoted 100% NOx. Further leaning of the air/fuel mix reduces NOx. Blending 15 % vol to 30 % vol hydrogen into CNG fuel extends the lean combustion limit. To leverage the NOx reduction of the extended lean limit, engine development would include retarded spark timing investigations.

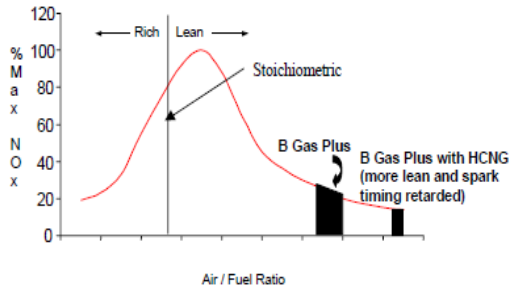

Fig. 10. Effect of air/fuel ratio on percentage maximum NOx emissions.

VII. Benifits Of H-CNG

Following are some of the benefits of using H-CNG as fuel. It is usable with the existing CNG infrastructure.

1) Hydrogen addition to natural gas can decrease engine's unburned hydrocarbons and NO*x* emissions (by lean burn) and speed up the combustion process.
2) It improves the engine efficiency and lowers fuel consumption.
3) It requires only small hydrogen storage and a column for the mixing of hydrogen with natural gas.
4) Safety properties are similar to CNG. It is safer to handle than hydrogen, because of lower risk due to very low energy content from hydrogen (only up to 30 vol.%).
5) It extends the lean misfire limit of CNG.
6) Minor modifications are required in the engine due the moderate concentration of hydrogen in the fuel mixture; the excellent anti-knock characteristics of CNG are not under-mined.
7) The phenomenon of hydrogen embrittlement does not occur with respect to the engine components. Hence, no major change is anticipated in the fuel system and engine components.

VIII. Challenges Of H-CNG

1) Today H2 is more expensive than CNG; however this can be mitigated by relying on NOx credits or by calibration that favours efficiency over NOx
2) When the hydrogen fraction increases above certain extent, abnormal combustion such as pre-ignition, knock and back-fire, will occur unless the spark timing and air-fuel ratio are adequately adjusted. This is due to the low quench distance and higher burning velocity of hydrogen which causes the combustion.
3) Combustion chamber walls become hotter, which causes more heat loss to the cooling water.
4) Storage of H-CNG and supply infrastructure cost is high.
5) Efforts to be focused on responding to fuel system performance, material compatibility.
6) Continuous availability of H-CNG needs to be assured before embarking on its major use in IC engines.
7) Quality & emission test cost is high.

IX. FUTURE RESEARCH

Future research of the hydrogen enriched compressed natural gas fuel include continuous improvement on performance and emissions, especially to reduce the hydrocarbon emissions which are currently not heavily regulated but will probably be more closely regulated in the future. Additional optimization is also necessary for the H-CNG fuel in order to obtain the ideal combination of excess air ratio, hydrogen ratio and spark timing. This should be further followed by the implementation of an adequate control system. Other potential improvements include the reduction of emissions which can be transpire with the addition of a catalytic converter or by implementing an exhaust gas recycle system, lastly there is potential for performance improvements with an increase in the compression ratio.

X. Conclusion

Natural gas is employed as fuel for IC Engines since it is the cleanest fossil fuel with exhaust emissions from natural gas vehicles lower than those of gasoline-powered vehicles. Some of its drawbacks can be mitigated by enriching it with hydrogen to produce the so called hydrogen-natural gas blends.

The laminar flame speed of methane is lower than the gasoline one and the addition of hydrogen, which presents a laminar flame speed about eight times that of methane, significantly improves this main combustion property.

Addition of hydrogen to CNG as a fuel in SI engines gives significant and positive impact on efficiency, especially close to the lean limit. H-CNG makes it possible to run the engine leaner, resulting in lower emissions of CO2, CO and HC at certain relative air/fuel ratio and higher NO*x* emissions at constant excess ratio. Future experimental developments would prophesy the optimization of emissions along with the reduction of fuel consumption. Finally, it has been concluded that H-CNG fuels pave the road for the use of hydrogen vehicles in the future due to expensive after treatment technologies. That benefit, combined with the energy issue awareness impact in public transportation, cannot be overestimated.

Acronyms

AFR	—	Air-fuel ratio [kg*air*/kg*f uel*]
Avg	—	avg – Average
CA	—	Crank angle
COV	—	Coefficient of variation
BMEP	—	Brake mean effective pressure
BTDC	—	Before top dead center
EGR	—	Exhaust gas recirculation
HCNG	—	Hydrogen-natural gas blend
Imep	—	Indicated mean effective pressure [Pa]
LHV	—	Lower heating value [MJ/kg or MJ/Nm3]
MAP	—	Manifold absolute pressure
MBT	—	Maximum brake torque
NG	—	Natural gas

NMHC — Non methane hydrocarbons
NOx — Nitrogen oxides
THC — Total Hydrocarbons

REFERENCES

[1] Nanthagopal, K., et al.: Hydrogen Enriched Compressed Natural Gas, Thermal Science, Year 2011, Vol. 15, No. 4, pp. 1145-1154

[2] Collier K, et al, Emissions results from the new development of a dedicated hydrogen-enriched natural gas heavy duty engine, SAE Paper 2005-01-0235.

[3] Reduced Turbine Emissions Using Hydrogen-Enriched Fuels R.W. Schefer Combustion Research Facility Sandia National Laboratories Livermore, CA 94551-0969

[4] Development and Demonstration of Hydrogen and Compressed Natural Gas (H/CNG) Blend Transit Buses - *Technical Report* /NREL/TP-540-38707 , November 2005

[5] Hign percentage H-CNG Blend Ford F-150 Operating Summary - Don Karner ,James Francfort , January 2003 ,Idaho National Engineering and Environmental Laboratory Bechtel BWXT Idaho, LLC

[6] Experimental Tests of Blends of Hydrogen and Natural Gas in Light Duty Vehicles , HYSYDAYS – 2ND Word Congress of Young Scientist on Hydrogen Energy Systems , Turiin 2007 Fernando Ortenzi, Maria Chiesa, Brescia,Francesco Conigli

[7] Properties of fuel table, Alternative fuels and advanced vehicle data centre, US Department of energy

[8] Hydrogen Enrichment Via Chemical Recuperation to Increase Efficiency and Reduce Emissions in Engines , David Vernon

[9] Development of HCNG Blended Fuel Engine with Control of NOx Emissions. - K R Patil, P.M. Khanwalkar, S.S.Thipse, K.P.Kavathekar, S.D.Rairikar

[10] A Review of Hydrogen-Natural Gas Blend Fuels in Internal Combustion Engines, Antonio Mariani, Biagio Morrone and Andrea Unich, Dept. of Aerospace and Mechanical Engineering - Seconda Universitá degli Studi di Napoli, Italy

[11] Hydrogen-enriched compressed natural gas as a fuel for engines, Fanhua Ma, Nashay Naeve, Mingyue Wang, Long Jiang, Renzhe Chen and Shuli Zhao State Key Laboratory of Automotive Safety and Energy Tsinghua University China.

[12] Test of blends of hydrogen and natural gas in a light duty vehicle, JSAE paper 2007, Giovanni Pede, Ennio Rossi

[13] HCNG Heavy Duty Vehicle Prime Mover Kirk Collier (Primary Contact), Neal Mulligan, Ranson Roser Collier Technologies, LLC , FY 2003

[14] Progress Report H- NG Mixtures for increased emgine efficiency and decreased emissions. R. SIERENS University of Gent, Laboratory of Transporttechnology Sint-Pietersnieuwstraat B-9000 Gent, Belgium

[15] HCNG - A Dead End or a Bridge to the Future? - C. Nelsson, C. Hulteberg, J. Saint-Just, M. Kaiadi, 18th World Hydrogen Energy Conference 2010 - WHEC 2010.

AUTHORS

[1] Kaustubh R Kapadani
[2] Shyam S Darewar
[3] Ravindra F Dunde
[4] Chunilal K Gosavi
[5] Kavita R Kapadni

S N 163/1A Arihant Avenue, Road no. 6, Airport Road, Pune - 411032, Maharashtra State, INDIA.
[1]anuragkapadanida@gmail.com,
[2]s_darewar@gmail.com,
[3]ravidunde@gmail.com,
[4]chunilal.gosavi@gmail.com,
[5]kavita.kapadni@gmail.com

Authors are Professor(s) [1] and student [4] of Mechanical Engineering branch from PES Modern College of Engineering & MES COE Pune and perusing their master degree in Mechanical/Automotive branch in Pune University. Their areas of interest are Alternative fuels, Emission control and Development of low cost – high performance car.

"A Case Study on Gas Recovery Unit for R-22"

[1]YOGESH K. MHATRE, [2]GANESH V. JADHAV, [3]YOGESH R. JAGTAP, [4]SANKET A. BHANDARKAR, [5]T. Z. QUAZI.

Department Of Mechanical Engineering
Saraswati College Of Engineering,
Sector-5, Kharghar, Navi Mumbai – 410210, University Of Mumbai.

Abstract-The present research is concerned with proper recovery of the R-22 [1] gas, which is widely used in various R.A.C. fields on the system failure and reusing these recovered gases again for the future use. It is well known that various cooling units are widely spread in their applications and are circulating R-22 as a refrigerant. It is intended to recover this type of refrigerant by any means preventing its ill effects on environment. The time required for recovering is less, hence the system requires less time. The recovery rate of the unit ranges between 1 to 2 kg/min for 1 ton capacity of the system. We can use the unit for any ton capacity of the breakdown system refrigeration and air conditioning system to recover the gas. The. Global warming [2] is the process wherein the average temperature of the Earth's near surface air increases, owing largely to various man-made activities. Though there are some natural causes for this rise in temperature, they stand to be insignificant when compared to the man-made causes. Understanding global warming & green house gas causes and effects can give us a brief idea of the dreadful phenomena our future generations may have to face. There are some of the prominent global warming causes and effects.

Keywords- *R-22, recovery rate, global warming, energy consumption*.

I. INTRODUCTION

Refrigeration and Air conditioning system are used worldwide for various applications like Air conditions, Refrigerators etc.They are commonly used in food industry, homes, automobiles and glass industries etc.The Refrigerants are used to produce cooling effect as per requirement. But if any component or element of system fails we have to extract the refrigerant from system or released it into atmosphere. But some of these refrigerant are harmful to the environment they are responsible for O.D.P & G.W.P. Hence to release this refrigerant in atmosphere is not desirable, so they must be stored or recovered by some means.

As we are using R.A.C systems its maintenance is also an important factor. It is done periodically. The care of the breakdown maintenance is manly the leakage of the refrigerant gases in the system. The leakage is found by various methods of detecting leaks [3].

Sometimes the compressors fails, at that time the gas is trapped in the system. In such cases we cannot do the maintenance work by keeping the gas in the system. Hence either the gas in the system was released in the atmosphere and then the new compressor was installed in the system or the compressor maintenance was done by restarting the system and again filling the fresh refrigerant gas in it and then system was started. But by the use of Gas

Recovery Unit we can recover the gas in the system i.e. we can extract the gas from the system and store in the cylinder which could be further used according to the requirement.

By this means we can firstly recover the gas which was released into the atmosphere because of the breakdown repairs and secondly we can reduce the percentage of the gas released into the atmosphere which is harmful for ozone layer by being the genuine reason for Global Warming effects. So this unit is helpful for the environment and it reduces the costs of recovering and reusing the same recovered gas. VCRS [4] system is used in the unit where the compression is done by the 1 ton capacity compressor and the expansion is done by the capillary tube. The condensation done by the condenser and for evaporation copper tube is surrounded inside the tray.

II. EXPERIMENTAL WORK

A] Apparatus Description:

A gas recovery unit of 1 ton of the refrigeration capacity was selected for experimental testing. The overall physical external dimensions of the recovery unit are (620 x480 x850) mm and 15 kg weight. The figure (a) shows a schematic diagram of the unit and manifests the instrumentation and measurement tools. The unit is powered by a single electricity phase at (49.36) cc/rev speed rotary vane compressor.

The unit utilizes (R-22) as a circulating refrigerant. The expansion is controlled by copper capillary tube of 450 mm length and 1mm diameter. All components of the unit are connected by copper tubing with brazed connection.

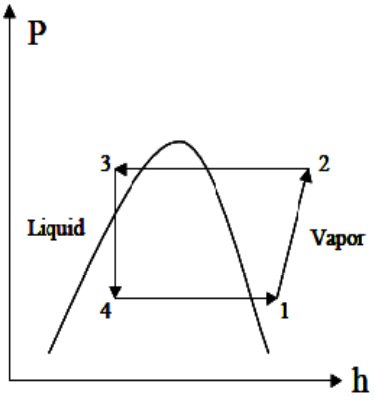

Fig 1. Schematic diagram of unit

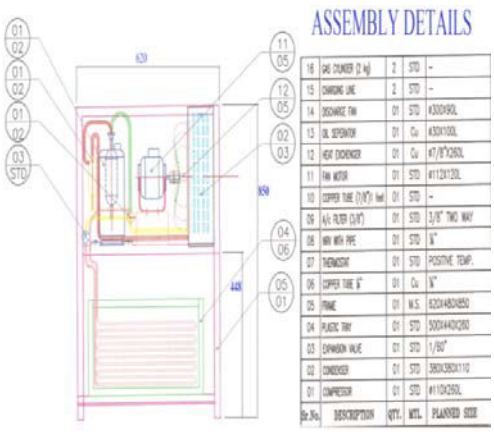

B] Refrigeration System Testing Methods:

1] Pressure test:

The pressure test is carried out by using dry nitrogen gas at pressure of 300 psi. This test held for 24hrs & the leakages are checked by soap tests

2] Evacuation test:

The system is dehydrated by the means of high vacuum pumps up to pressure of 30 Hg for 24 hrs and the whole system was heated by the torch flame.

3] Charging test:

After the evacuation is carried out the vacuum is broken by addition of refrigerant to the pressurized system at suction pressure of 50-55 psi and discharge pressure of 230 psi. The system is filled with 200-400 grams of R-22.

TABLE I

Comparative Refrigerant Performance per Ton of Refrigeration [2]

C] Methodology

Sr. no.	Properties	R-22
1.	Evaporator pressure (Mpa)	0.296
2.	Condenser pressure (Mpa)	1.192
3.	Compression ratio	4.03
4.	Refrigeration effect (kj/kg)	162.46
5.	Refrigerant flow rate (kg/s)	0.00616
6.	Sp. Vol. of suction gas	0.0774
7.	Compressor disp.	0.476
8.	Compressor power (kw)	0.210
9.	COP	4.75
10.	Compressor discharge temp (^{o} K)	326
11.	O.D.P	0.055
12.	G.W.P	1810

Process 1-2: Isentropic compression of saturated vapour in compression.
Process 2-3: Isobaric heat rejection in condenser

Process 3-4: Isenthalpic expansion of saturated liquid in expansion device
Process 4-1: Isobaric heat extraction in the evaporator

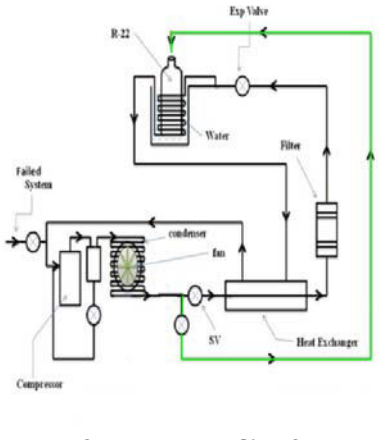

D] Analysis of The Cycle:

1) Refrigerating Effect:

The refrigerating effect accomplished by evaporator can be stated as:
$q_{evap}=(h_1-h_4)$

2) Evaporator Capacity:

The evaporator capacity can be calculated from the air side process by:
$Q_{evap} = m_a(h_{ai} - h_{ao})$

Mass of the refrigerant $(m_r) = Q_{evap} / q_{evap}$

3) Condenser Capacity:

The condenser capacity = $Q_{cond} = m_r(h_2-h_3)$

4) Useful Work:

This work used by the refrigerant can be expressed as:
$W = m_r(h_2-h_1)$

III. WORKING

We used two cylinders one as failed system and another for recovery purpose. The failed system is connected to the compressor by using hand operated valve. At first R-22 was allowed to circulate in the system to achieve the temp. of the water placed in plastic tray upto 16-18 ^oC and s.p. upto 45-55 psi. Once the steady state was achieved thermostat was cut off & compressor stopped automatically. During this process the discharge valve was closed and the R-22 flows through the circuit indicated by black linings as shown in the figure.

Fig.3 Line diagram of refrigerant gas recovery unit

After maintaining suitable pressure limit, the R-22 from the failed system flows through the compressor, condenser and circuit shown by the green line during this process charging line was closed and discharge valve was opened which is connected to the recovery cylinder placed in the water tray. During this recovery process weight of the cylinder was measured for every 10 pulses and the time required was noted

IV. OBSERVATION TABLE

TABLE II
The table shows sample readings.

Sr. No.	Input (Gas from the failed system)	Gas recovered by the system (in grams)	Time required (in seconds)	No. of pulses
1.	210	120	10.34	10
2	250	250	9.93	10
3.	210	340	8.89	10
4.	230	350	8.72	10

V. CALCULATIONS:

A) Recovery Rate:
Weight of each cylinder = 1380 grams
Weight of each charging line = 100 grams

$$\text{Recovery rate} = \left\{ \frac{\sum \text{Gas recovered}}{\sum \text{Total time taken}} \right\}$$

Gas in the system = 600 grams
Gas in failed cylinder = 1440 grams
Gas in the empty cylinder = 170 grams

Recovery rate = (1060/37.26)
= 28 grams/sec
= 1.67 kg/min

Graph 1: For the weight of the gas recovered (grams) to the time required (sec) to recover the gas.
Scale: On X– axis 1 unit = 100 grams
On Y – axis 1 unit = 0.2 sec

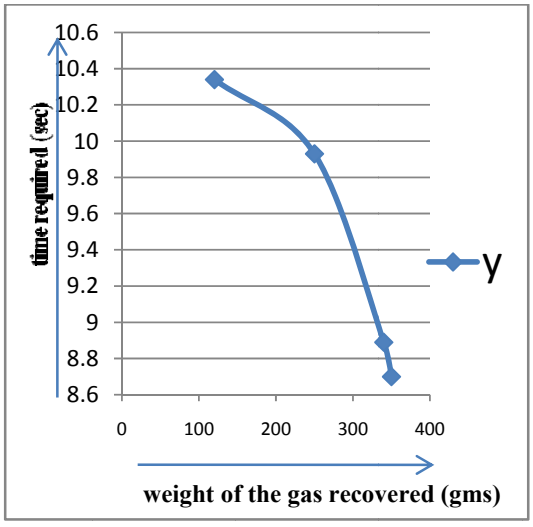

B) Energy calculations:

$$\text{Energy required} = \frac{\text{No. of pulses (for 10)} * 3600}{\text{EMC} * \text{time reqd. for}}$$

no. of pulses where ,

E.M.C = Energy Meter Constant for 10 pulses
= 3200

TABLE III
Energy calculations

Sr. No.	Gas recovered (gms)	Time reqd. (sec)	Energy reqd. (W)
1.	120	10.34	1.088
2.	250	9.93	1.133
3.	340	8.89	1.265
4.	350	8.7	1.293

Graph 2**:** For the weight of the gas recovered (grams) to the energy required (Watts).

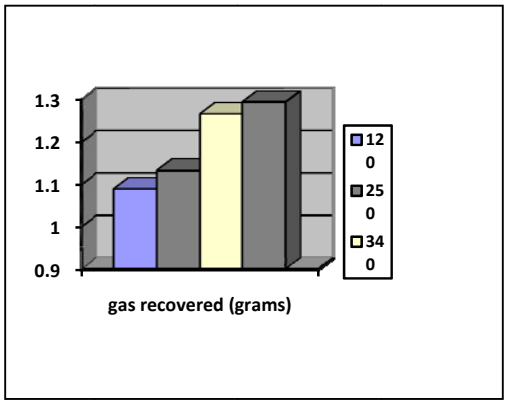

VI. CONCLUSION:

From the above discussion we conclude that

(i) Performance of VCRS decreases with increase in outdoor temp.
(ii) When we circulated the R-22 in the system to achieve the temp of the water up to 16-18 ^{o}C this is because temp. of the water reduces more gas will be recovered.
(iii) The time required for recovering is less, hence the system requires less time.
(iv) The recovery rate of the unit ranges between 1 to 2 kg/min for 1 ton capacity of the system.
(v) We can use the unit for any ton capacity of the breakdown system refrigeration and air conditioning system to recover the gas.
(vi) We can store the recovered gas and can use for another or same system in the future.
(vii) The money wastage for the new gas is reduced due to usage of the old gas, hence it is money saving project.
(viii) It minimizes the global warming effect and the ozone depletion potential due to the release of the gases in the atmosphere.

VII. NOMENCLATURE:

Temp : Temperature
ODP: Ozone Depletion Potential
GWP: Global Warming Potential
Reqd. :Required
W: Watts

REFERENCES:

[1] Sukumar Devetta, Saroja Asthana, Rahul Joshi, Process Development Division, National Chemical Lab, Pune 411008, India Received 3rd July,2003 Accepted 26th Oct 2003.Material Safety Datasheet For R-22 By National Refrigerant Inc, 661 Kenyon Avenue Bridgeton, New Jersey 080302.

[2] www.effectivepapers.blogspot.com/2010/10/research-paper-on-global- warming.html?m=1

[3] http://www.air-conditioner-selection.com/refrigerant-leak-detection-simple.html
ASHRAE refrigeration handbook chapter. 29, 19.

[4] Lesson 25 , Analysis Of Complete Vapour Compression Refrigeration Systems,Version 1 ME, IIT Kharagpur

Research papers by Ali Hussain Tarrad and Ayad Khudhair Abbas, Dept. Of Mech. Engg., Baghdad [Emirates Journal For Engg. Research Volume 15, No.2]
Research paper by Samuel F. Yana Motta and Piotr A . Domanski NIST Gaithersburg, USA.

Research paper by J.U.Ahamed1,2, R.Saidaur1, H.H.Masjubi, Dept. of Mechanical Engg. University of Malaya 50603 Kuda Lumpur, Malaysia.
"REFRIGERATION AND AIR CONDITION " BY R.S.Khurmi & Gupta

◈◈◈

Calculated and Evaluating Seven Cubic Equations of State in Predicting Gas and Liquid Phase Volumetric Properties of nine Ozone-Safe Refrigerants

[1]MOHAMMADREZA MOBINIPOUYA, [2]MARZIEH SHIDAEI

[1]Institute for Teacher Education, Organization of Fars Province, Shiraz, Iran
[2]Islamic Azad University, Marvdasht Branch, Marvdasht,Fars, Iran

Abstract— The present work is devoted to evaluating seven cubic equations of state (EOS) in predicting gas and liquid phase volumetric properties of nine ozone-safe refrigerants both in super and sub-critical regions. The evaluations, in sub-critical region, show that TWU and PR EOS are capable of predicting PVT properties of refrigerants R32 within 2%, R22, R134a, R152a and R143a within 1% and R123, R124, R125, and y TWU and PR EOS's, from literature data are 0.5% for R22, R32, R152a, R143a, and R125, 1% for R123, R134a, and R141b, and 2% for R124. Moreover, SRK EOS predicts PVT properties of R22, R125, and R123 to within aforementioned errors. The remaining EOS's predicts volumetric properties of this class of fluids with higher errors than those above mentioned which are at most 8%.In general, the results are in favor of the preference of TWU and PR EOS over other remaining EOS's in predicting densities of all mentioned refrigerants in both super and sub critical regions. Typically, this refrigerant is known to offer advantages such as ozone depleting potential equal to zero, Global warming potential equal to 140, and no toxic.

Keywords-component; *volumetric properties; refrigerant; super and sub-critical regions*

INTRODUCTION

Since van der Waals (1873) proposed his well-known cubic equation of state over a century ago, numerous equations of state have been proposed to calculate the thermodynamic properties of both pure components and mixtures in vapor and liquid phases.

The ability of a CEOS to correlate the phase equilibria of mixtures depends not only on the mixing rule, but also on the alpha function. Remarkable success in the development of a generalized alpha function was shown by Soave (1972) .He recognized that a prerequisite for the correlation of the phase equilibria of mixtures is the correlation of the vapor pressures of the pure components. The soave modification of the Redlich and Kwonog(1949) equation has been a major success in correlation of the phase behavior of multi-component systems containing non-polar and slightly polar components. The soave approach was subsequently used in work by peng and Robinson (1976). This also helped the PR equation to become one of the most widely used

equations of state in industry for correlating the vapor – liquid equilibria (VLE) of systems containing non-polar and slightly polar components.

I. Review of Equations of State Van der Waals EOS

$$\left(P+\frac{a}{V^2{}_m}\right)\left(V_m-b\right)=RT \tag{1}$$

Where p represents pressure, T is temperature, V_m is molar volume and R is the molar gas constant.The parameter a is a measure of the attractive forces between the molecules and the parameter b is a measure of the size of the molecules (hard body term). Both adjustable parameters a and b can be obtained from the critical properties of the fluid. The van der Waals equation can be regarded as a "hard-sphere (repulsive) + attractive" term equation of state composed from the contribution of repulsive and attractive intermolecular interactions, respectively.

It gives a qualitative description of the vapour and liquid phases and phase transitions (Van Konynenburg and Scott, 1980), but it is rarely sufficiently accurate for critical properties and phase equilibria calculations. A simple example is that for all fluids, the critical compressibility predicted by Eq. (1) is 0.375, whereas the real value for different hydrocarbons varies from 0.24 to 0.29. The van der Waals equation has been superseded by a large number of other, more accurate equations of state.

Where a, b and R are constants that depend on the specific material. They can be calculated from the critical properties as:

$$a=0.421875\frac{R^2T_c{}^2}{P_c} \tag{2}$$

$$b=0.125\frac{RT_c}{P_c} \tag{3}$$

In 1873, the van der Waals equation of state was one of the first to perform markedly better than the ideal gas law. In this landmark equation a is called the attraction parameter and b the repulsion parameter or the effective molecular volume. While the equation is definitely superior to the ideal gas law and does

predict the formation of a liquid phase, the agreement with experimental data is limited for conditions where the liquid forms. While the van der Waals equation is commonly referenced in text-books and papers for historical reasons, it is now obsolete. Other modern equations of only slightly greater complexity are much more accurate. Van der Waals equation may be considered as the ideal gas law, "improved" due to two independent reasons:

1. Molecules are thought as particles with volume, not material points. Thus V cannot be too little, less than some constant. So we get (V - b) instead of V.
2. While ideal gas molecules do not interact, we consider molecules attracting others within a distance of several molecules' radii. It makes no effect inside material, but surface molecules attract to inside. We see this as diminishing of pressure on the outer shell (which is used in the ideal gas law), so we write (P + something) instead of P. To evaluate this 'something', let's examine addition force acting on an element of gas surface.

A. Redlich-Kwong EOS

Introduced in 1949 the Redlich-Kwong equation of state was a considerable improvement over other equations of the time. It is still of interest primarily due to its relatively simple form. While superior to the van der Waals equation of state, it performs poorly with respect to the liquid phase and thus cannot be used for accurately calculating vapor-liquid equilibria. However, it can be used in conjunction with separate liquid-phase correlations for this purpose.

The Redlich-Kwong equation is adequate for calculation of gas phase properties when the ratio of the pressure to the critical pressure (reduced pressure) is less than about one-half of the ratio of the temperature to the critical temperature (reduced temperature).The Redlich-Kwong EOS by Redlich and Kwong is a modification of the Van der Waals EOS it should only be used in order to demonstrate the inabilities of simple EOS ,because better EOS exist . Use of this EOS only requires the input of Tc and Pc.

The parameters a and b (for each component):

$$p = \frac{RT}{v - b} - \frac{a/T^{0.5}}{v(v+b)} \quad (4)$$

$$a = \frac{0.42748 R^2 T_C^{2.5}}{P_C} \quad (5)$$

$$b = \frac{0.08664 R^2 T_C}{P_C} \quad (6)$$

B. Peng-Robinson EOS

This equation of state is fairly similar to the Soave-Redlich-Kwong equation ,but with a slightly different denominator for the second term.Again , the parameter α has a temperature dependence, and the parameter giving its dependence ω have been found by comparing the predictions of the equation with experimental boiling points.The Peng-Robinson equation is particularly accurate for predicting the properties of ydrocarbons, including the behavior of mixtures and vapor-liquid equilibrium. It is not expected to be accurate when predicting properties properties of highly polar molecules, particularly those that are capable of hydrogen bonding.The Peng-Robinson EOS is the EOS most widely used in chemical engineering thermodynamics.The EOS requires three inputs per compound: Tc, Pc and the acentric factor ω.

The Peng-Robinson EOS is the EOS most widely used in chemical engineering thermodynamics.The EOS requires three inputs per compound: Tc, Pc and the acentric factor ω.

$$P = \frac{RT}{V-b} - \frac{a}{V(V+b)+b(V-b)} \quad (7)$$

Where ω is the acentric factor for the species

The Peng-Robinson equation was developed in 1976 in order to satisfy the following goals:

1. The parameters should be expressible in terms of the critical properties and the acentric factor.
2. The model should provide reasonable accuracy near the critical point, particularly for calculations of the Compressibility factor and liquid density.

II. CALCULATION

Figure 1 illustrates deviation plot of the calculated vapor density from the literature data for refrigerant R152a in super-critical (T= 2700 K) region.

Figure 2 demonstrates a plot of the calculated a comparison between the calculated and literature values of saturated vapor of R134a system.

III. Second virial coefficient

A close look at figures reveals that PR and SRK are in good agreement with those obtained from recent correlations obtained by Tsonopoulos and Weber and speed of sound measurements.Therefore, these two EOS stand over other EOS both in sub and super critical regions.All EOS follow two-parameter principle of corresponding states at T/Tc higher than 8 and lower than 1 except NM EOS.In the temperature range 1<T/Tc<8, PR and SRK still follow above mentioned principle.The same trend has been observed for other refrigerants

1. The present work is devoted to evaluating seven cubic equations of state (EOS) in predicting gas and

liquid phase thermodynamic properties of several refrigerants both in super and sub- critical regions.
2. Refrigerants include R22, R32, R123, R124, R125, R134a, R141b, R143,and R152a and equations of state, considered here, are Ihm-Song-Mason (ISM), Peng-Robinson (PR), Redlich-Kwong (RK), Soave-Redlich-Kwong (SRK), Modified Redlickh-Kwong (MRK), Nasrifar-Moshfeghian (NM), and Twu-Coon- Cunningham (TCC).
3. The evaluations, in sub-critical region, show that TCC and PR EOS are capable of predicting PVT properties of refrigerants R32 within 2%, R22, R134a, R152a and R143a within 1% and R123, R124, R125, and R141b to within 0.5%. It should be mentioned that NM EOS can also predict volumetric properties of R22, R32, R123, R152a, and R143a within aforecited estimated accuracies. Moreover, in this region, the ISM EOS predicts these properties of R123 and R141b with above-mentioned accuracies.
4. In super-critical region, the deviations of calculated vapor densities, obtained by TCC and PR EOS's, from literature data are 0.5% for R22, R32, R152a, R143a, and R125, 1% for R123, R134a, and R141b, and 2% for R124. Moreover, SRK EOS predicts PVT properties of R22, R125, and R123 to within aforementioned errors.

IV. In Sun

The results are in favor of the preference of TCC and PR EOS's over other emaining EOS's in predicting vapor densities of all mentioned refrigerants in both super and sub critical regions.
As a thermodynamic property , second virial coefficients of R143a have been calculated from NM EOS.,PR EOS. ,SRK EOS. TCC EOS. Our calculations are in agreement with literature values especially at high temperatures

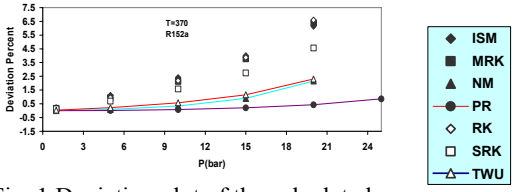

Fig. 1 Deviation plot of the calculated vapor density from
the literature data for refrigerant R134a in super-critical (T= 500 K) region

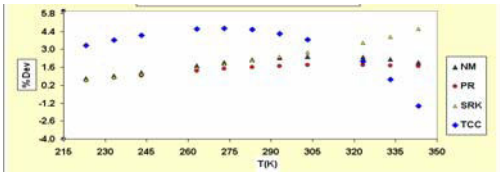

Fig.2 Comparison between the calculated and literature values of saturated vapor of R134a system.

NOMENCLATURE

p	pressure (bar)
T	temperature (K)
Z	compressibility factor
V	volume
V_m	molar volume
R	ideal gas constant (8.31451 J/ (mol K))
ω	acentric factor

REFERENCES

[1] C. H. Twu, J. E. Coon, J. R. Cunningham, *Fluid Phase Equilib*., 105, (1995) 49-54 http://webbook.nist.gov
[2] C. Tsonopoulos, Fluid Phase Equilibria, 21 (2003), 35-39
[3] D. Y. Peng, and D. B. Robinson, *Ind. Eng. Chem. Fundam*. 15, 59 (1976) 59-66
[4] G. Soave, *Chem. Eng. Sci*. 27 (1972), 1197-1204
[5] G. Soave, *Fluid Phase Equilib* (1993) 82-88
[6] Kh. Nasrifar, M. Moshfeghian, *Fluid Phase Equilibria* 190, 3(2001)
[7] L. A. Weber, Int. J. Thermophys, 15 (1994), 461-468
[8] O. Redlich and J. N. S. Kwong, *Chem. Rev*. 44, 461 (1949), 461-469

◈◈◈